

ELINE
VAN DER KRUK

PARAMETER ANALYSIS for SPEED SKATING PERFORMANCE



PARAMETER ANALYSIS for SPEED SKATING PERFORMANCE

ELINE VAN DER KRUK

TECHNISCHE UNIVERSITEIT DELFT FEBRUARI 2019

Parameter analysis for speed skating performance

Proefschrift

Ter verkrijging van de graad van doctor
aan de Technische Universiteit Delft,
op gezag van Rector Magnificus, Prof. dr. ir. T.H.J.J. van der Hagen,
voorzitter van het College voor Promoties,
in het openbaar te verdedigen op
donderdag 08 februari 2018 om 15:00 uur

door

Eline VAN DER KRUK

*Master of Science in Mechanical Engineering,
Technische Universiteit Delft, Nederland,
geboren te Albrandswaard, Nederland.*

Dit proefschrift is goedgekeurd door de promotoren.

Samenstelling promotiecommissie bestaat uit:

Rector magnificus,	voorzitter
Prof. dr. F.C.T. van der Helm,	Technische Universiteit Delft, promotor
Prof. dr. H.E.J. Veeger,	Technische Universiteit Delft, promotor
Dr. ir. A.L. Schwab,	Technische Universiteit Delft, copromotor

onafhankelijke leden:	
Prof. dr. A.J. van den Bogert,	Cleveland State University
Prof. dr. G. Jongbloed,	Technische Universiteit Delft
Prof. dr. R.H.M. Goossens,	Technische Universiteit Delft
Dr. H. Houdijk,	Vrije Universiteit Amsterdam
Prof. dr. H. Vallery,	Technische Universiteit Delft, reservelid



Parameter analysis for speed skating performance
Dissertation at Delft University of Technology
Copyright © 2018 by E. van der Kruk

An electronic version of this dissertation is available at
<http://repository.tudelft.nl/>

Cover design by E van der Kruk

Table of Contents

Summary	5
Samenvatting	7
CH 1. Introduction	11
Part I Capturing 3D kinetic data	
CH 2. Accuracy of Body Motion Capture Systems for Sport Applications	23
CH 3. Wireless Instrumented Klapskates for Long-track Speed Skating	41
Part II Speed skating technique	
CH 4. Two body dynamic model driven by the skater's leg extension	55
Part III Mechanical Power in Speed Skating	
CH 5. Power in Sports: a literature review on the application, assumptions, terminology and validity of mechanical power in sport research.	73
CH 6. Getting in shape: reconstructing three-dimensional long-track speed skating kinematics by comparing several body pose reconstruction techniques.	99
CH 7. Balancing Power: determining the mechanical power balance in speed skating with a new proposed inverse dynamics method.	123
Part IV Real-time feedback systems	
CH 8. Getting the angles straight in speed skating: a validation study on an IMU filter design to measure the lean angle of the skate on the straights	141
CH 9. Push-off forces in elite short-track speed skating.	149
CH 10. Discussion & Conclusions	161
Acknowledgements	197
Curriculum vitae	201
List of Publications	204

1

2

3

4

5

6

7

8

9

10

SUMMARY

Although speed skating has existed for centuries, it is not yet clear what the optimal skating technique actually is. Skating is a motion with many interconnected variables, and there seem to be different optimal techniques for different speed skaters.

The **aim of this dissertation** is to determine the interconnectivity of technique variables and performance determining variables within a skating stroke by measuring and modelling the speed skating motion, which eventually can be used for real-time feedback in speed skating training. This is done by the development and verification of a simple 3D biomechanical skater model that simulates the skating motion, and developing new instrumented klapskates to measure the push-off forces. To analyse the mechanical power, a well-known performance characteristic, a mechanical power model of a speed skater is developed.

Capturing kinematic data of a speed skater on an ice rink proved to be challenging due to the large volume one skating stroke covers. CH2 presents a literature review with an aim to assist researchers in the selection of suitable **motion capture systems** for their experimental setup in sport applications. Concluded from the review is that state-of the art human motion capture measurement systems are not capable of measuring position indoors with a <50mm accuracy in a volume of an indoor ice rink (area of 12,000 m²). The largest volume, captured in this dissertation, with an extensive measurement set-up was 50x4x2 m, with an accuracy of 4.5-4.7 mm.

A pair of **wireless force measuring instrumented klapskates** have been constructed in this dissertation, to measure the push-off forces of skaters. They are calibrated on a tensile testing machine, where they proved to be unaffected by temperature conditions and accurate up to 1.7% in normal direction and 4.4% in lateral direction. The design of the skate allows skaters to attach their own shoe and Maple blade to the bridge. On-ice measurements showed the possibility of recording with the skates simultaneously and synchronously both straights and curves, and the capability of the system to send data wirelessly and real-time to other devices, which makes it possible to eventually provide skaters and coaches with visual real-time feedback during practice (CH3).

The search for the optimal skating motion starts in the second part of this dissertation, where a **simple biomechanical skating model** (SSM) is presented, which mimics the observed forces and motion of a speed skater on the straights. The model simulates the upper body transverse translation of the skater together with the forces exerted by the skates on the ice. The input of the model is the changing distance between the upper body and the skate, referred to as the leg extension (Euclidean distance in 3D space). The model has been verified with 3D kinetic data of elite speed skaters measured at an ice rink (CH4). The model is most accurate for the position and velocity estimation (respectively 1.2% and 2.9% maximum residuals) and least accurate for the force estimations (underestimation of 4.5-10%). The model can be used to further investigate variables in the skating motion. For this, the input of the model, the leg extension, are optimized to obtain a maximal forward velocity of the upper body.

Power is one of the key parameters in speed skating, repeatedly brought forward by skaters, coaches, and trainers. A **systematic literature overview of the studies on mechanical power in sports** revealed that estimates of mechanical power are usually limited by the capabilities of measurement systems, resulting in the need for simplified power models. Validation of these simplifications has however only been done for running. Furthermore, inconsistency and imprecision were found in the determination of joint power, resulting from inverse dynamics methods, incorporation of translational joint powers, division in negative and positive work, and power flow over segments. Most inconsistency in terminology was found in the definition

and application of external, and internal work, and power (CH5). By structuring the existing literature, we identified some obstacles that may hamper sport research from making headway in mechanical power research.

Two proceedings are inevitable in determining the mechanical power in speed skating: inverse kinematics and inverse dynamics. In gait studies **body pose reconstruction (BPR) techniques** for inverse kinematics, have been widely explored, but no previous protocols have been developed for speed skating, while the peculiarities of the skating posture and technique do not automatically allow for the transfer of the results of those explorations to kinematic skating data. An eight body segment model (8SM) together with a global optimization method with revolute joint in the knee and in the lumbosacral joint showed to be the most realistic model to use for the inverse kinematics in long-track speed skating (CH6). Reporting on the Body Pose Reconstruction (BPR) technique and the inverse dynamic method is crucial to enable comparison between studies. This dissertation showed an underestimation of up to 74% in mean joint power when no optimization procedure was applied for BPR and an underestimation of up to 31% when a bottom-up inverse dynamics method was chosen instead of a least square error approach (LSE) (CH6).

Additionally, this dissertation introduced **a new inverse dynamics method**, PLS. The new proposed inverse dynamics method PLS allows minor modifications to the input variables under the assumption that the measurements can be slightly off. Different from other methods, the PLS method introduces the mechanical power balance as a constraint to the optimization function. PLS improves therefore both the input data and the power estimation. For speed skating, PLS showed significantly reduced residual powers in the complete mechanical power balance compared to the existing LSE method, by improving the kinetic power estimation (CH7).

The final part of this thesis describes several real-time measurement systems that were built for this dissertation to provide real-time feedback during speed skating practices. A **lean-angle algorithm for an IMU** is presented to measure the lean angle of the skate on the straights. Two aspects render measuring with commercially available IMUs and their filters on an ice rink rather difficult, first the ferromagnetic materials in the vicinity of the IMU and secondly the large linear accelerations. A complementary filter based on the assumption that the lean angle can be reset to zero when there is no change in steer angle (angular velocity, measured with a gyroscope) of the skate was used to bypass these problems for the real-time lean angle measurements (CH8); verification showed a maximum mean RMSE of 5.3° for this filter. There is no ambulant system to accurately measure the steering angle of the skate in a global frame.

In addition to feedback systems for the long-track discipline in speed skating, knowledge was spread to the short-track discipline, resulting in an **instrumented short-track skate** to measure push-off forces. A wireless force measuring instrumented skate for short-track speed skating, which has been developed and calibrated in this project, showed that there are four distinctive strokes in short-track speed skating. An explorative study performed on the Dutch national team revealed that the COP on the blade and the lateral forces are related to the level of the skater (CH9).

SAMENVATTING

Hoewel schaatsen al eeuwen lang bestaat, is nog steeds niet bepaald wat de optimale schaatstechniek is. Schaatsen is een beweging met veel verbonden parameters, en bovendien lijken er verschillende optimale technieken te bestaan voor verschillende schaatsers, wat ertoe leidt dat coaches en trainers lang op zoek zijn naar de ideale individuele techniek voor een individuele schaatser.

Het **doel van dit proefschrift** is om de onderlinge verbanden van de parameters binnen een schaatsslag te bepalen door het meten en modeleren van de schaatsbeweging, wat uiteindelijk gebruikt kan gaan worden voor directe terugkoppeling tijdens de schaatstraining. Hiervoor werd een 3D biomechanisch model van een schaatser ontwikkeld en geverifieerd, en zijn er nieuwe geïstrumenteerde meetschaatsen ontwikkeld die de afzetkrachten van de schaatser meten. Daarnaast werd, om mechanisch vermogen te kunnen meten, wat een bekende prestatie maat is, een mechanisch model van een schaatser ontwikkeld.

Het meten van kinematische data van een schaatser op een ijsbaan is een uitdaging vanwege het grote volume dat één schaatsslag bestrijkt. In H2 wordt een literatuurstudie gepresenteerd met als doel onderzoekers te helpen in het vinden van het juiste **kinematische meetsysteem voor onderzoek op sportgebied**. Uit de literatuurstudie kan geconcludeerd worden dat de huidige (state-of-the-art) meetsystemen niet in staat zijn om in het volume van een overdekte schaatsbaan (oppervlakte van 12.000m²) met een nauwkeurigheid van <50mm te meten. Het grootste volume waar wij in geslaagd zijn om 3D kinematische data te meten was 50x4x2m, met een nauwkeurigheid van 4.5 – 4.7 mm.

Dit proefschrift presenteert zelf-ontwikkelde **geïstrumenteerde klapschaatsen** voor het meten van afzetkrachten bij schaatsers. Deze zijn gekalibreerd op de trekbank, waar ze temperatuuroonafhankelijk en accuraat tot 1.7% in normale richting en 4.4% in laterale richting zijn gebleken. Het ontwerp van de schaats maakt het mogelijk voor schaatsers om hun eigen schoenen op de geïstrumenteerde bruggen te plaatsen en een Maple ijzer naar keuze. Metingen op de ijsbaan toonden aan dat het mogelijk is om met beide schaatsen continue en gesynchroniseerd zowel rechte stukken als bochten te meten. De data worden draadloos verzonden naar andere systemen, wat het mogelijk maakt om de schaatsers en coaches uiteindelijk van visuele real-time feedback te voorzien tijdens trainingen (H3).

De zoektocht naar de optimale schaatsslag begint in het tweede deel van dit proefschrift. Hier wordt een **eenvoudig biomechanisch schaatsmodel** gepresenteerd, dat de gemeten krachten en bewegingen van een schaatser op het rechte eind simuleert. Het model simuleert de transversale beweging van het bovenlichaam van de schaatser samen met de afzetkrachten op het ijs. Input van het model is de veranderende afstand tussen het bovenlichaam en de schaats, wat de leg extension wordt genoemd (Euclidean afstand in 3D). Het model is geverifieerd met 3D kinetische data van elite schaatsers gemeten op een schaatsbaan (H4). Het model is het nauwkeurigst voor positie- en snelheidsmetingen (respectievelijk 1.2% en 2.9% maximum restanten) en minst nauwkeurig voor de krachtmetingen (onderschatting van 4.5%-10%). Het model kan in verdere onderzoeken gebruikt worden om de variabelen binnen een schaatsslag te onderzoeken. Hiervoor kan de input van het model, de leg extension, geoptimaliseerd worden zodat er een maximale voorwaartse snelheid ontstaat.

Vermogen is een belangrijke variabele in het schaatsen, welke regelmatig door coaches, schaatsers en trainers wordt genoemd. Door middel van een **systematische literatuurstudie** toont dit proefschrift aan dat de schattingen van **mechanisch vermogen in sport** meestal gelimiteerd worden door de mogelijkheden in meten, wat leidt tot het gebruik van versimpelde modellen (H5). Validatie van deze versimpelde modellen is echter alleen gedaan voor het

rennen. Bovendien, werden inconsistentie en onnauwkeurigheden gevonden voor het bepalen van de joint power, resulterend uit de gebruikte inverse dynamica methodes, het wel of niet bepalen van translatie componenten in de joint power, verdeling in negatieve en positieve arbeid, en de powerflow over de segmenten. De meeste inconsistentie werd gevonden in de definitie en het gebruik van externe, en interne arbeid en vermogen (H5). Door de bestaande literatuur te structureren, zijn enkele obstakels geïdentificeerd die mogelijk de vooruitgang op het onderzoeksgebied van mechanisch vermogen belemmeren.

Twee handelingen zijn onmisbaar bij het bepalen van mechanisch vermogen in het schaatsen: inverse dynamica en inverse kinematica. In looponderzoek zijn de **body pose reconstructie (BPR) technieken voor inverse kinematica** uitgebreid onderzocht, maar voor schaatsen waren zulke protocollen nog niet ontwikkeld, terwijl de eigenschappen van de schaatshouding en techniek ervoor zorgen dat de bestaande BPR technieken niet direct toepasbaar zijn op de kinematische data van een schaatser. In dit proefschrift wordt aangetoond dat een 8-segmenten model (8SM) in combinatie met een globale optimalisatie methode, met een 1-assig gewricht in de knie en het lumbrosacraal gewricht het meest realistisch bleek om te gebruiken voor inverse kinematica in langebaanschaatsen (H6). Het rapporteren van de gebruikte BPR techniek en de inverse dynamicamethode is cruciaal om studies onderling te kunnen vergelijken. In dit proefschrift wordt aangetoond dat een onderschatting tot 74% in gemiddelde joint power werd gevonden als er geen optimalisatie methode werd gebruikt voor BPR, en een onderschatting tot 31% wanneer een bottom-up inverse dynamicamethode werd gebruikt in plaats van een least-square error approach (LSE) (H6).

Daarnaast wordt er in dit proefschrift een **nieuwe inverse dynamica methode** gepresenteerd, PLS. Deze nieuwe methode staat kleine modificaties aan de inputvariabelen toe onder de aanname dat de metingen meetfouten kunnen bevatten. Anders dan de bestaande methodes, introduceert de PLS-methode de vermogensbalans als restrictie in de optimalisatiemethode. PLS verbetert daarom zowel de inputdata als de vermogensschatting. Voor schaatsen reduceerde PLS de residuen in de vermogensbalans substantieel vergeleken met de bestaande LSE-methode, met name door de kinetische vermogens schatting te verbeteren (H7).

Het laatste deel van dit proefschrift beschrijft twee real-time feedback systemen die gebouwd zijn tijdens dit project voor real-time feedback tijdens schaatstrainingen. Allereerst een **leunhoekalgoritme voor een Inertial Measurement Unit (IMU)**, dat de leunhoek van de schaats bepaalt op het rechte eind. Twee aspecten maken het meten met bestaande, commerciële IMUs lastig op een ijsbaan; allereerst de ferromagnetisch materialen in nabijheid van de IMU, en ten tweede de grote lineaire acceleraties. Een Complementair Filter, gebaseerd op de aanname dat de leunhoek gereset kan worden naar nul graden wanneer er geen verandering is in de stuurhoek van de schaats (hoeksnelheid gemeten met de gyroscope), werd gebruikt om deze problemen te omzeilen voor het real-time meten van de leunhoek (H8). Verificatie toont aan dat de maximum gemiddelde RMSE van dit filter 5.3° is. Het is niet mogelijk om ook de stuurhoek van de schaats nauwkeurig te meten in het globale frame met een IMU.

Naast de feedback- en meetsystemen in het langebaanschaatsen, is de kennis van dit proefschrift ook verspreid naar de short-track discipline. Er is een **draadloze geïnstrumenteerde shorttrackschaats** ontwikkeld voor het short-track schaatsen die de afzetkrachten meet. Vier verschillende schaatsslagen konden met deze schaatsen worden onderscheiden. Een exploratieve studie binnen het Nederlands short-track team laat zien dat het aangrijpingspunt van de kracht op het blad (COP) en de laterale krachten loodrecht op het blad gerelateerd zijn aan het niveau van de schaatser (H9).

1

Introduction

‘Most overnight successes took a long time’
-Steve Jobs-

Onderzoek gaat niet over één nacht ijs

Throughout evolution, humans and animals have shown to develop a wide range of motion strategies. The general consensus is that a large factor in this development has been the energy-saving principle, which forces creatures to adapt their movement to the environment, whether this is ground, water, air, or ice. The development of ice-skating has not been different. At least 3000 years ago in the Scandinavian countries and the Netherlands, humans were already developing an on-ice motion strategy, to speed-up locomotion (Formenti & Minetti, 2007). Locomotion over ice was simple, effective, and cheap, which allowed people to reach more distant destinations than they could do by walking or running. In the 13th century, in winter, skating was used in the Netherlands to maintain communication between villages. This development was definitely strengthened after the construction of windmills in the 15th century, which drained the lower-lying areas, resulting in a large network of canals. Therefore, ice skating was the most popular, and convenient, means of transport in the Dutch winters for centuries. This history is still embedded in the Dutch language, with countless sayings related to skating, and with no less than fifty expressions for ice (Dohle, 2004). And ice-skating was definitely not limited to the Netherlands and Scandinavian countries, the first iron-blade skates were for instance designed in Scotland (1592), and the first all-steel blade in North-America (1851).

Today still, speed skating is after cycling, the fastest human-powered way to propel over flat-land. Nowadays, of course, ice-skating is no longer a necessary means of transport, but practised as leisure, or sport. Long-track speed skating (400m rink) has been an Olympic sport since 1924 for men, and since 1960 for women; short-track speed skating (111m rink) has been an Olympic discipline since 1992. Speed skating has known several technological developments: introduction of refrigerated ovals in the late-50s, ice preparation in the 60s,



Figure 1.1 Old Dutch tableau of a speed skating competition. bron: 'Het Schaats Boek', John van Zuijlen



Figure 1.2 State-of-the-art real-time feedback in speed skating.

thigh fitting clothes in the 70s, the opening of indoor ovals in the mid-80s, and the (re-) introduction of the klapskates in the late 90s of last century (Kuper & Sterken, 2003). Coaches and athletes are always eager for more, better, and faster.

The starting point of this project was the wish of the Dutch skating federation to have real-time feedback during skating practice to improve performance. Currently, the only feedback skaters receive during training is when they pass their coach at the end of the straight part, which is once every 400m (Figure 1.2). Preferably a coach or trainer would therefore be able to provide his or her skater with continuous feedback during training. The main question arising when designing such a system is: what (continuous) feedback variable can actually improve skating performance? Since, although speed skating has existed for centuries, it is still unknown what the optimal skating technique actually is.

The enigma of the sport lies in the fact that elite skaters greatly differ in build and each seems to have a unique skating technique¹ (Konings et al., 2015). This implies that there probably is not just one optimal technique, but that there is a different optimal technique for each individual speed skater. Furthermore, when skaters return to the ice rink after a summer of strength and cycling practice, it happens that, although their muscle strength was improved, their skating performance does not increase, or even decreases. A phenomenon that skaters describe as “not being able to hit their stroke”. So the strongest skater is not necessarily the fastest (Van Ingen Schenau & De Groot, 1983), which emphasises the importance of applying the right skating technique.

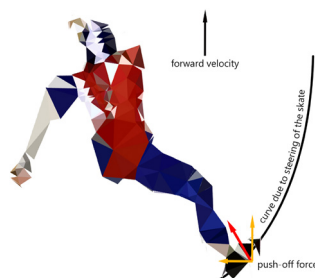
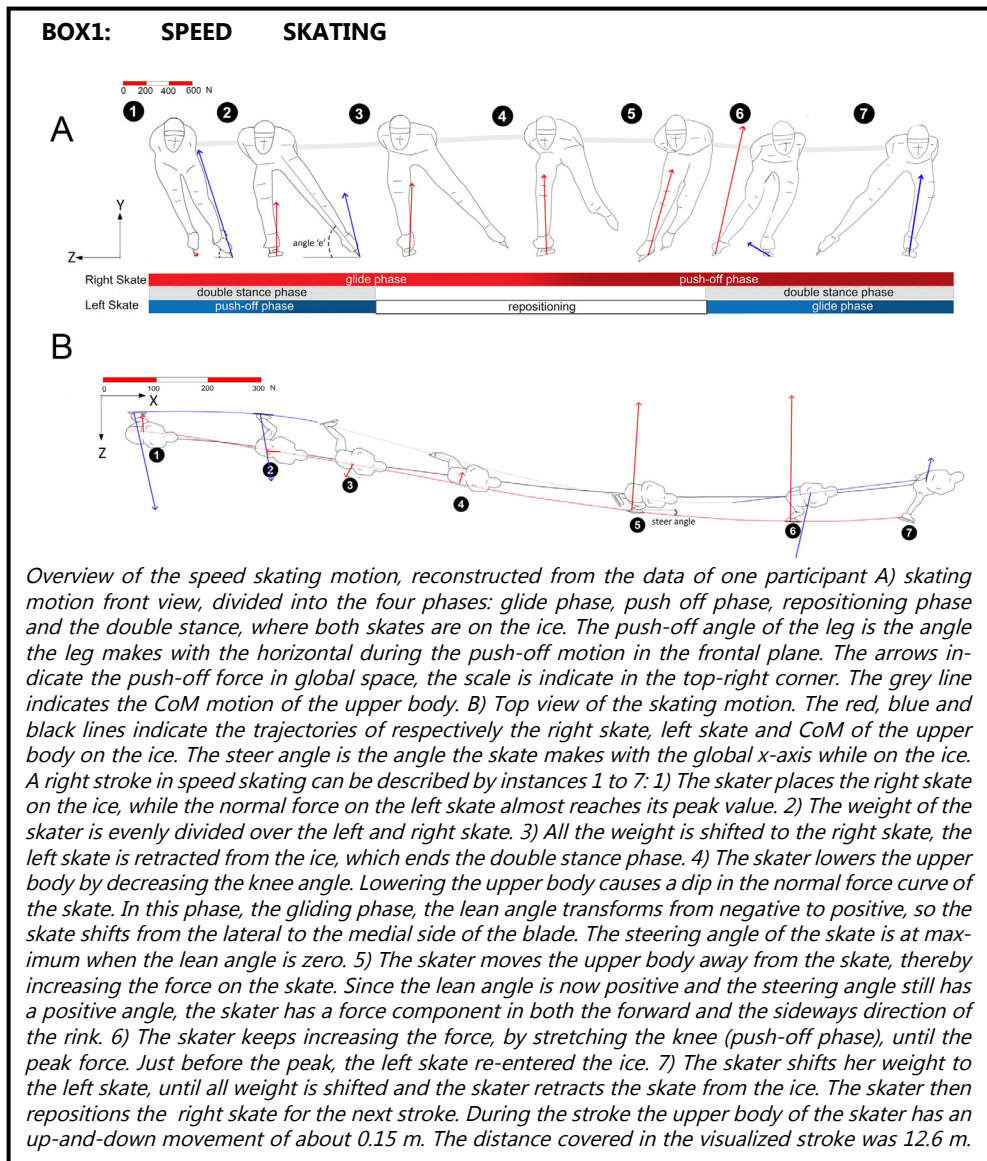
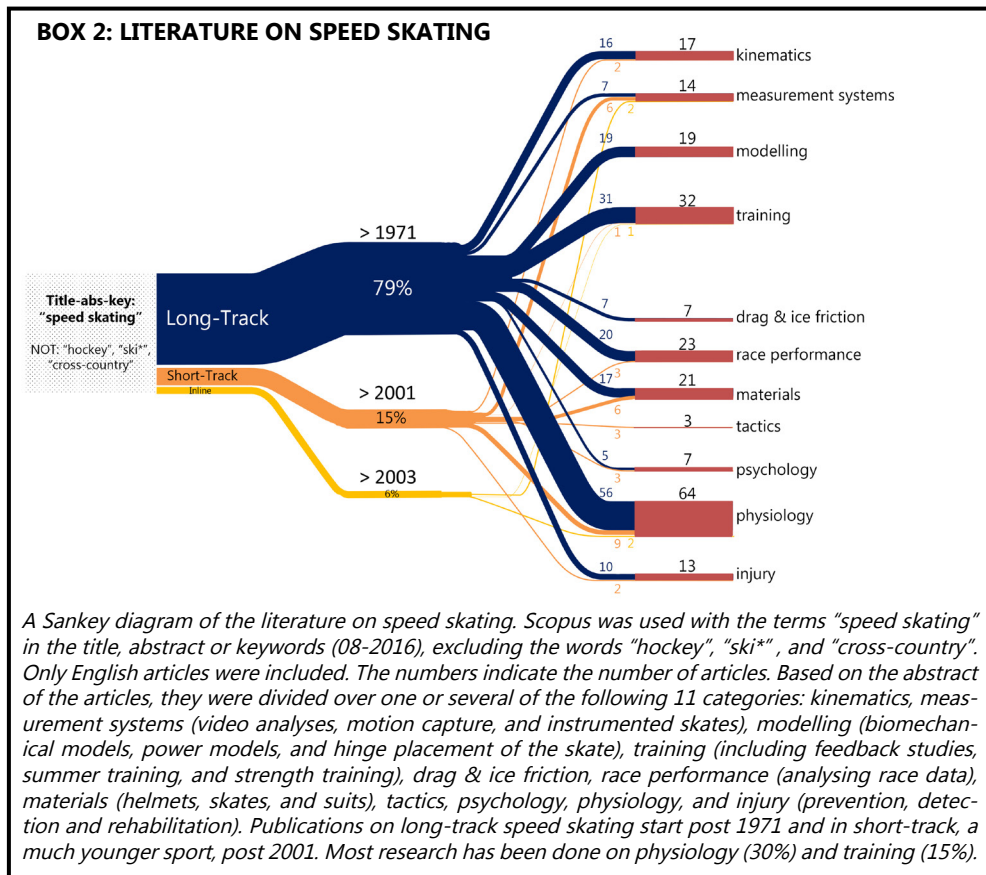


Figure 1.3 Skaters can push-off only lateral to the blade, while the skate can only glide in line with the blade. Skaters are therefore forced to steer their skate, thereby steering the push-off in both the forward and sideways direction.

¹Video: Sverre Lunde Pedersen and Havard Bøkkø imitate other skaters, A. (2010). <https://www.youtube.com/watch?v=k9Z9YHDVidA>.



Speed skating is a complex motion. The unique feature of ice is the very low friction, allowing a skater to glide. However, due to the slippery ice, it is impossible for a speed skater to push-off backwards. Trained skaters therefore steer their skate, making a curve over the ice (Figure 1.3). The push-off then results in both a forward and sideward motion, creating forward speed and making the skater move left and right over the rink. Skating is thus a trade-off between steering sideways and going forward. However, they do not only steer their skate but also lean the skate while applying force to it. At the same time lowering the upper body and repositioning the other skate, and deciding when and where to place the second skate on the ice (BOX 1). And then there is the fact that skaters have to make an even number of strokes on the straight part, to enter the curve with the correct leg. So skating is a motion with



many interconnected variables, pushing skaters, coaches and trainers to extremes to find that optimal individual technique.

This experiential search for the most optimal technique could be aided with scientific research. Reported scientific research on speed skating started in the early 1970s. A literature search using the terms "speed skating" (and eliminating the terms "ski" and "hockey") results in 193 scientific articles, starting in 1971. The articles, focussed on either long-track, short-track or inline skating, all aim at one or several of the categories indicated in box 2. Only 7% of research is aimed at the technique of speed skating, looking at single stroke variables (kinematics) of a speed skating stroke. The kinematic variables that were investigated were the push-off angle (de Boer et al., 1987; Noordhof, Foster, Hoozemans, & de Koning, 2013), push-off forces (de Boer et al., 1987; Houdijk, de Koning, de Groot, Bobbert, & van Ingen Schenau, 2000; Yuki, Ae, & Fujii, 1996), lean angle (Yuki et al., 1996), steer angle (Koga, Nishimura, Watanabe, Okamoto, & Wada, 1997), foot angle (Houdijk et al., 2000) and flexion angles of ankle, knee and hip (de Boer et al., 1987; Jos J. de Koning, de Groot, & Ingen Schenau, 1991; Houdijk et al., 2000; van Ingen Schenau, de Groot, & de Boer, 1985). These studies are all aimed at analysing single variables, rather than fitting the variables together into one technique. Statistical analyses of individual kinematic variables of skaters will, however, not be most efficient in finding the optimal skating motion (unless there are many skaters available, which for an elite level by

definition do not exist). After all, it is hypothesized that there is not one general optimal motion, but that there exists an optimal motion for each uniquely built speed skater. Therefore, we want to understand the techniques in a physical, interconnected, sense. A biomechanical model that accurately describes the speed skating motion can provide such insight.

Currently, there are two biomechanical speed skating models describing the coordination patterns of skaters. First, there is a dynamic model, consisting of 19 rigid bodies and 160 muscles, (Otten, 2003); second, there is an inverse dynamic model of a speed skater of Allinger & Bogert (1997), which is driven by individual strokes. However, both models have not been validated with actual (force) measurements, nor were the effects of the assumptions investigated. Furthermore, the application of the model by Allinger & Bogert (1997) is limited, since it is driven by a presumed function in time rather than measured leg extensions and the body height was assumed constant. Thus although (speed) skating models have been developed, none of them have been shown to accurately predict the observed coordination pattern and verification of the models with accurately measured kinetic data (kinematic and force data) of a speed skater was lacking. Therefore, there is a need for a verified biomechanical model that can accurately mimic observed forces and motions of a speed skater.

Collecting kinetic data of speed skaters is a challenge. Testing has to be performed outside laboratories at an actual ice rink, where the low temperatures, high humidity, ferromagnetic material, of e.g. the cooling pipes under the ice, and the reflections of the ice all interfere with measurements. Moreover, the high velocity of the skaters and the large volume one skating stroke covers (up to 18 m) are complicating factors for motion capture.

Also the measurement of force data is complicated. While in a gait lab a floor may be instrumented with force plates, an ice rink offers no such option. In the early nineties of the last century, instrumented skates have been developed that measure the push-off forces of skaters. At that time, speed skaters skated on the then conventional fixed skates, where the blade of the skate was fixed to the shoe (Jos J de Koning, de Boer, de Groot, & van Ingen Schenau, 1987; Van Ingen Schenau, 1981; Yuki et al., 1996). In the late-nineties, fixed skates were replaced by klapskates, which incorporate a hinge between the blade and the shoe. At the start of the 21st century, the first instrumented klapskates were introduced (Houdijk et al., 2000; Yuda, Yuki, Aoyanagi, Fujii, & Ae, 2004). These skates however, could not measure all essential (both normal and lateral) force components (Houdijk et al., 2000) or were not interchangeable between skaters (Yuda et al., 2004), and skaters had to carry a laptop to log the data. In order to perform accurate measurements and preserve participation of many skaters, skaters need to be able to wear their own skating shoes, and preferably blades, during measurements. Therefore, there is a need for a new design instrumented klapskate.

When coaches and trainers were asked the question what (continuous) real-time feedback variable could actually improve the skating performance, one variable was stated by all of them: power. Mechanical power is a metric often used by sport scientists, athletes, and coaches for research and training purposes. Speed skaters often train with power estimation systems (SRM) in their cycling trainings and therefore expressed their desire to also have real-time feedback on power during their speed skating practices. A SRM system calculates power as the product of pedal force and rotational velocity of the sprocket. Developing such a SRM-like system in speed skating, or running for that matter, proves to be more challenging than in cycling, since the center of mass of the skater continuously moves relatively to the push-off point, and the forces and velocities of both COM and the push-off point are directed into three-dimensions.

In literature, no study was found that determined the complete 3D mechanical power balance in speed skating, due to the limitations in measurements (which again emphasizes the complexity of performing kinetic measurements on an ice rink). As a consequence, simplified models have been used to estimate mechanical power (de Boer et al., 1987; de Boer & Nilsen, 1989; J.J. de Koning, de Groot, & van Ingen Schenau, 1992; Jos J de Koning, Foster, Lampen, Hettinga, & Bobbert, 2005; Houdijk et al., 2000). However, the validity of these simplifications have been disregarded, and although thorough reviews exist addressing the issues of the mechanical power equations (Aleshinsky, 1986; van Ingen Schenau & Cavanagh, 1990) and mechanical efficiency (van Ingen Schenau & Cavanagh, 1990), we found inconsistency in the power estimations and terminology. This not only makes the choice for a proper power model complicated, also interpretation and comparison to the literature is hampered. The speed skating literature, and more generally, sport research would clearly benefit from structuring and validating the research on mechanical power in sports.

Problem statement

Although speed skating has existed for centuries, it is still unknown what the optimal skating technique actually is. Skating is a motion with many interconnected variables, and there seem to be different optimal techniques for different speed skaters, which pushing skaters, coaches and trainers to extremes to find their optimal individual technique. A biomechanical model that accurately describes the speed skating motion can provide insight into the interconnectivity of the technique variables. Biomechanical skating models have been developed, but none of them have been shown to accurately predict the observed coordination pattern and verification of these models with accurately measured kinetic data (kinematic and force data) of a speed skater was lacking. This is mainly due to the fact that collecting kinematic and force data of speed skaters at an ice rink is challenging, as it requires instrumented skates that measure push-off forces and large-volume human motion capture. These limitations in measurements, also hamper the development of a power measurement system in speed skating, which is a desire of the skaters to have during training. No study determined the complete 3D mechanical power balance in speed skating. As a consequence, simplified models have been used to estimate mechanical power, but the validity of these simplifications have been disregarded.

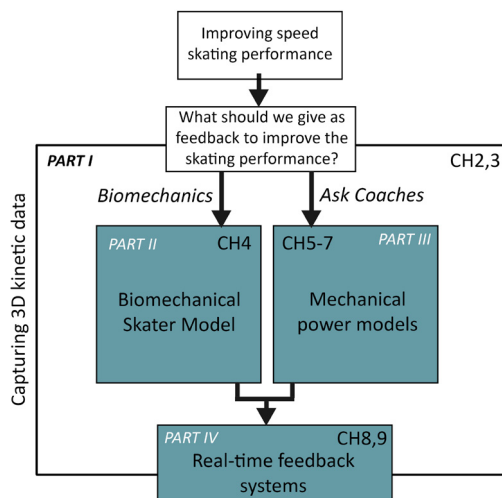


Figure 1.4 Dissertation Outline

Aim of this thesis

The aim of this dissertation is to determine the interconnectivity of technique variables and performance determining variables within a skating stroke by measuring and modelling the speed skating motion, which eventually can be used for real-time feedback in speed skating training. This is done by the development and verification of a simple 3D biomechanical skater model that simulates the skating motion, and developing new instrumented klapskates to measure the push-off forces. To analyse the mechanical power, a well-known performance characteristic, a mechanical power model of a speed skater is developed.

Outline

This thesis is divided into four parts. The interplay of the parts is sketched in Figure 1.4.

Part I (CH2, CH3) is concerned with capturing kinetic data on an ice rink, which is necessary for the validation of the studies performed in parts II, III and IV. Chapter 2 is a review of the available motion capture systems, concerned with the accuracy of the systems and their volume specifications. Chapter 3 focusses on measuring push-off forces in speed skating, describing the design and verification of a wireless instrumented klapskate.

Our search for the optimal skating motion starts in **Part II** (CH4). To understand the motion physically and optimize it, we use a biomechanical model. Chapter 4 describes the validation and design of this simple skating model.

Part III (CH5,CH6,CH7) is concerned with one of these key factors in speed skating. Power is the factor brought forward by skaters, coaches and trainers themselves, who requested a real-time feedback system on it. The term mechanical power however proved to be widely contained. Chapter 5 therefore considers the term mechanical power and how to determine it. The power estimation proves to be dependent on the model choice, measurement techniques and data processing, while in literature these influences are hardly quantified. Chapter 6 goes into several of the kinematic processing techniques, comparing inverse kinematics methods and their influence on power estimation. Chapter 7 proposes a new inverse dynamics technique, which incorporates the mechanical power balance as a constraint.

Part IV (CH8, CH9) describes several real-time measurement systems that were built for this dissertation to provide real-time feedback during speed skating practices. Chapter 8 describes the design and verification of an algorithm to determine the lean angle of the skate with the use of an IMU. In addition to feedback systems for the long-track discipline in speed skating, we spread our knowledge to the short-track discipline, resulting in an instrumented short-track skate to measure push-off forces, which is described in chapter 9.

References

Aleshinsky, S. Y. (1986). An energy "sources" and "fractions" approach to the mechanical energy expenditure problem - V. The mechanical energy expenditure reduction during motion of the multi-link system. *Journal of Biomechanics*, 19(4), 311–315.

Allinger, T. L., & Bogert, A. J. (1997). Skating technique for the straights based on the optimization of a simulation study. *Medicine and Science in Sports and Exercise*, 29, 279–286.

de Boer, R. W., Cabri, J., Vaes, W., Clarijs, J. P., Hollander, a P., de Groot, G., & van Ingen Schenau, G. J. (1987). Moments of force, power, and muscle coordination in speed-skating. *International*

Journal of Sports Medicine, 8(6), 371–378. <http://doi.org/10.1055/s-2008-1025688>

de Boer, R. W., & Nilsen, K. L. (1989). Work per stroke and stroke frequency regulation in Olympic speed skating. *Int J Sport Biomech*, (1987), 135–150.

de Koning, J. J., de Boer, R. W., de Groot, G., & van Ingen Schenau, G. J. (1987). Push-Off Force in Speed Skating, 103–109.

de Koning, J. J., de Groot, G., & Ingen Schenau, G. J. van. (1991). Coordination of leg muscles during speed skating. *Journal of Biomechanics*, 24(2), 137–146. [http://doi.org/10.1016/0021-9290\(91\)90358-T](http://doi.org/10.1016/0021-9290(91)90358-T)

de Koning, J. J., de Groot, G., & van Ingen Schenau, G. J. (1992). A power equation for the sprint in speed skating. *Journal of Biomechanics*, 25(6). [http://doi.org/10.1016/0021-9290\(92\)90100-F](http://doi.org/10.1016/0021-9290(92)90100-F)

de Koning, J. J., Foster, C., Lampen, J., Hettinga, F., & Bobbert, M. F. (2005). Experimental evaluation of the power balance model of speed skating. *Journal of Applied Physiology*, 98(1), 227–233. <http://doi.org/10.1152/jappphysiol.01095.2003>

Dohle, M. (2004). *Over een nacht ijs, een schaatsalfabet*. Amsterdam: Prometheus.

Formenti, F., & Minetti, A. E. (2007). Human locomotion on ice: The evolution of ice-skating energetics through history. *Journal of Experimental Biology*, 210(10), 1825–1833. <http://doi.org/10.1242/jeb.002162>

Houdijk, H., de Koning, J. J., de Groot, G., Bobbert, M. F., & van Ingen Schenau, G. J. (2000). Push-off mechanics in speed skating with conventional skates and klapskates. *Medicine and Science in Sports and Exercise*, 32(3), 635–641. <http://doi.org/10.1097/00005768-200003000-00013>

Koga, Y., Nishimura, T., Watanabe, N., Okamoto, K., & Wada, Y. (1997). Analysis for Motion on Speed Skating. In *SPIE* (pp. 464–469).

Konings, M. J., Elferink-Gemser, M. T., Stoter, I. K., van der Meer, D., Otten, E., & Hettinga, F. J. (2015). Performance Characteristics of Long-Track Speed Skaters: A Literature Review. *Sports Medicine*, 45(4), 505–516. <http://doi.org/10.1007/s40279-014-0298-z>

Kuper, G. H., & Sterken, E. (2003). Endurance in speed skating: The development of world records. *European Journal of Operational Research*, 148(2), 293–301. [http://doi.org/10.1016/S0377-2217\(02\)00685-9](http://doi.org/10.1016/S0377-2217(02)00685-9)

Noordhof, D. A., Foster, C., Hoozemans, M. J., & de Koning, J. J. (2013). Changes in speed skating velocity in relation to push-off effectiveness. *Int J Sports Physiol Perform.*, 8(2), 188–94.

Otten, E. (2003). Inverse and forward dynamics: models of multi-body systems. *Philosophical Transactions of the Royal Society of London B: Biological Sciences*, 358, 1493–1500.

Van Ingen Schenau, G. J. (1981). *A power balance applied to speed skating*. PhD. thesis. Vrije Universiteit Amsterdam.

Van Ingen Schenau, G. J., & Cavanagh, P. R. (1990). Power equations in endurance sports. *Journal of Biomechanics*, 23(9), 865–881. [http://doi.org/10.1016/0021-9290\(90\)90352-4](http://doi.org/10.1016/0021-9290(90)90352-4)

Van Ingen Schenau, G. J., & De Groot, G. (1983). On the origin of differences in performance level between elite male and female speed skaters. *Human Movement Science*, 2(3), 151–159. [http://doi.org/10.1016/0167-9457\(83\)90013-1](http://doi.org/10.1016/0167-9457(83)90013-1)

Van Ingen Schenau, G. J., de Groot, G., & de Boer, R. W. (1985). The control of speed in elite female speed skaters. *Journal of Biomechanics*, 18(2), 91–96. [http://doi.org/10.1016/0021-9290\(85\)90002-8](http://doi.org/10.1016/0021-9290(85)90002-8)

Video: Sverre Lunde Pedersen and Havard Bøkko imitate other skaters, A. (2010). <https://www.youtube.com/watch?v=k9Z9YHDVidA>.

Yuda, J., Yuki, M., Aoyanagi, T., Fujii, N., & Ae, M. (2004). Changes in blade reaction forces in speed skating the curve. *International Journal of Sport and Health Science*, 2(1996), 195–204.

Yuki, M., Ae, M., & Fujii, N. (1996). ドケットのド反 (Blade reaction forces in speed skating). *Society of Biomechanics*, 13, 41–51.

Capturing 3D Kinetic Data

PART I

2

Accuracy of human motion capture systems for sport applications; state-of-the-art review

Motus inter corpora relativus tantum est
-Huygens-

Accurate kinematic data are essential for the biomechanical analyses in speed skating; capturing kinematic data of a speed skater on an ice rink however, proved to be challenging due to the large volume one skating stroke covers. This chapter presents a review on the accuracy of body motion capture systems in sports application. The chapter consists of two parts; the first part is a literature study on available kinematic measurement systems; the second part contains guidelines for selecting a system for an experiment and on how to report on its accuracy.

E. van der Kruk & M.M. Reijne, *Accuracy of human motion capture systems for sport applications; state-of-the-art review* (2017), accepted with revisions at European Journal of Sport Sciences

Abstract

Objective: Sport research often requires human motion capture of an athlete. It can, however, be labor-intensive and difficult to select the right system, while manufacturers report on specifications which are determined in set-ups that largely differ from sport research in terms of volume, environment and motion. The aim of this review is to assist researchers in the selection of a suitable motion capture system for their experimental setup for sport applications. An open online platform is initiated, to support (sport)researchers in the selection of a system and to enable them to contribute and update the overview. Design: systematic review; Method: Electronic searches in Scopus, Web of Science, and Google Scholar were performed, and the reference lists of the screened articles were scrutinized to determine human motion capture systems used in academically published studies on sport analysis. Results: An overview of seventeen human motion capture systems is provided, reporting the general specifications given by the manufacturer (weight and size of the sensors, maximum capture volume, environmental feasibilities), and calibration specifications as determined in peer-reviewed studies. The accuracy of each system is plotted against the measurement range. Conclusion: The overview and chart can assist researchers in the selection of a suitable measurement system. To increase the robustness of the database and to keep up with technological developments, we encourage researchers to perform an accuracy test prior to their experiment and to add to the chart and the system overview (online, open access).

1.Introduction

Sport research often requires human motion capture of an athlete. Human motion capture is the process of recording human movement; in this review we specifically focus on recording global position of the body(segments) of an athlete. It can be labor-intensive and difficult to acquire information on the accuracy and practical usage of measurement systems. Specifications reported by manufacturers are determined in conditions and set-ups that diverge from the conditions in which sport research is performed; this can be attributed to four characteristics of the sport research area.

First, sport research is performed in non-laboratory settings, at the field, rink or arena that the sport is practiced on. Such an area outside the controlled laboratory environment brings several challenges, namely different locations (e.g. indoor versus outdoor), weather conditions (e.g. temperature and humidity), measurement interferences (e.g. noise, scattering or magnetic disturbances), and obstacles in the area resulting in occlusion.

Second, strongly related to the first characteristic, the measurement (capture) volume is often large (e.g. a ski-slope or a soccer field) (Figure 2.1). Typically, the accuracy is inversely proportional to the coverage of a positioning system (i.e. a lower accuracy for a larger measurement volume), which makes this generally the limiting factor in the selection of a measurement system. When the displacement of the participants becomes larger, ergometers are sometimes used to acquire a large number of movement cycles (e.g. treadmill, ergo cycle, or rowing-kayaking ergometers) (Begon, Colloud, Fohanno, Bahuaud, & Monnet, 2009). However, this is not always desirable, because movements on an ergometer might differ from the actual motion, or simply because there is no ergometer to replicate the motion on.

Third, research for sport analysis often deals with highly dynamic motions which are more difficult to capture than static or slow movements (e.g. gait analysis). High sample frequencies are a necessity in this case. For sport applications, typical sample frequencies are between 50-250 Hz (Table 2.2). It has the preference to prevent using too high sample frequencies to avoid excessive amounts of data and to avoid high frequency noise. Only in specific cases very high frequencies (>1000 Hz) are necessary, e.g. to study impact (such as jumping) or very high velocity movements (such as baseball pitching). Moreover, the system has to deal with motion dynamics, which, for instance, proves to be problematic in IMUs (inertial measurement units), where linear accelerations disturb gravity-based algorithms.

Fourth, the size and weight of the sensors are of importance when a measurement system

requires placement of sensors, markers, transponders, or tags directly on an athlete. Especially in high performance and high dynamic conditions, an athlete should be minimally hindered in her freedom of actions.

The aim of this paper is to assist researchers in the selection of a suitable motion capture system for their experimental setup for sport applications. For this purpose, a literature review was conducted on the available human motion capture systems used in peer-reviewed papers on sport analyses. This paper provides an overview of the found measurement systems and their specifications given by the manufacturer (weight and size of the sensors, maximum capture volume, environmental feasibilities), and reports the instrumental errors (accuracy) as determined in the peer-reviewed studies. Furthermore, the working principles of each of the systems are explained, as these determine the system limitations and characteristics. . Data processing, such as body pose reconstruction methods and filtering, falls outside of the scope of this survey. These results are made available via an open online platform, to enable (sport) researchers to contribute and update to the overview on measurement systems.

2. Method

We carried out a literature search between October 2012 and January 2013 and between December 2016 and February 2017. Both searches were performed in the databases of Scopus, Web of Science and Google Scholar using combinations of the keywords of the following three groups. Group 1: measure, analyze, system; Group 2: kinematic, motion, force, coordinate, rotation, orientation, location, position, velocity, speed, acceleration; Group 3: sport, skating, cycling, football, track, field, running, tennis, swimming, hockey, baseball, basketball, skiing and rowing. The search was limited to papers in the English language and published in peer-reviewed journals or conference proceedings. Additional literature was obtained through the reference lists of selected papers.

The abstracts of the retrieved papers were read to verify whether a human motion capture system was used in the work. We focused on papers sportsthat use measurement systems in a sport experimental setting. If this was not the case, the paper was excluded from further investigation. The remaining papers were read to obtain information about the accuracy of the measurement system and the context for which this accuracy was determined (environmental conditions, test set-up, type of motion and error definition). If the paper did not include an accuracy evaluation in the experimental context, we tried to retrieve this information from studies referenced by the paper. This information was then included, although not always determined in a sport context, and therefore marked in the results section. If no peer-reviewed papers were found on the accuracy, the paper and system were left out of further evaluation.

The accuracy of a system was set to be the 95th percentile (P_{95}) of the measurement error:

$$P_{95} = \mu + 2\sigma \quad (2.1)$$

In which μ is the reported mean (RMSE was used in case of absence of mean), and σ is the reported standard deviation. The range of a system was set to be the area (m^2) (global horizontal plane) of the measurement volume. We choose range instead of volume to obtain a general variable for both 2D and 3D systems.

3. Results

The literature study resulted in a total of twenty peer-reviewed studies on measurement accuracy, discussing 17 different human motion capture systems. The systems are listed in Table 2.1. This table provides the general specifications of the systems regarding environmental capabilities, weight, size and maximum volume as reported by the manufacturers. Table 2.2 lists the same systems with the corresponding published studies and the accuracy

Table 2.1 General Table : specifications of the manufacturers on the measurement systems. Given are the weight and size of the sensors and system, the type of sensor, and the maximum capture volume, number of markers, and sample frequency. The maximum capture volume is given for one camera or sensor; if a system is not restricted by the limitations of the number of sensors, this is indicated by '∞'. * indicates that the system was used in sport applications, but the accuracy was determined in a different context (found via reference list of paper).

system	environment		measure				marker			capture volume (1 camera)				maximum			sampling frequency			
	indoor	outdoor	position	velocity	acceleration	orientation	dimensions	weight	active	passive	markers	sensor	marker	tag	cameras	markers		sensors	tags	
Optoelectronic (OMS)																				
Optitrack 3020	3D	yes	x	-	x	x	-	x	<10 gr	x	-	-	-	infrared LED	-	8	512	-	-	3500 / (number of markers * 1 Hz)
Vicon i60 (datastation)	3D	yes	x	x	x	x	-	x	3 * 25 mm	<10 gr	x	-	-	reflective	-	6	8	-	-	2000 fps
Vicon T40	3D	no	x	x	x	x	-	x	3 * 25 mm	<10 gr	x	-	-	reflective	-	10	8	-	-	2000 fps
Vicon MX 13 & MX40 (cameras)	3D	no	x	x	x	x	-	x	3 * 25 mm	<10 gr	x	-	-	reflective	-	>24	8	-	-	2000 fps
IGFS	3D	yes	x	x	x	x	-	x	several sizes, starting at 80x20x20 mm	>30 gr	x	-	-	probe	-	8	-	8	-	50 Hz
Electromagnetic (EMS)																				
WASP	2D	yes	x	x	x	x	-	-	90x50x25 mm	?	x	-	x	-	x	-	8	-	8	125 Hz
LPM	2D	-	x	x	x	x	-	-	9,2 x 5,7 x 1,5 cm	60g	x	-	x	-	x	-	8	-	8	1000 Hz
Rfid carpet	2D	-	x	-	x	x	-	x	8,5 x 5,5 cm	-	-	x	-	x	-	8	-	8	-	dependent on reader
RTK GNSS (Javad Alpha G3T)	3D	no	-	x	x	x	-	-	148x85x35 mm	430 g	x	-	x	-	x	-	8	-	8	50 Hz
Ubisense Series 700 IP	3D	yes	x	x(?)	x	x	-	-	40x40x10 mm	x	-	-	x	-	x	-	8	-	8	10 Hz
Image processing (IPS)																				
panning camera, custom tracking algorithm	3D	no	x	-	x	x	-	-	-	-	-	-	-	-	-	camera dependent	1	-	-	?
color cameras combined with custom tracking algorithm	3D	no	x	-	x	x	-	x	-	-	-	-	-	-	-	camera dependent	1	-	-	200 fps
Kinect	3D	yes	x	-	x	x	-	x	-	-	-	-	-	-	-	1,8 x 2,8 m	1	-	-	30 fps
Lablacs	3D	-	x	-	x	x	-	x	-	-	x	-	-	-	LED	-	2	12	-	100 Hz
Ultrasonic (UWS)																				
WSN	3D	no	x	x	x	x	-	-	-	-	x	-	-	-	-	-	-	-	-	-
Inertial (IMs)																				
Fusion (FMS)																				
GPS, single frequency (u-box AB4) + MEMS IMU (Xsens Mt)	3D	no	-	x	x	x	x	x	50x56x32 mm (IMU) + 12,2x46x2,4 mm (u-box)	75	-	-	-	-	-	-	-	8	-	GPS: 1Hz, MEMS-IMU (100Hz)
Rolling Motion Capture system: SimiMotion 2.0 (Basler A602f)	3D	no	x	x	x	x	x	x	3 * 25 mm	<10 gr	-	x	-	reflective	-	system rolls along	depending on system	-	-	30 Hz

specifications. The accuracy specifications include the number of cameras, number of markers, sample frequency, reference system, motion, statistical value, measurement volume or range, and the reported accuracy. These results are processed in the online, interactive selection tool. In Figure 2.2, the accuracies are plotted against the range of the experimental setup. As expected, the accuracy of the systems (eq. 2.1) is inversely proportional to the coverage of a positioning system; in other words, a lower accuracy for a larger measurement volume.

The specifications in terms of the practical and technological difficulties associated with the types of measurement systems are highly dependent on their physical working principles. In human motion capture we distinguished five working principles: optoelectronic measurement systems (OMS), electromagnetic measurement systems (EMS), image processing systems (IMS), ultrasonic localization systems (UMS), and inertial sensory systems (IMU) (van der Kruk, 2013b). Arranged by these working principles, the measurement systems are explained in the next sections. The general pros and cons of each of the working principles are summarized in Figure 2.1.

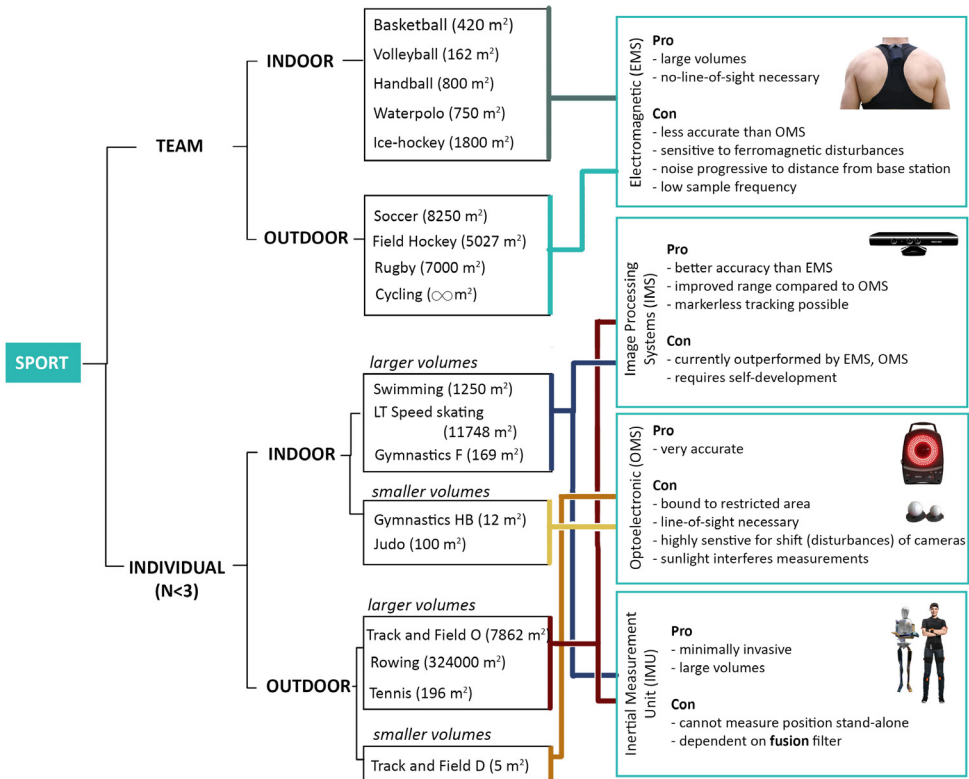


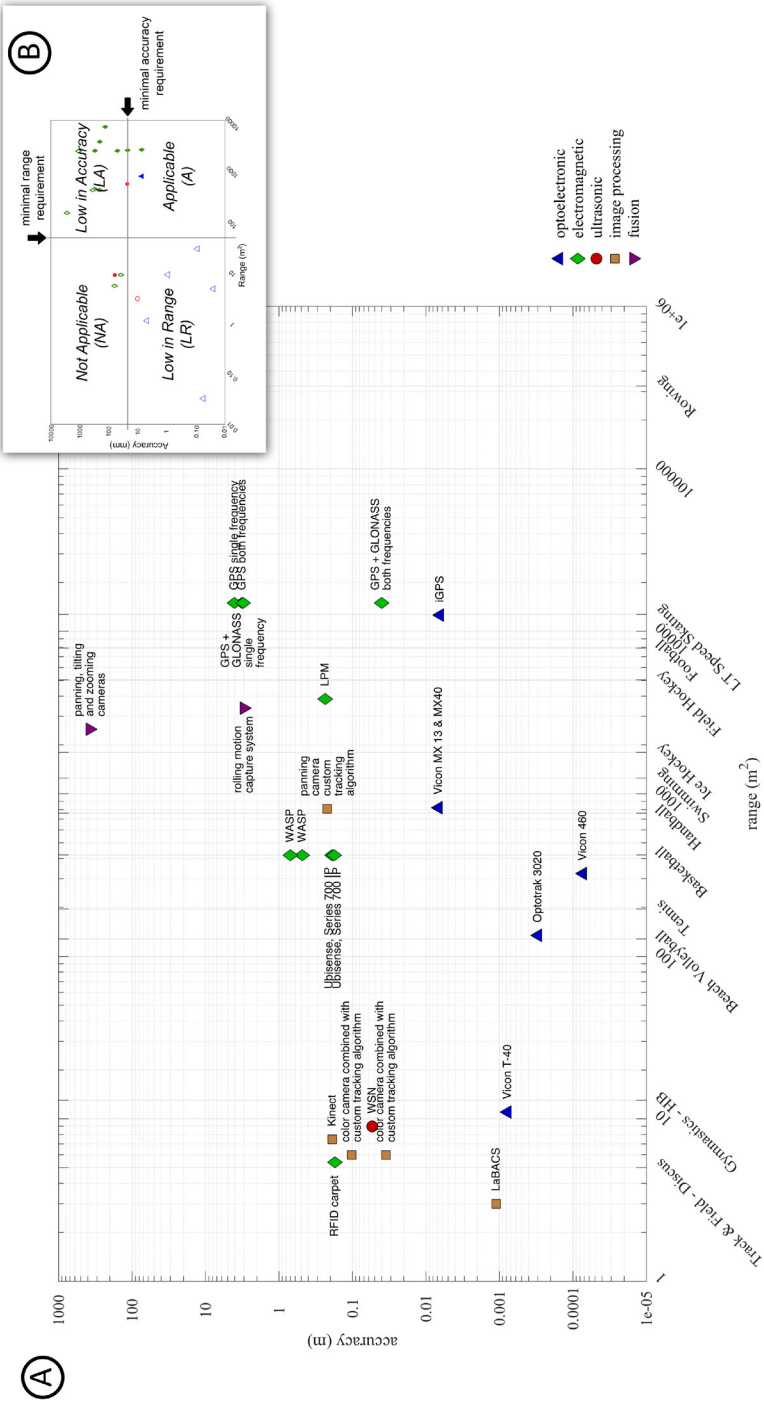
Figure 2.1 Sport categories with the most plausible measurement system categories. A division is made between team sports (more than three players), and individual sports. Team sports primarily involve large measurement volumes and occlusions. Since team sports are mainly concerned with tracking, the accuracy is less important than for individual sports, where technique factors are commonly analysed. The individual sports are apart from indoor vs outdoor, also divided into larger and smaller volume sports. Smaller volumes are covered by the highly accurate optoelectronic measurement systems. The individual sports in larger volumes are currently the most critical in terms of measuring kinematics. The most suitable options are IMS and IMU (fusion) systems. Gymnastics HB = High Bar, Gymnastics F = Floor, Track and Field R = Rink, Track and Field D = Discus;

Table 2.2 Accuracy Table: measurement systems and their accuracy in a certain range, as reported in peer-reviewed articles (column 2). The specifications of the experiment set-up are given in column 3–7. The last two columns (12–13) report the range and accuracy that are adopted in the chart of figure 1; chosen for this purpose was the maximum reported range (column 9), with the accuracy at 95% confidence interval (P95) (column 10). If the reported statistical values (column 8)) did not permit the estimation of the P95, this is indicated as a comment in column 11. Note that the maximum range in the peer-reviewed articles is not the maximum capture volumes of a system (for this see the general table (table 1)).

Optoelectronic (OMs)										comments	Range (m ²)	Accuracy (m)
study	system	cameras	markers	sampling freq	reference	movement	statistical value	range/volume/area [m]	reported accuracy			
Majumdar et al. (2006) ^{1, 2}	Optotrak 3020	3 (one unit)	246 (on each RGB)	30 Hz	machine's rotary table (resolution 0.005°) and linear slide and a sensor (reported resolution 0.006 mm)	static relative position between two rigid bodies	mean difference (SD)	range: 1.75, 2, 50, 3.25, 4.00, 4.75 m	Translation, in-plane 0.036 (0.109) mm, out-of-plane 0.017 (0.108) mm. Orientation, in-plane 0.151 (0.358) deg, out-of-plane 0.070 (0.393) deg	accuracy is of all data, 24 independent trials at each distance	13.5	0.000297
Winkel et al. (2009) ^{3, 2}	Vicon 460	4	4 (diameter 25 mm)	120 Hz	servo-motor-driven sliding carriage (reported accuracy 15 µm)	small translational movements (underwater)	RMSE (SD)	0.18x0.18x0.15 m	0.063 (0.095) mm		0.0324	0.000073
Monnet et al. (2014) ²	Vicon T-40	8	10	200 Hz	rigid bar	front crawl swimming (underwater)	RMSE	1.1x1x1 m	6.5 mm underwater, 0.77 mm in air	only RMSE	1.1	0.00077
Sgarbi et al. (2016) ¹⁰	Vicon MX 13 & MX40	24	51 (Plug-in-gait marker set + six and poles); 3 on magic wand	250 Hz	direct caliper measurements of rigid boot & magic wand	alpine skiing	mean difference (SD)	41.2x20 m	wand: 0.6 (0.4) mm fixed boot: 2.3 (2.2) mm (at 24.5 km/h)		824	0.0067
Van der Kuik 2013 ¹⁰	IGPS (Nikon)	8	2	30 Hz	Calibration Frame	Cycling on ice-rink (25 km/h)	mean(SD)	70mx180m	3.0 (1.7) mm	many gaps in the data in dynamic measurements	12600	0.0064
Electromagnetic (EMs)										comments	Range (m ²)	Accuracy (m)
study	system	cameras	markers	sampling freq	reference	movement	statistical value	range/volume/area [m]	reported accuracy			
Hadley et al. (2010) ¹⁷	WASP	12	2	10 Hz	distance between two tags attached to a piece of wood	quickly walking around	SD	28 x 15 m	0.24 m	Indoor basketball field, only SD	420	0.48
Sahyain et al. (2012) ²⁰	WASP	12	3	10 Hz	relative position between two tags fixed to a ruler attached to the upper back of each participant	run and sprint, straight and agility test course (length approx 28 m)	Cumulative density function	28 x 15 m	Indoor, linear, 0.7 m, 0.24 m, non-linear, 0.3 m, outdoor, linear, 0.25 m, outdoor non-linear, 0.45	accuracies are read from probability density graph at 95 %	420	0.7
Quares et al. (2012) ¹	LPM	12	1	45-45 Hz	Vicon (6 cameras, 24 x 36.5 m) (reported accuracy 10.9 mm)	small slides across game (2x2, 2x3 or 3x3)	RMSE	80 x 48 m	0.234 m (at 23 km/h)	only RMSE	3840	0.234
Shreejini et al. (2013) ^{18, 10}	RFD carpet	4	585	-	unknown	ten static positions with different orientations	mean error (SD)	3 x 1.8 m	position: 6.5 (5.4) cm, orientation: 0.96 (4.9) deg		5.4	0.173
Phadnis et al. (2014) ¹⁰	Ubisense, Series 700 IP	6	3	sensors: 137 tags: 16 Hz	position: laser total station (Leica TS-30, reported accuracy 0.004 m), velocity: wireless timing gates (Brower Timing Systems)	position: static, velocity: maximum sprint and multidirectional (wheelchair rugby) in indoor sports hall equipped with wooden sprung flooring	mean error (SD)	28 x 15 m	position: 0.19 m, velocity sprint: 4.00 (0.009) m/s, velocity multidirectional movements: 2.07 (0.13) m/s	system focuses more on measuring distance, velocity instead of position.	420	0.19
Pour et al. (2015) ¹¹	Ubisense, Series 700 IP	5	9	tags: (3x 16 Hz, 3x 8 Hz and 3x 4 Hz)	Leica TS-30 (reported accuracy 3 mm)	practice wheelchair rugby match	mean error (SD)	28 x 15 m	0.37 (0.24) m		420	0.1776
Gillman et al. (2016) ⁴	RTK, GNSS (Javad Alpha-GT)	3	-	50 Hz	GPS + Gnomas dual frequency at circular elevation angle of 10 deg (reported accuracy 0.075(0.025) m, based on photogrammetric reference system)	alpine skiing giant slalom	(see below)	300 x 50 m (estimated from figure)	(see below)	noted accuracy at 30 deg circular elevation angle		

	GPS + GONASS, both frequencies						mean error (SD)			0.02(0.01) m		15000	0.04
	GPS + GONASS, single frequency						mean error (SD)			0.09(2.22) m		15000	3.0636
	GPS, both frequencies						mean error (SD)			0.47(1.39) m		15000	3.17
	GPS, single frequency						mean error (SD)			0.70(1.67) m		15000	4.04
Image processing (IMS)													
Liu et al. (2009) ⁴⁰	panning camera, custom tracking algorithm	1	14				RMSE (SD)		static markers on short-track rink	short-track rink (45x18 m)	average of 14 markers (table 4 in Rosenblatt (2006))	810	0.22
Corazza et al. (2009) ⁴¹	color cameras combined with custom tracking algorithm	4	-	60 Hz	12 camera Vicon system (120 Hz), marker protocol proposed by manufacturer	walking	mean absolute error (SD)				data used from Humanive database	6	0.102
Corazza et al. (2009) ⁴¹	color cameras combined with custom tracking algorithm	8	-	120 Hz	8 camera Qualisys system (120 Hz), point cluster technique protocol	walking	mean absolute error (SD)				range estimated based on 'backwards gymnastic flip'	6	0.035
Datta (2012) ⁴²	Kinect	1	-	30 Hz	7 camera Vicon system (3 Mx 3 x 4 Mx 40 cameras, 100 Hz)	104 static positions of 10 cm large cubes	RMSE (SD)			range: 1.3-6 m, volume: 1.0-2.3 m ³ , precision: 1.0-3.06x240/71-2.13	x-direction: 0.0169 (0.0299) m, y-direction: 0.0348 (0.0765) m, z-direction: 0.0341 (0.0250) m	7.5	0.1878
Standic et al. (2013) ⁴³	LiRaCS	2	2	100 Hz	manipulator arm was rotated with precision servo motor controlled by AT MEGA 2560 microcontroller	single degree of freedom motion of rigid body with five increments of linear velocity from 0.5 to 2.5 m/s.	mean difference			not mentioned	0.23-1.1 mm (lowest - highest velocity)	3	0.0011
Kious et al. (2010) ³⁹	panning, tilting and zooming camera	5	25 mm squared markers (approx. 100 markers)	50 Hz	fixed measured distance of markers on ski pole	5 ski trials and 2 snowboard trials, slope inclination was uniformly 21 deg. One turn.	average difference (SD)			35x15 m	31 (3.3) mm	2500	0.0376
Ultrasonic (UMS)													
Bischoff et al. (2013) ⁴⁴	WSN	transmitter and 5 receivers	-		-	8 static positions	RMSE (SD)			3 x 3 m	fusion ultrasound + radio frequency	9	0.0535
Fusion (FMS)													
Wassell & Salsdon (2009) ³	GPS, single frequency (u-blox ALE4) + MEMS IMU (Xsens Mt)	GPS + 1 MEMS IMU	-	GPS: 1 Hz, MEMS-IMU (100 Hz)	GPS + GLONASS, dual frequency (Javad) and tactical grade IMU (LH200), reported accuracy 5 cm (roll, pitch) and 0.01 deg (heading).	six downhill skiing runs of approximately 1 min length performed by a professional skier	RMSE			400x450	accuracy read from graph, accuracy determined by manufacturer software, reduced the number of satellites on purpose to evaluate performance with IMU fusion	180000	0.65
Kersting et al. 2009 ¹⁶	Rolling Motion Capture system: SimiMotion 7.0 (Basler A602f) attached to moving frame	3	51	30 Hz	8-camera motion capture system Vicon MX	Rowing, nine elite level athletes in various boat categories were analysed during training and race pace	mean joint centre			4.5°x2.5 m	exact verification process is unclear, prior work shows research set up for gait (Bagot et al. 2009)	33.75	0.03

Figure 2.2 A) Chart on range versus accuracy as reported in peer-reviewed papers (see Table 2). Indicated are the ranges of several common sport fields. Note that the reported ranges are not the maximal ranges of a measurement systems (for this see Table 1J). B) Selection procedure for a suited measurement system. The graph can be divided into four quadrants, which are defined by the minimal measurement range and the minimal accuracy requirement of the research set-up in question. The upper left area now contains the systems that have a small range and low accuracy, we will refer to them as not applicable (NA). The lower right area is the area with measurement systems that meet the accuracy requirement, but do not have the required range; we refer to those systems as low in range (LR). The upper right area is the area with systems that meet the range requirement, but lack the accuracy requirement, referred to as low in accuracy (LA). It might be the case that there are no systems in the chart that meet the volume-accuracy requirements (A). Then it might be possible to combine systems from the LR or LA quadrant via sensor integration (James B. Lee, Ohgi, & James, 2012). Data from different measurement systems are then combined to determine one variable. A fusion motion capture system requires a fusion algorithm to combine the data of both measurement units (e.g. a Kalman filter or Comparative filter).



3.1 Optoelectronic measurement systems

The optoelectronic measurement systems (OMS) are more accurate than the other systems (see Figure 2.1). Not surprisingly, the optical systems (e.g. Optotrak or Vicon) are in literature often regarded as the gold standard in motion capture (Corazza, Mündermann, Gambaretto, Ferrigno, & Andriacchi, 2010). An OMS detects light and uses this detection to estimate the 3D position of a marker via time-of-flight triangulation. Accuracy of the systems is dependent on the following parts of the experimental set-up: the locations of the cameras relative to each other, the distance between the cameras and the markers, the position, number, and type of the markers in the field, and the motion of the markers within the capture volume (Maletsky, Sun, & Morton, 2007). Also, there is a trade-off between camera resolution and sample frequency.

OMS are based on fixed cameras and can therefore acquire data only in a restricted area (Begon et al., 2009). The capture volume is dependent on the maximum number of cameras and the field of view of each camera. The largest measured range with OMS is 824 m², described in Spörri et al. (2016), obtained with a Vicon MX13 measurement system (Spörri, Schieffmüller, & Müller, 2016). For this range, 24 cameras were required. This number of cameras results in significant practical difficulties regarding cost, portability, calibration, synchronization, labor, and set-up. Further limitations of the system are the necessity of a line-of-sight, which means that the data output will be interrupted when the cameras lose sight of the markers (Panjkota, Stancic, & Supuk, 2009; Spörri et al., 2016). Furthermore, the systems are highly sensitive to alterations in the setup, e.g. due to accidental shifting of a camera (Windolf, Götzen, & Morlock, 2008). The systems are mostly used in dark areas (indoors), because bright sunlight interferes with the measurements (Spörri et al., 2016).

There are two categories within the optoelectronic systems: active marker systems and passive marker systems. Passive systems use markers that reflect light back to the sensor. The Vicon systems (460, T-40, MX13 and MX40) in the chart (Figure 2.1) are examples of passive motion capture systems. Active systems utilize markers that contain the source of light for the sensors (often infrared) (Richards, 1999). In the chart, Optotrak 3020 is an active marker optical system. The benefit of active markers over passive ones is that the measurements are more robust. However, active markers do require additional cables and batteries, so the freedom of movement is more limited (Stancic, Supuk, & Panjkota, 2013). In addition, the maximum sample frequency is lowered when multiple markers are used as the signal of each individual marker needs to have distinguishable frequency by which it can be identified.

A rather original way of increasing the range of a marker-based optoelectronic measurement system is the rolling motion capture system (Begon et al., 2009; Colloud, Chèze, André, & Bahuau, 2008). With this method, cameras are placed on a fixed moving frame, to meet the requirement of fixed relative positions between the cameras. The method was applied in a 3D kinematic analysis of rowing, with a three-camera-recording-system mounted on a boat, which stayed next to the rowers (Kersting, Kurpiers, Darlow, & Nolte, 2008); this study showed an accuracy of about 30 mm in mean joint centres. Kersting et al. concluded, however, that the method is very time consuming - mainly due to calibration- and not suitable for general training purposes.

Indoor GPS (iGPS) is a OMS that is not based on markers, but on receivers that are attached to the tracked object or participant (Nikon, 2017). In contrast to what the name may indicate, the (physical) working principle is entirely different from a regular GPS system: the system has a transmitter which uses laser and infrared light to transmit position information from the transmitter to the receiver (Nikon, 2017). This is a one-way procedure. The advantage of this system is that there is practically no limit to the scalability of the system. Therefore it is possible to add as many transmitters as needed to cover a (factory) wide area and an unlimited number of receivers can be used (Khouri & Kamat, 2009). The accuracy of the system, determined on an indoor ice rink (12600 m²), was 6.4 mm (van der Kruk, 2013a). Important drawbacks for the application of this system in sport, are the size and weight of the receivers that need to be attached to the athlete (see Table 2.1).

3.2 Electromagnetic measurement systems

Electromagnetic systems (EMS) find the unknown positions of the measurement transponders by means of time-of-flight of the electromagnetic waves - radio waves - travelling from the transponder to the base stations (Stelzer, 2004). EMS provide large capture volumes (see Figure 2.1), but are less accurate than OMS: each EMS in the chart has a lower accuracy than the worst performing optoelectronic system. Unlike an OMS, no line-of-sight is necessary to find the positions of the transponders; also the human body is transparent for the field applied (Schepers & Veltink, 2010). Limitations of the system are the sensitivity for ferromagnetic material in the environment, which decrease the accuracy of the data (Day, Dumas, & Murdoch, 1998); moreover, when the distance between the base station and the transponder is increased, noise increases and the quality of the signal decreases (Day et al., 1998; Schuler, Bey, Shearn, & Butler, 2005). Furthermore, EMS often have a low sample frequency, which, as discussed in the introduction, is a drawback for sport analysis. The frequencies are lowered when using multiple markers.

Of the EMS systems, the GPS-GLONASS dual frequency system (one of the GNSS systems) shows a promising range-accuracy combination: 0.04m accuracy in a range of 15000 m². GNSS are satellite navigation systems of which GPS, GLONASS and GALILEO are examples. Satellites transmit data containing information on the location of the satellite and the global time. Since all satellites have a different position, the time it takes for the data to reach the receiver is different, which gives the option of determining the distance of the satellites. If the receiver gets the information from four satellites, the position in 3D can be estimated, although height information is determined 2 to 3 times worse than horizontal displacement (Berber, Ustun, & Yetkin, 2012). Note that in the graph, all GNSS systems are differential GNSS systems, which have an additional GNSS receiver as static base station within 5 km of the test site. The measurement of the satellite signals of the base station can be combined with the measurements of the mobile GNSS to increase accuracy.

Drawback of GNSS systems are the limitations associated with the cost, weight, and dimensions of the GNSS receivers and antenna. The GNSS system cannot be used indoors and is also sensitive to occlusions and the weather outside (a clear sky is necessary). The accuracy of a GNSS system is dependent on its specifications; for example, (low cost) single frequency GNSS units are of substantially lower accuracy (up to 4 m) than high cost dual frequency units (up to 0.04 m), especially under poor conditions (Duffield, Reid, Baker, & Spratford, 2010; Tan, Wilson, & Lowe, 2008). The high-end dual frequency units are however more bulky.

Contrary to GNSS, all other EMS systems can be used indoors, since they utilize local base stations instead of satellite signals. LPM (Local Position Measurement) consists of base stations, positioned throughout the area, and transponders, worn by the subjects. The main base station first sends a trigger to each transponder, whereupon each transmitter sends tagged electromagnetic waves to all other base stations. The same as for GNSS, at least four base stations need to receive a signal to determine the 3D position of the transponder via time-of-flight. The system functions both indoors and outdoors. The accuracy of the system presented in the chart is 0.23 m for a dynamic situation (23 km/h) in an area of 3840 m².

Comparable to the working principle of LPM, but less accurate, is the WASP system (Wireless Ad-hoc System for Positioning); WASP uses tags and anchor nodes, placed at fixed positions, to track participants in 2D. The accuracy that can be achieved is dependent upon the venue, varying from 0.25m in indoor sporting venues to a couple of meters when operating through multiple walls (Hedley et al., 2010). In sport studies, accuracies between 0.48-0.7 m were found at an indoor basketball field (420 m²) (Hedley, Sathyan, & MacKintosh, 2011; Sathyan, Shuttleworth, Hedley, & Davids, 2012). The accuracy is also limited by the bandwidth of the transmitted radio signal.

RFID is a wireless non-contact system which uses electromagnetic waves and electromagnetic fields to transfer data from a tag attached to an object, to the RFID reader. There are two sort of tags: active tags, which actively emit radio waves, and passive tags, which can be read only

over short ranges since they are powered and read via magnetic fields (induction). Passive tags practically have no lifetime, since they do not require any power from batteries (Shirehjini, Yassine, & Shirmohammadi, 2012). The RFID carpet of Shirehjini et al. (2012) consists of passive tags and reported accuracies of 0.17 m in a 5.4 m² area (Shirehjini et al., 2012). Ubisense is a commercially available system, originally designed for enterprises to track assets and personnel, that uses the active RFID technology. In sports, the system was tested at an indoor basketball field (420 m²), reporting an accuracy of 0.19 m (Perrat, Smith, Mason, Rhodes, & Goosey-Tolfrey, 2015; Rhodes, Mason, Perrat, Smith, & Goosey-Tolfrey, 2014).

Factors such as attenuation, cross paths of signals and interference from other RFID tags, RFID readers, and different Radio Frequency devices can affect the communication between the tags and RFID readers (Ting, Kwok, Tsang, & Ho, 2011).

3.3 Image Processing systems

Image processing systems (IMS) generally have better accuracy compared to the EMS, and an improved range when compared to the OMS. In image processing captured films or photos are digitally analyzed. Oppositely to the other measurement methods which are sensor-based, this method is vision-based, using optical cameras and computer vision algorithms. This marker-less tracking can be a big advantage in sports, such as for event-detection (Zhong & Chang, 2004). Image processing also has some drawbacks: it is not easy to perform image recognition in real-time, it might require expensive high quality and/or high speed cameras. The accuracy is also dependent on the experimental set-up, namely the position of the camera in relation to the object trajectory, and the number of cameras. (Lluna, Santiago, Defez, Dunai, & Peris-Fajarnes, 2011). Furthermore, generally, an increase in camera resolution results in a decrease in feasible maximum sampling frequencies.

Vision based systems can be divided into two categories: Model-based tracking and feature-based tracking. Model-based tracking uses a 3D model of the tracked object. In the basic concept of the model-based tracking, the pose information is updated in each video frame, first by using a dynamic model via a prediction filter and then by measurements in the video frame. A drawback of model-based tracking systems is that they are hard to use in unknown environments and restrict camera motion, due to the necessity of additional information such as 3D models of participants and environment (Bader, 2011; Ceseracciu et al., 2011).

Feature-based tracking algorithms use interest points in the frames to track the object. There are two kind of feature-based tracking algorithms: marker tracking, which uses known-markers, and marker-less tracking, which focuses on tracking 2D features such as corners, edges or texture (Akman, 2012). Note that the marker tracking in IMS differs from OMS, because IMS uses (for humans) visible light, whereas OMS works with infrared light.

For marker tracking, known-markers are used to track the object. This is usually more accurate than to detect natural features (e.g. existing corners or edges), however the markers must be put precisely in place before the experiment (grid set-up) and occlusion of markers may occur. In sports, marker-based feature tracking has been applied in the collection of kinematic data on a ski and snowboard track, where an accuracy of 0.04m was obtained in a 2500 m² range (Klous, Müller, & Schwameder, 2010).

Marker-less tracking eliminates the dependency on prior knowledge about the environment and extends the operation range. This natural tracking is a hot topic in, for instance, robot vision and augmented reality. However, in those applications, the cameras are actually attached to the object that is being tracked, in contrast to the sports application, where, up-to-know, the camera is static, while panning, tilting, and/or zooming (Liu, Tang, Cheng, Huang, & Liu, 2009). Liu et al. (2009) mounted a panning camera to the ceiling to track short-track speed skaters during a match, using a color-histogram of the skaters; they obtained an accuracy of 0.23 m (area 810 m²).

The KinectTM sensor – which was originally designed to allow users to interact with a gaming system without the need of a traditional handheld controller – can also be classified as a

marker-less tracking device, although the working principle is slightly different from what was previously described. The system projects an infrared laser speckle pattern onto the viewing area of the infrared camera. This infrared camera detects the pattern and enables the creation of a 3-D map by measuring deformations in the reference speckle pattern. Due to its low-costs and reasonable accuracy (0.19 m at 7.5 m² (Dutta, 2012)), the device is often used in scientific research (Bonnechere et al., 2014; Choppin, Lane, & Wheat, 2014; Dutta, 2012). The drawback of the Kinect camera is the small field of view; furthermore, the system struggles with the detection of dark surfaces that absorb light, shiny surfaces that result in specular reflection and rough surfaces if the angle of incidence of incoming light is too large (Dutta, 2012).

At present, available computer-vision-based measurement systems are outperformed by either optoelectronic or electromagnetic measurement systems and their maximal range is small. Although no mature system exists at the present (July 2017), a large number of open source codes are available and progress is rapid (Scaramuzza & Fraundorfer, 2011). Open-source databases with human kinematic data are provided to enable developers to verify their algorithms (HumanEva, 2017). This not only enables the verification of the developed systems, but also eases the comparison between systems for researchers developing their study setup.

3.4 Ultrasonic localization systems

Ultrasonic localization systems (UMS) are most commonly used in short-range measurements. UMS determine the position of an object by means of Time-of-Flight of an ultrasound wave travelling through the air. These systems are also called acoustic measurement systems, because the system functions by means of sound waves. The difference between sound and ultrasound is that ultrasound is stealthy for the human ear. This is, of course, beneficial in research. A drawback of ultrasound is that the range is limited compared to sound. Also, the directionality of ultrasound can be a disadvantage when working with dynamic measurements. In the chart (Figure 2.2), one system is included, which is based on ultrasonic localization in sports, with an accuracy of 0.05 m in an area of 9 m² (Bischoff, Heidmann, Rust, & Paul, 2012). Note, however, that this result was obtained via a fusion with a radio frequency transceiver.

3.5 Inertial sensor measurement systems

An inertial measurement unit (IMU) is a device consisting of an accelerometer, gyroscope, and often a magnetometer. By combining the information from the accelerometer – gravitational force – with the data from the gyroscope – rotational velocity –, the orientation of the device can be determined (M Brodie, Walmsley, & Page, 2008). The magnetometer is used to track the magnetic-north, to determine the heading of the IMU. There are many commercially available IMUs on the market.

As stand-alone system, the device cannot determine its (global) position, and is therefore not added to the chart. In principle, the accelerometer could be used to determine position by performing a double integration; however, the data will suffer from large integration drifts. When, however, the systems are placed on body segments, the orientation of these segments are determined, and the position in global space can be estimated with a rigid-body model of a human (Neuron, 2017; Xsens, 2017). IMUs do not have a base station and are therefore the most mobile of all available measurement systems. Additionally, the system is capable of detecting very rapid motion (Zohlandt, Walk, & Nawara, 2012) and is non-invasive for the user, which makes it an attractive system in sports (e.g. gymnastics (Zohlandt et al., 2012), swimming (James Bruce Lee, Burkett, Thiel, & James, 2011)). A drawback is that the system is susceptible to measurement errors due to nearby metal (experimental set-up). Moreover, the gravity-based algorithms are sensitive to linear acceleration.

IMU systems cannot be used for global position measurements as a stand-alone system (only orientation accuracy (M Brodie et al., 2008)); however, the systems do appear in the table as fusion motion capture systems (more on this in the next section).

4. Discussion & Conclusion: system selection

Choosing the right motion capture system for sport experiments can be difficult. Figure 2.2 is designed to support researchers in this choice. The selection procedure is explained in the caption of Figure 2.2, and also available online via an interactive selection tool.

Based on the results of this survey, we defined some broad sport categories, which require roughly the same characteristics in a measurement system (Figure 2.1). A division is made between team sports and individual sports. In team sports, systems are typically used for position, distance, velocity, and acceleration tracking of players, whereas individual sports usually involve some sort of technique analysis. Team sports primarily involve large measurement volumes, and occlusions are common. Accuracy is for these tracking applications not as important as for technique analysis. Therefore, EMS are the most suitable. The individual sports are apart from indoor versus outdoor, also divided into larger and smaller volume sports. Individual sports typically require higher accuracies. Smaller volumes can be covered by the highly accurate OMS. Individual sports in larger volumes are currently the most critical in terms of measuring kinematics. The most suitable options are IMS and IMU (fusion) systems, however these measurement categories often require development of a suitable algorithm (either for tracking in case of IMS, or fusion filtering in case of IMU). Therefore, overall we can conclude that there is a gap in measurement system supply for capturing large volumes at high accuracy (Figure 2.2). These specifications are mainly necessary for large volume individual sports, both indoor (among others swimming, speed skating, gymnastics), and outdoor (among others rowing, tennis, track and field).

The (online) selection tool enables researchers to make a faster and better informed selection for a measurement system suited to their experimental setup. Instrumental errors are dependent on the context of the study (section 2.2). Therefore, we encourage researchers to always perform and report a calibration procedure prior to their experiment (system, number of cameras, markers, sampling frequency, calibration procedure, statistical value (e.g. SD, mean, RMSE), range/volume, and accuracy). Furthermore, we invite researchers to add to the here presented chart (Figure 2.2) and system overview online.

Acknowledgements

We want to thank dr. Dimitra Dodou for proof reading our work. This study was supported by NWO-STW 12870.

References

- Akman, O. (2012). *Robust augmented reality*. TU Delft, Delft University of Technology.
- Bader, J. (2011). *Validation of a dynamic calibration method for video supported movement analysis*. Unpublished Master's Thesis). Technische Universitat, Munchen.
- Begon, M., Colloud, F., Fohanno, V., Bahuaud, P., & Monnet, T. (2009). Computation of the 3D kinematics in a global frame over a 40 m-long pathway using a rolling motion analysis system. *Journal of Biomechanics*, 42(16), 2649–2653. <http://doi.org/10.1016/j.jbiomech.2009.08.020>
- Berber, M., Ustun, A., & Yetkin, M. (2012). Comparison of accuracy of GPS techniques. *Measurement: Journal of the International Measurement Confederation*, 45(7), 1742–1746. <http://doi.org/10.1016/j.measurement.2012.04.010>
- Bischoff, O., Heidmann, N., Rust, J., & Paul, S. (2012). Design and implementation of an ultrasonic localization system for wireless sensor networks using angle-of-arrival and distance measurement. *Procedia Engineering*, 47, 953–956. <http://doi.org/10.1016/j.proeng.2012.09.304>

Bonnechere, B., Jansen, B., Salvia, P., Bouzahouene, H., Omelina, L., Moiseev, F., ... Jan, S. V. S. (2014). Validity and reliability of the Kinect within functional assessment activities: comparison with standard stereophotogrammetry. *Gait & Posture*, 39(1), 593–598.

Brodie, M., Walmsley, A., & Page, W. (2008). Dynamic accuracy of inertial measurement units during simple pendulum motion: Technical Note. *Computer Methods in Biomechanics and Biomedical Engineering*, 11(3), 235–242.

Brodie, M., Walmsley, A., & Page, W. (2008). Fusion motion capture : a prototype system using inertial measurement units and GPS for the biomechanical analysis of ski racing Research Article. *Sports Technology*, 1(1), 17–28. <http://doi.org/10.1002/jst.6>

Ceseracciu, E., Sawacha, Z., Fantozzi, S., Cortesi, M., Gatta, G., Corazza, S., & Cobelli, C. (2011). Markerless analysis of front crawl swimming. *Journal of Biomechanics*, 44(12), 2236–2242. <http://doi.org/10.1016/j.jbiomech.2011.06.003>

Choppin, S., Lane, B., & Wheat, J. (2014). The accuracy of the Microsoft Kinect in joint angle measurement. *Sports Technology*, 7(1–2), 98–105.

Colloud, F., Chèze, L., André, N., & Bahuaud, P. (2008). An innovative solution for 3d kinematics measurement for large volumes. *Journal of Biomechanics*, 41, S57.

Corazza, S., Mündermann, L., Gambaretto, E., Ferrigno, G., & Andriacchi, T. P. (2010). Markerless motion capture through visual hull, articulated icp and subject specific model generation. *International Journal of Computer Vision*, 87(1), 156–169.

Day, J. S., Dumas, G. a., & Murdoch, D. J. (1998). Evaluation of a long-range transmitter for use with a magnetic tracking device in motion analysis. *Journal of Biomechanics*, 31(10), 957–961. [http://doi.org/10.1016/S0021-9290\(98\)00089-X](http://doi.org/10.1016/S0021-9290(98)00089-X)

Duffield, R., Reid, M., Baker, J., & Spratford, W. (2010). Accuracy and reliability of GPS devices for measurement of movement patterns in confined spaces for court-based sports. *Journal of Science and Medicine in Sport*, 13(5), 523–525.

Dutta, T. (2012). Evaluation of the Kinect??? sensor for 3-D kinematic measurement in the workplace. *Applied Ergonomics*, 43(4), 645–649. <http://doi.org/10.1016/j.apergo.2011.09.011>

Gilgien, M., Spörri, J., Limpach, P., Geiger, A., & Müller, E. (2014). The effect of different Global Navigation Satellite System methods on positioning accuracy in elite alpine skiing. *Sensors*, 14(10), 18433–18453.

Hedley, M., Mackintosh, C., Shuttleworth, R., Humphrey, D., Sathyan, T., & Ho, P. (2010). Wireless tracking system for sports training indoors and outdoors. *Procedia Engineering*, 2(2), 2999–3004. <http://doi.org/10.1016/j.proeng.2010.04.101>

Hedley, M., Sathyan, T., & MacKintosh, C. (2011). Improved wireless tracking for indoor sports. *Procedia Engineering*, 13, 439–444. <http://doi.org/10.1016/j.proeng.2011.05.111>
HumanEva. (2017). HumanEva.

Kersting, U. G., Kurpiers, N., Darlow, B. J. S., & Nolte, V. W. (2008). Three-dimensional assessment of on water rowing technique: a methodological study. In *ISBS-Conference Proceedings Archive (Vol. 1)*.

Khoury, H. M., & Kamat, V. R. (2009). Evaluation of position tracking technologies for user localization in indoor construction environments. *Automation in Construction*. <http://doi.org/10.1016/j.autcon.2008.10.011>

Klous, M., Müller, E., & Schwameder, H. (2010). Collecting kinematic data on a ski/snowboard track with panning, tilting, and zooming cameras: is there sufficient accuracy for a biomechanical analysis? *Journal of Sports Sciences*, 28(12), 1345–1353. <http://doi.org/10.1080/02640414.2010.507253>

Lee, J. B., Burkett, B. J., Thiel, D. V., & James, D. A. (2011). Inertial sensor, 3D and 2D assessment of stroke phases in freestyle swimming. *Procedia Engineering*, 13, 148–153.

Lee, J. B., Ohgi, Y., & James, D. a. (2012). Sensor fusion: Let's enhance the performance of performance enhancement. *Procedia Engineering*. <http://doi.org/10.1016/j.proeng.2012.04.136>

Liu, G., Tang, X., Cheng, H. D., Huang, J., & Liu, J. (2009). A novel approach for tracking high speed skaters in sports using a panning camera. *Pattern Recognition*, 42(11), 2922–2935. <http://doi.org/10.1016/j.patcog.2009.03.022>

Lluna, E., Santiago, V., Defez, B., Dunai, L., & Peris-Fajarnes, G. (2011). Velocity vector (3D) measurement for spherical objects using an electro-optical device. *Measurement: Journal of the International Measurement Confederation*, 44(9), 1723–1729. <http://doi.org/10.1016/j.measurement.2011.07.006>

Maletsky, L. P., Sun, J., & Morton, N. a. (2007). Accuracy of an optical active-marker system to track the relative motion of rigid bodies. *Journal of Biomechanics*, 40(3), 682–685. <http://doi.org/10.1016/j.jbiomech.2006.01.017>

Monnet, T., Samson, M., Bernard, A., David, L., & Lacouture, P. (2014). Measurement of three-dimensional hand kinematics during swimming with a motion capture system: a feasibility study. *Sports Engineering*, 3(17), 171–181.

Neuron, P. (2017). <https://neuronmocap.com/>.

Nikon. (2017). <https://www.nikonmetrology.com/en-gb/product/igps>.

Ogris, G., Leser, R., Horsak, B., Kornfeind, P., Heller, M., & Baca, A. (2012). Accuracy of the LPM tracking system considering dynamic position changes. *Journal of Sports Sciences*, 30(14), 1503–1511.

Panjkota, A., Stancic, I., & Supuk, T. (2009). Outline of a qualitative analysis for the human motion in case of ergometer rowing. In *WSEAS International Conference. Proceedings. Mathematics and Computers in Science and Engineering*. WSEAS.

Perrat, B., Smith, M. J., Mason, B. S., Rhodes, J. M., & Goosey-Tolfrey, V. L. (2015). Quality assessment of an Ultra-Wide Band positioning system for indoor wheelchair court sports. *Proceedings of the Institution of Mechanical Engineers, Part P: Journal of Sports Engineering and Technology*, 229(2), 81–91.

Rhodes, J., Mason, B., Perrat, B., Smith, M., & Goosey-Tolfrey, V. (2014). The validity and reliability of a novel indoor player tracking system for use within wheelchair court sports. *Journal of Sports Sciences*, 32(17), 1639–1647.

Richards, J. G. (1999). *The measurement of human motion: A comparison of commercially available systems*. *Human Movement Science*, 18(5), 589–602. [http://doi.org/10.1016/S0167-9457\(99\)00023-8](http://doi.org/10.1016/S0167-9457(99)00023-8)

Sathyan, T., Shuttleworth, R., Hedley, M., & Davids, K. (2012). *Validity and reliability of a radio positioning system for tracking athletes in indoor and outdoor team sports*. *Behavior Research Methods*, 44(4), 1108–1114.

Scaramuzza, D., & Fraundorfer, F. (2011). *Visual odometry [tutorial]*. *IEEE Robotics & Automation Magazine*, 18(4), 80–92.

Schepers, H. M., & Veltink, P. H. (2010). *Stochastic magnetic measurement model for relative position and orientation estimation*. *Measurement Science and Technology*, 21(6), 65801. <http://doi.org/10.1088/0957-0233/21/6/065801>

Schuler, N. B., Bey, M. J., Shearn, J. T., & Butler, D. L. (2005). *Evaluation of an electromagnetic position tracking device for measuring in vivo, dynamic joint kinematics*. *Journal of Biomechanics*, 38(10), 2113–2117.

Shirehjini, A. A. N., Yassine, A., & Shirmohammadi, S. (2012). *An RFID-based position and orientation measurement system for mobile objects in intelligent environments*. *IEEE Transactions on Instrumentation and Measurement*, 61(6), 1664–1675. <http://doi.org/10.1109/TIM.2011.2181912>

Spörri, J., Schiefermüller, C., & Müller, E. (2016). *Collecting Kinematic Data on a Ski Track with Optoelectronic Stereophotogrammetry: A Methodological Study Assessing the Feasibility of Bringing the Biomechanics Lab to the Field*. *PloS One*, 11(8), e0161757.

Stancic, I., Supuk, T. G., & Panjkota, A. (2013). *Design, development and evaluation of optical motion-tracking system based on active white light markers*. *IET Science, Measurement & Technology*, 7(4), 206–214.

Stelzer, a. (2004). *Concept and application of LPM-a novel 3-D local position measurement system*. *IEEE Transactions on Microwave Theory and Techniques*, 52(12), 2664–2669. <http://doi.org/10.1109/TMTT.2004.838281>

Tan, H., Wilson, A. M., & Lowe, J. (2008). *Measurement of stride parameters using a wearable GPS and inertial measurement unit*. *Journal of Biomechanics*. <http://doi.org/10.1016/j.jbiomech.2008.02.021>

Ting, S. L., Kwok, S. K., Tsang, A. H. C., & Ho, G. T. S. (2011). *The Study on Using Passive RFID Tags for Indoor Positioning*. *International Journal of Engineering Business Management*, 3(1), 1. <http://doi.org/10.5772/45678>

van der Kruk, E. (2013a). *Modelling and Measuring 3D Movements of a Speed Skater*. TU Delft.

van der Kruk, E. (2013b). *Smooth Measuring; What measurement systems could serve the purpose of finding accurate kinematic data of skaters on an ice rink?*

Waegli, A., & Skalous, J. (2009). *Optimization of two GPS/MEMS-IMU integration strategies with application to sports*. *GPS Solutions*, 13(4), 315–326.

Windolf, M., Götzen, N., & Morlock, M. (2008). Systematic accuracy and precision analysis of video motion capturing systems-exemplified on the Vicon-460 system. *Journal of Biomechanics*, 41(12), 2776–2780. <http://doi.org/10.1016/j.jbiomech.2008.06.024>

Xsens. (2017). www.xsens.com.

Zhong, D., & Chang, S. F. (2004). Real-time view recognition and event detection for sports video. *Journal of Visual Communication and Image Representation*, 15(3), 330–347. <http://doi.org/10.1016/j.jvcir.2004.04.009>

Zohlandt, C., Walk, L., & Nawara, W. (2012). Classification of Vault Jumps in Gymnastics, 1–9.

3

Wireless instrumented klapskates for long-track speed skating.

'Ik heb het nog nooit gedaan, dus
ik denk dat ik het wel kan'
-Pippi Langkous-

Apart from measuring kinematic data (CH2), force measurements are a necessity for biomechanical research in speed skating. In human movement studies these are mostly measured with force plates; an ice rink however cannot be instrumented with this equipment, hence the need for an instrumented klapskate with integrated force sensors. This chapter describes the design and validation of the wireless instrumented klapskate, employed for the biomechanical measurements in chapters 4 to 8; it starts with an overview of the design, followed by the calibration procedure and the accuracy determination; subsequently the measured force data of eight Dutch elite speed skaters is presented.

van der Kruk, E., den Braver, O., Schwab, A. L., van der Helm, F. C. T., & Veeger, H. E. J. (2016). *Wireless instrumented klapskates for long-track speed skating*. Sports Engineering, 19(4), 273-281.

Abstract

In the current project we aim to provide speed skaters with real-time feedback on how to improve their skating performance within an individual stroke. The elite skaters and their coaches wish for a system that determines the mechanical power per stroke. The push-off force of the skater is a crucial variable in this power determination. In this study we present the construction and calibration of a pair of wireless instrumented klapskates that can continuously and synchronously measure this push-off force in both the lateral and normal direction of the skate and the centre of pressure of these forces. The skate consists of a newly designed rigid bridge (0.6 kg), embedding two three-dimensional force sensors (Kistler 9602, Kistler Group, Winterthur, Switzerland), which fits between most individual skate shoes and Maple skate blades. The instrumented klapskates were calibrated on a tensile testing machine, where they proved to be unaffected to temperature conditions and accurate up to a RMS of 42 N (SEM = 1 N) in normal and up to a RMS of 27 N (SEM = 1N) in lateral direction. Furthermore the centre of pressure of these forces on the blade was determined up to a mean error of 10.1 mm (SD = 6.9 mm). On-ice measurements showed the possibility of recording with both skates simultaneously and synchronously, straights as well as curves. The option to send data wirelessly and real-time to other devices makes it possible to eventually provide skaters and coaches with visual real-time feedback during practice.

1. Introduction

Force and power production are crucial factors in any performance sport. Insight in the force pattern produced by an athlete and the related relevant velocities, can help understand the technique and performance of that athlete. Ideally we would like to provide speed skaters with real-time feedback on their skating performance within an individual stroke. The Dutch elite skaters and their coaches would like to have access to a system that determines the power per stroke, which is a familiar variable for them from cycling practices. The push-off force of the skater is a crucial variable in this power determination (Van Ingen Schenau & Cavanagh, 1990). For power estimations the velocity of the skater and the orientation of the skate in the global frame are a necessity. Therefore, to fulfil the wish of the skaters, accurate measurement systems that can capture the kinetic and kinematic data of a skater, and preferably send it real-time to a device for feedback (e.g. phone, tablet, smart glasses), are essential. Since the accuracy of all these measurements are of utmost importance for the quality of the feedback, we will deal with these in separate studies. In this paper we present the construction and validation of a set of wireless instrumented klapskates that can measure the forces applied by the skater. The validation and measurements of the orientation of the skate, which will be performed with an IMU and self-designed filter, and the velocity of the skater are presented in a follow-up study.

Publication on instrumented skates started in the early nineties of the last century. At that time, speed skaters skated on the then conventional fixed skates, where the blade of the skate was fixed to the shoe. Two studies were published on instrumented fixed skates. The pioneers in this field aimed at measuring normal forces in speed skating on the straights and in a curve (Jos J de Koning, de Boer, de Groot, & van Ingen Schenau, 1987; Van Ingen Schenau, 1981). They constructed a right skate with three temperature compensated strain gauges that could measure in normal and longitudinal direction in a local coordinate system (Jobse, Schuurhof, Cserep, Schreurs, & Koning, 1990)(Figure 3.1). Their study on ice friction (J. J. De Koning, De Groot, & Van Ingen Schenau, 1992) measured the longitudinal forces on the blade and demonstrated that the maximal forces in longitudinal direction were 10 N, which is less than 1% of the force in normal direction. From these studies we conclude that measuring this small component of force is a technical challenge, while it is negligible relative to the total force.

Yuki et al. (1996) measured the normal and lateral forces in speed skating on the straight. For this study two sensor-skates were built, which consisted of strain gauges between the shoe and the blade. Their study aimed at measuring the horizontal (F_H , Figure 3.1) and vertical (F_V)

blade reaction forces for two different skating velocities, slow (9.1 m/s) and fast (11.5 m/s). Their study was the first to also report the centre of pressure of these static resultant forces on the skate blade (COP). Their results, based on one skilled skater ($n = 1$), indicated that the peak lateral forces were considerable, namely between the $f_L = 0.3\text{--}0.6$ BW (BW = body weight), which is equal to 25–45% of the peak normal force. Since the lateral force proved to be considerable, measuring this component seems inevitable when analysing speed skating forces. Furthermore a relationship was found between the performance of the speed skater and the COP. This makes the COP an esteemed variable for feedback.

In the mid-nineties, fixed skates were replaced by klapskates, which incorporate a hinge between the blade and the shoe. The first constructed instrumented klapskate measured forces in normal direction, thereby again neglecting the forces in lateral direction (Houdijk, de Koning, de Groot, Bobbert, & van Ingen Schenau, 2000). Not long after, Yuda et al. (2004) constructed a (left) instrumented klapskate that could measure in normal and lateral direction. The skate was equipped with two quartz voltage sensors which measured three components between the boot and the bridge of the skate. The data were logged on a computer carried on the skater's back. Their study reports on measurements in the curve with the left instrumented skate. Unfortunately no data on the calibration or accuracy of the force measurements were reported. Drawback of the design of this instrumented klapskate was the necessity for the skaters to carry a laptop to log the data (3.3 kg). Also, the sensors were placed between the skate shoe and the blade as a result of which every participant had to wear (and fit) the same (only left) skate shoe. In order to perform true measurements and preserve participation of many skaters, a skater needs to be able to wear his own skate shoe, and preferably blade, during measurements.

Three previous studies have described calibration procedures for instrumented skates in long track speed skating (J. J. De Koning et al., 1992; Jobse et al., 1990; Yuki et al., 1996). In all three studies, which use static calibration with weights, the accuracy determination focused on the crosstalk between the force directions rather than the accuracy of the force directions itself. Since also the relationship between the forward velocity (performance) and the measured forces had not completely been grasped yet, literature did not provide us with an adequate benchmark for the accuracy requirement for an instrumented skate. One study has been published on the construction and calibration of an instrumented ice hockey skate, which measured the forces in normal and lateral direction, with strain gauges, and reported on the calibration accuracies in the separate directions (Stidwill, Turcotte, Dixon, & Pearsall, 2010). Their skates were calibrated with an error of 68N in normal and 40N in lateral direction.

In this study we present the construction and calibration of a pair of instrumented klapskates that can continuously and synchronously measure both the lateral and normal forces in a local frame and the COP of these forces. The skate is designed to fit most individual skate shoes and Maple skate blades (Maple, 2015). Additionally the developed system can log data wirelessly and locally through a logger at the rear of the skate. In the design, the longitudinal force is neglected, since this is assumed to be less than 1% of the normal force. The skate is built to be part of the instrumentation to provide speed skaters with real-time feedback during practice on improving their performance within a single stroke.

2. Method

In this section first the design of the instrumented klapskates is described. Subsequently the calibration set-up, the calibration routine and calibration analyses are explained. The section closes with the description of the on-ice skating measurements.

2.1 Instrumented klapskates

The instrumented klapskate consists of a custom-made rigid aluminium bridge (mountable on Maple skates), with two three-dimensional piezoelectric force sensors with integrated

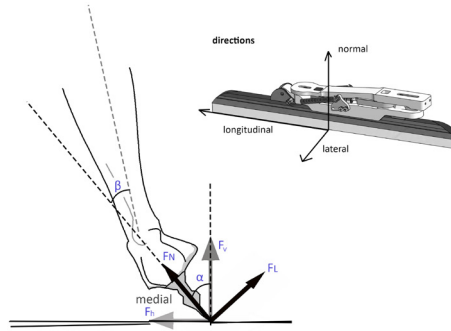


Figure 3.1 The normal force (F_N) and lateral force (F_L) are the forces measured in the local skate coordinate system (as in (Jos J de Koning et al., 1987; Houdijk et al., 2000; Jobse et al., 1990)). The forces F_v and F_h are the vertical and horizontal components (as in (Yuda et al., 2004; Yuki et al., 1996)) of the push-off forces F_N and F_L . α is the lean angle of the skate and describes the angle between the skate and the ice. β is the angle between the shank and the skate and describes the eversion of the ankle. Given is the rear view of the right skate, the force F_L is for both the right and the left skate negative in medial direction. The lean angle is positive while the blade is on the medial side.

electronics (Kistler 9602, Kistler Group, Winterthur, Switzerland) (Figure 3.2). Due to the design of the bridge, the sensors are not aligned with the bridge. The voltage output of the front (V_{fx} , V_{fy} , V_{fz}) and rear (V_{rx} , V_{ry} , V_{rz}) sensor are logged on a SD card and sent over Bluetooth via a data logger (Shimmer3, 2015). The logger is further equipped with an accelerometer, gyroscope and magnetometer (IMU) and logs temperature for temperature-compensation. The IMU will be used in future application for orientation measurements, these are however not discussed in this study. The force sensors are powered by rechargeable Li-Ion batteries. Synchronisation between the two skates is done over Bluetooth. To enable synchronisation with external measurement devices, a digital start-end pulse can be logged. The weight of the instrumented bridge and electronics is 600 g. The instrumented bridge replaces the normal bridge in a klapskate. It can be attached to any Maple blade via the hinge mechanism and any skate shoe can be placed on it. The instrumented bridge does not increase the height of the skate.

2.2 Calibration

The calibration of the instrumented skates was performed using a tensile testing machine (Zwick Z100, Zwick Roell, Ulm, Germany, principal accuracy 1N). The aim of the calibration was to calibrate the forces on the instrumented skates in normal and lateral direction and the centre of pressure of these resultant forces on the blade (COP). Since it was uncertain whether the measurements of the skate were influenced by the low environmental temperature on the ice rink, ranging between -5°C to 0°C on the ice and 0°C to 5°C just above the ice, first the temperature dependency was determined.

The tensile testing machine was placed in a climate-controlled chamber to regulate the temperature. Each skate was positioned blade up in four different positions (P1-P4) on the fixed lower head of the testing machine. The reference force F_{LC} exerted by the movable upper head of the machine ($\varnothing 50$ mm), was applied directly to the blade via a constant displacement, up to a maximum force, and released by the same constant displacement. A wedge was designed to place the skate under five tilting angles (λ_{ta}) with $\lambda_{ta} = -70, 70, 00, -200, 200$, to distribute the applied force F_{LC} into a normal (F_N) and lateral (F_L) force on the skate.

2.2.1 Temperature

The temperature dependency test was conducted under four different temperatures (-5°C , 0°C , 5°C and 19°C) at position P2, by applying a rising force up to 1100N. From each condition

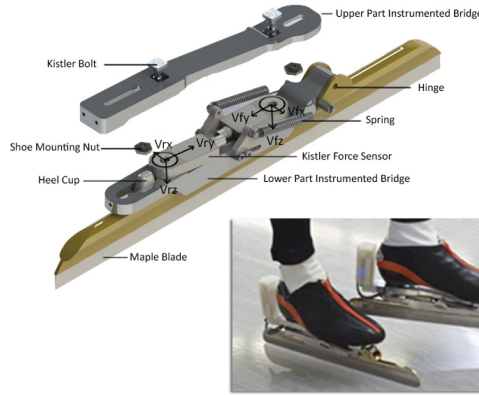


Figure 3.2 Overview of the instrumented bridge and an attached blade. The lower part of the bridge is only attached to the blade via the hinge. The upper part of the bridge is attached to the lower part via the Kistler bolts under pre-stress. The skater can place its own shoe on the bridge via the Shoe mounting nuts. The small white box near the heel is the recording and transmission unit for the measured data.

12 samples were taken (every 100 N) and the combined output voltages $V_{fz} + V_{rz}$ were compared between temperature conditions. Results showed that the output voltages were uncorrelated to the temperature conditions ($R = -0.015$, $p = 0.89$ for left skate and $R = -0.0037$, $p = 0.9712$ for the right skate). Therefore the remaining calibration could be performed at room temperature (19°C).

2.2.2 Normal and Lateral Force

The calibration in normal and lateral direction was performed at room temperature (19°C), in four different positions (P1-P4) under the five tilting conditions λ_{-70} , λ_{-70} , λ_0 , λ_{200} and λ_{-200} . At each position, under each condition, 12 samples were taken from the force data, equally divided from zero up to the maximum measured force. The maximum forces differed between conditions due to the applied tilting angle, but ranged from 1600 N to 2500 N in normal direction and from -610 N up to 610 N in lateral direction.

Calibration was done using a forced entry regression analysis with a second order fit in both the normal and lateral direction. This second order fit was believed to be necessary due to non-linearity in the material deformations of the bridge, the heel cup and the spring and to intercept any differences in pre-stress of the sensors. The characteristics of the heel cup and the spring mainly influence the force transition in lateral direction and its influence varies with the position of the applied forces in lateral direction. Therefore the ratio RV was introduced as a measure of this position:

$$RV = \frac{V_{fz} - V_{rz}}{V_{fz} + V_{rz}} \quad (3.1)$$

This ratio was introduced as an input into the lateral regression, to improve the lateral force estimation. Overall, input for the second order regression analysis in normal direction were the voltages measured in the vertical plane (V_{fz} and V_{rz}). Input to the second order model in lateral direction were the voltages measured in the lateral direction (V_{fx} and V_{rx}) and a the ratio RV.

2.2.3 Centre of Pressure

The COP is the position on the skate blade where the resultant force acts on. Input for a forced linear regression for determination of the COP was the ratio RV:

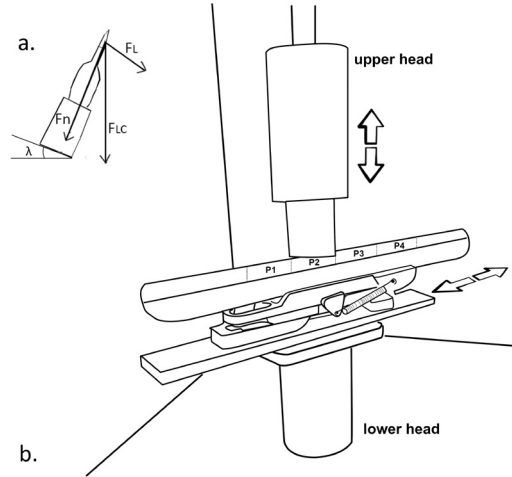


Figure 3.3 Calibration Set-up; a) The tensile strength machine exerts the force F_{LC} due to the tilting angle λ under which the skate is positioned, this results in a force in normal and lateral direction. B) The upper head moves down to exert force on the blade of the instrumented skate. The skate can be placed in 5 different positions (P1-P5) to calibrate the COP and can be placed under an angle λ to calibrate the normal and lateral forces.

$$COP = c_0 + c_1 \cdot RV \quad (3.2)$$

Where c_0 and c_1 are the variables to be determined by regression. The assumption was made that the applied force acts at the centre of the moving upper head, neglecting the curving of the blade, and that the point of application at the blade is equal for the normal and lateral applied forces.

2.3 Measurements on the ice rink

To demonstrate the practical use of the measurement system, data were collected in 2015 on the indoor ice rink of Thialf, which is located at Heerenveen in the Netherlands. Seven Dutch elite speed skaters (5 men, 2 women; 22 ± 1.1 years; 77.3 ± 6.8 kg; PR at 1000m: men: 1.10-1.12s, women: 1.16-1.18s) were equipped with two instrumented skates, on which their own skating shoes were positioned. The average velocity over a straight part or a curve was measured by a local position measurement system (LPM, 2015). Skaters familiarized themselves with the equipment before the start of the test. The test was divided into three parts, each at a different velocity, which each consisted of skating three laps at a constant velocity, of which we employed the data at 10.3 m/s for the current paper. The push-off forces were normalized to ratio of total body weight and equipment (BW). The onset of a stroke was defined as the time at which the normal force attained 100 N (Jos J de Koning et al., 1987), the end of the stroke the time at which the normal force fell back to 100 N. The time is normalized in units of stroke time.

2.4 Statistics

The statistics applied in this paper, are based on three strokes per participant, per side. Therefore 21 strokes for each skate (left and right). In order to establish any differences in peak forces or mean COP between left and right, a paired sample t-test was performed in which the mean value of three strokes was used as an input for each participant.

3. Results

3.1 Calibration results

Calibration in normal direction with a second order regression equation resulted in correlations of $R^2 = 0.995$ and $R^2 = 0.997$ for the left and the right skate respectively, with a root mean square error (RMS) of 42 N (SEM = 1 N) and 38 N (SEM = 1 N) (Figure 3.4) (SEM is the standard error of the mean). Calibration in lateral direction performed with a second order regression, incorporated the factor RV. The correlation for the lateral direction yielded $R^2 = 0.991$ for both skates with the corresponding RMS errors of 25 N (SEM = 1 N) and 27 N (SEM = 1N) for respectively the left and the right skate. The remaining error of the fit proved to be random. The absolute mean error of the center of pressure estimation, based on linear regression (eq. 3.2), is 8.5 mm (SD = 6.4 mm) for the left skate and 10.1 mm (SD = 6.9 mm) for the right skate.

3.2 Measurements on the rink

Figure 3.5 shows an example of the force registration for two straights and a curve. The curve is characterized by a higher stroke frequency and lower normal forces compared to the straight parts. Furthermore the lateral forces of the left skate change direction when entering the curve, since the skater changes the push-off for this skate from the medial to the lateral side of the blade. Except for normal forces in the curve, all other forces show a clear peak at the end of the stroke. Figure 3.6 presents the normalized forces (mean \pm SD of seven participants, each three strokes) with a velocity of 10.3(\pm 0.6) m/s for the straight part. The mean peak values of the normalized normal forces at the straight part were $\bar{f}_N = 1.35(\pm 0.09)$ BW and $\bar{f}_N = 1.38(\pm 0.08)$ BW for the left and right stroke respectively. The mean maximum normal forces in the curve (Figure 3.7) go up to $\bar{f}_N = 1.30(\pm 0.07)$ BW and $\bar{f}_N = 1.32(\pm 0.09)$ BW for the left and the right stroke respectively. The lateral forces showed mean peak values at the straight part of $\bar{f}_L = 0.74(\pm 0.14)$ BW and $\bar{f}_L = 0.79 (\pm 0.25)$ BW for the left and right skate. There is no significant difference between left and right for any of these maximum forces ($p > 0.1$), however the lateral forces in the curve do have mean peak values that differ between sides ($p < 0.00$), with $\bar{f}_L = 0.35(\pm 0.09)$ BW for the left and $\bar{f}_L = 0.73(\pm 0.25)$ BW for the right stroke.

The mean COP (Figure 3.8) showed no difference between left and right on the straight part ($p = 0.58$), while in the curve there is a clear difference. In the curve the COP moves faster toward the front of the blade compared to the straight, which is most evident in the left skate. The timing of the peak forces is indicated by the vertical grey bar in the figure. Except for the left COP in the curve, all peak forces occur while the COP moves to the front of the blade. For the left skate in the curve, the COP already shifts towards the hinge (at 0 mm) before the occurrence of peak forces, and levels while the peak forces occur.

4. Discussion

4.1 Construction and Calibration

In this paper we have described the construction and calibration of two wireless instrumented klapskates that can measure the lateral and normal forces during high-speed skating with an accuracy of RMS of 42 N (SEM = 1 N) in normal and up to a RMS of 27 N (SEM = 1N) in lateral direction. As mentioned in the introduction, we cannot determine yet whether the found accuracy will be sufficient for the purpose of providing elite speed skaters with adequate feedback on improving their performance, since the relation between the forward velocity (performance) and the applied forces is yet to be discovered. This relationship can however be established with for instance a dynamic model of skating that describes the complete path from push-off force to forward velocity. The current skate can be of use in validating such a model (van der Kruk, Veeger, van der Helm, & Schwab, 2015).

Apart from crosstalk, previous papers on the calibration of instrumented skates for speed skating, did not give an accuracy indication for separate force directions. The study on the construction and calibration of an instrumented ice hockey skate did (Stidwill et al., 2010). The

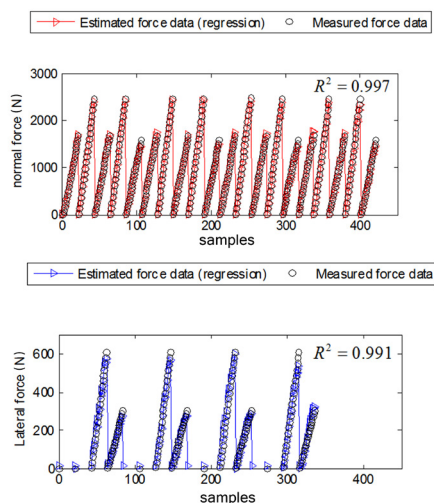


Figure 3.4 Forces estimated by the right instrumented skate with the second order regression functions and the forces measured by the tensile test machine for each sample. The upper graph shows the results for the normal direction, the lower graph the results for the lateral direction. Given are the regression coefficients of the fit.

RMS errors of the instrumented klapskates are similar to those of the ice hockey skates, with a RMS in normal direction of 42 N for the klapskates versus 68 N for the ice hockey skates and a RMS in lateral direction of 27 N for the klapskates and 40 N for the ice hockey skates.

The skates were calibrated in two directions, lateral and normal, while the sensors are capable of measuring in three directions. We intentionally chose to neglect the longitudinal direction, due to the relatively small forces acting in this direction. Considering the crosstalk of $\approx 3\%$ between the vertical and transverse plane of the applied sensors, as reported by the manufacturer, it will be impossible to observe ice friction forces lower than 1% of the body weight with the current design. If in future research we do want to determine these forces, a construction needs to be made whereby the normal forces are completely decoupled from the transverse plane, in order to avoid crosstalk. With the current design, this will not be feasible.

The aim to build wireless instrumented klapskates, was accomplished in this paper. Although the instrumented skates function as a klapskate, the skate was only calibrated while it was closed. As soon as the skate opens, the force measurements are therefore no longer reliable. Previous studies indicate that the opening of the skate happens at the very last part of the stroke (50ms before lifting the skate) and that the forces are small in this time span (Houdijk et al., 2000). As a consequence we expect this not to be a major problem for the power determination. The benefit of the hinge mechanism in the system, is to preserve the skating movement of speed skaters during testing. The presented instrumented skate has high resemblance to a standard klapskate. Still the influence of the added weight of the instrumented bridge on the skaters technique should not be disregarded in future analyses. A follow-up research in which the skating technique while skating on the instrumented skate is compared to the technique employed while skating on common klapskates, can identify such specific differences.

4.2 Practical results

The recorded normal peak forces at the straight partially agree with previous studies, where normal peaks between the 1.2-1.5 BW at 9 m/s to 11.5 m/s on a conventional skate were reported (Jos J de Koning et al., 1987; Yuki et al., 1996). In line with the current study, previous studies report that no clear normal peak forces were found in the curve. The lateral forces measured in the curve are higher than the reported lateral forces of Yuki et al. (Yuki et al.,

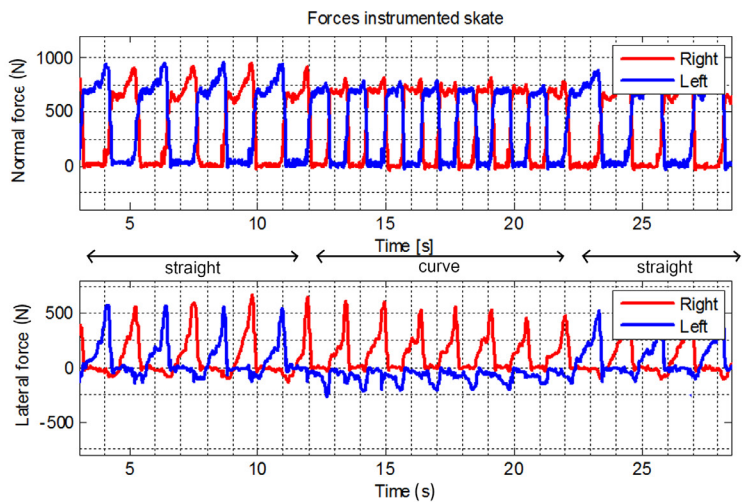


Figure 3.5 Example of a force registration of a female elite skater (65 kg) on two straights and a curve part at 10 m/s. The lateral forces are positive for both the left and the right skate at the straight parts. In the curve, the force on the left skate is applied on the medial side of the blade.

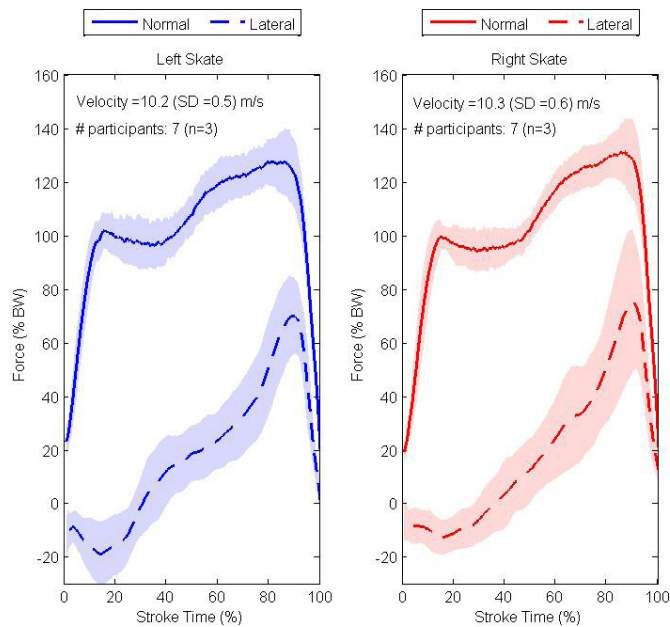


Figure 3.6 The mean and standard deviation for the normal and lateral forces for seven elite speed skaters measured at the straight. The forces are presented per stroke, from each skater three strokes were incorporated. The forces are normalized to body weight and the stroke is normalized to stroke time.

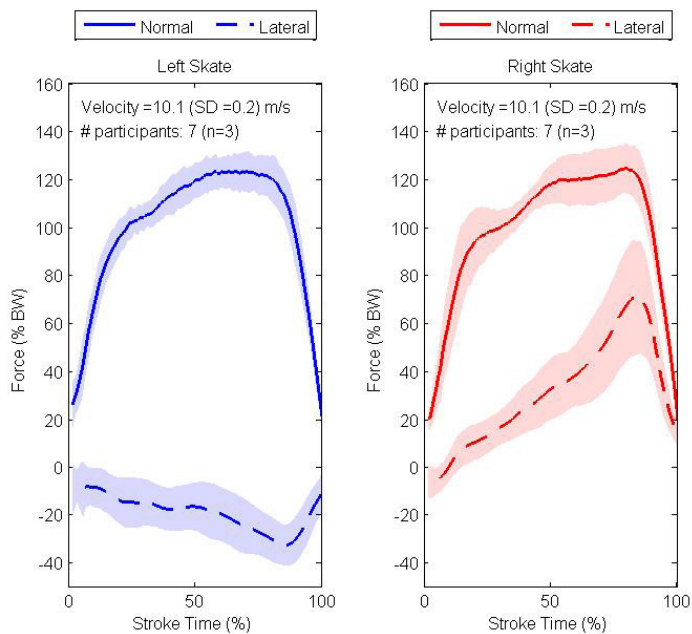


Figure 3.7 The mean and standard deviation for the normal and lateral forces for seven elite speed skaters measured at the curve. The forces are presented per stroke, from each skater three strokes were incorporated. The forces are normalized to body weight and the stroke is normalized to stroke time.

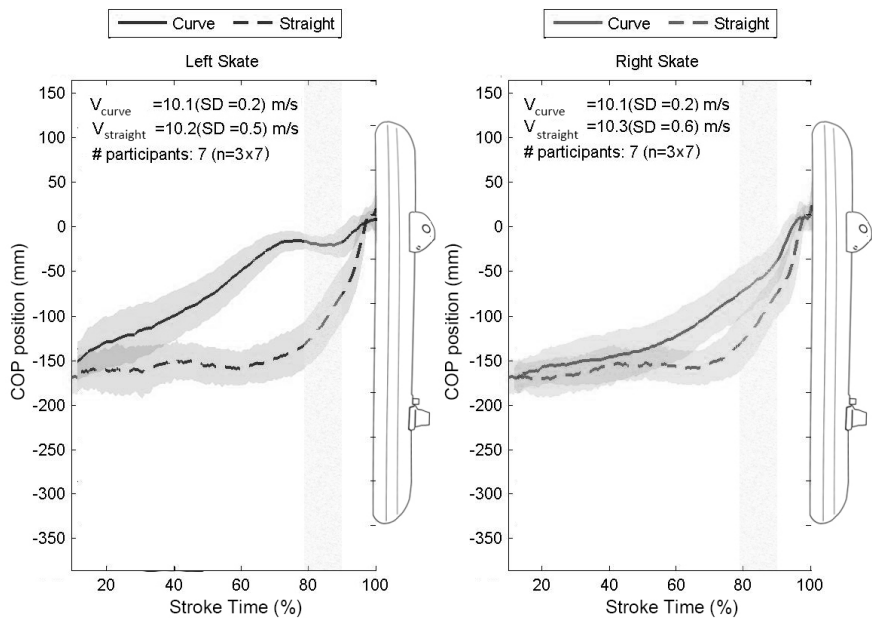


Figure 3.8 Centre of Pressure of the resultant force (COP) for the straight part and the curve. Given are the mean and standard deviation of the measured COP of 7 participants, each three strokes. The grey area indicates the occurrence of peak forces. The hinge is located at 0 mm, the damper at -205 mm and the centre of the heel cup at -220 mm.

1996), who found lateral forces on the straight part of 0.4 BW for both sides, and in the curve 0.3 BW for the left and 0.6 BW for the right skate, for one typical example. Direct comparison is however not feasible, since the velocity and the skill level of this skater will influence these values, and these were unfortunately not mentioned in his study. Nonetheless, both studies showed that the lateral force is a major component in the push-off force. The lateral forces are related to the lean angle of the skate and the eversion of the skate, which causes the foot and the lower leg to be unaligned. Whether the lateral force is of benefit or counterproductive to the forward motion of the skater, depends on the orientation of the skate, determined by both the lean and steer angle. The lean angle of the skate has a direct effect on the distribution of a push force over the local vertical and transverse component, while the steer angle determines the direction of push-off in the horizontal plane (forward or sideways).

4.3 Centre of Pressure

The centre of pressure indicates where the resultant measured forces act on the skate blade. On the straight part, the centre of pressure of the resultant force levelled at about 20-70 mm ahead of the heel cup, for the first 80% of the stroke. Then the COP shifted towards the hinge of the skate, in which time the peak forces occurred, followed by the opening of the skate. Since the hinge is taken as origin, the skate would open when the COP becomes positive if it wasn't for a spring acting on the hinge, which makes it difficult to interpret the exact opening of the klapskate. The curve showed different COP patterns for left and right. Both lack the levelled phase at the start of the stroke, since the COP continuously shifts towards the front. The left skate has a faster shift and levels at the end of the stroke while the peak forces occur. This pattern arises from the fact that the skater has to cross his right leg over his left in the curve. Therefore the skater is forced to move his left leg backwards faster, whereby his COP quickly shifts towards the point of his blade.

4.4 Real-Time feedback

Measured outputs were sent wirelessly and real-time over Bluetooth to a phone carried by the speed skater during the test. It is possible to link the phone via wifi or a mobile network to a tablet or smart glasses, in order to provide both coach and skater with real-time visual feedback on the force level and COP during training. Eventually the forces will be combined with kinematic measurement systems, to provide feedback on power per stroke. During this experiment the possibility of synchronising the skates with other measurement equipment via a digital end-start pulse proved to be easy.

5. Conclusion

Two wireless force measuring instrumented klapskates were constructed and calibrated on a tensile testing machine, where they proved to be unaffected by temperature conditions and accurate up to a RMS of 42 N (SEM = 1 N) in normal and 27 N (SEM = 1N) in lateral direction. Furthermore the centre of pressure of these forces on the blade was determined up to a mean error of 10.1 mm (SD = 6.9 mm). The design of the skate allows a skater to attach his own shoe and Maple blade to the bridge. On-ice measurements showed the possibility of recording with both skates simultaneously and synchronously both straights and curves, and the capability of the system to send data wirelessly and real-time to other devices, which makes it possible to eventually provide skaters and coaches with visual real-time feedback during practice. With the construction of these instrumented klapskates we are one step closer to fulfilling the wish of the Dutch elite skaters and their coaches for a system determining the mechanical power per stroke.

References

de Koning, J. J., de Boer, R. W., de Groot, G., & van Ingen Schenau, G. J. (1987). Push-Off Force in Speed Skating, 103–109.

De Koning, J. J., De Groot, G., & Van Ingen Schenau, G. J. (1992). Ice friction during speed skating. *Journal of Biomechanics*, 25(6), 565–571. [http://doi.org/10.1016/0021-9290\(92\)90099-M](http://doi.org/10.1016/0021-9290(92)90099-M)

Houdijk, H., de Koning, J. J., de Groot, G., Bobbert, M. F., & van Ingen Schenau, G. J. (2000). Push-off mechanics in speed skating with conventional skates and klapskates. *Medicine and Science in Sports and Exercise*, 32(3), 635–641. <http://doi.org/10.1097/00005768-200003000-00013>

Jobse, H., Schuurhof, R., Cserep, F., Schreurs, a W., & Koning, J. J. De. (1990). Measurement of Push-Off Force and Ice Friction During Speed Skating. *International Journal of Sports Biomechanics*, 6, 92–100.

LPM. (2015). LPM.

Maple. (2015). Maple.

Shimmer3. (2015). Shimmer. Retrieved from www.shimmersensing.com

Stidwill, T. J., Turcotte, R. A., Dixon, P., & Pearsall, D. J. (2010). Force transducer system for measurement of ice hockey skating force. In *International Sports Engineering Association 2010*.

van der Kruk, E., Veeger, H. E. J., van der Helm, F. C. T., & Schwab, A. L. (2015). Two Body Dynamic Model for Speed Skating Driven by the Skaters Leg Extension. In *icSports conference 2015*.

Van Ingen Schenau, G. J. (1981). A power balance applied to speed skating. PhD. thesis. Vrije Universiteit Amsterdam.

Van Ingen Schenau, G. J., & Cavanagh, P. R. (1990). Power equations in endurance sports. *Journal of Biomechanics*, 23(9), 865–881. [http://doi.org/10.1016/0021-9290\(90\)90352-4](http://doi.org/10.1016/0021-9290(90)90352-4)

Yuda, J., Yuki, M., Aoyanagi, T., Fujii, N., & Ae, M. (2004). Changes in blade reaction forces in speed skating the curve. *International Journal of Sport and Health Science*, 2(1996), 195–204.

Yuki, M., Ae, M., & Fujii, N. (1996). ドケットのド反 (Blade reaction forces in speed skating). *Society of Biomechanics*, 13, 41–51.

Speed Skating Technique

PART II

4

Design and verification of a simple 3D dynamic model of speed skating which mimics observed forces and motions

Everything should be made as simple as possible, but not simpler.
-Einstein-

This is where our search for the optimal skating motion starts. Each speed skater has its own implementation of the speed skating technique, which makes statistical analyses of the skating technique ineffective for finding the optimal motion. Therefore we want to understand the physical principles of the speed skaters coordination pattern, which can be done with a simple biomechanical model. This chapter describes such a model; first the biomechanical speed skater model is presented, followed by its validation using the kinetic data measured at an ice rink (CH2, CH3).

van der Kruk, E., H.E.J. Veeger, F.C.T. van der Helm and A.L. Schwab, (2017) *Design and verification of a simple 3D dynamic model of speed skating which mimics observed forces and motions*, journal of biomechanics, 64, 93-102.

Abstract

Advice about the optimal coordination pattern for an individual speed skater, could be addressed by simulation and optimization of a biomechanical speed skating model. But before getting to this optimization approach one needs a model that can reasonably match observed behaviour. Therefore, the objective of this study is to present a verified three dimensional inverse skater model with minimal complexity, which models the speed skating motion on the straights. The model simulates the upper body transverse translation of the skater together with the forces exerted by the skates on the ice. The input of the model is the changing distance between the upper body and the skate, referred to as the leg extension (Euclidean distance in 3D space). Verification shows that the model mimics the observed forces and motions well. The model is most accurate for the position and velocity estimation (respectively 1.2% and 2.9% maximum residuals) and least accurate for the force estimations (underestimation of 4.5-10%). The model can be used to further investigate variables in the skating motion. For this, the input of the model, the leg extension, can be optimized to obtain a maximal forward velocity of the upper body.

1. Introduction

Speed skaters can only push-off laterally to their blade, therefore they are restricted to a specific motion pattern. A skating stroke during speed skating the straights can be divided into three phases: the glide phase, the push-off phase and the re-position phase (Figure 4.1) (Van Ingen Schenau, 1981). During the glide phase, the mass of the skater is supported over one leg, whereby the ankle-hip distance remains more or less constant. The skater then starts to increase this distance by introducing a leg extension, thereby moving the center of mass away from the skate, which indicates the start of the push-off phase. The push-off phase ends when the leg is at its maximal extension. Since the leg extension velocity can no longer keep up with the upper body velocity in this phase, the skate leaves the ice. During the re-positioning phase the skate is retracted under the body of the skater, until the skater places the skate again on the ice, whereby the glide phase begins, which completes the motion cycle. Double support (both skates on the ice) exists when one leg is at the start of the glide phase while the other leg is at the end of push-off. This coordination pattern results in a sinus-wave like transverse trajectory of the upper body over the ice.

Within the restriction of this motion, still a distinct difference in coordination patterns among (elite) speed skaters is observed. This indicates room for individual optimization of the speed skating motion. Finding this optimal coordination pattern could well be addressed by simulation and optimization of a biomechanical model of speed skating. But before getting to this optimization approach one needs a model that can reasonably match observed behaviour.

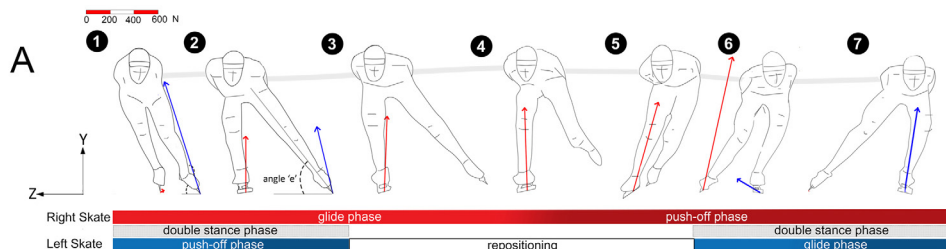


Figure 4.1 Phases in the skating motion; the figure is adopted from (van der Kruk et al., 2017). Skating is divided into the four phases: glide phase, push off phase, repositioning phase and the double stance, where both skates are on the ice. The push-off angle of the leg is the angle the leg makes with the horizontal during the push-off motion in the frontal plane. The arrows indicate the push-off force in global space, the scale is indicate in the top-right corner. The grey line indicates the CoM motion of the HAT.

Currently, there are two speed skating models describing the coordination patterns of skaters. First, there is a dynamic model, consisting of 19 rigid bodies and 160 muscles, which can simulate the speed skating motion and gives insight in the forces and motions acting in the joints (Otten, 2003); Second, there is an inverse dynamic model of a speed skater of Allinger & Bogert (1997), which is driven by individual strokes and gives insight in the coordination pattern of the speed skater. To the best knowledge of the authors, both models have not been validated with actual (force) measurements, nor were the effects of the assumptions investigated. Furthermore, the application of the model by Allinger & Bogert (1997) is limited, since it is driven by a presumed function in time rather than measured leg extensions and the body height was assumed constant. Apart from speed skating, there is one other skating model developed, simulating the skating push-off force in cross-country skiing (Bruzzo et al., 2016). This is a multibody model of a two-segment leg (with the upper body mass attached to the top of the leg), using the orientation of each leg segment as input for their simulation. The aim of their model was to estimate the push-off force rather than a model which could be used for technique optimization. Thus although (speed) skating models have been developed, none of them have been shown to accurately predict the observed coordination pattern.

The objectives of this study are to present a verified three dimensional dynamic skater model with minimal complexity – built on previous work in rowing (Cabrera, Ruina, & Kleshnev, 2006) and speed skating (Fintelman, Den Braver, & Schwab, 2011; van der Kruk, Veeger, van der Helm, & Schwab, 2015) - modelling the speed skating motion on the straights. The model is driven by the leg extension - the changing distance between the upper body and the skate - and the skate steering, which we call motion coordination. In this paper we present the verification of this novel model through correlation with observed kinematics and forces.

2. Methods

2.1 Model description

The skater is considered as a combination of three point masses, which are situated at the upper body (mass B) and at each skate (mass S) (Figure 4.2). Since the double stance phase is rather short, it is assumed that there exists no double stance phase. Therefore, only one skate at the time is on the ice, alternating left and right. The point of alternation is defined as the moment in time where the forces exerted on both skates are equal. So at any point in time, only two masses are considered in the model, which we refer to as the *active masses* (mass B and one of the skates). The repositioning phase of the inactive skate in the air is therefore neglected. Each mass has three degrees of freedom. The set of parameters is restricted to the position coordinates of mass B (x_b, y_b, z_b), two translations in the transverse plane of mass S, with the position coordinates (x_s, y_s) (because the skate is assumed to be on the ice, making

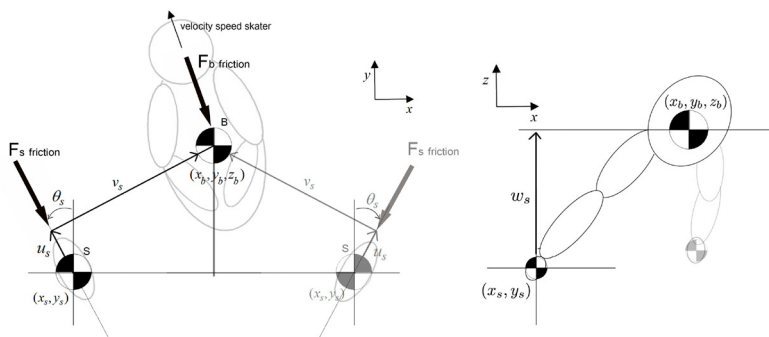


Figure 4.2 Simple skater model; a) top view of the skater; b) rear view of skater. The skater is considered as two point masses, which are situated at the upper body (mass B) and at each skate (mass S). The position of mass B was estimated at the CoM of the HAT (head, arms and trunk). The position of mass S was positioned at the CoM of the foot segment. The generalized coordinates are explained in Table 4.1.

$z_s=0$ at all times) and one rotation in the same plane, the steer angle (θ_s). This steer angle is of importance for the constraint forces acting on the skate, since we assume that the skate can only glide in the direction of the blade, restricting lateral slip. All other rotations of the skates and the upper body rotations are neglected. The bodyweight of the skater is distributed over the two active masses by a constant mass distribution coefficient (η). Furthermore, the arm movements are assumed to be of marginal effect on the overall power and are therefore neglected.

The input of the model is the changing distance between the point mass position of the upper body and the skate (Euclidean distance in 3D space), which will be indicated as the leg extension in the remainder of this paper, and the steering angle of the skate; these are relative measures. The output of the model is the upper body motion of the skater in global space together with the forces exerted by the skates on the ice.

2.2 Generalized coordinates

The global coordinates describing the position of upper body B and skate S are,

$$\mathbf{x} = [x_b \quad y_b \quad z_b \quad x_s \quad y_s \quad \phi_s] \quad (4.1)$$

We want to express the coordination of the skater in terms of leg extension. Instead of describing the position and orientation of the body together with the constraints imposed by the joints on these coordinates \mathbf{x} we use a minimum set of coordinates \mathbf{q} ,

$$\mathbf{q} = [u_b \quad v_b \quad w_s \quad u_s \quad v_s \quad \theta_s] \quad (4.2)$$

Where (w_s, u_s, v_s, θ_s) describe the leg extension that is actively controlled by the skater and therefore serve as the input coordinates to the model (Figure 4.2). The remaining coordinates

(u_b, v_b) are the generalized coordinates of the upper body, which will be a result of the system dynamics. The global coordinates \mathbf{x} can be expressed in terms of the generalized coordinates

$$\mathbf{x} = T(\mathbf{q}) \quad (4.3)$$

$$\begin{bmatrix} x_b \\ y_b \\ z_b \\ x_s \\ y_s \\ \phi_s \end{bmatrix} = \begin{bmatrix} u_b \\ v_b \\ w_s \\ u_b - kk \cdot \cos(\theta_s) \cdot v_s + kk \cdot \sin(\theta_s) \cdot u_s \\ v_b - \sin(\theta_s) \cdot v_s - \cos(\theta_s) \cdot u_s \\ kk \cdot \theta_s \end{bmatrix} \quad (4.4)$$

Where kk is the parameter introduced to distinct the alternating left active skate ($kk = 1$) and the right active skate ($kk = -1$). A derivation of these relations lead to a Jacobian matrix \mathbf{T} , which maps global velocities onto generalized velocities.

Table 4.1 Clarification on the generalized coordinates.

q	Generalized coordinates
u_b	Absolute position of mass B in x-direction (global)
v_b	Absolute position of mass B in y-direction (global)
w_s	Vertical distance between the mass S and mass B
u_s	Horizontal distance between mass S and mass B in heading direction of the skate
v_s	Horizontal distance between mass S and mass B perpendicular to the heading direction of the skate
θ_s	Heading of the skate (counterclockwise)

$$\dot{\mathbf{x}} = \frac{\partial T}{\partial \dot{\mathbf{q}}} \dot{\mathbf{q}} = \mathbf{T} \dot{\mathbf{q}} \quad (4.5)$$

The matrix \mathbf{T} can also be used to transform the global mass and force matrix into mass and force matrices that act on the generalized coordinates (local frame).

2.3 Unconstrained Equations of Motion

We first determine the unconstrained equations of motion and then add a non-holonomic constraint to the skate to restrict any lateral slip in the next section. The unconstrained equations of motion in terms of generalized coordinates according to Newton's law are then described by

$$\bar{\mathbf{M}} \cdot \ddot{\mathbf{q}} = \bar{\mathbf{F}} \quad (4.6)$$

Where $\ddot{\mathbf{q}}$ is the second derivative of \mathbf{q} with respect to time. $\bar{\mathbf{M}}$ and $\bar{\mathbf{F}}$ are respectively the mass and the force matrix acting on the generalized coordinates. $\bar{\mathbf{M}}$ is found by

$$\bar{\mathbf{M}} = \mathbf{T}^T \mathbf{M} \mathbf{T} \quad (4.7)$$

$$\mathbf{M} = \begin{bmatrix} m_b & 0 & 0 & 0 & 0 & 0 \\ 0 & m_b & 0 & 0 & 0 & 0 \\ 0 & 0 & m_b & 0 & 0 & 0 \\ 0 & 0 & 0 & m_s & 0 & 0 \\ 0 & 0 & 0 & 0 & m_s & 0 \\ 0 & 0 & 0 & 0 & 0 & I_s \end{bmatrix} \quad (4.8)$$

where m_b is the mass of B , m_s the mass of S and I_s the mass moment of inertia of S . The second reduced matrix, is the reduced force matrix $\bar{\mathbf{F}}$ which is defined as

$$\bar{\mathbf{F}} = \mathbf{T}^T (\mathbf{f} - \mathbf{M} \cdot \mathbf{h}_{con}) + \mathbf{Q} \quad (4.9)$$

where \mathbf{Q} are the forces exerted on the local frame and \mathbf{h}_{con} are the convective acceleration terms of \mathbf{x} ,

$$\ddot{\mathbf{x}} = \mathbf{T} \ddot{\mathbf{q}} + \mathbf{h}_{con} \quad (4.10)$$

With

$$\mathbf{h}_{con} = \frac{\partial \mathbf{T}}{\partial \dot{\mathbf{q}}} \dot{\mathbf{q}} \cdot \dot{\mathbf{q}} \quad (4.11)$$

The forces \mathbf{f} consist of gravitational and friction forces acting on \mathbf{x} . The external forces \mathbf{f} are described by:

$$\mathbf{f} = \begin{bmatrix} \sin(\theta_b) \cdot F_{b,f} \\ -\cos(\theta_b) \cdot F_{b,f} \\ -m_b \cdot g \\ k \sin(\theta_s) \cdot F_{s,f} \\ -\cos(\theta_s) \cdot F_{s,f} \\ k M_s \end{bmatrix} \quad (4.12)$$

$F_{b,f}$ represents the air friction working on the skater. We described the air friction forces based on the study of van Ingen Schenau (1982):

$$F_{b,f} = \frac{1}{2} A C_d \rho v_{xyz}^2 = k_1 v_{xyz}^2 \quad (4.13)$$

where C_d represents the drag coefficient, A the frontal projected area of the skater, ρ the air density and v_{xyz} the velocity of the air with respect to the skater. $F_{s,f}$ is the ice friction working on the skate, which is described using Coulomb's law of friction (J. J. De Koning, De Groot, & Van Ingen Schenau, 1992):

$$F_{s,f} = \mu F_N \quad (4.14)$$

where μ is the friction coefficient and F_N is the normal force of the skate on the ice. Since the normal force is one of the outcomes of the model and μ is small, the normal force is approximated by $F_N \approx mg$ in which m the mass of the skater and g the earth gravity.

2.4 Constrained Equations of Motion

The acting external forces are the air frictional forces acting on the body (located at mass B) and the ice frictional forces acting on the skate. The undetermined external force acting on the skate is the constraint force perpendicular to the skate blade in the transverse plane, restraining any lateral slip of the skate. This was implemented in the model by means of a non-holonomic constraint acting in the lateral direction of the skate.

$$C_s = -\sin(\theta_s) \cdot \dot{y}_s - k \cos(\theta_s) \cdot \dot{x}_s = 0 \quad (4.15)$$

Expressing C_s into the generalized coordinates and differentiating ones, leaves us with the equation

$$C\ddot{q} + C_{con} = 0 \quad (4.16)$$

In which C is the Jacobian of the constraints and C_{con} are the convective acceleration terms of the constraints. Adding these constraints to the total equation of motion, Eq. 4.5 results in:

$$\begin{bmatrix} \overline{\mathbf{M}} & \mathbf{C}^T \\ \mathbf{C} & \mathbf{0} \end{bmatrix} \begin{bmatrix} \ddot{\mathbf{q}} \\ \lambda \end{bmatrix} = \begin{bmatrix} \overline{\mathbf{F}} \\ -C_{con} \end{bmatrix} \quad (4.17)$$

where λ is the constraint force (Lagrange multiplier) acting in the lateral direction of the skate.

2.5 Finding the solution

The model is solved in two steps. First, since the parameters (w_s, u_s, v_s, θ_s) are considered as inputs and the air frictional forces acting on the upper body are assumed to be known, Eq. 4.14

can be reorganized in terms of known (q^o) and unknown (q^d) coordinates:

$$\begin{bmatrix} \overline{\mathbf{M}}^{dd} & \overline{\mathbf{M}}^{do} & \mathbf{C}^{dT} \\ \overline{\mathbf{M}}^{od} & \overline{\mathbf{M}}^{oo} & \mathbf{C}^{oT} \\ \mathbf{C}^d & \mathbf{C}^o & 0 \end{bmatrix} \begin{bmatrix} \ddot{\mathbf{q}}^d \\ \ddot{\mathbf{q}}^o \\ \lambda \end{bmatrix} = \begin{bmatrix} \overline{\mathbf{F}}^d \\ \overline{\mathbf{F}}^o \\ -C_{con} \end{bmatrix} \quad (4.18)$$

the constraint force λ and the transverse position of the upper body (u_b v_b) can be determined by solving

$$\begin{bmatrix} \ddot{q}^d \\ \lambda \end{bmatrix} = \begin{bmatrix} \overline{\mathbf{M}}^{dd} & C^{dT} \\ C^d & 0 \end{bmatrix}^{-1} \begin{bmatrix} \overline{\mathbf{F}}^d - \overline{\mathbf{M}}^{do} \cdot \ddot{q}^o \\ -C_{con} - C^o \cdot \ddot{q}^o \end{bmatrix} \quad (4.19)$$

The algebraic differential equations Eq 4.19 cannot be solved analytically. The equations are integrated using the classical fourth order Runge Kutta method. The integration time t_n has been chosen the sample time of the measurements ($t_n = 0.01$). The constraints are fulfilled for each integration step by a coordinate projection method (Eich-Soellner & Führer, 1998). Hereby a minimization problem was formulated, concerning the distance from the predicted solution to the solution which is on the constraint surface.

With above steps, the complete set of generalized coordinates q_i can be determined, with which the global coordinates x_i can be determined analytically via the kinematic relations in (Eq. 4.4). Finally, with the determined \ddot{q} and λ , the forces acting on the skate $\overline{\mathbf{F}}^o$ can be determined analytically so that a complete two-body dynamic model of the skater has been established:

$$\overline{\mathbf{F}}^o = \begin{bmatrix} F_{w_s} & F_{u_s} & F_{v_s} & M_{\theta_s} \end{bmatrix} \quad (4.20)$$

$$\overline{\mathbf{F}}^o = \begin{bmatrix} \overline{\mathbf{M}}^{od} & \overline{\mathbf{M}}^{oo} & C^o \end{bmatrix} \begin{bmatrix} \ddot{q}^d \\ \ddot{q}^o \\ \lambda \end{bmatrix} \quad (4.21)$$

Summarized the known generalized coordinates q^o , which we define as the leg extension were used as input. This was utilized to solve Eq. 4.19 to obtain the unknown coordinates q^d , defined as the upper body translation. The motion strategy was then used to find the forces applied on the skate, applying Eq. 4.21.

2.6 Data Collection

To verify the model, data were collected on the indoor ice rink of Thialf, Heerenveen (the Netherlands) in 2015. Four Dutch elite speed skater were equipped with two instrumented skates, on which their individual skating shoes and blades were positioned (in full detail described in: van der Kruk, den Braver, Schwab, van der Helm, & Veeger (2016)). The data were logged on a SD-card, with the data logger which is integrated into the instrumented skates. The skates measured the force acting in the normal and lateral direction of the local skate frame (100Hz). The ice-frictional forces (in longitudinal direction of the skates), were expected to be smaller than the cross-talk of the force sensors and therefore estimated (eq. 4.14) (van der Kruk, den Braver, et al., 2016). The 3D kinetic data collection is fully described in van der Kruk, Schwab, van der Helm, & Veeger (2017). The skater was equipped with 23 passive markers, which were captured by twenty motion capture cameras (300 Hz) on fifty meter of the straight part of the rink. Synchronisation between the instrumented skates and the motion capture system was done via a digital start-and-end-pulse.

To estimate the COM positions of the separate segments, we used a global optimization inverse kinematics method, employing an eight rigid body model with a revolute joint in the

knee, while keeping the other joints spherical (described and verified in van der Kruk et al. (2017)). The position of the mass S was estimated at the CoM of the foot; the position of mass B was estimated at the CoM of HAT (which is head, arms and trunk). Since mass B is much larger than the point masses at the skates, we initially set the mass distribution coefficient (η) to zero for the verification of the model, so that all bodyweight is located at mass B (Garcia, Chatterjee, Ruina, & Coleman, 1998). Since the skate can only glide in line with the blade, the steer angle was determined by the velocity vectors of the skates.

Skaters familiarized themselves with the equipment before the start of the test. The test was divided into three parts, each at a different velocity, which each consisted of skating three laps at a constant velocity. Skaters were asked to skate at a self-chosen velocity, corresponding to the low (70%), medium (80%), and high (90%) intensity, something they are familiar with in training. Due to the complexity of the measurements – foremost the large size of the capturing volume – not all datasets were applicable for verification. In total 28 trials of the four participants were recorded, of which 18 data sets consisting each of one straight part with several strokes (in total 39 strokes) at speeds varying from 8.5-12.3 m/s were complete and used for the verification of the model (Table 4.2). Of participant A, only data at low intensity was applicable for verification. In the remainder of this paper we refer to the trials by the participant character and trial number, e.g. C2 is participant C, trial 2.

2.7 Model Verification

The purpose of the model verification is to quantify the error between the simulated data and the measured forces and positions. Analysis of the model error is performed similar to the method of Cabrera et al. (2006). This method constructs two measures, first the residuals, defined as

$$R(y_j) = \frac{1}{N} \sum_{i=1}^N |\tilde{y}_{ij} - y_{ij}| \quad (4.22)$$

in which \tilde{y}_{ij} is the simulated value of a variable, y_{ij} the measured value of a variable and N is the number of samples. Second, a measurement error J_{\min} independent of scales and units:

$$E(y_j) = \frac{1}{N} \sum_{i=1}^N \frac{(\tilde{y}_{ij} - y_{ij})^2}{\bar{y}_j^2} \quad (4.23)$$

$$J_{\min} = \frac{\sum_{j=1}^M E(y_j)}{N} \quad (4.24)$$

In which \bar{y}_j is the characteristic value of the variable, N is the number of samples and M is the number of residuals. The errors of the upper body positions (x_b, y_b), the upper body velocity (\dot{x}_b, \dot{y}_b) and the magnitude of the force (F_{tot}) are taken into account. The peak to peak values of the upper body positions, average value of the body velocity in forward direction, peak value of the velocity in sideward direction and the maximum local measured normal peak force are used as the characteristic values of the parameters.

3. Results

3.1 Measured Data

An example of the measured leg extensions of both left and right strokes are shown in Figure 4.3. The motion pattern is similar for the left and the right stroke. For better comprehension of the movement, Figure 4.5 shows a motion plot of the skater. At the start of the stroke (the glide phase), the skate is positioned on the lateral opposite side of mass B, indicated by the negative v_s , and almost under mass B in the longitudinal direction, indicated by a close-to-zero u_s (Figure 4.3a,b, Figure 4.5a). The skate is then moved sideways (the push off phase) whereby v_s increases up to about 0.7 m (Figure 4.3b, Figure 4.5b-e). Only in the last part of the push-off (Figure 4.5d,e), the skate is moved backward from the upper body mass, indicated by the increase of u_s (Figure 4.3a). In the repositioning phase the skate is retracted to the upper body, thereby first moving the skate sideward (Figure 4.5f,g) and then forward (Figure 4.5h,i). The vertical distance between the skate and the upper body increases and decreases within the stroke, describing a sine wave like trajectory in the transverse plane, during speed skating the straights (Figure 4.3c). The measured normal and lateral forces were similar to previously published skating data (van der Kruk, den Braver, et al., 2016) (Figure 4.4).

3.2 Model Data

The simple skater model mimics the skaters observed motion and forces well as can be concluded from the results presented in Table 4.2, where the residuals and the J_{min} values are shown in column 9-25. We selected the best fit (C2, $J_{min} = 0.024$) and the worst fit (B4, $J_{min} = 0.094$) to present in Figure 4.6 and Figure 4.7. The model errors found in the verification process proved to be unrelated to the velocity in the trial or the participant (mass and technique).

The model performs best for the simulation of position and velocity of mass B with a maximal residual of 0.04 m in x- and 0.39 m in y-position (distance covered is 33 m) and 0.05 m/s for x-velocity (D2). Maximum residual in y-velocity is 0.31 m/s; the model simulates the average y-velocity over a stroke correctly, but lacks to simulate the occurring fluctuations within a stroke; We will elaborate on this in the discussion.

Force data have the least accurate fit and were underestimated in each test. The minimum force residual found is 47 N (C2), the maximum residual found is 135 N (D3) (peak forces here are 1000 N and 1250 N respectively). The success of the simulation is independent of subject and unrelated to the velocity of the skater and the number of strokes within a trial.

Table 4.2 Trials and results; In total the data of four participants were used for the verification of the model. The number of trials per participant differs, even as the number of strokes per trial. This was subject to the capturing volume and the accuracy of the motion capture system. P = participant, W = weight, T = trial, S = number of strokes in trial

P	W	η	k1	μ	T	S	velocity	Residuals		Error									
								Rxb	Ryb	Rdxb	Rdyb	RFtot	Exb	Eyb	Edxb	Edyb	EFtot	Jmin	
		(kg)					(m/s)	(m)	(m)	(m/s)	(m/s)	(N)	*e-3	*e-3	*e-3	*e-3			
A	F	70	0	0.19	0.006	1	2	9.8	0.03	0.19	0.04	0.20	111	0.726	0.125	0.631	0.495	0.011	0.065
						2	3	10.0	0.02	0.10	0.02	0.12	130	0.531	0.013	0.291	0.219	0.019	0.065
B	F	65	0	0.18	0.006	1	2	8.7	0.02	0.09	0.02	0.13	83	0.307	0.026	0.192	0.316	0.011	0.046
						2	3	9.5	0.01	0.05	0.02	0.14	94	0.196	0.004	0.203	0.361	0.01	0.034
						3	2	9.9	0.04	0.33	0.04	0.24	88	0.679	0.238	0.468	0.803	0.011	0.052
						4	2	9.9	0.04	0.32	0.04	0.29	121	1.158	0.28	0.585	1.172	0.017	0.094
C	M	76	0	0.14	0.006	1	2	10.3	0.03	0.16	0.03	0.15	54	0.418	0.054	0.303	0.303	0.006	0.029
						2	2	11.1	0.03	0.15	0.03	0.16	47	0.339	0.039	0.199	0.288	0.005	0.024
						3	2	11.2	0.03	0.09	0.03	0.15	62	0.33	0.017	0.293	0.23	0.007	0.032
						4	2	11.2	0.02	0.09	0.02	0.12	65	0.258	0.014	0.199	0.165	0.008	0.036
						5	2	11.8	0.03	0.13	0.03	0.18	72	0.756	0.046	0.495	0.332	0.008	0.051
						6	3	12.4	0.02	0.13	0.03	0.14	80	0.247	0.02	0.354	0.179	0.008	0.034
						7	2	12.8	0.02	0.15	0.03	0.19	83	0.6	0.056	0.477	0.278	0.009	0.055
						1	2	10.5	0.03	0.27	0.03	0.21	72	0.294	0.097	0.302	0.515	0.007	0.027
D	M	81	0	0.14	0.006	2	2	10.7	0.04	0.39	0.05	0.31	82	0.508	0.222	0.653	0.926	0.007	0.034
						3	2	10.8	0.04	0.32	0.04	0.25	135	0.556	0.17	0.444	0.673	0.017	0.073
						4	2	11.1	0.03	0.24	0.03	0.22	132	0.432	0.106	0.389	0.513	0.014	0.066
						5	2	12.3	0.02	0.21	0.04	0.23	128	0.471	0.115	0.43	0.408	0.011	0.067

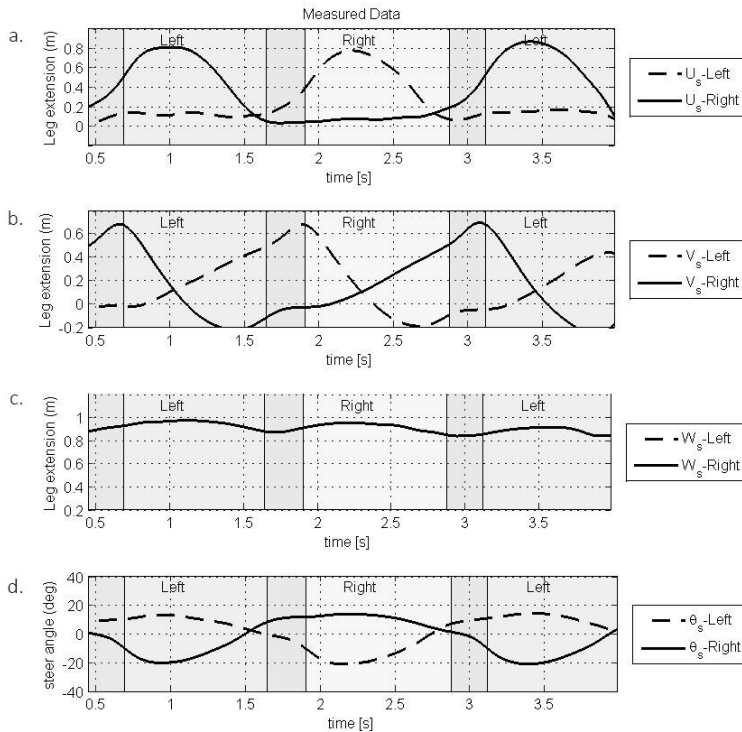


Figure 4.3 Typical example of the (filtered) measured leg extension of a speed skater. The text indicates which skate is active (on the ice). The double stance phase – where both skates are on the ice – is indicated by the vertical lines and the dark grey area.

4. Discussion

The simplified model of a skater proved to mimic the observed forces and motions of a speed skater well. The model can therefore be used to further investigate variables in the skating motion. For this, the input of the model, the leg extension, can be optimized to obtain a maximal forward velocity of the upper body. The leg extension is an indirect measure of the knee flexion-extension, the ankle eversion, the lean angle of the skate, hip abduction and the steering of the skate. Anatomic restrictions and maximum leg extension velocity would be part of the constraints in such an optimization procedure.

The model errors found in the verification process proved to be unrelated to the velocity in the trial or the participant (mass and technique). The differences found between trials are therefore related to the accuracy of the measured data, and the correctness of the estimated data, e.g. air friction; this is further discussed in section 4.2. The model does have two general

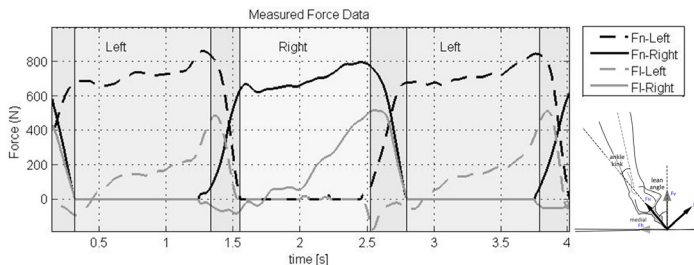


Figure 4.4 Typical example of the (filtered) measured normal (F_n) and lateral (F_l) forces of a speed skater. The text indicates which skate is active (on the ice). The double stance phase – where both skates are on the ice – is indicated by the vertical lines and the dark grey area.

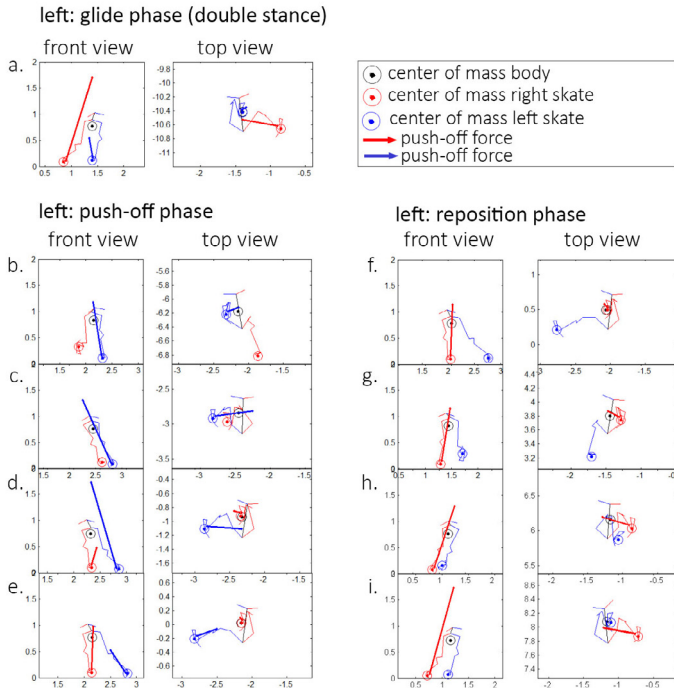


Figure 4.5 Position of the skates relative to the center of mass throughout the speed skating stroke. Focus is on the left (blue) skate. The arrows indicate the force applied on the skate. When the skate does not have an arrow, there is no force on the skate, meaning that it is lifted from the ice (repositioning).

limitations; first the forward velocity, where the model showed to be incapable of simulating the within-stroke fluctuations, and second the underestimation of the forces. Since both limitations also provide insight into the skating mechanics, they are discussed next.

4.1 Swing Leg Error

The fluctuation – or dip – in the measured forward velocity of mass B is probably caused by the swinging leg in repositioning, which was neglected in our simplified model. To get a rough idea on the magnitude of the necessary acceleration of the swinging leg to cause the deceleration and acceleration of the mass B, we simplified the system again in two masses; assume this time that mass 1 (m_1) is the swinging leg and mass 2 (m_2) is the remaining body and the sum of the forces is zero. Then, with the momentum conservation principle, we know that:

$$m_1 \ddot{x}_1 + m_2 \ddot{x}_2 = 0 \quad (4.25)$$

From Dumas, Chèze, & Verriest (2007) most of the predictive equations are ambiguously applicable in the conventional 3D segment coordinate systems (SCSs) we know that the mass of one foot, one shank and one thigh is 0.161 times the body mass. So the ratio for the acceleration of the swinging leg and the rest of the body should be around 0.192; In the data the acceleration of the mass B is around -2 m/s^2 , which requires a 10 m/s^2 acceleration of the swinging leg. This swinging leg reaches accelerations of 12 m/s^2 and could therefore well explain the fluctuation in velocity within the skating stroke. This is an interesting fact, while the swinging leg was, up to now, always neglected in speed skating analyses.

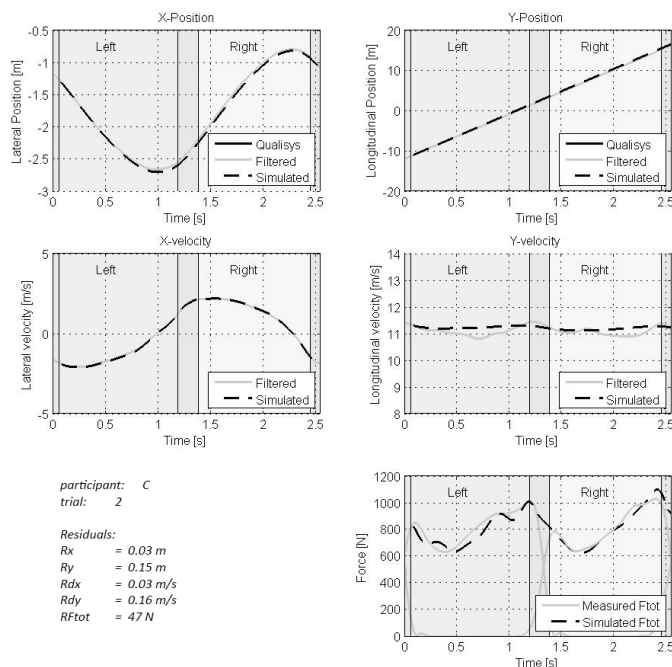


Figure 4.6 Results on the measured and model data of the best fit of the model (C2);

Other simplifications that influence the forward velocity estimation are the negligence of arm movements, body-segment rotations, and change in frontal area (air friction). However their influence is not as large as the one inflicted by the swinging leg. For the arm-movements this was determined in a simple post-hoc analysis, by comparing the model fit of the skaters performing an arm swing (skaters A,B,C) to the skater which kept his arms on his back (skater D) (based on video analysis). Table 4.2 shows us that the model fit of skater D is not better compared to the others, so the HAT segment assumption cannot be of large influence on the model fit.

For the underestimation of the measured force, the cause is less straightforward, while we expect that it is a conjunction of simplifications. The model assumes that all force is directed at mass B, the HAT segment. However, in reality the push-off of the skater is not that utter efficient; ankle eversion and damping in the leg cause that not all the force we measured at the skate is directly addressed to mass B. Some of this is lost to segment rotations or friction, both of which were not accounted for in the model. Furthermore, we neglected the double stance phase, in which both skates are on the ice. The neglected skate – which starts in the glide phase – does not add much force, but will increase the ice friction (although small), and, when placed incorrectly, can cause a force detrimental to the forward velocity (van der Kruk, van der Helm, Schwab, & Veeger, 2016).

4.2 Sensitivity Analysis

In the model, three inputs were kept constant: the mass distribution, the ice friction coefficient and the air friction coefficient (k_1). The sensitivity of the model to these mechanical constants can be determined by changing one of them while keeping the remaining constants fixed. The results of this sensitivity analysis for again B4 and C2 are shown in Figure 4.8. The ice friction coefficient has least impact on the fit, indicating that ice friction has relatively little impact on the skating velocity. The mass distribution coefficient has more impact, but was zero in our verification process and thus close to optimal.

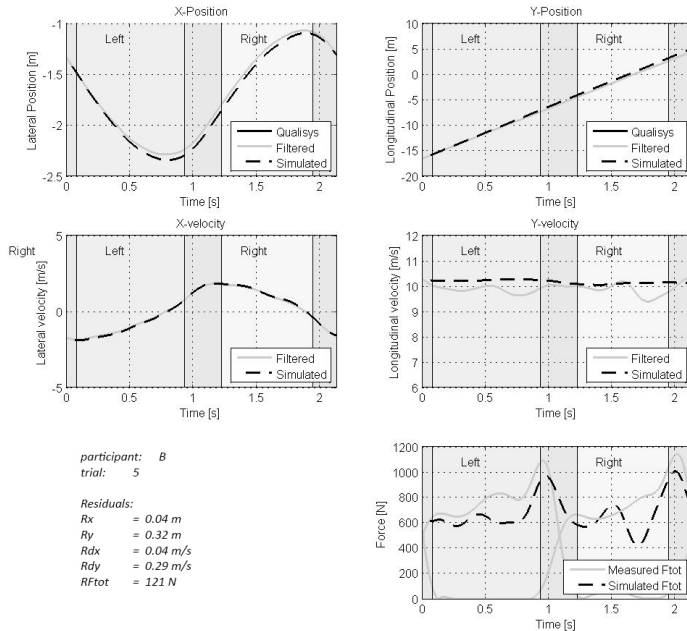


Figure 4.7 Results on the measured and model data of the worst fit of the model (B4);

The model is most sensitive to the air friction coefficient (k_1), which was expected; after all there are power models purely based on this air friction (Jos J de Koning, Foster, Lampen, Hettinga, & Bobbert, 2005). For the verification process, k_1 was kept at a constant value based on previous literature (van Ingen Schenau, 1982). We could, however, also determine the air friction coefficient via optimization of the model, fitting the model to the measured data. The sensitivity analysis shows that the k_1 used in C2 (our best fit) is close to optimal (0.14), while the k_1 used in B4 - our worst fit - could be improved by increasing the coefficient from 0.18 to 0.25. Adjusting k_1 in B4, benefits the estimated y-position and velocity most, while their residuals are respectively reduced from 0.32 m to 0.23 m and 0.29 m/s to 0.23 m/s (a 27% and 21% improvement). The model could therefore benefit from an improved estimation, or measurement, of air frictional forces (Terra, Sciacchitano, & Scarano, 2017).

5. Conclusion

We modelled a speed skater as two point masses, one at the foot and one at the upper body, and used the leg extension (the changing distance between these two masses) and the steering of the skate as input for the model. Verification shows that the model mimics the observed forces and motions well. The model is most accurate for the position and velocity estimation (respectively 1.2% and 2.9% maximum residuals). It is least accurate for the force estimations which, due to simplifications, are underestimated with 4.5–10%. The model can be used to further investigate variables in the skating motion. For this, the input of the model, the leg extension, can be optimized to obtain a maximal forward velocity of the upper body.

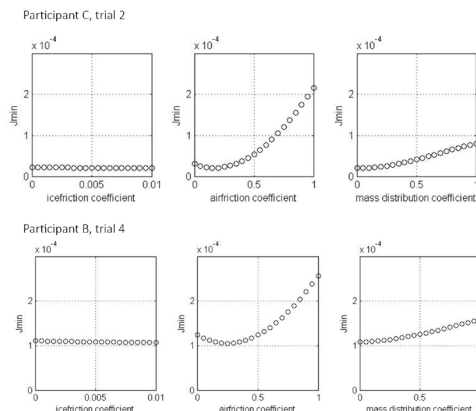


Figure 4.8 Results on the sensitivity analysis for C2 and B4.

Acknowledgement

The authors express their gratitude to Frida Bakkman, Daniel Thompson, Erik Westerström and Marcus Johansson of Qualisys, Wouter van der Ploeg of the KNSB, Andre Zschernig of the company Moticon and Frédérique Meeuwse, Niels Lommers and Jos Koop of the TU Delft and the Hague university of applied sciences for their help and support during the measurements. Also we express gratitude to Thialf for giving us the opportunity of overnight measurements at their rink. Furthermore we thank dr. D.M. Fintelman for her work on this project. This study was supported by the NWO-STW under grant 12870.

References

- Allinger, T. L., & Bogert, A. J. (1997). *Skating technique for the straights based on the optimization of a simulation study. Medicine and Science in Sports and Exercise*, 29, 279–286.
- Bruzzo, J., Schwab, A. L., Valkeapää, A., Mikkola, A., Ohtonen, O., & Linnamo, V. (2016). *A simple mechanical model for simulating cross-country skiing, skating technique. Sports Engineering*, 19(2), 91–104.
- Cabrera, D., Ruina, a., & Kleshnev, V. (2006). *A simple 1+ dimensional model of rowing mimics observed forces and motions. Human Movement Science*, 25(2), 192–220. <http://doi.org/10.1016/j.humov.2005.11.002>
- De Koning, J. J., De Groot, G., & Van Ingen Schenau, G. J. (1992). *Ice friction during speed skating. Journal of Biomechanics*, 25(6), 565–571. [http://doi.org/10.1016/0021-9290\(92\)90099-M](http://doi.org/10.1016/0021-9290(92)90099-M)
- de Koning, J. J., Foster, C., Lampen, J., Hettinga, F., & Bobbert, M. F. (2005). *Experimental evaluation of the power balance model of speed skating. Journal of Applied Physiology*, 98(1), 227–233. <http://doi.org/10.1152/jappphysiol.01095.2003>
- Dumas, R., Chèze, L., & Verriest, J. P. (2007). *Adjustments to McConville et al. and Young et al. body segment inertial parameters. Journal of Biomechanics*, 40(3), 543–553. <http://doi.org/10.1016/j.jbiomech.2006.02.013>
- Eich-Soellner, E., & Führer, C. (1998). *Numerical methods in multibody dynamics (Vol. 45). Springer.*

Fintelman, D. M., Den Braver, O., & Schwab, A. L. (2011). A simple 2-dimensional model of speed skating which mimics observed forces and motions. In *Multibody dynamics, ECCOMAS Thematic Conference, Brugge, Belgium*. (Vol. 511).

Garcia, M., Chatterjee, A., Ruina, A., & Coleman, M. (1998). The simplest walking model: stability, complexity, and scaling. *Journal Biomechanical Engineering*, 120(2), 281–288.

Otten, E. (2003). Inverse and forward dynamics: models of multi-body systems. *Philosophical Transactions of the Royal Society of London B: Biological Sciences*, 358, 1493–1500.

Terra, W., Sciacchitano, A., & Scarano, F. (2017). Aerodynamic drag of transiting objects by large-scale tomographic-PIV. *Experiments in Fluids*, 58(7), 83.

van der Kruk, E., den Braver, O., Schwab, A. L., van der Helm, F. C. T., & Veeger, H. E. J. (2016). Wireless instrumented klapskates for long-track speed skating. *Journal of Sports Engineering*, 19(4), 273–281. <http://doi.org/10.1007/s12283-016-0208-8>

van der Kruk, E., Schwab, A. L., van der Helm, F. C. T., & Veeger, H. E. J. (2017). Getting in shape: reconstructing three-dimensional long-track speed skating kinematics by comparing several body pose reconstruction techniques. Under Review at *Journal of Biomechanics*.

van der Kruk, E., Veeger, H. E. J., van der Helm, F. C. T., & Schwab, A. L. (2015). Two Body Dynamic Model for Speed Skating Driven by the Skaters Leg Extension. In *icSports conference 2015*.

van Ingen Schenau, G. J. (1982). The influence of air friction in speed skating. *Journal of Biomechanics*, 15(6), 449–458. [http://doi.org/10.1016/0021-9290\(82\)90081-1](http://doi.org/10.1016/0021-9290(82)90081-1)

Van Ingen Schenau, G. J. (1981). A power balance applied to speed skating. PhD. thesis. Vrije Universiteit Amsterdam.

Mechanical Power in Speed Skating

PART III

5

Power in Sports: a literature review on the application, assumptions, terminology and validity of mechanical power in sport research.

'If enough people say it, it will eventually become the truth.'
-Ex-director Atari:-

Previous chapter (CH4), explored the key factors in the speed skating technique. One of these key parameters, also repeatedly brought forward by skaters, coaches, and trainers, is power. The definition of power in human movement studies, however, proved to be ruffled up and inconsistent throughout literature. The aim of this chapter is to review the term power in literature.

van der Kruk, E., F.C.T. van der Helm, H.E.J. Veeger & A.L. Schwab, *Power in Sports: a literature review on the application, assumptions, terminology and validity of mechanical power in sport research.* Accepted with revisions at Journal of Biomechanics

Abstract

Mechanical power can provide valuable insight in the capability of athletes to generate power, and in technique factors affecting the effective use of power for performance. Estimates are usually limited by the capabilities of measurement systems, resulting in the use of simplified power models. This review provides a systematic overview of the studies on mechanical power in sports, discussing the application and estimation of mechanical power, the validity of simplifications, and the terminology. The mechanical power balance consists of five parts, joint power, kinetic power, gravitational power, environmental power, and frictional power. Structuring literature based on these power components shows that simplifications in models are done on four levels: single versus multibody models, instantaneous power versus change in energy, the dimensions of a model (1D,2D,3D) and disregarding parts of the power balance. Validation of the simplifications has only been done for running, and shows differences ranging from 10 up to 250% compared to joint power models. Furthermore, inconsistency and imprecision were found in the determination of joint power, resulting from inverse dynamics methods, incorporation of translational joint powers, partitioning in negative and positive work, and power flow over segments. Most inconsistency in terminology was found in the definition and application of external, and internal work, and power. The awareness that these terms are not self-evident and therefore need explanation and interrelation to the complete power equation, will reduce the possibility of errors. Sport research would clearly benefit from structuring and validating the research on mechanical power in sports.

1. Introduction

Mechanical power is a metric often used by sport scientists, athletes, and coaches for research and training purposes. The estimates of mechanical power are usually limited by the capabilities of motion capture systems, resulting in the necessity to use simplified power models. However, due to the introduction of these simplified models, and thus variation, the overview in literature in the terminology and estimation of mechanical power is disordered. Furthermore, the validity of the simplifications is often disregarded.

The inconsistency in the use and definition of power came to our attention, when attempting to estimate the mechanical power balance in speed skating. Although thorough reviews exist addressing the issues of the mechanical power equations (Aleshinsky, 1986; van Ingen Schenau & Cavanagh, 1990) and mechanical efficiency (van Ingen Schenau & Cavanagh, 1990), we found in the (post 1990) literature still inconsistency in the power estimations and terminology. Moreover, the validity of simplifications has usually been disregarded. This not only makes the choice for a proper power model complicated, but also interpretation and comparison to the literature is hampered. Providing insight into the interrelations between the different models, estimations, and assumptions can benefit the interpretation of power results and assist scientists in performing power estimations. A power balance analysis can provide valuable insight in the capability of athletes to generate power, and also in technique factors affecting the effective use of power for performance.

The aim of this study is provide an overview of the existing papers on mechanical power in sports, discussing its application and estimation, the validity of simplifications, and the terminology.

2. Method

A literature search was carried out in July 2017 in the database Scopus. The keywords "mechanical power" and "sport" were used in the search (128 articles) (Search 1). The search was limited to papers in English. Abstracts of the retrieved papers were read to verify whether the article was suited to the aim of the paper, papers that estimated 'power' for a sporting exercise were included (resulting in 94 articles). With these papers, the problems and struggles of power estimation were determined. Three additional searches were performed in August 2017 addressing three specific power estimations, combining the keyword "sport" with

“external power” (30 articles)(Search 2), “internal power” (4 articles) (Search 3), and “joint power” (35 articles) (Search 4), restricted to articles published after 1990. Again, the abstracts of the retrieved papers were read to verify whether the paper was suited for the current review (resulting in respectively 13, 3, and 26 articles).

3. Application of the term power

When the terms mechanical power and sport were used in articles, the scope of the papers can roughly be divided into two categories: the term power was either used as a strength characteristic or performance measure (approximately 75% of the articles), or as an indication of mechanical energy expenditure (muscle power or metabolic power).

The first application was mainly found in fitness and strength studies. Power is then wrongly used as strength measure, attributed to a certain athlete. This would implicate that (peak) mechanical power is a synonym for short-term, high intensity neuromuscular performance characteristic, which is directly related to performance of an athlete. However, firstly, as Knudson (2009) also discusses, a peak power is not a fixed characteristic of a certain athlete: The power estimation in a certain exercise, e.g. the well-known vertical jump (Bosco, Komi, Tihanyi, Fekete, & Apor, 1983), cannot be directly translated into performance of an athlete for different movements. Secondly, while strength is a force measurement, power is a combination of force and velocity (Alberto E Minetti, 2002); these two are not interchangeable.

Power can of course be used as an indication of performance during endurance sports. In cycling practices, power meters (SRM systems) are widely accepted and used as an indication of the intensity of the training or race. Since a SRM system determines power as the product of pedal force and rotational velocity of the sprocket, under the same conditions (e.g. equal frictional and gravitational forces), the cyclist with the highest generated power will be fastest. This is, however, not a matter of course for every sport. For example, power generated by a skater not only generates a forward motion (in line with the rink), but also a lateral one (perpendicular to the rink). The result of this being that the skater that generates most power is not necessarily the fastest one finishing. Technique factors will determine the efficient use of the generated power for propulsion.

This review focusses on the second purpose of power estimation: as indication of mechanical energy expenditure. The relationship between mechanical power, muscle power and metabolic power is shown in Figure 5.1. Metabolic power can be measured by the rate of oxygen uptake, from which the energy expenditure for the complete body in time is estimated. The energy expenditure can be compared with the part of energy that is used for mechanical muscle power. Mechanical power can be determined by applying the laws of classic mechanics to the human body, and by modelling it as a linked segment model consisting of several bodies (Aleshinsky, 1986). Both metabolic power and mechanical power estimates eventually aim to approach muscle power (either via the metabolic or via the mechanical approach), which is closely related to the energy expenditure for the movement. However, mechanical power is far from an exact estimation of muscle power or energy expenditure.

The disparity between mechanical power and muscle power can, next to measurement inaccuracies, be attributed to physiological factors. In a mechanical approach, the part of the muscle power which is degraded into heat or non-conservative frictional forces inside the body or in antagonistic co-contraction is not taken into account (Figure 5.1). Neither is the power against conservative forces taken into account, such as tendon stretch, which in principle can be re-used (van Ingen Schenau & Cavanagh, 1990).

4. Mechanical power equations

Before elaborating on the interpretation of the literature on mechanical power, we first set-up the complete human power balance equations (based on the work of Aleshinsky (1986) and van Ingen Schenau & Cavanagh (1990)) to expound the terminology used in this review. The equations are based on the free body diagram shown in Figure 5.2.

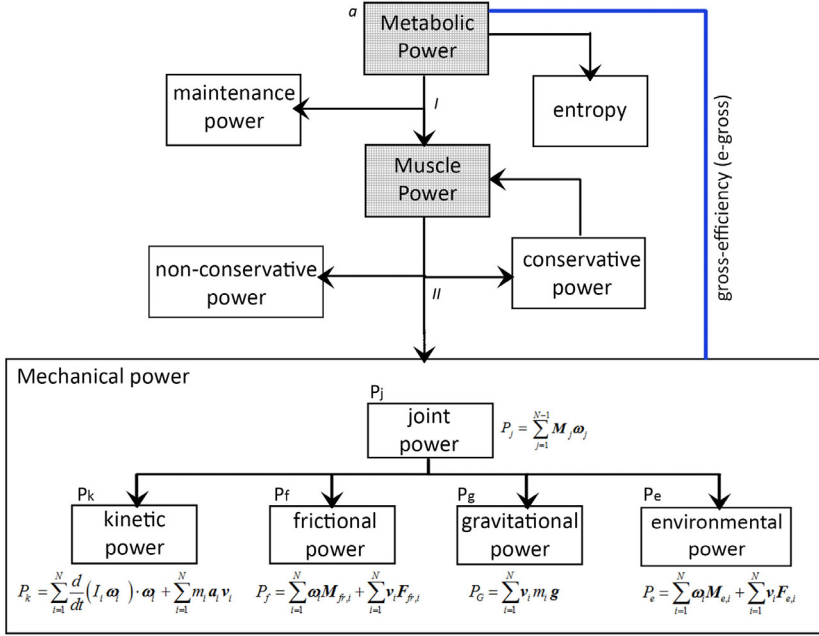


Figure 5.1 The power flow in human movement. Metabolic power is a chemical process, estimated by for example measuring lactate or oxygen uptake (α). Energy distributes into muscle power, maintenance power and entropy. Muscle power results in mechanical power (force times contraction velocity), except for the power that dissipates into heat or non-conservative frictional forces inside the body (or when muscles work against each other), nor the conservative forces, which in principle can be re-used (e.g. tendon stretch). It is possible to convert the mechanical power into an actual estimation of muscle power by the use of musculoskeletal models (II). The mechanical power balance consists of joint power, which is generated by the human, and which results in the kinetic power, which is the rate of change of the kinetic energy, the frictional power, due to e.g. air resistance, the environmental power, which is induced by external forces and moments, and the gravitational power. The mechanical power can therefore be estimated by the joint power alone, or by the combination of kinetic, frictional, environmental and gravitational power. E-gross is the ratio between the expended work (metabolic work) and the performed work (mechanical power).

The human is modelled as a chain of N linked rigid bodies ($N \geq 1$), where each body is identified as a segment with index i . We start by writing down the power balance of every segment and then add them to come to the power balance for the complete system. For a better understanding of the system behaviour we distinguish between the joint power, which is the power generated by the human in the joints, the frictional power losses, the kinetic power, which is the rate of change of the kinetic energy, the gravitational power, and the environmental power, which is the power from external forces and moments. We here use the term environmental power to avoid confusion, since the term external power has been used to describe several different models (e.g. the change in kinetic energy of the center of mass, as well as the power measured with a SRM system in cycling) (see section 5.2.1). Then, for one segment i we can determine these powers from the Newton-Euler equations of motion by multiplying them with the appropriate velocities.

Starting with the translational part, the Newton equations, we get for segment i ,

$$(\mathbf{F}_{j,i} + \mathbf{F}_{G,i} + \mathbf{F}_{f,i} + \mathbf{F}_{e,i}) \cdot \mathbf{v}_i = m_i \mathbf{a}_i \cdot \mathbf{v}_i \quad (5.1)$$

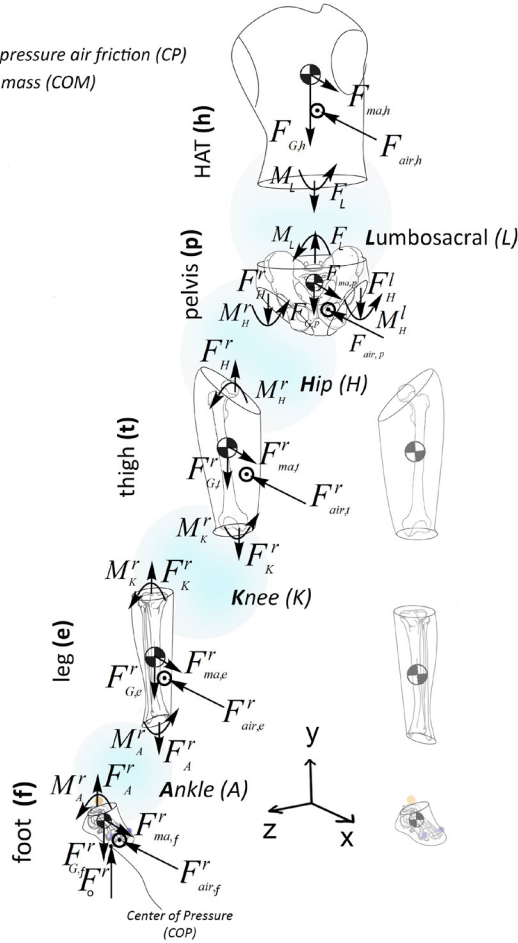


Figure 5.2 Free body diagram of a rigid segment model of a human. The human body is here divided into eight segments; the feet (f), the legs (e), the thighs (t), the pelvis (p) and a HAT (h). The forces acting on the human are the ground reaction forces and the air frictional forces. There are joint forces and moments acting in the Ankle (A), Knee (K), Hip (H) and Lumboseacral (L) joints. Indicated are the Center of Mass (COM) of each segment, the Center of Pressure of the air friction (CP), where the air frictional force acts upon, and the Center of pressure of the ground reaction force (COP).

In which $\mathbf{F}_{j,i}$ are the joint forces, $\mathbf{F}_{G,i}$ are the gravitational forces, $\mathbf{F}_{e,i}$ are the external forces and $\mathbf{F}_{f,i}$ are the frictional forces (e.g. air friction, ice friction). \mathbf{a}_i and \mathbf{v}_i are respectively the linear acceleration and velocity of the segment. We write the translational power balance equation as

$$P_{j,tr,i} + P_{G,tr,i} + P_{f,tr,i} + P_{e,tr,i} = P_{k,tr,i} \quad (5.2)$$

Where $P_{j,tr,i}$, $P_{G,tr,i}$, $P_{f,tr,i}$, $P_{e,tr,i}$ are respectively the translational joint power, the translational gravitational power, the translational frictional power, and the translational environmental

power. $P_{k,ir,i}$ is the translational kinetic power.

For the rotational power we can take the Euler equation of motion, expressed in the global reference system, and multiply by the angular velocities at the segment, to come to the rotational power equation, as in

$$\left(\mathbf{M}_{j,i} + \mathbf{M}_{f,i} + \mathbf{M}_{e,i} \right) \cdot \boldsymbol{\omega}_i = \frac{d}{dt} \left(\mathbf{I}_i \boldsymbol{\omega}_i \right) \cdot \boldsymbol{\omega}_i \quad (5.3)$$

Where $\mathbf{M}_{j,i}$ are the joint moments, $\mathbf{M}_{f,i}$ are the frictional moments, $\mathbf{M}_{e,i}$ are the external moments and $\boldsymbol{\omega}_i$ is the segment angular velocity. We write the power as

$$P_{j,ro,i} + P_{f,ro,i} + P_{e,ro,i} = P_{k,ro,i} \quad (5.4)$$

Next, we add up the rotational and translational segment powers of all segments. The constraint forces in the joints have no contribution to the total power equation, since only relative rotation at the joint between the two segments is assumed (linked segment model), and therefore will drop out of the equation. Joint forces can redistribute energy between segments and links, but not add energy to the total body system (Aleshinsky, 1986). Note however, that if an applied inverse kinematics method allows for translations in the joint, as in Ojeda et al. (2016), or a six degree of freedom joint is applied (e.g. OpenSim, Visual3D), joint forces do play a role and the constraint forces should be accounted for in the power determination (see section 5.1.3).

The total power equations for the system, now written in terms of joint power, gravitational power, frictional power and kinetic power are,

$$P_j = P_k + P_G + P_f + P_e \quad (5.5)$$

In which we have the joint power (P_j) which is directly calculated using the moments at the joint (\mathbf{M}_j) and the rotational velocities around the joint ($\boldsymbol{\omega}_j$), as in

$$P_j = \sum_{i=1}^{N-1} \mathbf{M}_{i,i+1} (\boldsymbol{\omega}_{i+1} - \boldsymbol{\omega}_i) = \sum_{j=1}^{N-1} \mathbf{M}_j \boldsymbol{\omega}_j \quad (5.6)$$

We find the gravitational power in equation 5.5 as in,

$$P_G = \sum_{i=1}^N \mathbf{v}_i m_i \mathbf{g} \quad (5.7)$$

And the frictional power, which consists of translational power and rotational power,

$$P_f = \sum_{i=1}^N \boldsymbol{\omega}_i \mathbf{M}_{fr,i} + \sum_{i=1}^N \mathbf{v}_i \mathbf{F}_{fr,i} \quad (5.8)$$

And the environmental power, which consists of translational power and rotational power,

$$P_e = \sum_{i=1}^N \boldsymbol{\omega}_i \mathbf{M}_{e,i} + \sum_{i=1}^N \mathbf{v}_i \mathbf{F}_{e,i} \quad (5.9)$$

And the change of kinetic energy in the segments:

$$P_k = d \sum \frac{E_{seg}}{dt} = \sum_{i=1}^N \frac{d}{dt} (I_i \boldsymbol{\omega}_i) \cdot \boldsymbol{\omega}_i + \sum_{i=1}^N m_i \mathbf{a}_i \mathbf{v}_i \quad (5.10)$$

In summary, the power balance consists of five parts, joint power, kinetic power, gravitational power, environmental power and frictional power. Joint power is generated by the human, and is the result of muscle power and its metabolic processes. Joint power is therefore closest related to *effort* or *energy expenditure*. This entails that for the most complete estimation of mechanical (human) power either the joint power should be determined directly through measurements of joint torques and angular velocity, or indirectly via the sum of frictional,

kinetic, environmental and gravitational power, P_f, P_k, P_e , and P_G (Figure 5.1). Usually, these terms are approximated depending on the available recording methods, and thereby might introduce a deviation from the total mechanical power.

Instantaneous power (IN) versus change of energy (EN)

Power is the amount of energy per unit of time. In the literature there are, apart from the different models, two different approaches to estimate power. First, what is referred to as instantaneous power (IN): the power balance is used to determine the power at any instant of time (van Ingen Schenau & Cavanagh, 1990). The second approach is by determining the change of kinetic and gravitational energy of a system (EN) over a larger time span, e.g. the cycle time, and divide this over the larger Δt . We know that the kinetic energy at time t is:

$$E_{k,i,t} = \frac{1}{2} m \mathbf{v}_{i,t}^T \mathbf{v}_{i,t} + \frac{1}{2} \boldsymbol{\omega}_{i,t}^T I_{i,t} \boldsymbol{\omega}_{i,t} \quad (5.11)$$

And the gravitational energy at time t :

$$E_{g,i,t} = m \cdot g \cdot y_{i,t} \quad (5.12)$$

Note that EN only estimates average mechanical power, and does not give insight into the power development, or peak powers. Also, oscillatory movements will result in a zero outcome with EN (e.g. walking).

5. Power models in the literature

Based on the mechanical power equations, we sorted the literature of Search 1-3 concerning the estimation of mechanical power as an indication of energy expenditure in Tables 5.1 &

5.2. For each study the power model (P_j, P_k, P_f, P_g, P_e), the estimation approach (IN, EN) and the dimensions (1D, 2D, 3D) are indicated. Results show that simplifications are done on three scales: the number of bodies (single body vs multibody), the measured data (kinematic versus kinetic), and the time interval (IN versus EN). The analysis on results for the literature of Search 4, are given separately in Table 5.3, divided into articles for single joints versus multi-joints, and energy versus power results.

Table 5.1 Structuring of the literature for single body models Indicated are the terminology, the power estimation, the dimensions of the model (1D, 2D, 3D) and whether the power is estimated instantaneously (Instantaneous power (IN)) or via the change in energy over a time span (EN). Inconsistent terminology and oversimplifications are indicated in the final column.

Article	Terminology	Dimensions	P _i	P _{k TRANS}	P _{k ROT}	P _i	P _g	P _e	IN / EN	Comments
SINGLE BODY MODELS										
RUNNING										
(Yanagiyva et al. 2003)	Mechanical power	1						X	IN	velocity of the belt times the horizontal force on the handle bar
(Fukunaga et al. 1981) (sprint)	Forward power	2						X	IN	
(Pantoja et al. 2016) (sprint)	Mechanical power	1	X						IN	
(di Prampero et al. 2014) (sprint)	Mechanical accelerating power	1	X				X		IN	
(Minetti et al. 2011) (skyscraper)	External power (internal power)	1					X		EN	Regression for internal power
(Gaudino et al. 2013) (soccer)	Mechanical power	1	X						EN	Inconsistent terminology: Internal and external work
(Adamantios Arampatzis et al. 2000)	Mechanical power	2		X				X	IN	Inconsistent terminology: Directional power
(Martin et al. 1993)	COM kinematics approach	2	X				X		EN	Oversimplified model: $F_{gft} \times V_{com}$
(Bezodis et al. 2015)	External power	1	X						EN	[Compared to joint power (in same experiment)] +14% mean mechanical power +28% mean mechanical power [compared to joint power (in same experiment)] -47% procent mean mechanical power [compared to joint power in same experiment]
CYCLING										
(Telli et al. 2017)	External power							X	IN	Inconsistent terminology: Internal and external work
(Van Ingen Schenau et al. 1992)	Additional External power	3	X				X		EN	Inconsistent terminology
	External power	1	X				X		EN	
SWIMMING										
(Seifert et al. 2010)	External power, Relative power, absolute power	1					X		IN	Fdrag measured
(Toussaint & Truijens 2005)		1	X				X		-	Theoretical, not measured
(Toussaint & Beek 1992)		1	X				X		-	Theoretical, not measured

Article	Terminology	Dimensions	P _j	P _{k TRANS}	P _{k ROT}	P _t	P _g	P _e	IN / EN	Comments
ROWING (Hofmijster et al. 2008) (Buckeridge et al. 2012) (Hofmijster et al. 2009) (Colloud et al. 2006)	External power	1						X	IN	Integral of handle displacement-handle force curve divided by time. Inconsistent terminology: internal and external power
	External power	1						X	IN	
	Internal Power	1	X							
	External mechanical power							X	IN	
SPEED SKATING (H. Houdijk et al. 2000) (de Koning et al. 2005) (de Koning et al. 1992) (sprint)	External power	1			X				EN	About 20% of the joint power consists of Pk+Pg based on (van der Kruk et al. 2017)
	Power output	1		X	X				EN	
	External Power	1		X	X				EN	
WHEELCHAIR (Mason et al. 2011) (Veege et al. 1991)	External Power Output	1			X				EN	Fdrag measured Fdrag measured
	External power	1			X				EN	
KAYAKING (Jackson 1995)										
(Nakamura et al. 2004)	Internal power	1		X	X				EN	Theoretical, not measured
										Regression function
										Inconsistent terminology: internal and external work
Sideway locomotion (Yamashita et al. 2017a)										
	External power, vertical power, horizontal power, lateral power	2						X	IN	Inconsistent terminology: internal and external work & Directional power
Bench press (Jandacka & Uchytíl 2011) (soccer)		1						X	IN	Vertical velocity of the COM x ground reaction force of the bench to the floor Oversimplified model: Fgrf x Vcom

Table 5.2 Structuring of the literature for multi body models. Indicated are the terminology, the power estimation, the dimensions of the model (1D, 2D, 3D) and whether the power is estimated directly (Instantaneous power (IN)) or via the change in energy over a time span (EN). Deviant terminology is indicated in the last column.

Article	Terminology	Dimensions	P _j	P _{k TRANS}	P _{k ROT}	P _t	P _g	P _e	IN / EN	Comments
MULTIBODY MODELS										
RUNNING										
(Willwacher et al. 2013) (Adamantios Arampatzis et al. 2000)	Joint power	3	X							▪
	Joint power	2	X							
(Martin et al. 1993) (sprint)	Mechanical power	2		X	X		X		IN	Reference 1 (15 segments)
									EN	11% difference in mean mechanical power [compared to joint power in same experiment]
										15 segments
	Joint power	2	X						IN	Reference 2 (14 segments)
	Segments kinematics approach	2		X	X		X		EN	-56% mean mechanical power [compared to joint power in same experiment]
										14 segments
CYCLING										
(De Groot et al. 1994) (Neptune & Van Den Bogert 1997)	Joint power		X							Inconsistent terminology: internal and external work
	Joint power	2	X						IN	
	Internal and external power	2		X	X	X	X		IN	
(Telli et al. 2017)	Internal Power	3		X	X				EN	Relative to COM
										Inconsistent terminology: internal and external work
GOLF										
(McNally et al. 2014)	Joint power	3	X							
WALKING										
69 (Royer & Martin 2005)	Mechanical work	2		X	X		X		EN	

5.1 Simplifications of power models

5.1.1 Single body models

When an athlete is simplified to a single mass, the assumption is that this mass is located at the center of mass (COM) of the full body. Constructing the mechanical power balance (eq. 5.5) for this single body system results in an equation with one body left, the COM, which automatically neglects any relative motions between the segments and the center of mass, and any power related to these motions. Although this single body approach is used quite often (see Table 5.1), validation or estimation of the impact of this simplification has only been performed in two studies, both on running.

A. Arampatzis et al. (2000) (see also Table 5.1) compared four mechanical power models in over-ground running at velocities ranging from 2.5–6.5 m/s. Their results show that the mean mechanical power estimated with the single body model, based on the change in potential and kinetic energy, is 32% higher than the power of the 2D joint power estimation at 3.5m/s running speed. Martin et al. (1993) determined the mechanical power in treadmill running with three methods (see Table 5.1). Based on their results, a single body kinematic approach results in a 47% lower mechanical power estimation compared to joint power, running at 3.35 m/s. Since the neglected frictional power (air friction) at these running speeds is relatively small (<1% of joint power, based on Tam et al. (2012)), the difference between joint power estimation and the kinematic single body estimation is attributed to the neglected relative motions of the segments to the COM and the fact that only kinematic data were used in the single body, which is expected to be less accurate than the combination of force and kinematic data. The difference in results between the two studies is surprising, since the mechanical equations, running speeds, and joint power models (14 versus 15 segments, 2D, absolute per joint) are similar for both studies, while the only difference was the treadmill versus over-ground condition. Unfortunately, A. Arampatzis et al. (2000) do not discuss this difference.

It is clear that, although there is no consensus on whether a single body model under- or overestimates the mechanical power in running (since the absolute is taken, part of the external power could instantaneously be cancelled out by the neglected internal power (see section 5.2.1)), both studies show significant differences between a single body model and a joint power model. Since this is the consequence of disregarding the motions of the segments and kinematic accuracy, validity will likely be different for different movements.

Three studies were found that determined the mechanical power in locomotion with a single body model by multiplication of the measured ground reaction forces times the velocity of the center of mass of the complete body (Arampatzis et al., 2000; Jandacka & Uchytel, 2011; Yamashita, Fujii, Yoshioka, Isaka, & Kouzaki, 2017). Theory of this model lays in the simplification of an athlete to one rigid body being propelled by a force. Therefore, the ground reaction force, which acts on the foot is now shifted to the COM and assumed to cause the movement of the complete (rigid) body. However, although a force can be replaced by a resultant force acting at the COM without changing the motion of the system, the work of the system will divert from the actual work. For example, the ground reaction force in running, acting on the foot, in principle hardly generates power, after all the foot has close to zero velocity (Zelik, Takahashi, & Sawicki, 2015). By assuming that the force acts on the COM of the athlete, the force suddenly generates all power (and therefore work). So although mechanically, with the rigid body assumption, the simplified model is in balance, the validity of modelling an athlete as a point mass (single body) driven by the ground reaction force is highly doubtful. The results of such a model should in no case be interpreted as an indication of muscle power or mechanical energy expenditure, while the relationship with actual joint power is lost by the oversimplification of an athlete.

For single body power estimations, both IN approaches (e.g. Pantoja et al. 2016; di Prampero et al. 2014; Seifert et al. 2010) and EN approaches (e.g. Minetti et al. 2011; Gaudino et al. 2013; Houdijk et al. 2000) were found. An EN approach results in an average mechanical power

estimate. Consequently, there is no insight into the course of power during the motion cycle, e.g. peak power, but also oscillatory motions are neglected, which are tricky assumptions for several sports like running, cycling, swimming, etc. This certainly applies for speed skating at constant speed where the mean kinetic and gravitational power on a straight part is zero, as there is usually no forward acceleration. Using the EN approach causes that both the lateral and upward oscillatory motion (zig-zag motion of the upper body) are not incorporated in the estimation. However, the kinetic and gravitational power related to these oscillatory motions, appeared to account for almost 20% of the joint power (van der Kruk, Schwab, & van der Helm, 2017). Therefore, assumptions on ignoring velocity fluctuations, or motions that do not directly contribute in the forward motion, should be well validated. Especially when working with top-athletes or highly technical sports, these components could be the key-factors in an athlete's performance, therefore IN models seem more appropriate than EN models for understanding performance (Caldwell & Forrester, 1992).

5.1.2 Multibody models

Using a multi-body approach is much more complex than the single body approach, since the motion of the separate body parts needs to be measured. Benefit is that the power per segment gives insight into the distribution of power over the body. In the kinematic approach, only kinematic data are used to indirectly estimate joint power: frictional power, kinetic power and gravitational power (, and). The main difference with the joint power estimation, is therefore the absence of force data. Furthermore, in the kinematic approach frictional power is neglected in running and walking studies, and gravitational power in cycling studies.

The studies by A. Arampatzis et al. (2000) and Martin et al. (1993), which were mentioned earlier, enable the comparison of a kinematic multi-body approach, which resulted in respectively 10% more mechanical power and 56% less mechanical power when compared to the joint power estimation (at respectively 3.5 m/s and 3.35 m/s) (Table 5.2). Again, their results are contradictory and largely diverge in magnitude. However, the results do stress the need of accurate kinematic measurements in the models. The kinetic-based expressions of effort correlated better with the aerobic demand than kinematic-based expressions (Martin et al., 1993).

5.1.3 Joint Power

Since we found several inconsistencies in estimating joint power in the articles of Search 1-3 (see Table 5.2), we performed a specific search for joint power (Search 4). Analysis of these studies lets us identify three classes of differences in joint power estimation: the inverse dynamics method, the degrees of freedom of the joints and the estimation of mechanical energy expenditure (MEE) (see Table 5.3).

Joint power estimation requires the determination of joint moments and forces via an inverse dynamics method. Although several methods exist to estimate joint moments (e.g. Dumas, Rachid, & Guise, 2004; Kuo, 1998; van der Kruk et al., 2017), the bottom-up approach (Elftman, 1939; Miller & Nelson, 1973; Winter, 2009) is still the most applied method, and referred to as the 'standard inverse dynamics method' or 'Newton(-Euler) inverse dynamics approach' without citing further reference. However, since the bottom-up approach can leave large residuals at the trunk and the joint power is largely influence by the inverse dynamics method (up to 31%) (van der Kruk et al., 2017), there should be more attention towards this part of the power estimation.

A second class of difference was found in the degrees of freedom of the joint. If translation is allowed in the joints, the joint forces suddenly generate power (see eq. 5.2). Application of 6 DOF joints, and therefore incorporation of translational joint power is more common, due to the ever more detailed 3D human joint models (e.g. OpenSim, Visual3D); The effect of these forces on the joint power, and whether the translations are not part of residuals of the choice in inverse kinematics method, rather than a physiological phenomenon falls outside of the

scope of this review (Ojeda et al., 2016; Zelik, Takahashi, & Sawicki, 2015). However, we want to make the reader aware that differences do occur and thereby influence the joint power estimations, where the increase in complexity will not automatically imply improvement.

The third class of difference was found in the integration of joint power to work (mechanical energy expenditure). For the power in a single joint, a separation is made between negative and positive power. Negative power occurs when the moment around the joint is opposite to the angular velocity of the joint, which would denote braking (dissipation of energy). With only mono-articular muscles, this would imply the production of eccentric power. However, bi-articular muscles can 'transfer' power to adjacent joints. Translating power into work is done by taking the integral of the power curve over time. In the literature, the division is made between positive work and negative work (Hamill, Gruber, & Derrick, 2014; Schache et al., 2011; Sorenson et al., 2010; Yeow, Lee, & Goh, 2009). This is done, since, from a biomechanical perspective, it is assumed that, for negative muscle work (or eccentric muscle contraction), the metabolic cost is lower than for positive muscle power requiring concentric muscle contraction. However, there is no general consensus on the exact magnitude of this difference. Caldwell & Forrester (1992) even argue that the division into positive and negative work should be rejected, since mechanical power is an indication of muscle power, not metabolic cost and thus 1 J of negative power reflects 1 J of positive power. However, currently the general consensus is to separate negative from positive work; musculoskeletal simulations might shed light on the difference in magnitude in the future.

For power estimation in multiple joints, the estimation of MEE becomes more complicated due to the power flow between segments (and thus joints); bi-articular muscles activations can induce both negative and positive power simultaneously around adjacent joints (Van Ingen Schenau & Cavanagh, 1990). When no power flow is assumed, the integral of the absolute joint power per joint is taken and summed over the joints (Attenborough, Smith, & Sinclair, 2012). If power flow is assumed, the joint powers are first summed over the joints and then the integral over time is taken, again allowing for the separation of negative and positive power (Devita, Hunter, & Skelly, 1992; Lees, Vanrenterghem, & De Clercq, 2006). What the best approach is, has yet to be determined. Hansen (2003) found in cycling that the energy expenditure was most accurately measured with a model that allowed for energy transfer only between segments of the same limb. Articles that do not report the method for MEE estimation are inappropriate for comparison (e.g. (Greene, Sinclair, Dickson, Colloud, & Smith, 2013)), since the difference between the two methods can go up to >2.5x the MEE (measured in running (Martin et al. (1993))). Note that this power flow issue not only accounts for the estimation of joint power over several joints, but also for power transfer between segments in other kinematic multi-body models (Willems, Cavagna, & Heglund, 1995).

5.2 Inconsistent Terminology

5.2.1 Internal and external work

The terms internal and external power and work are often used. However, these terms are ill-defined, terminology is inconsistent, and the actual purpose of separation is dubious. We will discuss these issues by considering a simple 2D two-link model (Figure 5.3). The mechanical power equations of this simple model can be divided into external powers and internal powers. We here employ the definition of internal power as the energy changes of the segments, relative to the center of mass of the complete body (Aleshinsky, 1986). The power equation for this model can be divided as follows:

$$\frac{dE}{dt} = \frac{d}{dt} \left\{ \frac{M(\dot{x}_{com}^2 + \dot{y}_{com}^2)}{2} + M \cdot g \cdot \dot{y}_{com} \right\} + \frac{d}{dt} \left\{ \sum_{i=1}^N \left[\frac{m_i(\dot{x}_{ci/com}^2 + \dot{y}_{ci/com}^2)}{2} + \frac{I_{ci}\dot{\phi}_i}{2} \right] \right\} =$$

$$\boxed{F_o^x \dot{x}_{com} - F_d^x \dot{x}_{com} + F_o^y \dot{y}_{com} - F_d^y \dot{y}_{com}} + \boxed{F_o^x \dot{x}_{ol/com} + F_o^y \dot{y}_{ol/com} + \left[\sum_{i=1}^{N-1} M_{1,2}(\dot{\phi}_2 - \dot{\phi}_1) \right] + M_o \dot{\phi}_1} \quad (5.13)$$

Table 5.3 Articles found with the search terms joint power and sport. The literature was divided into estimating power or energy of a single joint, and power and energy of multiple joints. Noted are the applied inverse dynamics technique with reference (N.M. = not mentioned). For the energy estimation, the conversion from power to energy is given and whether positive and negative work are separated. Articles are sorted on year of publication.

JOINT POWER				
Power per joint	Movement	Inverse dynamics method		
(Paquette et al. 2017)	running	"Newtonian inverse dynamics"	N.M.	
(Middleton et al. 2016)	cricket	"Standard inverse dynamics analysis"	N.M.	
(Barratt et al. 2016)	cycling	Inverse dynamics method	(Elftman 1939)	
(Pauli et al. 2016)	Squats, jumps	N.M.	N.M.	
(Van Lieshout et al. 2014)	exercises	N.M.	N.M.	
(Creveaux et al. 2013)	tennis	[Method is fully described in paper]	n.a.	
(Kuntze et al. 2010)	badminton	N.M.	N.M.	
(Riley et al. 2008)	running	"Vicon plug-in-gait"	Vicon	
(Dumas & Cheze 2008)	gait	"Inverse dynamics based on wrenches and quaternions"	(Dumas et al. 2004)	
(Vanrenterghem et al. 2008)	jumping	N.M.	N.M.	
(Schwameder et al. 2005)	walking	"Standard 2D inverse dynamics routine"	N.M.	
(Rodacki & Fowler 2001)	Exercise	"Newtonian equations of motion"	N.M.	
(Jacobs & van Ingen Schenau 1992)	sprint	"Linked segment model"	(Elftman 1939)	
(Houdijk et al. 2000)	Speed Skating	"An inverse dynamics analysis"	N.M.	
Energy per Joint	Movement	Inverse dynamics method		
(Schache et al. 2011)	running	"A standard inverse dynamics technique"	(Winter 2009)	Power to work integral of joint power over time N.M.
(Hamill et al. 2014)	running	"Newton-Euler inverse dynamics approach"	N.M.	Not absolute (pos and neg work)
(Sorenson et al. 2010)	Jump	Inverse Dynamics	Visual 3d	Not absolute (pos and neg work)
(Yeow et al. 2010; Yeow et al. 2009)	Landing jump	N.M.	N.M.	Not absolute (pos and neg work)
Power multiple joints	Movement	Inverse dynamics method		
(Strutzenberger et al. 2014)	cycling	"Sagittal plane inverse dynamics"	Visual 3D	sum of ankle, knee and hip powers -

Energy multiple joints	Movement	Inverse dynamics method		Power to work	Absolute
(Greene et al. 2013; Greene et al. 2009) (Attenborough et al. 2012)	rowing	Custom program	(Winter 2009)	Sum of the joint mechanical energy	N.M.
	rowing	Inverse dynamics	(Winter 2009)	Integration of the absolute value of the power time series curve for each joint	Absolute per joint
(Lees et al. 2006)	jumping	"Inverse dynamics using standard procedures"	(Miller & Nelson 1973), (Winter 2009)	Time integral per joint 'Standard procedure', (de Koning & van Ingen Schenau 1994); sum of left and right limb;	Not absolute (pos and neg work)
(Devita et al. 1992)	running	"An inverse dynamics method"	N.M.	Resultant joint powers around hip, knee and ankle joint were summed at each time point.	Not absolute (pos and neg work)
(Houdijk et al. 2000)	Speed Skating	"An inverse dynamics analysis"	N.M.	Integrating joint power over time	N.M.

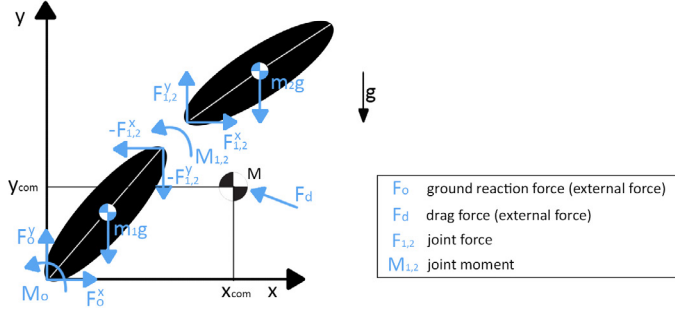


Figure 5.3 Free body diagram of a two-link segment body

in which the parts in the blue boxes represent the external powers, and the parts in the green boxes the internal powers. Note that the external force F_o acts at O , and:

$$\dot{x}_o = \dot{x}_{com} + \dot{x}_{o/com}; \quad \dot{y}_o = \dot{y}_{com} + \dot{y}_{o/com} \quad (5.14)$$

Although these equations show that the system energy can be presented as a sum of external and internal power, the total work is *not equal* to the sum of the 'internal' and 'external' work (Aleshinsky, 1986; Zatsiorsky, 1998). Take into consideration that:

$$\dot{x}_{com} = \dot{x}_o - \dot{x}_{o/com}; \quad \dot{y}_{com} = \dot{y}_o - \dot{y}_{o/com} \quad (5.15)$$

If we then determine work (or mechanical energy expenditure) by taking the absolute integral of the power equations separated into internal and external power, we obtain:

$$\begin{aligned} & \int_{T_1}^{T_2} \left| \frac{d}{dt} \left\{ \frac{M(\dot{x}_{com}^2 + \dot{y}_{com}^2)}{2} + M \cdot g \cdot \dot{y}_{com} \right\} \right| dt + \int_{T_1}^{T_2} \left| \frac{d}{dt} \left\{ \sum_{i=1}^N \left[\frac{m_i(\dot{x}_{ci/com}^2 + \dot{y}_{ci/com}^2)}{2} + \frac{I_{ci} \dot{\phi}_i}{2} \right] \right\} \right| dt \neq \\ & \int_{T_1}^{T_2} \left| F_o^x \dot{x}_o - F_d^x \dot{x}_{com} + F_o^y \dot{y}_o - F_d^y \dot{y}_{com} - F_o^x \dot{x}_{o/com} - F_o^y \dot{y}_{o/com} \right| dt + \\ & \int_{T_1}^{T_2} \left| F_o^x \dot{x}_{o/com} + F_o^y \dot{y}_{o/com} + \left[\sum_{i=1}^{N-1} M_{1,2} (\dot{\phi}_2 - \dot{\phi}_1) \right] + M_o \dot{\phi}_1 \right| dt \end{aligned} \quad (5.16)$$

As mentioned by Aleshinsky in 1986, there are external forces () inside the 'internal' work, therefore the internal and external work are not independent measures. Moreover, the absolute values (due to positive and negative work) destroy the balance. Members of the expressions in the internal and external work, are powers which regularly fluctuate out of phase, thereby cancelling each other out. By treating them as independent measures, the work doubles instead of cancelling out, while in reality these powers do not cost any energetically charge (e.g. pendulum motion). Replacing an actual system of forces applied to a body by the resultant force and couple does not change the body motion. It can change, however, the estimation of performed work. Therefore, the power of the external forces as a hypothetical drag force, when assumed this acts at the COM, can be seen separate from the internal power (there is no relative velocity between the point of application of the force and the COM). However, ground reaction forces, or any other forces with a point of application different from the COM will be part of both the 'internal' and 'external' work, and therefore are not independent measures (see also section 5.1.1).

Despite the mechanical incorrectness of the separation of internal from external work, and

the discussion involving these measures (van Ingen Schenau, 1998; Zatsiorsky, 1998), more recent publications still make this distinction (e.g. Minetti et al. 2011; Nakamura et al. 2004), raising the question what the benefit is of separating the mechanical energy into internal and external energies if the separation is mechanically incorrect? In cases where the whole power balance is estimated, there seems no point in dividing the power in internal and external power or work. This separation has not given additional useful insight into human power performance so far. Only application of the separation could be when a single body model is used and therefore only external power can be measured. The balance ratio between internal and external power can then be used to provide insight into the validity of the simplification.

Adding to the confusion of the interpretation of external and internal power, is the inconsistent use of the terms. The use of the term 'internal' is logically diffuse, while it might refer to muscular or metabolic work (Williams, 1985). In this literature review, two articles were found that used the internal power for estimations different from the definition given above, defining internal mechanical power loss as the part of power absorbed by the muscles that is lost to heat (estimated as fluctuations in kinetic energy of the back and forth moving of the rower on an ergometer) (Hofmijster, Van Soest, & De Koning, 2009), or the total energy required to move segments (Neptune & Van Den Bogert, 1997). However, more models and interpretations of internal power have been published, that all largely (up to 3x) differ in power output estimation (Hansen, Jørgensen, & Sjøgaard, 2004).

Also the term external power is inconsistently used. Aleshinsky (1986) defined the term as the change in energy of the center of mass of the athlete, and can therefore be seen as a single body model. The origin of the term lies in the assumption that the human generates power only to overcome external forces (e.g. air friction, ground friction). In speed skating (Houdijk et al. 2000; de Koning et al. 1992), wheelchair sports (Mason, Van Der Woude, De Groot, & Goosey-Tolfrey, 2011; Veeger, Yahmed, Van Der Woude, & Charpentier, 1991) and swimming (Seifert et al., 2010), the term external power is used for the estimation of frictional power (P_f), assuming that, under constant velocity, this is equal to the power generated by the human. In rowing (Buckeridge, Hislop, Bull, & McGregor, 2012; Colloud, Bahuaud, Doriot, Champely, & Chèze, 2006; Hofmijster, Van Soest, & De Koning, 2008) and cycling (Telli, Seminati, Pavei, & Minetti, 2017), where ergometers are available, the term external power is used to describe the power output measured by the ergometer, what we define as environmental power (P_e). Note however, that the power output measured with an ergometer or a SRM system is not necessarily the same as the COM movement. If a cyclist stops pedalling on an ergometer but moves his or her upper body up and down, there is a COM movement (due to joint power), but there is no power measured at the ergometer (P_e) (the cyclist of course does not have to stop pedalling for the same effect). In running and walking, where the frictional power is only marginal and environmental power in principle is zero, the term external power is used to describe the change in kinetic energy (P_k) (Bezodis, Salo, & Trewartha, 2015) and/or gravitational energy (P_g) (Minetti et al., 2011) of the COM, but also for an estimation done by multiplication of the ground reaction forces times the COM velocity (see section 5.1.1 on the validity of this model). More interpretations of external power can be found in Table 5.1.

So even though the term external power is well known and frequently used, the estimation is not straightforward and interrelations are not always clear. The terms internal and external power can, however, be structuralized and classified by the mechanical power balance from section 3, as was done in Table 5.1 and 5.2. We propose a standard in section 6.

5.2.2 Directional power

In the studies on running and walking, we found many power terms related to some sort of direction: forward power, lateral power, etc. (see Table 5.1 and 5.2). Since power is a scalar, it is in principle incorrect to give the power a certain direction, although of course the forces and velocities related to power have a direction. The separation of the mechanical power equations into these different directions is actually not beneficial. Take for example a situation

where there is no environmental power acting on the human e.g. walking; in that situation the power equation simplifies to:

$$\frac{d}{dt} \left\{ \frac{M(\dot{x}_{com}^2 + \dot{y}_{com}^2)}{2} + M \cdot g \cdot \dot{y}_{com} \right\} + \frac{d}{dt} \left\{ \sum_{i=1}^N \left[\frac{m_i(\dot{x}_{cilcom}^2 + \dot{y}_{cilcom}^2)}{2} + \frac{I_{ci}\dot{\phi}_i}{2} \right] \right\} = \left[\sum_{i=1}^{N-1} M_{i,i+1}(\dot{\phi}_{i+1} - \dot{\phi}_i) \right]$$

(5.17)

17)

Although the translational left side of this equation can be divided into terms related to a certain translational direction, the eventual power production, on the right side of this equation, cannot be separated into these directions. Separating the left side of the equation into directional terms, is completely dependent on the chosen global frame; moreover, 'vertical' power can very easily be translated into a 'lateral power' without adding power to the system, e.g. due to centrifugal forces.

5.3 E-gross

This review clearly showed that there arise large differences in mechanical power estimation based on the choice for a model. This also impacts the metabolic power research studies when gross-efficiency is used (e-gross), which is the ratio between the expended work (metabolic work) and the performed work (mechanical work). E-gross is often determined in a lab, using VO₂-measurements, to convert mechanical power into energy expenditure (EE). Main causes in the differences among athletes and inaccuracies in measurement of e-gross are searched in the metabolic side of the equation. However, determination of the mechanical power with simplified models influences the e-gross estimation evenly well. When only part of the mechanical power balance is determined, for example with a single body model, the dependency of e-gross to the relative movements of the segments is neglected (e.g. de Koning et al. (2005)). If an athlete would then change movement coordination (technique) between the submaximal experiment (where e-gross is set) and the actual experiment, the change in segment motion is neglected in the mechanical power and thus in the metabolic power estimation. Especially for technique dependent sports (e.g. swimming, speed skating), this seems an important fact.

6. Discussion

This review provided an overview of the existing papers on mechanical power in sports, discussing the application and the estimation of mechanical power, the validity of simplifications, mechanically inconsistent models, and the terminology on mechanical power. Structuring the literature shows that simplifications in models are done on four levels: single vs multibody models, instantaneous power (IN) versus change in energy (EN), the dimensions of a model (1D,2D,3D) and neglecting parts of the power balance. Except for the difference between single versus multibody model in running, no studies were found that validated or quantified the consequences of simplifying the mechanical power balance in sport. Furthermore, inconsistency was found in joint power estimations between studies in the applied inverse dynamics methods, the incorporation of translational joint power, and the integration of joint power to energy. Both the validation of simplification of models and the lack of a general method for joint power or work are research areas well worth investigating. These topics could be addressed with accurate musculoskeletal models.

The terms internal power and external power/work are, apart from the discussion on the actual usefulness (and validity in case of energy) of the separation, confusing, since several meanings were attributed to the terms. The interrelations between the different interpretations of external power have been discussed here. We argue to abolish the terms internal, and external power, and work by replacing them with the terms from the power balance: joint power (eq. 5.6), gravitational power (eq. 5.7), frictional power (eq. 5.8), environmental power (eq. 5.9) and kinetic power (eq. 5.10). In case the power due to motion of the COM and

due to motion of the segments relative to the COM are to be separated for measurement conveniences, we propose to work with the term Peripheral Power for moving body segments relative to the COM (Riddick & Kuo, 2016; Zelik & Kuo, 2012). Note however, that these should not be interpreted as separate energy measures (work). The awareness that terms internal and external work/power are not self-evident and therefore need explanation and interrelation to the complete power equation, will reduce the possibility of errors and increase the comprehension for the reader.

To quote (E. M. Winter et al., (2016): ‘if sport and exercise science is to advance, it must uphold the principles and practices of science’. This review only revealed the tip of the iceberg of the studies concerned with estimating power in sport (the search term power and sport results in 9,751 articles (August 2017)), but illustrates clearly that the sport literature would benefit from structuring and validating the research on (mechanical) power in sports. By structuring the existing literature, we identified some obstacles that may hamper sport research from making headway in mechanical power research.

7. Conclusions

- Power is not a direct translation of performance
- Mechanical power is not a direct estimation of muscle power or (when integrated) energy expenditure for movement.
- Mechanical power is estimated via the joint power directly, or via the sum of kinetic, frictional, gravitational and environmental power; all other estimations are simplifications.
- Due to limitations in human motion capture in sports, simplified models are employed to determine power. Simplifications in models are done on four levels: single vs multibody models, instantaneous power (IN) versus change in energy (EN), the dimensions of a model (1D,2D,3D) and neglecting parts of the power balance.
- Single body models by definition neglect the relative motion of the separate body segments to the CoM of the body. The resulting underestimation in power, as an indication of muscle power, is rarely determined in sports, whereas this part of power is an essential part of the power balance in technique driven sports as e.g. speed skating, swimming or skiing.
- IN models are more appropriate than EN models for understanding performance of elite athletes. EN automatically results in determination of average power and therefore negligence of any oscillatory movements.
- Little attention is given to the chosen inverse dynamics technique to estimate joint moments and forces, although its influence on joint power estimation is large (e.g. 31% in speed skating).
- When 6DOF joints are applied (e.g. OpenSim, Visual3D), joint forces not only distribute energy, as in the classical 3DOF joint rotational models, but also allow for translational power; Sport researchers should be aware of the differences between these joint power estimations.
- There is no consensus on how negative and positive work in a single joint should be summed. On the same note, there is no standard on whether to allow for energy flow between joints. The chosen approach is not always clear from the articles, although factors of 2.5x difference between approaches have been found.
- The terms external and internal power and work are inconsistent. The terms can easily be replaced by the terms joint power, kinetic power, gravitational power, frictional power and environmental power mentioned in the power balance of this review paper, which will avoid future confusion.
- Gross-efficiency (e-gross) is not constant within and between athletes. Apart from metabolic causes, this can also be caused by the procedure of mechanical power determination.

References

Aleshinsky, S. Y. (1986). An energy “sources” and “fractions” approach to the mechanical energy expenditure problem- II. movement of the multi-link chain model. *Journal of Biomechanics*, 19(4).

Arampatzis, A. et al., 2000. Mechanical power in running: a comparison of different approaches. *Journal of Biomechanics*, 33(4), pp.457–463. Available at: <http://www.scopus.com/inward/record.url?eid=2-s2.0-0033968709&partnerID=tZOtx3y1> [Accessed September 27, 2015].

Arampatzis, A. et al., 2000. Mechanical power in running: A comparison of different approaches. *Journal of Biomechanics*, 33(4).

Attenborough, A.S., Smith, R.M. & Sinclair, P.J., 2012. Effect of gender and stroke rate on joint power characteristics of the upper extremity during simulated rowing. *Journal of Sports Sciences*, 30(5).

Barratt, P.R. et al., 2016. Effects of pedal speed and crank length on pedaling mechanics during submaximal cycling. *Medicine and Science in Sports and Exercise*, 48(4).

Bezodis, N.E., Salo, A.I.T. & Trewartha, G., 2015. Relationships between lower-limb kinematics and block phase performance in a cross section of sprinters. *European Journal of Sport Science*, 15(2).

Bosco, C. et al., 1983. Mechanical power test and fiber composition of human leg extensor muscles. *European Journal of Applied Physiology and Occupational Physiology*, 51(1).

Buckeridge, E. et al., 2012. Kinematic asymmetries of the lower limbs during ergometer rowing. *Medicine and Science in Sports and Exercise*, 44(11).

Caldwell, G.E. & Forrester, L.W., 1992. Estimates of mechanical work and energy transfers: Demonstration of a rigid body power model of the recovery leg in gait. *Medicine and Science in Sports and Exercise*, 24(12).

Colloud, F. et al., 2006. Fixed versus free-floating stretcher mechanism in rowing ergometers: Mechanical aspects. *Journal of Sports Sciences*, 24(5).

Creveaux, T. et al., 2013. Joint kinetics to assess the influence of the racket on a tennis player's shoulder. *Journal of Sports Science and Medicine*, 12(2).

Devita, P., Hunter, P.B. & Skelly, W.A., 1992. Effects of a functional knee brace on the biomechanics of running. *Medicine and Science in Sports and Exercise*, 24(7).

Dumas, R. & Cheze, L., 2008. Hip and knee joints are more stabilized than driven during the stance phase of gait: An analysis of the 3D angle between joint moment and joint angular velocity. *Gait and Posture*, 28(2).

Dumas, R., Rachid, A. & Guise, J.A. de, 2004. A 3D generic inverse dynamic method using wrench notation and quaternion algebra. *Computer methods in biomechanics and biomedical engineering*, 7(3), pp.159–166.

Elftman, H.O., 1939. Forces and energy changes in the leg during walking. *American Journal of Physiology*, 125(2), pp.339–356. Available at: <http://ajplegacy.physiology.org/>

content/125/2/339.

Fukunaga, A., Matsuo, A. & Ichikawa, M., 1981. Mechanical energy output and joint movements in sprint running. *Ergonomics*, 24(10).

Gaudino, P. et al., 2013. Biomechanics and predicted energetics of sprinting on sand: Hints for soccer training. *Journal of Science and Medicine in Sport*, 16(3).

Greene, A.J. et al., 2009. Relative shank to thigh length is associated with different mechanisms of power production during elite male ergometer rowing. *Sports Biomechanics*, 8(4).

Greene, A.J. et al., 2013. The effect of ergometer design on rowing stroke mechanics. *Scandinavian Journal of Medicine and Science in Sports*, 23(4).

De Groot, G. et al., 1994. Power, muscular work, and external forces in cycling. *Ergonomics*, 37(1).

Haakonssen, E.C. et al., 2013. Energy expenditure of constant- and variable-intensity cycling: Power meter estimates. *Medicine and Science in Sports and Exercise*, 45(9).

Hamill, J., Gruber, A.H. & Derrick, T.R., 2014. Lower extremity joint stiffness characteristics during running with different footfall patterns. *European Journal of Sport Science*, 14(2).

Hansen, E.A., Jørgensen, L.V. & Sjøgaard, G., 2004. A physiological counterpoint to mechanistic estimates of "internal power" during cycling at different pedal rates. *European journal of applied physiology*, 91(4), pp.435–442.

Hofmijster, M.J., Van Soest, A.J. & De Koning, J.J., 2009. Gross efficiency during rowing is not affected by stroke rate. *Medicine and Science in Sports and Exercise*, 41(5).

Hofmijster, M.J., Van Soest, A.J. & De Koning, J.J., 2008. Rowing skill affects power loss on a modified rowing ergometer. *Medicine and Science in Sports and Exercise*, 40(6).

Hopker, J.G. et al., 2012. Reliability of cycling gross efficiency using the douglas bag method. *Medicine and Science in Sports and Exercise*, 44(2).

Houdijk, H. et al., 2000. Physiological responses that account for the increased power output in speed skating using klapskates. *European Journal of Applied Physiology*, 83(4–5), pp.283–288.

Houdijk, H. et al., 2000. Push-off mechanics in speed skating with conventional skates and klapskates. *Medicine and science in sports and exercise*, 32(3), pp.635–641.

van Ingen Schenau, G.J., 1998. Positive work and its efficiency are at their dead-end: comments on a recent discussion. *Journal of biomechanics*, 31(2), pp.195–197.

Van Ingen Schenau, G.J. & Cavanagh, P.R., 1990. Power equations in endurance sports. *Journal of Biomechanics*, 23(9), pp.865–881.

Van Ingen Schenau, G.J., De Koning, J.J. & De Groot, G., 1992. The distribution of anaerobic energy in 1000 and 4000 metre cycling bouts. *International Journal of Sports Medicine*, 13(6).

Jackson, P.S., 1995. Performance prediction for olympic kayaks. *Journal of Sports Sciences*,

13(3).

Jacobs, R. & van Ingen Schenau, G.J., 1992. Intermuscular coordination in a sprint push-off. *Journal of Biomechanics*, 25(9), pp.953–965. Available at: <https://www.scopus.com/inward/record.uri?eid=2-s2.0-0026928534&partnerID=40&md5=1f747a5ef58b1d855ce7a121be90a1a6>.

Jandacka, D. & Uchytíl, J., 2011. Optimal load maximizes the mean mechanical power output during upper extremity exercise in highly trained soccer players. *Journal of Strength and Conditioning Research*, 25(10).

Knudson, D.V., 2009. Correcting the use of the term “power” in the strength and conditioning literature. *Journal of Strength and Conditioning Research*, 23(6).

de Koning, J.J. et al., 2005. Experimental evaluation of the power balance model of speed skating. *Journal of Applied Physiology*, 98(1), pp.227–233.

de Koning, J.J., de Groot, G. & van Ingen Schenau, G.J., 1992. A power equation for the sprint in speed skating. *Journal of Biomechanics*, 25(6), pp.573–580.

de Koning, J.J. & van Ingen Schenau, G.J., 1994. On the Estimation of Mechanical Power in Endurance Sports. *Sports Science Review*, 3(2), pp.34–54.

van der Kruk, E. & Reijne, M.M., 2017. Accuracy of human motion capture systems for sport applications; state-of-the-art review. under review at european journal for sport sciences.

van der Kruk, E., Schwab, A.L. & van der Helm, F.C.T., 2017. Balancing the power: determining the mechanical power balance in speed skating with a new proposed inverse dynamics method. submitted at journal of biomechanics.

Kuntze, G., Mansfield, N. & Sellers, W., 2010. A biomechanical analysis of common lunge tasks in badminton. *Journal of Sports Sciences*, 28(2).

Kuo, A.D., 1998. A least-squares estimation approach to improving the precision of inverse dynamics computations. *Journal of Biomechanical Engineering-Transactions of the Asme*, 120(1), pp.148–159.

Lees, A., Vanrenterghem, J. & De Clercq, D., 2006. The energetics and benefit of an arm swing in submaximal and maximal vertical jump performance. *Journal of Sports Sciences*, 24(1).

Van Lieshout, K.G. et al., 2014. Intensity rankings of plyometric exercises using joint power absorption. *Clinical Biomechanics*, 29(8).

Martin, P.E., Heise, G.D. & Morgan, D.W., 1993. Interrelationships between mechanical power, energy transfers, and walking and running economy. *Medicine and Science in Sports and Exercise*, 25(4).

Mason, B. et al., 2011. Effects of camber on the ergonomics of propulsion in wheelchair athletes. *Medicine and Science in Sports and Exercise*, 43(2).

McNally, M.P., Yontz, N. & Chaudhari, A.M., 2014. Lower extremity work is associated with club head velocity during the golf swing in experienced golfers. *International Journal of Sports Medicine*, 35(9).

Middleton, K.J. et al., 2016. The association between lower limb biomechanics and ball release speed in cricket fast bowlers: A comparison of high-performance and amateur competitors. *Sports Biomechanics*, 15(3).

Miller, D.I. & Nelson, R.C., 1973. *Biomechanics of Sport*,

Minetti, A. E. (2002). On the mechanical power of joint extensions as affected by the change in muscle force (or cross-sectional area), *ceteris paribus*. *European Journal of Applied Physiology*, 86(4), 363–369.

Minetti, A.E. et al., 2011. Skyscraper running: Physiological and biomechanical profile of a novel sport activity. *Scandinavian Journal of Medicine and Science in Sports*, 21(2).

Nakamura, F.Y. et al., 2004. Energetic cost estimation and contribution of different metabolic pathways in speed kayaking. *Revista Brasileira de Medicina do Esporte*, 10(2).

Neptune, R.R. & Van Den Bogert, A.J., 1997. Standard mechanical energy analyses do not correlate with muscle work in cycling. *Journal of Biomechanics*, 31(3), pp.239–245.

Noordhof, D.A. et al., 2010. The between and within day variation in gross efficiency. *European journal of applied physiology*, 109(6), pp.1209–1218.

Ojeda, J., Martínez-Reina, J. & Mayo, J., 2016. The effect of kinematic constraints in the inverse dynamics problem in biomechanics. *Multibody System Dynamics*, 37(3), pp.291–309.

Pantoja, P.D. et al., 2016. Sprint Acceleration Mechanics in Masters Athletes. *Medicine and Science in Sports and Exercise*, 48(12).

Paquette, M.R. et al., 2017. Soreness-related changes in three-dimensional running biomechanics following eccentric knee extensor exercise. *European Journal of Sport Science*, 17(5).

Pauli, C.A. et al., 2016. Kinematics and kinetics of squats, drop jumps and imitation jumps of ski jumpers. *Journal of Strength and Conditioning Research*, 30(3).

di Prampero, P.E., Botter, A. & Osgnach, C., 2014. The energy cost of sprint running and the role of metabolic power in setting top performances. *European Journal of Applied Physiology*, 115(3).

Riley, P.O. et al., 2008. A kinematics and kinetic comparison of overground and treadmill running. *Medicine and Science in Sports and Exercise*, 40(6).

Rodacki, A.L.F. & Fowler, N.E., 2001. Intermuscular coordination during pendulum rebound exercises. *Journal of Sports Sciences*, 19(6).

Royer, T.D. & Martin, P.E., 2005. Manipulations of leg mass and moment of inertia: Effects on energy cost of walking. *Medicine and Science in Sports and Exercise*, 37(4).

Schache, A.G. et al., 2011. Effect of running speed on lower limb joint kinetics. *Medicine and Science in Sports and Exercise*, 43(7).

Schwameder, H., Lindenhofer, E. & Müller, E., 2005. Walking: Effect of walking speed on lower extremity joint loading in graded ramp walking. *Sports Biomechanics*, 4(2).

Seifert, L. et al., 2010. Arm coordination, power, and swim efficiency in national and regional front crawl swimmers. *Human Movement Science*, 29(3).

Sorenson, S.C. et al., 2010. Knee extensor dynamics in the volleyball approach jump: The influence of Patellar Tendinopathy. *Journal of Orthopaedic and Sports Physical Therapy*, 40(9).

Strutzenberger, G. et al., 2014. Effect of chainring ovality on joint power during cycling at different workloads and cadences. *Sports Biomechanics*, 13(2).

Tam, E. et al., 2012. Energetics of running in top-level marathon runners from Kenya. *European journal of applied physiology*, 112(11), pp.3797–3806.

Telli, R. et al., 2017. Recumbent vs. upright bicycles: 3D trajectory of body centre of mass, limb mechanical work, and operative range of propulsive muscles. *Journal of Sports Sciences*, 35(5).

Toussaint, H. & Truijens, M., 2005. Biomechanical aspects of peak performance in human swimming. *Animal Biology*, 55(1).

Toussaint, H.M. & Beek, P.J., 1992. Biomechanics of Competitive Front Crawl Swimming. *Sports Medicine: An International Journal of Applied Medicine and Science in Sport and Exercise*, 13(1).

Vanrenterghem, J., Lees, A. & Clercq, D.D., 2008. Effect of forward trunk inclination on joint power output in vertical jumping. *Journal of Strength and Conditioning Research*, 22(3).

Veeger, H.E.J. et al., 1991. Peak oxygen uptake and maximal power output of olympic wheelchair-dependent athletes. *Medicine and Science in Sports and Exercise*, 23(10).

Willems, P.A., Cavagna, G.A. & Heglund, N.C., 1995. External, internal and total work in human locomotion. *Journal of Experimental Biology*, 198.

Williams, K.R., 1985. The relationship between mechanical and physiological energy estimates. *Medicine and Science in Sports and Exercise*, 17(3).

Williams, K.R. & Cavanagh, P.R., 1983. A model for the calculation of mechanical power during distance running. *Journal of Biomechanics*, 16(2), pp.115–128.

Willwacher, S. et al., 2013. Does specific footwear facilitate energy storage and return at the metatarsophalangeal joint in running? *Journal of Applied Biomechanics*, 29(5).

Winter, D.A., 2009. *Biomechanics and motor control of human movement*, John Wiley & Sons.

Yamashita, D. et al., 2017b. Asymmetric interlimb role-sharing in mechanical power during human sideways locomotion. *Journal of Biomechanics*, 57.

Yanagiya, T. et al., 2003. Effect of gender on mechanical power output during repeated bouts of maximal running in trained teenagers. *International Journal of Sports Medicine*, 24(4).

Yeow, C.H., Lee, P.V.S. & Goh, J.C.H., 2009. Regression relationships of landing height with

ground reaction forces, knee flexion angles, angular velocities and joint powers during double-leg landing. Knee, 16(5).

Yeow, C.H., Lee, P.V.S. & Goh, J.C.H., 2010. Sagittal knee joint kinematics and energetics in response to different landing heights and techniques. Knee, 17(2).

Zatsiorsky, V.M., 1998. Can total work be computed as a sum of the "external" and "internal" work? Journal of biomechanics, 31(2), pp.191–3.

Zelik, K. E., & Kuo, A. D. (2012). Mechanical work as an indirect measure of subjective costs influencing human movement. PLoS One, 7(2), e31143.

Zelik, K.E., Takahashi, K.Z. & Sawicki, G.S., 2015. Six degree-of-freedom analysis of hip, knee, ankle and foot provides updated understanding of biomechanical work during human walking. Journal of experimental biology, 218(6), pp.876–886.

6

Getting in shape: reconstructing three-dimensional long-track speed skating kinematics by comparing several body pose reconstruction techniques.

'Besides, it is a disgrace to grow old through sheer carelessness before seeing what manner of man you may become by developing your bodily strength and beauty to their highest limit. But you cannot see that, if you are careless; for it will not come of its own accord.' -Socrates-

The definition of power became clear in the previous chapter (CH 5); now we can move on to the mechanical power determination in speed skating. Two proceedings are inevitable in determining the mechanical power in speed skating: inverse kinematics and inverse dynamics. The methods for each of them have been widely explored in other human movement studies, e.g. gait studies, but now need to be addressed for the speed skating motion. This chapter discusses the inverse kinematics handlings. The aim of this chapter is to determine to what extent the choice for a body pose reconstruction technique influences the estimation of joint power. We compare four global optimization methods in terms of marker residual reduction and model fidelity.

E. van der Kruk, A.L. Schwab, F.C.T. van der Helm & H.E.J. Veeger (2017), *Getting in shape: reconstructing three-dimensional long-track speed skating kinematics by comparing several body pose reconstruction techniques.* Accepted with revisions at Journal of Biomechanics

Abstract

In gait studies body pose reconstruction (BPR) techniques have been widely explored, but no previous protocols have been developed for speed skating, while the peculiarities of the skating posture and technique do not automatically allow for the transfer of the results of those explorations to kinematic skating data. The aim of this paper is to determine the best procedure for body pose reconstruction and inverse dynamics of speed skating, and to what extent this choice in BPR influences the estimation of joint power. The results show that an eight body segment model together with a global optimization method with revolute joint in the knee and in the lumbosacral joint, while keeping the other joints spherical, would be the most realistic model to use for the inverse kinematics in speed skating. To determine joint power, this method should be combined with a least-square error method for the inverse dynamics. Reporting on the BPR technique and the inverse dynamic method is crucial to enable comparison between studies. Our data showed an underestimation of up to 74% in mean joint power when no optimization procedure was applied for BPR and an underestimation of up to 31% in mean joint power when a bottom-up inverse dynamics method was chosen instead of a least square error approach. Although these results are aimed at speed skating, reporting on the BPR procedure and the inverse dynamics method, together with setting a standard should be common practice in all human movement research to allow comparison between studies.

1. Introduction

Speed skating is, except for cycling, the fastest way for humans to propel themselves over flat land. Humans seem to have developed several skating techniques, each subjected to the one constraint that, due to the construction of the skate, there can only be a push-off lateral to the gliding direction of the blade. What the optimal technique is, has yet to be discovered. Kinetic data for biomechanical analysis are essential in this search.

A complicating factor in the biomechanical research of speed skating is the complexity of performing three-dimensional kinetic measurements on an ice rink. One skating stroke can cover a distance of 18m, which results in a huge volume (18m x 4m x 2m) in terms of motion capture. However, with the recently developed wireless instrumented klapskates (van der Kruk, den Braver, Schwab, van der Helm, & Veeger, 2016) and the rapidly improving techniques for 3D motion capture, we managed to capture 3D kinetic data of elite speed skaters for 50m of the straight part, which implies about three to four speed skating strokes, for this project.

For a full biomechanical analysis, recorded marker positions need to be transformed into segment position and orientation. The general assumption is that the body segments are rigid. The actual marker data will however never exactly describe actual rigid bodies, due to instrumental errors and soft tissue artefacts, a well-known phenomenon (Cappozzo, Cappello, Croce, & Pensalfini, 1997; Cappozzo, Catani, Leardini, Benedetti, & Della Croce, 1996).

Therefore, body pose reconstruction techniques (BPR) play an important role. State-of-the-art BPR technique is the global optimization method (GOM) (Lu & O'Connor, 1999), which searches for the optimal pose of the multi-body system, such that the measured data points and the estimated data points from the biomechanical model are minimized in a least-square error sense. The biomechanical model can vary in model complexity e.g. number of segments and joint constraints (Andersen, Benoit, Damsgaard, Ramsey, & Rasmussen, 2010; Charlton, Tate, Smyth, & Roren, 2004; Duprey, Cheze, & Dumas, 2010; Reinbolt et al., 2005).

In gait studies these techniques have been widely explored (Ojeda, Martínez-Reina, & Mayo, 2016), but no previous protocols have been developed for BPR in speed skating, while the peculiarities of the skating posture and technique do not automatically allow for the transfer of the results of those explorations to kinematic skating data. Moreover, previous studies on speed skating do not report on any of the methods used for the inverse kinematics or the inverse dynamics to determine joint power (van der Kruk, van der Helm, Veeger, & Schwab, 2017). It is also unclear to what extent the choice for these methods influences the joint power estimations.

The aim of this paper is to determine the best procedure for body pose reconstruction and inverse dynamics of speed skating, and to what extent this choice influences the estimation of joint power. We present an eight segment rigid body model and compare two inverse dynamics methods - bottom-up and least square error-, and four global optimization methods in terms of marker residual reduction and model fidelity - such that the joint angles obtained from the inverse kinematics meet the biomechanical restrictions of the human joints.

This paper is organized as follows; first the data collection, the body pose reconstruction techniques and the evaluation criteria are presented in the method section. Second we present the results on the marker residuals reduction and the model fidelity together with the effect of the choice of a BPR technique on the joint power estimation. Finally the results are discussed to determine the best BPR procedure for speed skating analysis.

2. Method

2.1 Experimental set-up

Data for this study were drawn from a larger study on eight Dutch elite speed skaters. Here we use the data of three strokes for one participant, since the objective of this paper is to show the influence of the different data manipulation procedures on the inverse kinematics and kinetics on the same set of data.

Data were collected on an indoor ice rink in Thialf Heerenveen, the Netherlands. Twenty Qualisys cameras (300 Hz) were placed on both sides of the straight part of the rink, covering an area of 50m (Qualisys, 2015) (Figure 6.1). Subjects were equipped with a full body passive marker set consisting of 22 markers (Van Sint Jan, 2007) (Figure 6.2). Equipped with a LPM motion tracking sensor, the skaters were tracked by four dome cameras to gather video footage (30 Hz).

The subjects skated on two wireless instrumented klapskates (van der Kruk et al., 2016). The instrumented skates each consist of two three-dimensional force sensors which measure the force in normal (F_N) and lateral direction (F_L) between the shoe and the blade (Figure 6.2C) (100Hz). Additionally the position of force application, the center of pressure (COP) was

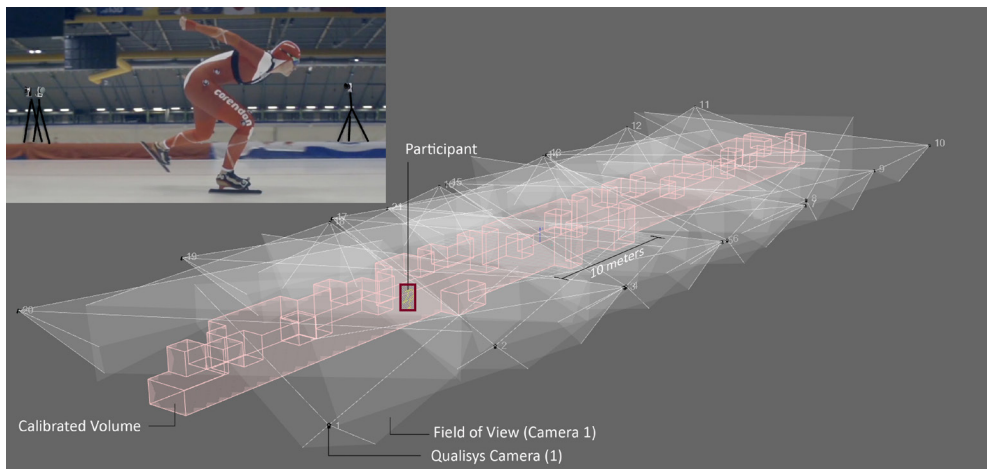


Figure 6.1 Research set up of the Qualisys system. Twenty cameras were located along the straight part of the rink. 50 meters of the straight part were covered by the calibrated volume. The participants were equipped with a full body marker set consisting of 29 markers of which six markers were used only in the static trials. The pink areas indicate the calibrated volumes. The field of view of each camera is shown.

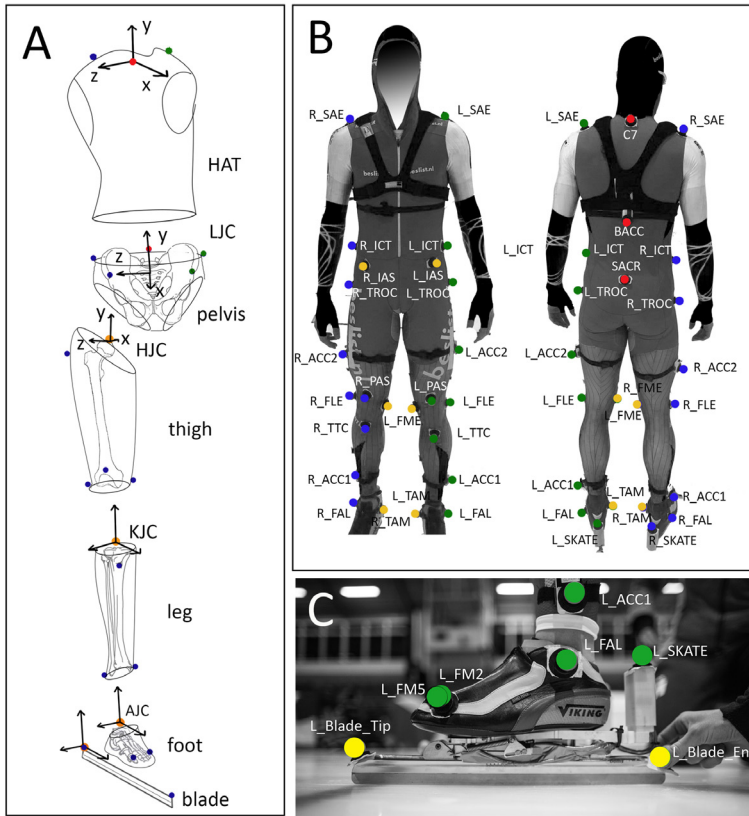


Figure 6.2 A) Local coordinate systems (SCS) of each segment with the markers defining them; see appendix A for further explanation on the SCS. B) Skater equipped with the markerset of 23 markers - marker names adopted from (Van Sint Jan, 2007). Green indicates the marker on the right side, blue the markers on the left side, and yellow are the six markers that were removed after the static trial. Markers indicated with ACC were positioned at an IMU. C) The instrumented klapskate to measure the push-off forces of the skaters (normal and lateral direction). The force sensors are integrated in the bridge; data were logged on the logger on the rear side of the skate (van der Kruk et al., 2016).

measured. The moment of the environment acting on the blade, M_B^d , was not measured since it was expected to be small. The skates were equipped with a Maple hinge mechanism and Maple blades (Maplez, 2017). Each skater placed his or her own shoe in the instrumented bridge. Force data, kinematic data and the IMUs were synchronized via a digital start-end pulse (Shimmer3, 2015). The dome cameras run on a global time stamp (GMT), equal to the timestamp of the kinematic measurement system.

The longitudinal force (ice friction) was not measured, but estimated using Coulomb's law of friction $F_{ice} = \mu F_N$ (De Koning, De Groot, & Van Ingen Schenau, 1992), where μ is the friction coefficient and F_N is the normal force of the skate on the ice. The air frictional forces were estimated based on the study of van Ingen Schenau (1982) (Appendix 6.B.5).

2.2 Rigid body model

The skater is modelled as a chain of linked rigid bodies (i), or segments. After a first analysis on the number of segments, we divided the skater into eight segments: the skates (s), the legs

(e), the thighs (t), pelvis (p) and the HAT (h), which is the head, arms and torso (Figure 6.3). The arm movements are thus neglected, since we assume HAT is a rigid body. A seven segment model in which the pelvis was part of the HAT segment was tested in our first analysis, but proved to be insufficient, since the COM of the HAT then showed unacceptable translations. Therefore the lumbosacral joint (LJ) was added to obtain an eight segment model. The local axes of the system are specified in appendix 6.A. The global reference frame xyz is specified, where y is up, x is in the longitudinal direction of the straight and z is in the lateral direction of the straight part of the rink (right, facing forward), in agreement with the ISB convention. The Euler rotations of a segment correspond to the order Y,X and Z, which are referred to as yaw, roll, pitch. The joint rotation, which is the rotation between two segments, is rotated in the Euler sequence Z, X, and Y, around the SCS of the proximal segment, further referred to as the flexion-extension (Z'), internal-external rotation (Y'') and adduction-abduction (X''').

2.3 Inverse dynamics and joint power

To apply inverse dynamic techniques, first the Newton-Euler equations of motion for each of the segments need to be determined in a global reference frame. These equations of motion are laid out in Appendix 6.B. The center of mass (COM) and the mass of the separate segments were determined by the specifications as given in Table 4.1 of Winter (2009). The inertial tensor specifications given in Table 2 of Dumas, Chèze, & Verriest (2007) most of the predictive equations are ambiguously applicable in the conventional 3D segment coordinate systems (SCSs are applied to determine the inertial matrix for each segment.

2.3.1 inverse dynamics: LSE and CS

The joint moments and forces can be determined via different inverse dynamics methods. In this paper two commonly applied methods were used in order to determine if the impact of the choice for a BPR procedure on the joint moments differs for different inverse dynamics techniques.

Consecutive Solving (CS) or the bottom-up technique for lower extremities (Miller & Nelson, 1973). The equations of motion are solved from distal to proximal until the upper joint is reached, in our case the lumbosacral joint. This method leaves residual moments and forces at the HAT, in previous studies also referred to as *the hand of god*, which are indicative of the accuracy of the approximation procedure.

Least-Square Error (LSE) Since the system of equations for the speed skater model is overdetermined (in our system we have 39 variables and 48 equations, see Appendix 6.B), the solution can be found by solving the system of linear equations with a least-square error fit (Kuo, 1998). The method minimizes the moment and forces residuals and spreads the remaining residuals out over the seven joints. The system equations and minimization problem are explained in Appendix 6.C.

2.3.2 Joint Power

Joint power is part of the mechanical power balance in speed skating and stands for the mechanical power generated in the joints. A precise definition of mechanical power in speed skating is presented in van der Kruk et al. (2017). The joint power is calculated with the moments in the joint and the rotations around the joint, as in

$$P_{j,tot} = \sum_{i=1}^7 \mathbf{M}_{o,o+1} (\boldsymbol{\omega}_{o+1} - \boldsymbol{\omega}_o) = \sum_{j=1}^7 \mathbf{M}_j \boldsymbol{\omega}_j \quad (6.1)$$

In which $\boldsymbol{\omega}_o$ is the segment angular velocity, \mathbf{M}_j are the joint moments and $\boldsymbol{\omega}_j$ are the

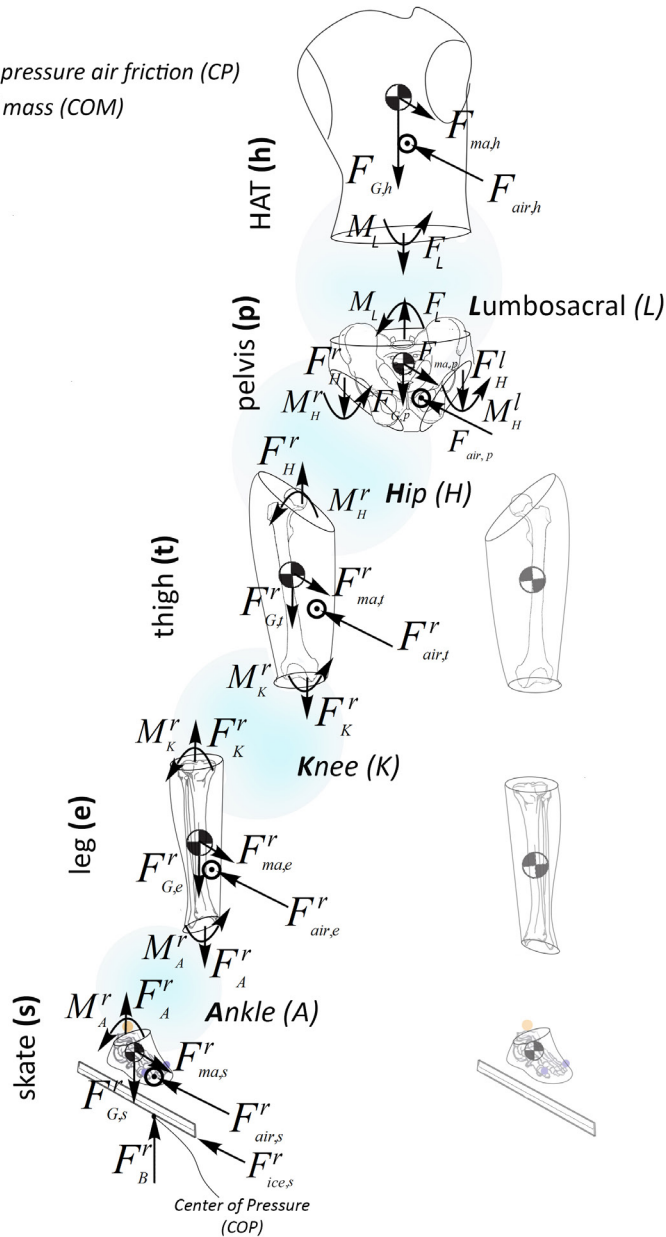


Figure 6.3 The skater is divided into eight segments; the skates (s), the legs (l), the thighs (t), the pelvis (p) and a HAT (h). The forces acting on the skater are the ground reaction forces, ice frictional forces and the air frictional forces. There are joint forces and moments acting in the Ankle (A), Knee (K), Hip (H) and Lumbo-sacral (L) joints. Indicated are the Center of Mass (COM) of each segment, the Center of Pressure of the air friction (CP), where the air frictional force acts upon, and the Center of pressure of the ground reaction force (COP). Although indicated at different positions in the figure, in this paper it was assumed that the CP is positioned at the COM of each segment. The Newton-Euler equations for this FBD are presented in Appendix B.

joint angular velocities. If we now write the complete equation for all joints, we obtain:

$$P_{j,tot} = \sum_d M_A^d (\omega_s^d - \omega_e^d) + \sum_d M_K^d (\omega_e^d - \omega_t^d) + \sum_d M_H^d (\omega_t^d - \omega_p) + M_L (\omega_p - \omega_h) \quad (6.2)$$

In which the subscripts denote the segments (s, e, t, p, h) and the joints (ankle (A), knee (K), hip (H) and lumbosacral joint (L)). d denotes either left of right, so both sides (legs) are incorporated in the joint power.

2.4 Body pose reconstruction procedures

In this paper we compare four different body pose reconstruction procedures based on global optimization (GOM) with different joint modelling and an un-optimized technique (UNO). The names are adopted from (Ojeda et al., 2016).

Un-Optimized (UNO) The un-optimized technique defines a segment by the origin and three orthogonal axes which are defined by single markers measured at each frame, with a minimum of three markers per segment. UNO method constructs the local reference frame at each point time point in the movement. The vector running from the origin to the markers is measured in the static trial and used in every frame, without a least-square error estimation. UNO does not correct for skin tissue artefacts and has no kinematic constraint, which entails that the separate segments can detach during movement and the length of the segments may vary. The UNO method and the local coordinate systems are expounded in appendix 6.A.

Global Optimization Method (GOM) This technique searches for the optimal pose of the multi-body system, such that the measured data points and the estimated data points from the biomechanical model are minimized in a least-square error sense (Lu & O'connor, 1999).

The position of a marker at any moment in time $\mathbf{r}_{0,i}^m$ can be described by

$$\mathbf{r}_{0,i}^m = \mathbf{JC}_{o,i} + R_{g \rightarrow o,i} \cdot \mathbf{v}'_{JC_0 \rightarrow m} \quad (6.3)$$

In which \mathbf{JC}_o is the joint center as well as the origin of the segment o , $R_{g \rightarrow o}$ is the rotation matrix from the global system to the segment system and $\mathbf{v}'_{JC_0 \rightarrow m}$ is the vector running from the joint center to marker m , expressed in the segment coordinate system, measured in the static trial. When the linked segment system is indeed completely rigid, the estimated marker

position $\mathbf{r}_{0,i}^m$ should be consistent with the measured marker position $\mathbf{r}_{0,i}^{m,meas}$. The difference

Table 6.1 Overview of the Body Pose Reconstruction Procedures.

Procedure	Joints	Kinematic constraints	STA reduction
UNO	-	NO	NO
GOMs	All spherical	no translations in joints	YES
GOMt	Ankle, Lumbosacral and Hip spherical, Knee joint two-axes.	- no translations in joints - two-degree knee joint (flexion-extension, internal-external)	YES
GOMr	Ankle, Lumbosacral, and Hip spherical, Knee joint revolute	- no translations in joints - one-degree knee joint (flexion-extension)	YES
GOMrr	Ankle and Hip spherical, Lumbosacral and Knee joint revolute	- no translations in joints - one-degree knee joint (flexion-extension) - one-degree lumbosacral joint (flexion-extension)	YES

between the two defines the marker residual

$$\mathbf{res}_{o,i}^m = \mathbf{r}_{o,i}^m - \mathbf{r}_{o,i}^{m,meas} \quad (6.4)$$

$$\|\mathbf{res}_{o,i}^m\| = \sqrt{\mathbf{res}_{o,i}^{mT} \mathbf{res}_{o,i}^m} \quad (6.5)$$

In which $\mathbf{res}_{o,i}^m$ is the residual vector (xyz) at time i for marker m , which in total makes 22 residuals. Input to the optimization function are the measured marker positions at each point

in time and $\vec{v}_{JC_0 \rightarrow m}$ measured in the static condition. The system is a non-linear multivariable function and was solved in a non-linear optimization using the function *fmincon*, in Matlab. The model uses the UNO technique to find a start position of the model. Output of the optimization are the rotation matrices for the skates, legs, thighs, pelvis and torso and the positions of AJC, KJC and HJC and LJC.

GOM reduces the residuals and adds kinematic constraints, restricting any translation within joints (between segments) and guarantees a constant segment length. Within this technique there are several ways to model the joint constraints. In this study we applied four (Table 6.1):

1. a model with only spherical joints (**GOMs**) (27 DOF);
2. a model with a two-axes knee joint allowing for only flexion-extension and internal-external rotation (**GOMt**); The lumbosacral, hip and ankle joint are spherical (25 DOF).
3. a model with a revolute (one-axis) knee joint, only allowing for flexion-extension (**GOMr**); The lumbosacral, hip and ankle joint are spherical (23 DOF).
4. a method in which in addition to the revolute joint in the knee, also the lumbosacral joint is modelled as a hinge joint, only allowing flexion-extension (**GOMrr**). Since the LS joint was only added to improve the CoM translation of the HAT in the inverse model, a revolute joint was deemed to be sufficient (21 DOF).

2.5 Criteria for evaluating the BPR procedures

To evaluate the various BPR procedures, we determined kinematic and kinetic criteria. For the kinematic criteria there are two evaluation measures. First, marker residuals, which are often used in literature to quantify the fit of the model on the experimental data (Lu & O'Connor, 1999; Ojeda, Martínez-Reina, & Mayo, 2014). The residuals depend on STA and instrumental errors as well as the global optimization fit. To evaluate the residuals for the procedures, the sum of the marker residuals over time for each marker RES^m is determined

$$RES^m = \frac{1}{T} \sum_{i=1}^T \|\mathbf{res}_{o,i}^m\| \quad (6.6)$$

In which T is the total time of the three consecutive strokes. Additionally, the average total marker residual of all markers ($N_m = 22$) was determined by:

$$RES^{tot} = \frac{1}{N_m} \frac{1}{T} \sum_{i=1}^T \sum_{m=1}^{22} \|\mathbf{res}_{o,i}^m\| \quad (6.7)$$

For the second kinematic evaluation criteria, the procedures were evaluated on the obtained joint kinematics which are the joint angles. The results were tested on their model fidelity. Since there are no results on 3D speed skating kinematics in literature to compare the results to, we can only evaluate these results based on general biomechanical knowledge.

For the kinetic evaluation criterion, the methods were evaluated on their dynamic consistency.

The joint forces and moments, obtained with the two inverse dynamics techniques, were evaluated based on the Newton-Euler residuals, i.e. the residuals left in each Newton ($\tilde{\mathbf{e}}_{F,o}^d$) and Euler ($\tilde{\mathbf{e}}_{M,o}^d$) equation of motion (Appendix 6.B):

$$\tilde{\mathbf{e}}_{F,i}^d = \sum \tilde{\mathbf{F}}_o^d - m_o^d \tilde{\mathbf{a}}_o^d \quad (6.8)$$

$$\tilde{\mathbf{e}}_{M,i}^d = \sum \tilde{\mathbf{M}}_o^d - \frac{d}{dt} (I_o^d \tilde{\boldsymbol{\omega}}_o^d) \quad (6.9)$$

The Newton-Euler residuals were summed over all segments and averaged over time. We normalized to the estimated joint forces and moments (also summed over the joints and averaged over time):

$$RES^{Newton} = \frac{\sum_{i=1}^T \sum_{o=1}^8 \sqrt{\tilde{\mathbf{e}}_{F,o}^{dT} \tilde{\mathbf{e}}_{F,o}^d}}{\sum_{i=1}^T \sum_{j=1}^7 \sqrt{\mathbf{F}_j^{dT} \mathbf{F}_j^d}} \cdot 100\% \quad (6.10)$$

$$RES^{Euler} = \frac{\sum_{i=1}^T \sum_{o=1}^8 \sqrt{\tilde{\mathbf{e}}_{M,o}^{dT} \tilde{\mathbf{e}}_{M,o}^d}}{\sum_{i=1}^T \sum_{j=1}^7 \sqrt{\mathbf{M}_j^{dT} \mathbf{M}_j^d}} \cdot 100\% \quad (6.11)$$

Note that for CS there are only Newton-Euler residuals at the HAT segment, while for

LSE there are residuals for every segment. Finally, the mean ($\bar{P}_{j,tot}$) and peak ($P_{j,tot}^{max}$) joint power (for two consecutive strokes) were estimated for each combination of BPR and inverse dynamics technique, to quantify the influence of a choice in terms of joint power estimation.

3. Results

For easier interpretation of the results and clarification on the terminology on the speed skating for this paper, an infographic was constructed from the measured 3D kinetic data (Figure 6.4). The caption provides a description of the phases and terms.

3.1 Marker residuals and joint gaps

The average values of the marker residuals for the three analysed strokes are shown in Figure 6.5. Among the GOM methods we only see small differences in marker residuals, none of the methods sticks out from these results. The largest residuals are found in the upper body, since the rigid body assumption will hold least for the HAT segment. UNO is the only method that allows joint gaps. The mean gaps for the Ankle, Knee, Hip and Lumbosacral joint were 2.1 cm, 7.3 cm, 0 cm and 3.9 cm respectively for both left and right.

Joint kinematics

The joint angles obtained using the five procedures (UNO, GOMs, GOMr, GOMt, GOMrr) for two consecutive strokes are given in Figure 6.6. Additionally a 3D visualisation whereby all five procedures are sketched together with the measured marker positions is given in Figure 6.7. The joint angles are clearly changed by the optimization method compared to the un-optimized method UNO, which shows unrealistic rotations (too large knee and hip extensions (Figure 6.6)). The GOMs method, with spherical joints only, shows unrealistic large knee joint adduction angles and hip endo rotations. The GOMt, GOMr and GOMrr methods all solve the

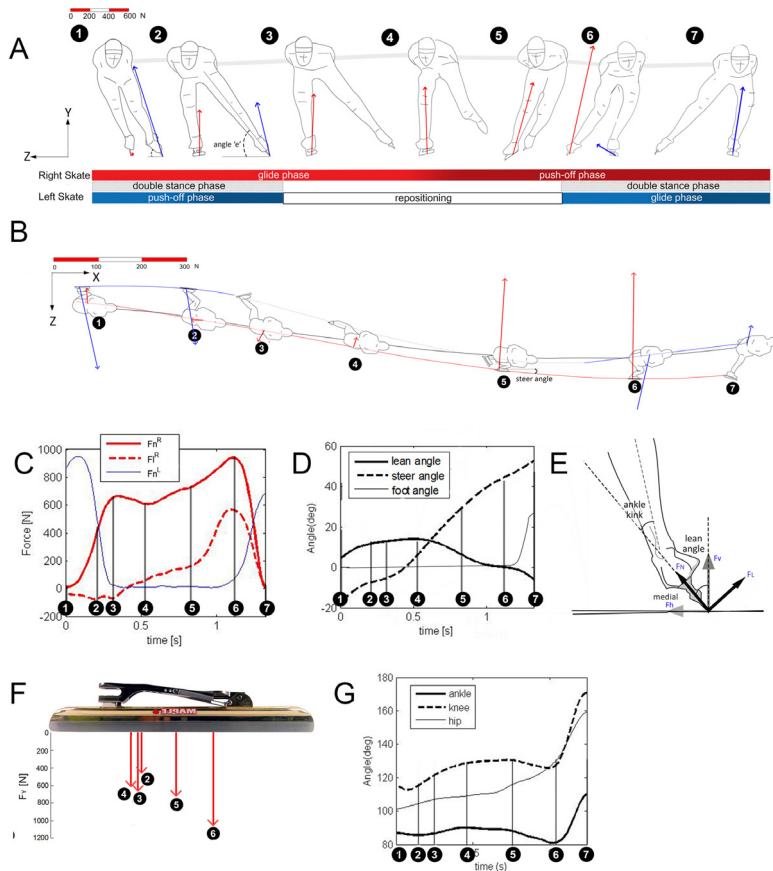


Figure 6.4 Overview of the speed skating motion, reconstructed from the data of one participant. A) skating motion front view, divided into the four phases: glide phase, push off phase, repositioning phase and the double stance, where both skates are on the ice. The push-off angle of the leg is the angle the leg makes with the horizontal during the push-off motion in the frontal plane. The arrows indicate the push-off force in global space, the scale is indicate in the top-right corner. The grey line indicates the CoM motion of the HAT. B) Top view of the skating motion. The red, blue and black lines indicate the trajectories of respectively the right skate, left skate and CoM of the HAT on the ice. The steer angle is the angle the skate makes with the global x-axis while on the ice. C) measured (local) normal and lateral push off force on the skate (see E) for the right (red) and left (blue) skate during the right stroke. D) lean angle (roll), steer angle (yaw) and foot angle (opening of the skate, pitch) in the global system (see E). E) Center of Pressure (COP) measured on the skate together with the upward global force (F_y). Instances 1 and 7 have too little force on the skate, to determine the COP. F) joint flexion angles of the angle knee and hip.

A right stroke in speed skating can be described by instances 1 to 7: 1) The skater places the right skate on the ice, while the normal force on the left skate almost reaches its peak value. 2) The weight of the skater is evenly distributed over the left and right skate. 3) All the weight is shifted to the right skate, the left skate is retracted from the ice, which ends the double stance phase. 4) The skater lowers his upper body by decreasing the knee angle. Lowering the upper body causes a dip in the normal force curve of the skate. In this phase, the gliding phase, the lean angle transforms from negative to positive, so the skate shifts from the lateral to the medial side of the blade. The steering angle of the skate is at maximum when the lean angle is zero. 5) The skater moves his upper body away from his skate, thereby increasing the force on his skate. Since the lean angle is now positive and the steering angle still has a positive angle, the skater has a force component in both the forward and the sideways direction of the rink. 6) The skater keeps increasing his force, by stretching his knee (push-off phase), until the peak force. Just before the peak, the left skate re-entered the ice. 7) The skater shifts his weight to the left skate, until all weight is shifted and the skater retracts his skate from the ice. The skater then repositions his right skate for the next stroke. During the stroke the upper body of the skater has an up-and-down movement of about 0.15 m. The distance covered in the visualized stroke was 12.6 m.

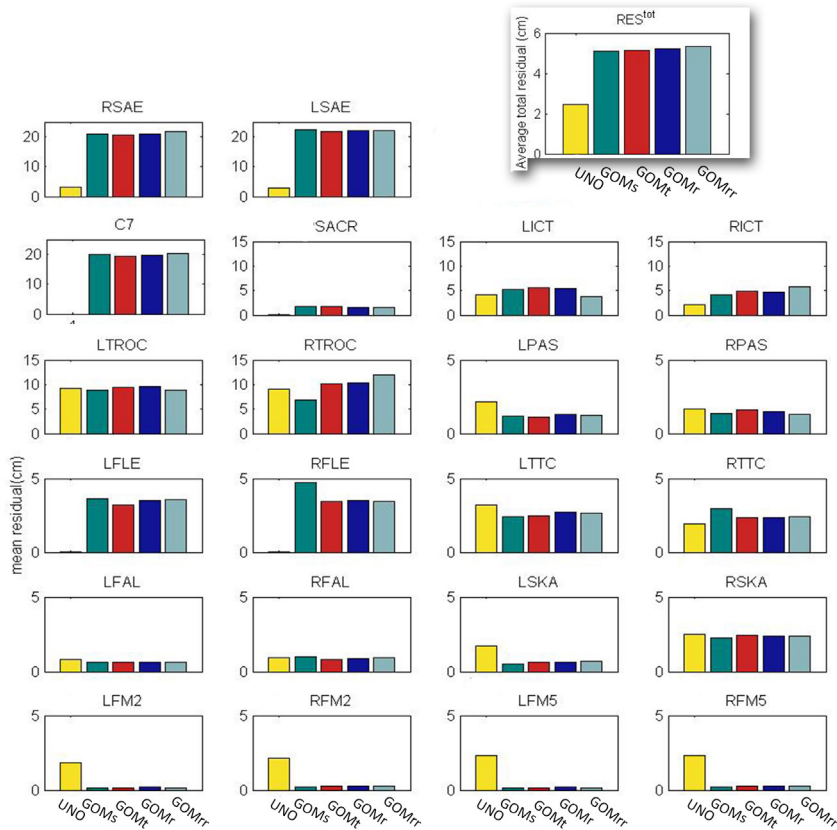


Figure 6.5 Marker residuals of each marker for the five BPR procedures. Marker definitions are given in figure 6.2; Note the graphs have different scaling, while we want to compare the BPR procedures rather than the mutual markers.

unrealistic knee adduction by restricting it and thereby also improve the hip endo rotation into more realistic values. Comparing the latter three, the GOMt method shows quite arbitrary endo-exo rotation in the knee joint, not related to the skating pattern. In the GOMr and GOMrr, where the knee endo-exo rotation is constrained, an increased ankle endo-exo rotation is visible up to about 30 degrees compared to GOMt, however these only occur when the skate is of the ice and are therefore feasible.

3.2 Newton-Euler residuals and Joint Power

The Newton-Euler residuals, relative to the summed joint forces and moments, are given in Table 6.2. For both inverse dynamics methods, the Newton residuals (RES^{Newton}) are lower than the Euler residuals (RES^{Euler}). LSE has significant lower RES^{Euler} compared to CS. In absolute numbers, the maximal average residual of CS, which only results in residuals at the HAT segment, is 160 N and 133 Nm. The maximal residual of the LSE method is 23 N and 9 Nm, at the skate segment. Within the LSE method, the influence of the BPR procedure on RES^{Euler} and RES^{Newton} is only marginal, where GOMs and GOMrr seem most dynamic consistent (Table 6.2). Estimation of joint power is influenced by both the BPR procedure and the inverse dynamics method, each of the combinations is presented in Figure 6.8. The figure makes clear that the differences in joint power between methods is large.

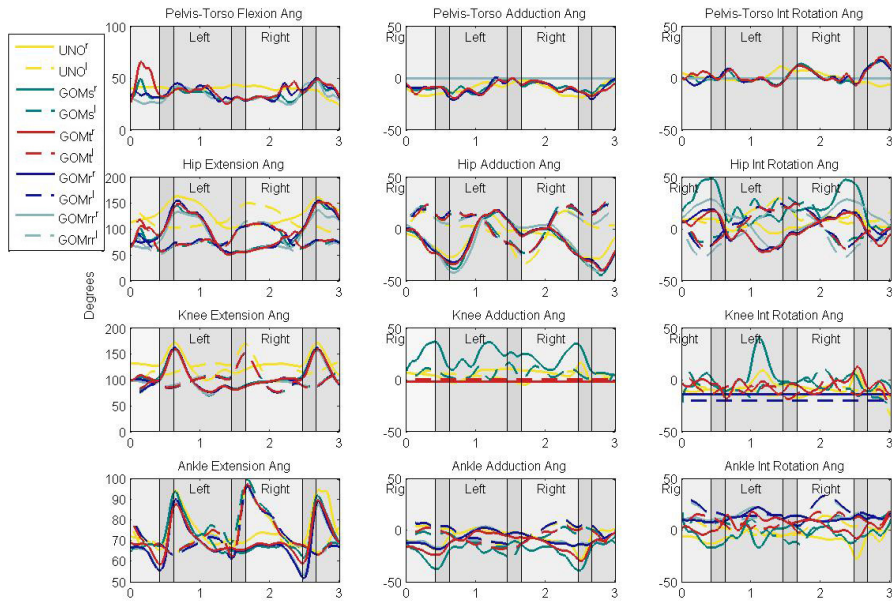


Figure 6.6 Joint angles in the segment coordination system for three consecutive strokes (right-left-right) with the five BPR techniques. The solid line is right (r), the dotted line denotes the left (l) side. The angles are in degrees. The grey areas indicate whether the right or left skate is on the ice and the double stance phases. The upright conditions for the extension angles are 180° for the knee and hip and 90° for the ankle. All other rotations have a 0° value in the standing upright position.

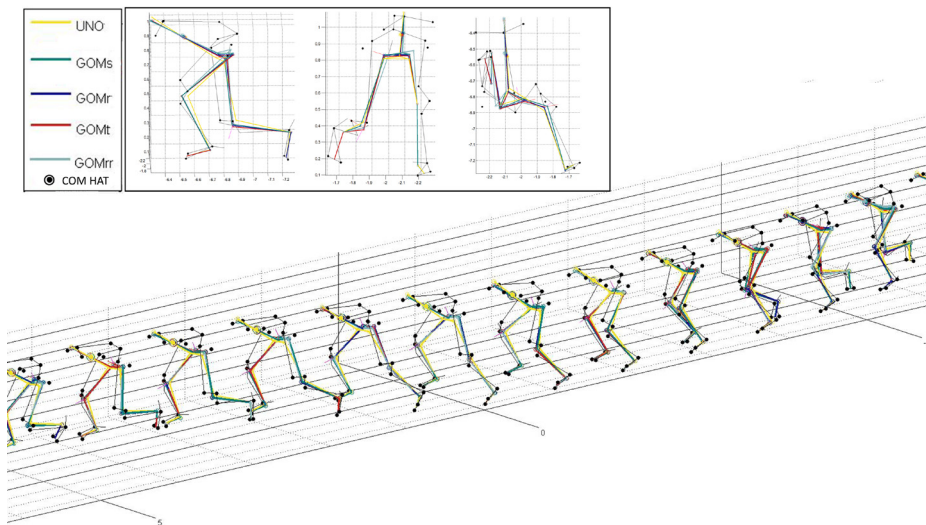


Figure 6.7 3D plot of the measured markers (black dots) and the estimated joint centers (coloured circles) for the five BPR procedures. A coloured line is drawn from joint to joint (the joint gaps for UNO are therefore not shown) and a thin black line from marker to marker.

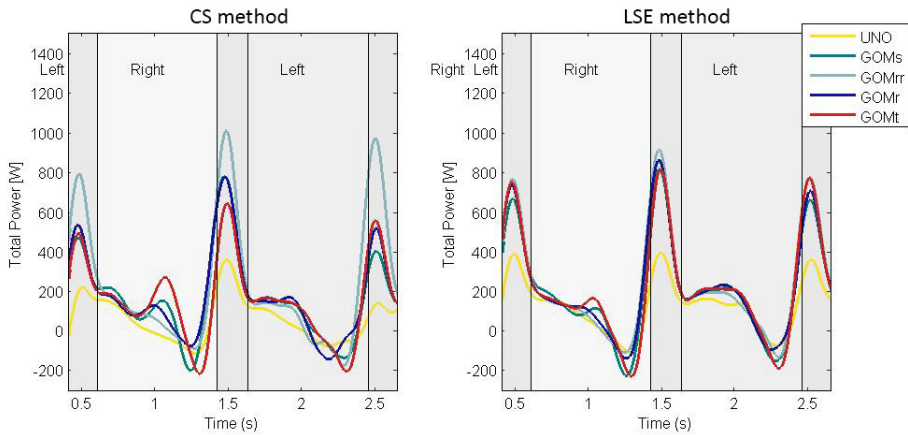


Figure 6.8 Joint power obtained with the five BPR procedures with the bottom-up approach (CS) (left) and least-square error approach (LSE) (right) for inverse dynamics.

4. Discussion

Both the choice in BPR procedure and inverse dynamics method have a large impact on the estimation of joint power. The results underline the importance for setting a standard for future studies and reporting on both procedures to allow for comparison of studies – also when these methods are embedded in a software. This applies not just for speed skating, but also to other studies, where motion capturing in large volumes is involved (van der Kruk & Reijne, 2017).

For the inverse dynamics method, the bottom-up approach (CS) is dynamically less consistent than the least-square error approach (LSE) (Table 2). In this speed skating study, where the accuracy of the motion capture data is low due to the large recording volume, the LSE method has made the results more robust by incorporating full body dynamics (Table 3). Therefore LSE is here the better choice for inverse dynamics.

An optimization procedure for BPR is essential, as the un-optimized procedure, UNO, results in unacceptable joint rotations (Figure 6.6). The results show that a model with spherical joints only (GOMs), results in unrealistic knee adduction and hip endo rotations and therefore is not sufficient. GOMt, with a two-degree knee joint, shows arbitrary endo-exo rotations in the joint angles, which is expected to be merely a compensation variable caused by the minimization problem, than an actually existing motion, since the motion is not periodically. Although GOMr and GOMrr show an increased ankle endo-exo rotation (compared to GOMt), these rotations occur when the skates are in the air, which makes these joint angles acceptable. Both methods seem sufficient for the inverse kinematics of a speed skater. The GOMrr however has a slightly better dynamic consistency compared to GOMr (Table 6.2), therefore GOMrr is the best choice in BPR procedure.

Table 6.3 presents the percentage differences between using the GOMrr for inverse kinematics together with a LSE inverse dynamics method, and using any of the other combinations. The table makes the necessity for reporting the applied methods clear; Compared to GOMrr, an un-optimized method estimates the joint power lower, with a 45 to 74 % difference. This structural underestimation is partly related to the neglected translational powers in the joint, which only apply for UNO. Using a GOM procedure, but a CS method instead of LSE, causes differences of up to 31% in mean joint power and 29% in peak power. As long as a GOM procedure with a LSE method is applied, the difference stays within the 10%, again ruling to always use a least-square error approach for the inverse dynamics.

Table 6.2 Dynamic residuals of each inverse kinematics and inverse dynamics combination. The Newton-Euler residuals were summed over all segments, averaged over time and normalized to joint forces and moments (eq.7.10 & 7.11).

RES	CS		LSE	
	Newton	Euler	Newton	Euler
UNO	7.3%	34.2%	8.0%	25.3%
GOMs	7.0%	33.7%	7.7%	22.5%
GOMt	7.2%	34.3%	7.8%	23.8%
GOMr	7.2%	34.0%	7.9%	23.2%
GOMrr	7.1%	33.6%	7.8%	22.6%

4.1 Soft tissue artefacts in speed skating

The residuals found in the speed skating experiment are sometimes ten times larger than in gait studies (Ojeda et al., 2014). The main cause of this difference is the size of the volume in which the data were captured, which influences the instrumental error of the marker data. The calibration error in this experiment was 4.5-4.7 mm, which in lab environments usually is <0.7mm (van der Kruk & Reijne, 2017). Second cause is the skating posture; while in gait analysis the dynamic posture is similar to the static (upright) trial, in speed skating the skater bends forward, with an increased knee and hip flexion. Due to this bending, the skating suit of the skaters with the attached markers will significantly shift relatively to the skin (and skeletal); this highly undermines the rigid body assumption. In future studies it is advised to use an additional static calibration, where the participant is positioned in a speed skating posture.

4.2 Inverse Dynamics

Accurate kinematic measurements are essential for inverse dynamics. Measurement data can benefit from sensor integration or sensor fusion. The least-square error approach used in this study, can be interpreted as a way of sensor fusion: adding the equations of the HAT segment to the total system of motion equations, forming a closed loop, enables the fusion of kinematic data and force data to solve the joint moment and forces in a least-square manner. Possible improvement of LSE as applied in the current study, is to use an inverse covariance matrix for the weighting as done in Van Den Bogert & Su (2008). This might further improve the Euler residuals for LSE. Also, in addition to the Newton-Euler equation, the power balance equation could be implemented to the system, thereby further improving the dynamic consistency of the model. Such a method is introduced and further discussed in a sequencing paper (van der Kruk, Schwab, & van der Helm, 2017), in which we also discuss the influence of instrumental errors and body parameters on joint power estimations.

Table 6.3 Difference between the mean and peak joint power of the best method (GOMrr with LSE), indicated by **, and the mean and peak joint power with any of the other combinations. Data are based on two consecutive strokes.

P_j	CS		LSE	
	mean	peak	mean	peak
UNO	-74%	-60%	-45%	-57%
GOMs	-29%	-15%	-9%	-10%
GOMt	-31%	-29%	-6%	-10%
GOMr	-26%	-15%	-3%	-6%
GOMrr	-3%	+9%	**	**

5. Conclusion

An eight body segment model together with a global optimization method with revolute joint in the knee and in the lumbosacral joint would be the most realistic model to use for the inverse kinematics in long-track speed skating. To determine joint power this method should be combined with a least-square error method for the inverse dynamics. Reporting on the BPR optimization technique and the inverse dynamic method is crucial to enable comparison between studies. Our data showed an underestimation of up to 74% in mean joint power when no optimization procedure was applied for BPR and an underestimation of up to 31% when a bottom-up inverse dynamics method was chosen instead of a least square error approach.

Acknowledgements

The authors express their gratitude to Frida Bakkman, Daniel Thompson, Erik Westerström, and Marcus Johansson of Qualisys, Wouter van der Ploeg of the KNSB, Andre Zschernig of the company Moticon, and Frédérique Meeuwsen, Niels Lommers, and Jos Koop of the TU Delft and the Hague university of applied sciences for their help and support during the measurements. Also we express gratitude to Thialf for giving us the opportunity of overnight measurements at their ice rink. This study was supported by the NWO-STW under grant 12870.

References

- Andersen, M. S., Benoit, D. L., Damsgaard, M., Ramsey, D. K., & Rasmussen, J. (2010). Do kinematic models reduce the effects of soft tissue artefacts in skin marker-based motion analysis? An in vivo study of knee kinematics. *Journal of Biomechanics*, 43(2), 268–273.
- Cappozzo, A., Cappello, A., Croce, U. Della, & Pensalfini, F. (1997). Surface-marker cluster design criteria for 3-D bone movement reconstruction. *IEEE Transactions on Biomedical Engineering*, 44(12), 1165–1174.
- Cappozzo, A., Catani, F., Leardini, A., Benedetti, M. G., & Della Croce, U. (1996). Position and orientation in space of bones during movement: experimental artefacts. *Clinical Biomechanics*, 11(2), 90–100.
- Charlton, I. W., Tate, P., Smyth, P., & Roren, L. (2004). Repeatability of an optimised lower body model. *Gait & Posture*, 20(2), 213–221.
- De Koning, J. J., De Groot, G., & Van Ingen Schenau, G. J. (1992). Ice friction during speed skating. *Journal of Biomechanics*, 25(6), 565–571. [http://doi.org/10.1016/0021-9290\(92\)90099-M](http://doi.org/10.1016/0021-9290(92)90099-M)
- Dumas, R., Chèze, L., & Verriest, J. P. (2007). Adjustments to McConville et al. and Young et al. body segment inertial parameters. *Journal of Biomechanics*, 40(3), 543–553. <http://doi.org/10.1016/j.jbiomech.2006.02.013>
- Duprey, S., Cheze, L., & Dumas, R. (2010). Influence of joint constraints on lower limb kinematics estimation from skin markers using global optimization. *Journal of Biomechanics*, 43(14), 2858–2862.
- Kuo, A. D. (1998). A least-squares estimation approach to improving the precision of inverse dynamics computations. *Journal of Biomechanical Engineering-Transactions of the Asme*, 120(1), 148–159. <http://doi.org/10.1115/1.2834295>
- Lu, T.-W., & O'connor, J. J. (1999). Bone position estimation from skin marker co-ordinates using global optimisation with joint constraints. *Journal of Biomechanics*, 32(2), 129–134.

Maplez. (2017). <http://www.mapleskate.com>.

Miller, D. I., & Nelson, R. C. (1973). *Biomechanics of Sport*.

Ojeda, J., Martínez-Reina, J., & Mayo, J. (2014). A method to evaluate human skeletal models using marker residuals and global optimization. *Mechanism and Machine Theory*, 73, 259–272.

Ojeda, J., Martínez-Reina, J., & Mayo, J. (2016). The effect of kinematic constraints in the inverse dynamics problem in biomechanics. *Multibody System Dynamics*, 37(3), 291–309.

Qualisys. (2015). <http://www.qualisys.com/>.

Reed, M. P., Manary, M. A., & Schneider, L. W. (1999). *Methods for Measuring and Representing Automotive Occupant Posture*. Society of Automotive Engineers, (724).

Reinbolt, J. A., Schutte, J. F., Fregly, B. J., Koh, B. II, Haftka, R. T., George, A. D., & Mitchell, K. H. (2005). Determination of patient-specific multi-joint kinematic models through two-level optimization. *Journal of Biomechanics*, 38(3), 621–626.

Shimmer3. (2015). Shimmer. Retrieved from www.shimmersensing.com

Van Den Bogert, A. J., & Su, A. (2008). A weighted least squares method for inverse dynamic analysis. *Computer Methods in Biomechanics and Biomedical Engineering*, 11(1), 3–9.

van der Kruk, E., van der Helm, F. C. T., Veeger, H. E. J., & Schwab, A. L. (2017). Power in Sports: a literature review on the application, assumptions, terminology and validity of mechanical power in sport research. Submitted at *Journal of Biomechanics*.

van der Kruk, E., den Braver, O., Schwab, A. L., van der Helm, F. C. T., & Veeger, H. E. J. (2016). Wireless instrumented klapskates for long-track speed skating. *Journal of Sports Engineering*, 19(4), 273–281. <http://doi.org/10.1007/s12283-016-0208-8>

van der Kruk, E., & Reijne, M. M. (2017). Accuracy of human motion capture systems for sport applications; state-of-the-art review. Under Review at *European Journal for Sport Sciences*.

van der Kruk, E., Schwab, A. L., & van der Helm, F. C. T. (2017). Balancing the power: determining the mechanical power balance in speed skating with a new proposed inverse dynamics method. Submitted at *Journal of Biomechanics*.

van Ingen Schenau, G. J. (1982). The influence of air friction in speed skating. *Journal of Biomechanics*, 15(6), 449–458. [http://doi.org/10.1016/0021-9290\(82\)90081-1](http://doi.org/10.1016/0021-9290(82)90081-1)

Van Sint Jan, S. (2007). *Color Atlas of Skeletal Landmark Definitions. Guidelines for Reproducible Manual and Virtual Palpations*. (C. Livingstone, Ed.). Edinburgh.

Winter, D. A. (2009). Anthropometry. In *Biomechanics and Motor Control of Human Movement* (4th ed., pp. 82–106).

Appendix 6.A Segment Coordinate Systems (SCS)

For each segment, a Segment Coordinate System (SCS) was determined (Figure 6.2). Symmetry is assumed between the left and the right leg.

A.1 Skate

The X-axis of the skate SCS runs from the AJC (estimated as the midpoint between FAL and TAM) to the midpoint of the FM2 and FM5 marker. The Y-axis is normal to a plane containing the AJC, FM2 and FM5 marker. The Z-axis is the cross product between the Y and X axes. The origin is AJC.

A.2 Leg

The Ankle joint Center (AJC) was estimated as the midpoint between FAL and TAM. The Y-axis of the leg runs from the AJC to the KJC (midpoint between LFE and MFE). The Z-axis is normal to a plane containing the AJC, KJC and TTC. The X-axis is the cross product between the Y and Z axis. The origin is AJC.

A.3 Thigh

The Knee joint Center (KJC) was estimated as the midpoint between LFE and MFE. The Y-axis of the thigh runs from the HJC to the KJC. The X-axis is normal to a plane containing the HJC, LFE and MFE, pointing anteriorly. The Z-axis is the cross product between the X and Y axis.

A.4 Pelvis

The SCS of the Pelvis has its Z-axis running through the markers R_IAS and L_IAS. The Y-axis is the vector perpendicular to the plane containing the R_IAS, L_IAS and SACR marker. The X-axis is the cross product of the Y and Z-axis. The origin is the midpoint MIAS between the R_IAS and L_IAS marker. The hip joint center (HJC) is estimated according to (Reed, Manary, & Schneider, 1999), where the vector from MIAS to HJC is estimated based on the pelvis width (PW): $[0.24PW \quad 0.30PW \quad kk \cdot 0.36PW]$, in which $kk = -$ for the left HJC (LHJC) and $kk = 1$ for the right HJC (RHJC).

A.5 HAT

The SCS of the HAT has his Y-Axis running through the markers C7 and SACR. The X-axis is the vector perpendicular to the plane containing the C7, RSAE and LSAE markers. The Z-axis is the cross product of the X- and Y-axis. The origin is the C7 marker.

Appendix 6.B Newton-Euler Equations of Motion

In this appendix the Newton-Euler equations for the seven-body-rigid model are given. The body consists of eight segments: the skates, the legs, the thighs, the pelvis and the HAT which is the head, trunk and arms, see Figure 6.3.

B.1 Skate (S)

The Newton-Euler equations at the COM of the skate in the three global directions are,

$$\sum \mathbf{F}_s^d = \mathbf{F}_B^d + \mathbf{F}_{ice}^d + \mathbf{F}_A^d + \mathbf{F}_{G,s}^d + \mathbf{F}_{air,s}^d = m_s^d \mathbf{a}_s^d \quad (\text{B.1})$$

Where d indicates the left (L) or right (R) skate. $\mathbf{F}_{ice}^d + \mathbf{F}_B^d$ are the reaction forces acting at the COP of the blade of the skate, where \mathbf{F}_{ice}^d works in the longitudinal direction of the blade and \mathbf{F}_B^d in the normal (\mathbf{F}_N^d) and lateral direction (\mathbf{F}_L^d) of the blade. We make a distinction between the two, since we measure \mathbf{F}_B^d and can only estimate \mathbf{F}_{ice}^d . The air frictional force $\mathbf{F}_{air,s}^d$ has its own center of pressure (CP) on the segment, where the force acts. $\mathbf{F}_{G,s}^d$ is the gravitational force acting in the COM of the skate segment. \mathbf{F}_A^d is the force acting in the Ankle joint center (A). The sum of the forces should add up to the mass of the segment times the acceleration of the COM of this segment, $m_s^d \mathbf{a}_s^d$. For the rotational part we write the Euler equation at the COM expressed in the global reference frame in the three global directions:

$$\sum \mathbf{M}_s^d = \mathbf{M}_B^d + \mathbf{M}_{F_B}^d + \mathbf{M}_A^d + \mathbf{M}_{F_{A,s}}^d + \mathbf{M}_{air,s}^d + \mathbf{M}_{ice,s}^d = \frac{d}{dt} (\mathbf{I}_s^d \boldsymbol{\omega}_s^d) \quad (\text{B.2})$$

Where $\mathbf{M}_{F_B}^d$ is the moment caused by the force \mathbf{F}_B^d and $\mathbf{M}_{ice,s}^d$ is the moment due to the ice frictional force. $\mathbf{M}_{F_{A,s}}^d$ is the moment implied by the ankle joint force \mathbf{F}_A^d as in

$$\mathbf{M}_{F_{A,s}}^d = \mathbf{r}_{A/s}^d \times \mathbf{F}_A^d \quad (\text{B.3})$$

Where $\mathbf{r}_{A/s}^d$ is the vector running from the center of mass of the skate to the Ankle joint center.

\mathbf{M}_B^d is the external moment of the environment acting on the blade, which was assumed to be small and therefore neglected. $\mathbf{M}_{air,s}^d$ is the moment induced by the air frictional force. This moment only exists when the CP is different from the COM. After all, a force that acts at the COM, would, like the gravitational force and the acceleration force, not contribute to the sum of moments around the COM. To complete, there is a moment acting in the ankle joint \mathbf{M}_A^d . The sum of moments should add up to the change in angular momentum of the

segment at the COM $\frac{d}{dt} (\mathbf{I}_s^d \boldsymbol{\omega}_s^d)$, where $\boldsymbol{\omega}_s^d$ is the angular velocity and \mathbf{I}_s^d its inertia tensor of the skate expressed in a global reference frame. The global parameters $\boldsymbol{\omega}_o^d$ and \mathbf{I}_o^d were determined via the orientation of the segment. The segment orientation is described by the Euler sequence yaw (γ), roll (α), and pitch (β), with the rotation matrix of the segment \mathbf{R}_o :

$$\mathbf{R}_o^d = \mathbf{R}_{o\gamma}^d \mathbf{R}_{o\alpha}^d \mathbf{R}_{o\beta}^d \quad (\text{B.4})$$

The global angular velocity vector (ω_o^d) was then determined by:

$$\omega_o^d = \begin{bmatrix} 0 \\ \dot{\gamma}_o^d \\ 0 \end{bmatrix} + R_o^d \gamma \begin{bmatrix} \dot{\alpha}_o^d \\ 0 \\ 0 \end{bmatrix} + R_o^d \gamma R_o^d \alpha \begin{bmatrix} 0 \\ 0 \\ \dot{\beta}_o^d \end{bmatrix} \quad (B.5)$$

In which the Euler rotational velocities were determined by differentiation of the Euler angles, filtered with a two-way second order Butterworth filter with a 12Hz cut-off frequency. The global inertial tensor was determined by:

$$I_o^d = R_o^d I_o^{rd} R_o^{dT} \quad (B.6)$$

In which I_o^{rd} is the inertial tensor in the segment frame. Next, the global inertial tensor (I_o^d) was multiplied by the global segment angular velocity (ω_o^d), differentiated once and filtered

with a second order Butterworth filter with a 4Hz cut-off frequency to obtain $\frac{d}{dt}(I_o^d \omega_o^d)$.

B.2 Leg (e) and thigh (t)

The equations of motion for the leg and the thigh are derived in a similar manner to that of the skate. Each segment introduces a force and a moment in the consecutive joint (Knee (K) and Hip (H)). The leg has the following equations of motion:

$$\sum F_e^d = -F_A^d + F_K^d + F_{G,e}^d + F_{air,e}^d = m_e^d a_e^d \quad (B.7)$$

$$\sum M_e^d = -M_A^d + M_K^d + M_{F_{A,e}}^d + M_{F_{K,e}}^d + M_{air,e}^d = \frac{d}{dt}(I_e^d \omega_e^d) \quad (B.8)$$

Where F_A^d is the force acting in the ankle joint, but with an opposite sign to the one acting in the skate segment. F_K^d is the force acting in the knee joint. The moments $M_{F_{A,e}}^d$ and $M_{F_{K,e}}^d$ are induced by the forces in the respective joints. $M_{F_{A,e}}^d$ is different from $M_{F_{A,s}}^d$ due to the different moment arm $r_{A/e}^d$, running from the center of mass of the segment e to the joint center A. The moment M_A^d is equal but opposite to the ankle moment as appearing in B.2. M_K^d is the moment in the Knee joint. $M_{air,e}^d$ is the moment induced by the air frictional force.

$\frac{d}{dt}(I_e^d \omega_e^d)$ is the change in angular momentum of the segment at the COM of the leg, where ω_e^d is the angular velocity and I_e^d its inertia tensor expressed in a global reference frame. Moving to the next segment, the equations of motion for the thigh are given by:

$$\sum F_t^d = -F_K^d + F_H^d + F_{G,t}^d + F_{air,t}^d = m_t^d a_t^d \quad (B.9)$$

$$\sum M_t^d = -M_K^d + M_H^d + M_{F_{K,t}}^d + M_{F_{H,t}}^d + M_{air,t}^d = \frac{d}{dt}(I_t^d \omega_t^d) \quad (B.10)$$

Where \mathbf{F}_H^d is the force acting in the hip joint and \mathbf{M}_H^d is the moment in the Hip joint.

$\mathbf{M}_{F_{K,t}}^d$ is again different from $\mathbf{M}_{F_{K,e}}^d$ due to the different moment arms $\mathbf{r}_{K/t}^d \cdot \frac{d}{dt}(\mathbf{I}_t^d \boldsymbol{\omega}_t^d)$ is the change in angular momentum of the segment at the COM of the thigh, where $\boldsymbol{\omega}_t^d$ is the angular velocity and \mathbf{I}_t^d its inertia tensor expressed in a global reference frame.

B.3 Pelvis (p)

Pelvis has the most forces and moments acting on it. There are three joints at the pelvis: the left and right HJC and the LJC. The Newton equation of motion for the pelvis is:

$$\sum \mathbf{F}_p = -\mathbf{F}_H^r - \mathbf{F}_H^l + \mathbf{F}_L + \mathbf{F}_{G,p} + \mathbf{F}_{air,p} = m_p \mathbf{a}_p \quad (\text{B.11})$$

Here \mathbf{F}_H^r and \mathbf{F}_H^l are the forces acting in respectively the right and the left hip and \mathbf{F}_L is the force acting at the lumbosacral joint. $\mathbf{F}_{G,p}$ is the gravitational force acting in the COM of the segment and $\mathbf{F}_{air,p}$ is the air frictional force acting on the pelvis. The Euler equation of motion for the pelvis is:

$$\sum \mathbf{M}_p = -\mathbf{M}_H^l - \mathbf{M}_H^r - \mathbf{M}_{F_{H,p}}^l - \mathbf{M}_{F_{H,p}}^r + \mathbf{M}_L + \mathbf{M}_{F_{L,p}} + \mathbf{M}_{air,p}^d = \frac{d}{dt}(\mathbf{I}_p \boldsymbol{\omega}_p) \quad (\text{B.12})$$

$\frac{d}{dt}(\mathbf{I}_p \boldsymbol{\omega}_p)$ is the change in angular momentum of the segment at the COM, where $\boldsymbol{\omega}_p$ is the angular velocity and \mathbf{I}_p its inertia tensor expressed in a global reference frame. $\mathbf{M}_{F_{H,p}}^d$ is again different from $\mathbf{M}_{F_{H,t}}^d$ due to the different moment arms $\mathbf{r}_{H/p}^d$. \mathbf{M}_L is the moment acting in the lumbosacral joint.

B.4 HAT (h)

We assume the trunk, head and arms to be one rigid body segment. Therefore the lumbosacral joint is the most superior joint. So in the equation of HAT, no additional joint force or moment is introduced. The Newton Equations of HAT are therefore:

$$\sum \mathbf{F}_h = -\mathbf{F}_L + \mathbf{F}_{G,h} + \mathbf{F}_{air,h} = m_h \mathbf{a}_h \quad (\text{B.13})$$

$\mathbf{F}_{G,h}$ is the gravitational force acting in the COM of the segment and $\mathbf{F}_{air,h}$ is the air frictional force acting on HAT. The Euler equation of motion of the HAT at the COM, expressed in a global reference frame is:

$$\sum \mathbf{M}_h = -\mathbf{M}_L - \mathbf{M}_{F_{L,h}} + \mathbf{M}_{air,h}^d = \frac{d}{dt}(\mathbf{I}_h \boldsymbol{\omega}_h) \quad (\text{B.14})$$

$\frac{d}{dt}(\mathbf{I}_h \boldsymbol{\omega}_h)$ is the change in angular momentum of the segment at the COM of the HAT, where $\boldsymbol{\omega}_h$ is the angular velocity and \mathbf{I}_h its inertia tensor expressed in a global reference frame.

B.5 Air frictional force

The air frictional force ($\mathbf{F}_{air,i}$) acting at a segment i was estimated by first determining the total air frictional force acting on the skater, based on the study of van Ingen Schenau (1982):

$$F_{air,tot} = \frac{1}{2} AC_d \rho \mathbf{v}_{xyz}^2 = k_1 \mathbf{v}_{xyz}^2 \quad (\text{B.15})$$

where C_d represents the drag coefficient, A the frontal projected area of the skater, ρ the air density and \mathbf{v}_{xyz} the velocity of the air with respect to the skater. Based on frontal video analysis of the experiment, the ratio in frontal area between the segments was estimated and used to determine the air frictional force per segment.

B.6 CS method: the bottom-up approach

The solution for the CS approach, was found as following; first, the ankle force (\mathbf{F}_A^d) was determined (eq. B.1) to find the moment in the ankle joint (\mathbf{M}_A^d) (eq. B.2). Next, using \mathbf{F}_A^d and \mathbf{M}_A^d , the knee force (\mathbf{F}_K^d) was determined (eq. B.4), in order to estimate the moment around the knee (\mathbf{M}_K^d) (eq. B.5). Then, using \mathbf{F}_K^d and \mathbf{M}_K^d , the forces in the hip joints (\mathbf{F}_H^d) are determined (eq. B.6), to then estimate the moments in the hip joints (\mathbf{M}_H^d) (eq. B.7). Finally, with \mathbf{F}_H^d and \mathbf{M}_H^d , the force in the lumbosacral joint (\mathbf{F}_L) is determined (eq. B.8), to estimate the moment in the lumbosacral joint (\mathbf{M}_L) (eq. B.9). Note that the equations of the HAT segment (eq. B.10, B.11) are not used in the CS approach.

Appendix 6.C LSE method: System Equations and the minimization problem

The LSE method is a least-square error method, based on a linear equation. First the Newton-Euler equations (appendix B) for all segments have to be written in terms of the unknown variables, which are the joint forces and joint moments. Therefore we have to rewrite the moment caused by the joint force in terms of this joint force. This moment is the cross product

between the vector that runs from the COM of segment o to the joint center of joint j ($\mathbf{r}_{j/o}^d$) and the force acting in this joint (\mathbf{F}_j^d), so that:

$$\mathbf{M}_{F_{j,o}}^d = \mathbf{r}_{j/o}^d \times \mathbf{F}_j^d = \begin{bmatrix} \mathbf{r}_{j/o,x}^d \\ \mathbf{r}_{j/o,y}^d \\ \mathbf{r}_{j/o,z}^d \end{bmatrix} \times \begin{bmatrix} F_{j,x}^d \\ F_{j,y}^d \\ F_{j,z}^d \end{bmatrix} \quad (\text{C.1})$$

In which $\mathbf{M}_{F_{j,o}}^d$ is the moment induced by the forces acting in the joint. To obtain a linear equation, we can replace the cross product, by introducing the matrix $\tilde{\mathbf{r}}_{j/o}^d$:

$$\mathbf{M}_{F_{j,o}}^d = \tilde{\mathbf{r}}_{j/o}^d \mathbf{F}_j^d = \begin{bmatrix} 0 & -r_{j/o,z}^d & r_{j/o,y}^d \\ r_{j/o,z}^d & 0 & -r_{j/o,x}^d \\ -r_{j/o,y}^d & r_{j/o,x}^d & 0 \end{bmatrix} \begin{bmatrix} F_{j,x}^d \\ F_{j,y}^d \\ F_{j,z}^d \end{bmatrix} \quad (\text{C.2})$$

We use this matrix in the set of linear equations. The complete system of equations (eq. B.1, B.2, B.4-B.11) is:

$$\begin{bmatrix} \mathbf{I} & 0 & 0 & 0 & 0 & 0 & 0 & 0 & 0 & 0 & 0 & 0 \\ 0 & \mathbf{I} & 0 & 0 & 0 & 0 & 0 & 0 & 0 & 0 & 0 & 0 \\ -\mathbf{I} & 0 & \mathbf{I} & 0 & 0 & 0 & 0 & 0 & 0 & 0 & 0 & 0 \\ 0 & -\mathbf{I} & 0 & \mathbf{I} & 0 & 0 & 0 & 0 & 0 & 0 & 0 & 0 \\ 0 & 0 & -\mathbf{I} & 0 & \mathbf{I} & 0 & 0 & 0 & 0 & 0 & 0 & 0 \\ 0 & 0 & 0 & -\mathbf{I} & 0 & \mathbf{I} & 0 & 0 & 0 & 0 & 0 & 0 \\ 0 & 0 & 0 & 0 & -\mathbf{I} & -\mathbf{I} & 0 & 0 & 0 & 0 & 0 & 0 \\ \mathbf{r}_{A/s}^{rc} & 0 & 0 & 0 & 0 & 0 & \mathbf{I} & 0 & 0 & 0 & 0 & 0 \\ 0 & \mathbf{r}_{A/s}^{lc} & 0 & 0 & 0 & 0 & 0 & \mathbf{I} & 0 & 0 & 0 & 0 \\ -\mathbf{r}_{A/e}^{rc} & 0 & \mathbf{r}_{K/e}^{rc} & 0 & 0 & 0 & -\mathbf{I} & 0 & \mathbf{I} & 0 & 0 & 0 \\ 0 & -\mathbf{r}_{A/e}^{lc} & 0 & \mathbf{r}_{K/e}^{lc} & 0 & 0 & 0 & 0 & -\mathbf{I} & 0 & \mathbf{I} & 0 \\ 0 & 0 & -\mathbf{r}_{K/t}^{rc} & 0 & \mathbf{r}_{H/t}^{rc} & 0 & 0 & 0 & 0 & -\mathbf{I} & 0 & \mathbf{I} \\ 0 & 0 & 0 & -\mathbf{r}_{K/t}^{lc} & 0 & \mathbf{r}_{H/t}^{lc} & 0 & 0 & 0 & 0 & -\mathbf{I} & \mathbf{I} \\ 0 & 0 & 0 & 0 & -\mathbf{r}_{H/h}^{rc} & -\mathbf{r}_{H/h}^{lc} & 0 & 0 & 0 & 0 & -\mathbf{I} & -\mathbf{I} \end{bmatrix} \begin{bmatrix} \mathbf{F}_A^r \\ \mathbf{F}_A^l \\ \mathbf{F}_K^r \\ \mathbf{F}_K^l \\ \mathbf{F}_H^r \\ \mathbf{F}_H^l \\ \mathbf{M}_A^r \\ \mathbf{M}_A^l \\ \mathbf{M}_K^r \\ \mathbf{M}_K^l \\ \mathbf{M}_H^r \\ \mathbf{M}_H^l \end{bmatrix} = \begin{bmatrix} m_s^r \mathbf{a}_s^r - \mathbf{F}_B^r - \mathbf{F}_{G,s}^r - \mathbf{F}_{air,s}^r - \mathbf{F}_{ice}^r \\ m_s^l \mathbf{a}_s^l - \mathbf{F}_B^l - \mathbf{F}_{G,s}^l - \mathbf{F}_{air,s}^l - \mathbf{F}_{ice}^l \\ m_e^r \mathbf{a}_e^r - \mathbf{F}_{G,e}^r - \mathbf{F}_{air,e}^r \\ m_e^l \mathbf{a}_e^l - \mathbf{F}_{G,e}^l - \mathbf{F}_{air,e}^l \\ m_i^r \mathbf{a}_i^r - \mathbf{F}_{G,i}^r - \mathbf{F}_{air,i}^r \\ m_i^l \mathbf{a}_i^l - \mathbf{F}_{G,i}^l - \mathbf{F}_{air,i}^l \\ m_h \mathbf{a}_h - \mathbf{F}_{G,h} - \mathbf{F}_{air,h} \\ \frac{d}{dt} (I_s^r \omega_s^r) - M_B^r - M_{F_B}^r - M_{ice,s}^r - M_{air,s}^r \\ \frac{d}{dt} (I_s^l \omega_s^l) - M_B^l - M_{F_B}^l - M_{ice,s}^l - M_{air,s}^l \\ \frac{d}{dt} (I_e^r \omega_e^r) - M_{air,e}^r \\ \frac{d}{dt} (I_e^l \omega_e^l) - M_{air,e}^l \\ \frac{d}{dt} (I_t^r \omega_t^r) - M_{air,t}^r \\ \frac{d}{dt} (I_t^l \omega_t^l) - M_{air,t}^l \\ \frac{d}{dt} (I_h \omega_h) - M_{air,h} \end{bmatrix} \quad (\text{C.3})$$

In which I is a three by three identity matrix. We can write this equation as

$$Cf = n \quad (C.4)$$

When solving the system, we will obtain an error $e_{q,o}^d$, where q is either a translational (tr) or rotation (ro) error

$$e_{q,o}^d = (Cf - n) \quad (C.5)$$

The system in C.3 is overdetermined and therefore is solved in a least-square manner. We minimize hereby the error $e_{q,o}^d$ while solving for f

$$e_{q,o}^{d\ T} e_{q,o}^d = \min_f \quad (C.6)$$

Optionally a weighing factor can be added to the minimization problem, adding a weighing factor $w_{q,o}^d$. This could be an option when it is known that one of the segment measurements is less reliable than others.

$$e_{q,o}^{d\ T} w_{q,o}^d e_{q,o}^d = \min_f \quad (C.7)$$

In this paper we choose to keep $w_{q,o}^d = I$. The solution is computed by performing a least-squares fit, which minimizes the sum of squares of the deviations of the data from the model, via the solution:

$$f = (C^T C)^{-1} \cdot C^T n \quad (C.8)$$

7

Balancing Power: determining the mechanical power balance in speed skating with a new proposed inverse dynamics method.

'Het kenmerk van een goeie tandarts en een echte theoreticus is om niet alles te slopen wat er is, maar in tact te laten wat kan en erop voortbouwen.' -Vincent Icke-

As introduced in the previous paper (CH 6), the inverse dynamics proceedings influence the determined mechanical power in speed skating. This chapter addresses the impact of the choice for the right inverse dynamics method on the mechanical power estimate and proposes a new method. To thereupon address the quantification of the sensitivity of the mechanical power balance to instrumental errors and inaccuracy in estimated parameters, the new proposed inverse dynamics method is used to determine the mechanical power balance of one skater (joint power, kinetic power, frictional power and gravitational power) with measured 3D kinetic data.

E. van der Kruk, F.C.T. van der Helm, H.E.J. Veeger & A.L. Schwab, *Balancing power: determining the mechanical power balance in speed skating with a new proposed inverse dynamics method.* (2017), under review at Journal of Biomechanics (May 2017)

Abstract

The aim of this paper is to determine the complete mechanical power balance in speed skating (joint power, kinetic power, gravitational power, frictional power) with a new proposed power least-square error optimization for inverse dynamics (PLS), which incorporates the mechanical power balance as a constraint. Attention is given to the sensitivity of the power balance to instrumental errors and inaccuracies in estimated body parameters. The conventional least-square error method (LSE) and PLS perform equally well for the estimation of joint power. The new proposed inverse dynamics method PLS significantly reduced residual power errors in the mechanical power balance compared to the existing LSE method, by improving the kinetic power estimation. This was mainly induced by an improvement in estimation of the upper body acceleration. Modelling results indicated that, frictional power alone is not a good estimate of joint power –even at constant forward speeds–, because on average 20% of the joint power dissipates to upwards and lateral oscillatory motions (kinetic and gravitational power). Sensitivity analyses showed that the normal force and steering angle accuracy, as well as the COM position of the HAT segment, are of significant influence on the joint power estimation; a 5° inaccuracy in steer or 5 cm inaccuracy of the COM position of the HAT resulted in a 9.7 % and 12.6 % mean error in joint power estimation respectively.

1. Introduction

Mechanical power estimations can provide valuable insight into the performance of an athlete. Currently, work is done on the design of a real-time power meter that can be used during speed skating practices. Due to the real-time feedback demand and the restricted number of sensors, the design of such a system requires a simplified mechanical power model with minimal inputs. As discussed in CH5, it is important to quantify the consequences for a simplified power model. For this quantification, or in other words verification, the complete mechanical power balance should be determined. The mechanical power balance in speed skating consists of four components: joint power, kinetic power, frictional power and gravitational power. To determine these components, one needs measured 3D kinetic data of a speed skater, a rigid body model and body segment parameters (Dumas, Chèze, & Verriest, 2007). CH6 discussed that a skater can be modelled with an eight segment rigid body model (skates, shanks, thighs, pelvis and HAT (which is the head, arms and torso)), with a revolute joint in the knee, while keeping all other joints spherical. Furthermore, a global optimization technique in which the marker residuals were minimized, was used for the inverse kinematics. A least square error method which minimized the residuals in the Newton-Euler equations of motion (LSE), optimized the estimation of joint forces and moments (inverse dynamics), in order to determine the joint power. However, that study focussed on joint power only, neglecting the remaining terms in the balance, namely the kinetic, frictional and gravitational power. Since we now want to determine the complete power balance with all four components, an additional constraint will be added to the least-square error method for inverse dynamics: the power balance. Since if the system is not balanced, superfluous power dissipates to or from the system. By adding this constraint to the least-square error optimization problem, not only the estimation of the joint forces and moments is improved – as in LSE (Kuo, 1998; van der Kruk, Schwab, et al., 2017), but also the input data of the model.

The aim of this paper is to determine the complete mechanical power balance in speed skating (joint power, kinetic power, gravitational power, frictional power), for an eight rigid body model, with a new proposed least-square error optimization, minimizing the power residual. Special attention will be given to the sensitivity to measurement errors and estimated body parameters. The paper is organized as follows; first, the data collection, rigid body model and inverse dynamics methods are presented, together with the evaluation criteria for the methods. Second, the residuals of the methods, the estimated mechanical power balance, and the

sensitivity of the model are given. Finally, based on the results, the new proposed method is evaluated.

2. Method

2.1 Data collection and processing

Kinetic data of eight elite speed skaters were collected on an indoor ice rink (Thialf, Heerenveen) using a passive motion capture system (Qualisys, 2015) and a pair of wireless instrumented klapskates (van der Kruk, den Braver, Schwab, van der Helm, & Veeger, 2016). The data collection is fully described in CH6. The data were post-processed with a global optimization method (GOM) for body pose reconstruction (BPR). The knee was hereby modelled as a revolute joint, all other joints were spherical. In this paper the data of one participant for one straight (three strokes) is presented, since we want to show the influence of different data manipulation techniques for the inverse dynamics and sensitivity analyses; adding more data may occlude these effects.

The Euler rotations of a segment correspond to the order Y,X and Z, for the skate segment referred to as steer, lean, pitch. The joint rotation, which is the rotation between two segments, is rotated in the Euler sequence Z', X', and Y', around the SCS, further referred to as the flexion-extension (Z'), adduction-abduction (X') and internal-external rotation (Y').

2.2 Mechanical Power

2.2.1 Equations of motion

To determine the equations of motion of a speed skater, first the skater is modelled as a chain of linked rigid bodies, segments. The skater is divided into eight segments: the skates (s), the legs (e), the thighs (t), the pelvis (p) and the HAT (h) (Figure 6.3). Now we set-up the Newton-Euler equations of motion for each of these segments expressed in a global reference frame xyz, where y is up, x is in the longitudinal direction of the straight and z is in the lateral direction of the straight part of the rink (right, facing forward), in agreement with the ISB convention. These equations of motion are presented in Appendix 6.A.

2.2.2 Inverse Dynamics: Determine the joint forces and moments

Given the acceleration of the body segments and the measured ground reaction forces, the system of equations to determine the unknown joint forces and moments can be solved. Since there are more equations than unknowns, it is solved in a least square error manner.

Least-Square Error (LSE) The system of equations for the eight rigid body speed skater is overdetermined (in our system we have 39 variables and 48 equations, see Appendix 6.C). Therefore the solution can be found by solving this system of linear equations with a least-square error fit (Kuo, 1998). The method minimizes the moment and force residuals in the Newton-Euler equations of motion (Appendix 6.C). The objective function for the minimization, J_{\min} , now consists of residuals in the Newton and Euler equations of motion (EoM) of each body segment. The objective function is determined for every timestep t_i . The residuals for the Newton EoM are:

$$E_{F_o}^d = \left(\frac{\left(\sum F_o^d - m_o^d a_o^d \right)}{\bar{F}_o^d} \right)^2 \quad (7.1)$$

In which d is either left or right, o is the segment (s,e,t,p,h) and \bar{F}_o^d is a scaling factor that scales the error found in this equation. These scaling factors were introduced, since all equations in J_{\min} each have a different unity and magnitude. Furthermore the scaling factors

can add significance or an indication of reliability of measurement or estimation to each of the variables. The residuals in the EoMs for the Euler equations of motion are:

$$\mathbf{E}_{M_o}^d = \left(\frac{\left(\sum \mathbf{M}_o^d - \frac{d}{dt} (I_o^d \boldsymbol{\omega}_o^d) \right)}{\bar{M}_o^d} \right)^2 \quad (7.2)$$

In which \bar{M}_o^d is the scaling factor of each segment. We allow an error or residue in these Newton-Euler equations of motion to relax the rigid body assumption on the segments. The optimization variable for the error in the EoM of both the forces and moments is:

$$E_{EM} = \sum_o \left(\mathbf{E}_{F_o}^d + \mathbf{E}_{M_o}^d \right) \quad (7.3)$$

And the objective function for the minimization, J_{\min} , is

$$J_{\min}(X_{LSE}) = E_{EM} \quad (7.4)$$

In which \mathbf{X} are the variables to be estimated with the optimization consisting of the joint forces and moments,

$$X_{LSE} = \begin{bmatrix} \mathbf{F}_j^d & \mathbf{M}_j^d \end{bmatrix} \quad (7.5)$$

Power Least-Square error (PLS) In the PLS method minor modifications are allowed to the input variables under the assumption that the measurements can be slightly off. Different from other methods, the PLS method introduces the mechanical power balance as a constraint to the optimization function. PLS improves therefore both the input data and the power estimation. The objective function for the minimization, J_{\min} , now consists of three parts.

The first part are the residuals in the Newton Euler equations of motion (EoM) of each body segment, E_{EM} (eq 7.3). The second part of J_{\min} consists of the power balance. This is to make sure that no superfluous power gets pumped in or dissipates. Also this equation was weighted, with a scaling factor \bar{P} .

$$E_p = \left(\frac{P_k - P_f - P_g - P_j}{\bar{P}} \right)^2 \quad (7.6)$$

The third, and last part of J_{\min} consists of the measured variables (V), since it is foreseen that instrumental errors are present. In order to keep the estimated data close to the actual measurements, the following equations were added to the minimization variable:

$$\sum \left(\frac{V^d - \hat{V}^d}{\bar{V}^d} \right) \quad (7.7)$$

Where \bar{V}^d are the scaling factors and V^d are the estimated optimization data; \hat{V}^d is the

measured variable or estimated parameter. Taken into account are the global forces F_b^d (indirect measure of the orientation of the skate and the measured force) and the ice frictional force F_{ice}^d . Furthermore, for each segment o , the estimated air frictional force $F_{air,o}^d$, the measured acceleration a_o^d , and the change in angular momentum dIw_o^d were included. For the angular momentum we took the derivative of the inertial tensor times the rotational velocity as one variable that could be altered:

$$dIw_o^d = \frac{d}{dt}(I_o \omega_o)^d \quad (7.8)$$

Adding the different errors, gives us the minimization criteria:

$$J_{\min}(X_{PLS}) = E_{EM} + E_P + E_V \quad (7.9)$$

In which X are the variables to be estimated with the optimization consisting of the joint forces and moments, the measured global forces, the estimated ice frictional force, the estimated air frictional force, the measured accelerations of each segment and the change in angular momentum:

$$X_{PLS} = \begin{bmatrix} F_j^d & M_j^d & F_B^d & F_{ice}^d & F_{air,o}^d & a_o^d & dIw_o^d \end{bmatrix} \quad (7.10)$$

The linear set of equations is solved in a least-square error manner. The mechanical power balance resulting from the PLS method, is discussed in the results section of this paper. The alterations made to the input variables (\tilde{X}) due to the least-square error optimizations are presented in Appendix 7.A.

2.2.3 Power Equations

Since the joint forces and moments are determined, the mechanical power balance can be determined. A precise definition of mechanical power in speed skating is presented in CH5; here we repeat the main results. The total power equations for the system can be written in terms of joint power (P_j), gravitational power (P_G), frictional power (P_f), kinetic power (P_k), and environmental power (P_e) as in,

$$P_j = P_k + P_G + P_f + P_e \quad (7.11)$$

In which we have the joint power (P_j) which is directly calculated using the moments at the joint (M_j) and the rotational velocities around the joint (ω_j), as in

$$P_j = \sum_{i=1}^{N-1} M_{i,i+1} (\omega_{i+1} - \omega_i) = \sum_{j=1}^{N-1} M_j \omega_j \quad (7.12)$$

$$P_j = M_A^d (\omega_s^d - \omega_e^d) + M_K^d (\omega_e^d - \omega_t^d) + M_H^d (\omega_t^d - \omega_p^d) + M_J^d (\omega_p^d - \omega_h^d) \quad (7.13)$$

In which the subscripts denote the segments (s, e, t, p, h) and the joints (ankle (A), knee (K),

hip (H) and lumbosacral joint (L)), $\mathbf{M}_{j,o}$ are the joint moments and $\boldsymbol{\omega}_o$ is the segment angular velocity. d denotes either left or right, so both sides (legs) are incorporated in the joint power.

We find the gravitational power in equation 7.11 as in,

$$P_G = \sum_{i=1}^N \mathbf{v}_i m_i \mathbf{g} \quad (7.14)$$

$$P_G = \mathbf{v}_i \sum m_i \mathbf{g} = \mathbf{v}_s^d \mathbf{F}_{G,s}^d + \mathbf{v}_e^d \mathbf{F}_{G,e}^d + \mathbf{v}_t^d \mathbf{F}_{G,t}^d + \mathbf{v}_p \mathbf{F}_{G,p} + \mathbf{v}_h \mathbf{F}_{G,h} \quad (7.15)$$

In which $\mathbf{F}_{G,o}$ are the gravitational forces and \mathbf{v}_o is the linear velocity of the segment. And the frictional power, which consists of translational power and rotational power,

$$P_f = \sum_{i=1}^N \boldsymbol{\omega}_i \mathbf{M}_{fr,i} + \sum_{i=1}^N \mathbf{v}_i \mathbf{F}_{fr,i} \quad (7.16)$$

With the individual contributions of the ice and air friction,

$$P_{ice} = \boldsymbol{\omega}_s^d \mathbf{M}_{ice,s}^d + \dot{\mathbf{x}}_s^d \mathbf{F}_{ice} \quad (7.17)$$

$$P_{air} = \dot{\mathbf{x}}_s^d \mathbf{F}_{air,s}^d + \dot{\mathbf{x}}_e^d \mathbf{F}_{air,e}^d + \dot{\mathbf{x}}_t^d \mathbf{F}_{air,t}^d + \dot{\mathbf{x}}_p \mathbf{F}_{air,p} + \dot{\mathbf{x}}_h \mathbf{F}_{air,h} \quad (7.18)$$

And the environmental power, which consists of translational power and rotational power,

$$P_e = \sum_{i=1}^N \boldsymbol{\omega}_i \mathbf{M}_{e,i} + \sum_{i=1}^N \mathbf{v}_i \mathbf{F}_{e,i} \quad (7.19)$$

And the change of kinetic energy in the segments:

$$P_k = d \sum \frac{E_{seg}}{dt} = \sum_{i=1}^N \frac{d}{dt} (I_i \boldsymbol{\omega}_i) \cdot \boldsymbol{\omega}_i + \sum_{i=1}^N m_i \mathbf{a}_i \cdot \mathbf{v}_i \quad (7.20)$$

2.3 Criteria for evaluation of the inverse dynamics methods

The inverse dynamics techniques are evaluated based on two variables: the Newton-Euler

residuals ($\tilde{\mathbf{e}}_{F,o}^d, \tilde{\mathbf{e}}_{M,o}^d$) and the power residual ($\tilde{\mathbf{e}}_{POW}$). The Newton-Euler residuals are the errors, which are left in each Newton and Euler equations of motion after the inverse dynamics for each segment.

$$\tilde{\mathbf{e}}_{F,o}^d = \tilde{\mathbf{F}}_o^d - m_o^d \tilde{\mathbf{a}}_o^d \quad (7.21)$$

$$\tilde{\mathbf{e}}_{M,o}^d = \tilde{\mathbf{M}}_o^d - \frac{d}{dt} I_o^d \tilde{\boldsymbol{\omega}}_o^d \quad (7.22)$$

Even if $\tilde{\mathbf{e}}_{F,o}^d$ and $\tilde{\mathbf{e}}_{M,o}^d$ are optimal, there can still be an imbalance in the mechanical power equation. The power residual is based on the mechanical power balance; theoretically the kinetic power, the gravitational power, the environmental power, and the frictional power should add up to the joint power at any instant in time. This is generally not the case, due to

Table 7.1 Left column: relative error added to the variable or parameter. The absolute error differs over time and per variable. The maximum absolute errors added to each variable or parameter are given in the remaining columns.

Error	Skate				Fair	Acc	COM				
	<i>Fn</i>	<i>Fl</i>	<i>steer</i>	<i>lean</i>			<i>Skate</i>	<i>Leg</i>	<i>Thigh</i>	<i>Pelvis</i>	<i>HAT</i>
10%	96 N	66 N	5°	5.5°	1 N	0.2 m/s	0.02 m	0.04 m	0.05 m	0.02 m	0.05 m

measurement errors and model assumptions:

$$\tilde{e}_{POW} = \tilde{P}_j - \tilde{P}_k - \tilde{P}_f - \tilde{P}_G - \tilde{P}_e \quad (7.23)$$

2.4 Sensitivity of the model

To determine the necessary accuracy of measured variables and estimated parameters to establish the joint power with the PLS method and to determine the robustness of the method, a sensitivity analysis was performed. The analysis was done for three sets of measured variables and three sets of estimated parameters, namely the measurements of the push-off forces, orientation of the skate, and the segment accelerations, and the estimations of the air frictional forces, and COM position of the segments. The sensitivity of the joint power estimation to the ice frictional force estimation, possible movements within the joints and the CP position was not tested, since their influence is small. The influence of the rigid body assumption, marker motion and local coordinate system determination were covered in van der Kruk et al. 2017.

The sensitivity of the joint power model for each variable was determined for one stroke. The specific variable or parameter was changed by adding a perturbation in time to the data. The absolute error therefore differs over time and per variable. A 10% perturbation was chosen for each variable, the resulting maximum absolute perturbations are shown in Table 7.1.

The sensitivity of the model for this specific variable is defined in the usual manner as,

$$S_p = 100 \cdot \frac{1}{N} \sum_{t_i} \left\| \frac{P_{pp}(x \pm x_{err}) - P_{pp}(x)}{P_{pp}(x)} \right\| \quad (7.24)$$

Where x is the variable or parameter that is changed, x_{err} the change and N are the number of data points. pp indicates kinetic, gravitational, frictional or joint power. The measured variables of the normal and lateral force and of the orientation of the skates (lean, steer and pitch), were changed by adding a constant error (10%). The air frictional force and the acceleration were varied for each segment. The position of the COM of the segments were varied in position in the local X-axis for the skate and the local Y-axis for the leg, thigh, pelvis and HAT.

3. Results

3.1 Mechanical Power Balance

Regarding the residuals from the Newton-Euler equations of motion, LSE and PLS perform equally well. LSE has lower residuals than PLS for the Euler equations (average \tilde{e}_M is 9 Nm for both methods), while PLS has lower residuals than LSE for the Newton equations (\tilde{e}_F is 23N for LSE and 20N for PLS). Figure 7.2 shows the individual contributions to the power balance (joint power, frictional power, kinetic power and gravitational power) for one of the strokes obtained with LSE

Table 7.2 Average and peak joint power (P_j), frictional power (P_f), kinetic power (P_k) and gravitational power (P_g) for three separate strokes for the PLS and LSE method in Watt. Especially for the residual power, E_p , PLS has lower values. The peak E_p values of LSE are up to two times the peak joint powers.

	Stroke 1 (R)				Stroke 2 (L)				Stroke 3 (R)			
	LSE		PLS		LSE		PLS		LSE		PLS	
W	avg	peak	avg	peak	avg	peak	avg	peak	avg	peak	avg	peak
P_j	261	998	264	1001	276	998	280	1001	233	877	232	862
P_f	-231	-245	-223	-245	-240	-255	-231	-275	-240	-254	-231	-252
P_g	-7	217	-7	217	-7	191	-7	191	-1	221	-1	221
P_k	121	1162	22	715	60	1827	28	715	77	1115	-16	467
E_p	-99	981	11	68	-32	1799	13	138	-85	1491	16	132

and PLS. The powers of PLS (optimized) are clearly more in balance (average \tilde{e}_{POW} is 11 W, peak is 68 W) than the powers of LSE (un-optimized) (average \tilde{e}_{POW} is -99 W, peak is 981 W), see Table 7.2. This difference is caused by the difference in kinetic power. LSE uses the measured data directly (filtered by minimizing the marker differences and with a second order Butterworth filter with a cut-off at 2Hz) as input, whereas PLS adjusts these data with the power balance as a constraint. The largest adjustments made in PLS were found for the longitudinal acceleration of the HAT (x-direction, forward direction for the skater) (see Figure 7.3). The difference in joint power between the LSE and PLS method is small, with 261W and

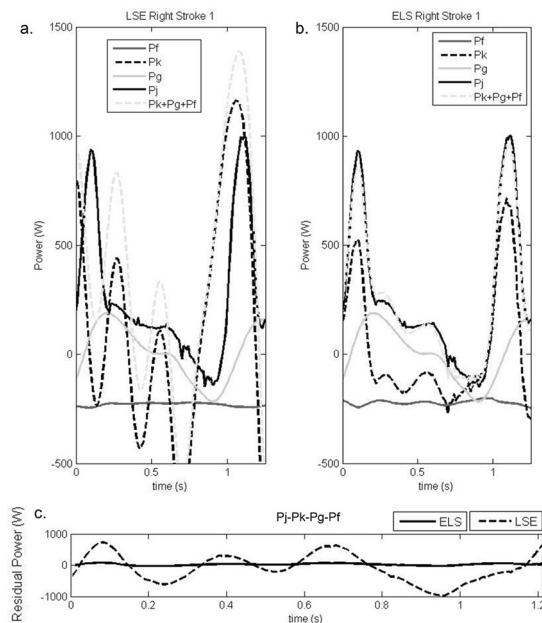


Figure 7.2 a,b) Specific power contributions to the complete mechanical power balance in speed skating. P_f = frictional power, P_k = kinetic power, P_g = gravitational power, P_j = joint power. The dip in the kinetic power is attributed to the lateral fluctuation. The gravitational power is on average around zero, the skater moves his body up and down within a stroke. C) Theoretically the kinetic power, the gravitational power and the frictional power should add up to the joint power P_j at any instant in time. In this graph the residual powers are shown ($P_j - P_k - P_g - P_f$). The LSE method clearly shows higher residual powers than the PLS method.

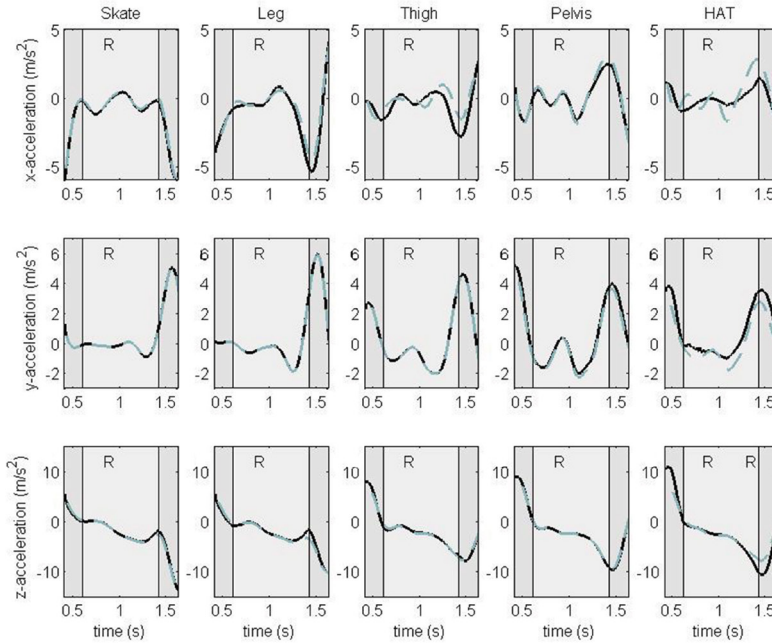


Figure 7.3 Optimizations done by the PLS method to the acceleration of the center of mass of the segments. Black line is the optimized data, the blue line are the measured data. Y is up, x is in the longitudinal direction of the straight and z is in the lateral direction of the straight part of the rink (right, facing forward), in agreement with the ISB convention.

264 W mean joint power respectively, and 998 W and 1001 W peak joint power respectively (see Table 7.2, stroke 1).

Table 7.2 presents the average and peak power from each component of the mechanical power balance for three individual strokes. Note that the average powers do not necessarily have to add up. Joint power mainly dissipates in frictional power (on average 80-99%); kinetic and gravitational power account for the remaining part. This ratio varies largely for separate data points in time throughout a stroke (see Figure 7.2).

3.2 Sensitivity of the model

The sensitivity of the power estimation (S_p) for the measured variables and estimated parameters is given in Table 7.3. The results show that, based on the deviations in joint power and the peak power residuals, PLS is more robust to perturbations than LSE, as expected. Overall, the table reveals the importance of accurate input data, particularly the estimation of the center of mass position of the HAT segment and the measurements of the push-off forces in global space – consisting of the normal and lateral forces with the lean and steer angle. Perturbations in these variables and parameter resulted in most increased power residuals, and the largest deviations in the joint power estimations for PLS. A 10% perturbation on the COM position of the HAT (maximum of 0.05m) resulted in an error in the joint power estimation of 12.6% for PLS. For the locally measured normal force, absolute mean difference in joint power was 11.6% for PLS (maximum perturbation 96N). Steer was most influential on the joint power regarding the orientation of the skate; a mean absolute difference of 9.7% was found (maximum perturbation was 5°).

Table 7.3 The sensitivity of the model (S_P) for each tested variable and parameter for Stroke 1. The sensitivities are in percentages. S_{P-LSE} = sensitivity of model with LSE method; S_{P-PLS} = sensitivity of model with PLS method. The power residuals are in Watt. The un-perturbed values of the power residuals (E_p) for PLS and LSE were respectively 11 W and -99 W on average with peaks of 68 W and 981 W (table 2). Overall, the PLS method is more robust than LSE, based on the joint power errors and the peak power residuals. The power balance is most sensitive to the orientation of the skate, the push-off forces and the position of the COM of the HAT segment.

Method		Skate				Fair	Acc	COM				
		<i>Fn</i>	<i>Fl</i>	<i>steer</i>	<i>lean</i>			<i>skate</i>	<i>leg</i>	<i>thigh</i>	<i>pelvis</i>	<i>HAT</i>
	Max	96N	66N	5°	5.5°	1 N	0.2 m/s	0.02 m	0.04m	0.05 m	0.02 m	0.05 m
	Perturbation											
S_{P-LSE}												
Pj	(%)	12.2	8.5	8.5	8.5	0.1	1.6	0.4	2.0	1.6	1.7	13.2
Pk	(%)	0	0	99.5	6.4	0	10.0	2.0	19.6	24.5	7.8	77.2
Pf	(%)	0.7	0.2	0.6	<0.1	9.0	0	<0.1	0.1	0.3	0.3	0.1
Pg	(%)	0	0	7.4	31.8	0	0	1	6.0	14.6	1.7	19.7
Ep avg	(W)	-72	-104	-55	-100	-119	-109	-98	-99	-103	-97	-59
Ep peak	(W)	944	1008	1181	1006	1002	1080	980	991	1041	978	1049
S_{P-PLS}												
Pj	(%)	11.6	6.4	9.7	6.7	0.7	1.3	0.2	1.4	1.7	1.4	12.6
Pk	(%)	10.5	4.1	18.1	5.7	14.3	3.9	0.4	2.3	4.3	0.8	8.3
Pf	(%)	0.8	0.2	1.2	0.1	9.2	0.4	<0.1	0.2	0.3	0.3	0.8
Pg	(%)	0	0	7.4	31.8	0	0	1	6.0	14.6	1.7	19.7
Ep avg	(W)	18	9	17	11	9.9	10	11	11	12	11	12
Ep peak	(W)	84	62	75	64	67	68	68	69	67	67	89

4. Discussion

4.1 Inverse Dynamics

The newly proposed inverse dynamics method (PLS) shows a better mechanical power balance compared to the existing LSE method, with minimum power residuals over time. The improvement is attributed to the optimization performed on the HAT acceleration data (mainly in forward (x) direction), which largely impacts the kinetic power estimation. The input data for both LSE and PLS had been filtered by minimizing the marker differences (van der Kruk, Schwab, et al., 2017) and a Butterworth second order filter (cut-off 2Hz) before entering the inverse dynamics method. However, a small measurement error in the HAT acceleration ($<1 \text{ m/s}^2$), resulted in residual powers in the power balance of the LSE method of up to 1800 W (almost twice the peak joint power). PLS optimizes the input for the mechanical power model; the largest adjustments were made to the acceleration of the HAT. The HAT is assumed to be the trunk, head and arms, which clearly is not a rigid body on an actual human. Adjustments to the measured data were therefore expected at the HAT segment, and not unrealistic ($\text{SD} = 1 \text{ m/s}^2$). So although the optimizations done on the input data are fairly small (see Appendix 7.A), they show to be very effective in optimizing the kinetic power (Pk), and thereby reducing the residual powers in the power balance.

4.2 Comparison to literature

Mechanical power can be estimated via either joint power, or the sum of frictional, kinetic and gravitational power. Existing mechanical power models in speed skating, however, omit the kinetic and gravitational power, thereby estimating the mechanical power with frictional power only, under the assumption of a constant forward velocity (De Boer & Nilsen, 1989; de

Koning, Foster, Lampen, Hettinga, & Bobbert, 2005; Houdijk, de Koning, de Groot, Bobbert, & van Ingen Schenau, 2000; Noordhof, Foster, Hoozemans, & De Koning, 2013; van Ingen Schenau, 1982; Van Ingen Schenau & Bakker, 1980; van Ingen Schenau & Cavanagh, 1990). As expected, on average, this underestimates the mechanical power estimation up to 20%, varying largely for separate data points in time throughout a stroke (Table 7.2, Figure 7.2). Although the skater in this study moved at an almost constant forward velocity, the kinetic and gravitational power do fluctuate within a stroke, due to the oscillatory lateral and upward velocity. So apart from frictional power, the kinetic and gravitational power are essential for an accurate mechanical power estimation. The results indicate that accurate kinematic data of the HAT segment (velocity and acceleration) are important for the estimation of kinetic power, and that small perturbations have a large impact on the eventual estimation. The PLS method is a form of sensor fusion where the measured force data and the measured kinematic data are combined to improve the kinetic power estimation. When force data are not available, one could also think of other sensor fusion options, such as Kalman filtering.

4.3 Sensitivity of the model to measured variables.

The sensitivity analysis showed that the accuracy with which the orientation of the skate (steer) and the push-off forces (normal and lateral) are measured is of high influence on the joint power estimation. This was expected, since the moments around the joint are mainly determined by the direction and magnitude of the global push-off force. The applied instrumented skate (van der Kruk, den Braver, et al., 2016b), with an accuracy in forces of around 4 % in the normal and 6% in the lateral direction, would account for an error in joint power of 3.5% and 1.7% respectively with the PLS method. The estimation of a steer angle within a 5% error ($<2.5^\circ$) or the estimation of the COM position at the HAT segment with 5 cm accuracy, are more challenging, if not impossible, at an ice rink with the current state of technology.

The sensitivity analysis is of high value to create insight into the model reliability and to determine the necessary accuracy of a human motion capture system. It would, however, be easy to get mislead into the thought that this analysis also decides on the importance of the variables in the skating stroke for an optimal performance. However, the variables were treated as independent measures, whereas when skaters change e.g. their steering, this would affect the overall velocity of the skater. This analysis does therefore not predict what the change in performance or power would be in case skaters would change this variable themselves. When one would like to determine what the influence of one of the parameters or variables is on the produced joint power, a forward dynamic model is needed (CH4).

5. Conclusion

- The inverse dynamics method PLS showed significantly reduced residual powers in the complete mechanical power balance compared to the existing LSE method, by improving the kinetic power estimation.
- Frictional power alone is not a good estimate of joint power –even at constant forward speeds–, because on average 20% of the joint power dissipates to upwards and lateral oscillatory motions (kinetic and gravitational power).
- Sensitivity analyses showed that the normal force and steering angle accuracy, as well as the COM position of the HAT, are of significant influence on the joint power estimation; a 5° inaccuracy in steer or 5 cm inaccuracy of the COM position of the HAT resulted in a 9.7 % and 12.6 % error in joint power estimation respectively.
- Accurate estimation of the kinetic and gravitational power depends heavily on the kinematic measurements of the HAT segment (upper body);

Acknowledgements

This study was supported by NWO-STW 12870.

References

- De Boer, R. W., & Nilsen, K. (1989). *The gliding and push-off technique of male and female Olympic speed skaters*. *International Journal of Sport Biomechanics*, 119–134.
- De Koning, J. J., Foster, C., Lampen, J., Hettinga, F., & Bobbert, M. F. (2005). *Experimental evaluation of the power balance model of speed skating*. *Journal of Applied Physiology* (Bethesda, Md. : 1985), 98(1), 227–233. <http://doi.org/10.1152/jappphysiol.01095.2003>
- Dumas, R., Chèze, L., & Verriest, J. P. (2007). *Adjustments to McConville et al. and Young et al. body segment inertial parameters*. *Journal of Biomechanics*, 40(3), 543–553. <http://doi.org/10.1016/j.jbiomech.2006.02.013>
- Houdijk, H., de Koning, J. J., de Groot, G., Bobbert, M. F., & van Ingen Schenau, G. J. (2000). *Push-off mechanics in speed skating with conventional skates and klapskates*. *Medicine and Science in Sports and Exercise*, 32(3), 635–641. <http://doi.org/10.1097/00005768-200003000-00013>
- Kuo, A. D. (1998). *A least-squares estimation approach to improving the precision of inverse dynamics computations*. *Journal of Biomechanical Engineering-Transactions of the Asme*, 120(1), 148–159. <http://doi.org/10.1115/1.2834295>
- Noordhof, D. A., Foster, C., Hoozemans, M. J., & De Koning, J. J. (2013). *Changes in speed skating velocity in relation to push-off effectiveness*. *International Journal of Sports Physiology and Performance*, 8(2), 188–194.
- Qualisys. (2015). <http://www.qualisys.com/>.
- Van der Kruk, E. ., van der Helm, F. C. T. ., Veeger, H. E. J. ., & Schwab, A. L. . (2017). *Power relations: a literature review on the terminology of power in sports with an application in speed skating*. Submitted at *Journal of Biomechanics*.
- Van der Kruk, E., den Braver, O., Schwab, A. L., van der Helm, F. C. T., & Veeger, H. E. J. (2016). *Wireless instrumented klapskates for long-track speed skating*. *Journal of Sports Engineering*, 19(4), 273–281. <http://doi.org/10.1007/s12283-016-0208-8>
- Van der Kruk, E., Schwab, A. L., van der Helm, F. C. T., & Veeger, H. E. J. (2017). *Getting in shape: reconstructing three-dimensional long-track speed skating kinematics by comparing several body pose reconstruction techniques*. Submitted at *Journal of Biomechanics*.
- Van Ingen Schenau, G. J. (1982). *The influence of air friction in speed skating*. *Journal of Biomechanics*, 15(6), 449–458. [http://doi.org/10.1016/0021-9290\(82\)90081-1](http://doi.org/10.1016/0021-9290(82)90081-1)
- Van Ingen Schenau, G. J., & Bakker, K. (1980). *A biomechanical model of speed skating*. *Journal of Human Movement Studies*, 6, 1–18.
- Van Ingen Schenau, G. J., & Cavanagh, P. R. (1990). *Power equations in endurance sports*. *Journal of Biomechanics*, 23(9), 865–881. [http://doi.org/10.1016/0021-9290\(90\)90352-4](http://doi.org/10.1016/0021-9290(90)90352-4)

Appendix 7.A PLS Method input variables

The PLS method allows modification to the input data to find an optimal solution in which the constraint equations (Newton-Euler equations of motion, the power balance and the measured variables) are best satisfied. In Table 7.4 we present the adjustments to the input data. The mean and standard deviation of the difference between the measured data are given, together with maximum of the measured data itself. The measured data are presented together with the optimized input data for the measured forces and ice frictional forces (Figure 7.4), the angular momentum (Figure 7.5), and the air frictional forces (Figure 7.6).

Table 7.4 Adjustments made to the input data by the PLS optimization. R = right, L = left; Difference estimated is the difference between the measured data and the optimized data in the PLS method. The reference is the peak value of the variable or parameter in the measured data.

Forces		Difference estimated		Reference	SD/ref
		mean	SD	Max	
Fb	R	-6 N	20 N	1100.7 N	1.8 %
Fb	L	-5 N	19 N	1143.9 N	1.7 %
Fice	R	0.0 N	0.1 N	3.1 N	3.2 %
Fice	L	0.0 N	0.1 N	3.3 N	3.0 %
Air friction					
Skate	R	0.0 N	0.1 N	1.2 N	8.3 %
Skate	L	0.0 N	0.1 N	1.2 N	8.3 %
Leg	R	0.0 N	0.1 N	2.1 N	4.8 %
Leg	L	0.0 N	0.1 N	2.0 N	5.0 %
Thigh	R	0.0 N	0.1 N	3.6 N	2.8 %
Thigh	L	0.1 N	0.1 N	3.4 N	2.9 %
Pelvis	-	0.0 N	0.1 N	1.9 N	5.3 %
HAT	-	0.0 N	0.1 N	9.9 N	1.0 %
Acceleration					
Skate	R	-0.0 m/s ²	0.1 m/s ²	15.7 m/s ²	0.6 %
Skate	L	-0.0 m/s ²	0.1 m/s ²	15.9 m/s ²	0.6 %
Leg	R	-0.1 m/s ²	0.3 m/s ²	11.7 m/s ²	2.6 %
Leg	L	-0.1 m/s ²	0.3 m/s ²	11.8 m/s ²	2.5 %
Thigh	R	-0.1 m/s ²	0.5 m/s ²	8.2 m/s ²	6.1 %
Thigh	L	-0.1 m/s ²	0.4 m/s ²	7.8 m/s ²	5.1 %
Pelvis	-	0.0 m/s ²	0.2 m/s ²	20.2 m/s ²	<0.1 %
HAT	-	0.1 m/s ²	1 m/s ²	7.7 m/s ²	13 %
dlw					
Skate	R	-0.0 Nm	0.2 Nm	0.1 Nm	200 %
Skate	L	-0.0 Nm	0.2 Nm	0.1 Nm	200 %
Leg	R	0.0 Nm	0.2 Nm	3.5 Nm	5.7 %
Leg	L	-0.0 Nm	0.2 Nm	2.2 Nm	9.1 %
Thigh	R	0.0 Nm	0.2 Nm	6.8 Nm	2.9 %
Thigh	L	0.0 Nm	0.2 Nm	5.5 Nm	3.6 %
Pelvis	-	0.0 Nm	0.2 Nm	47 Nm	<0.1 %
HAT	-	0.0 Nm	0.2 Nm	15.8 Nm	1.3 %

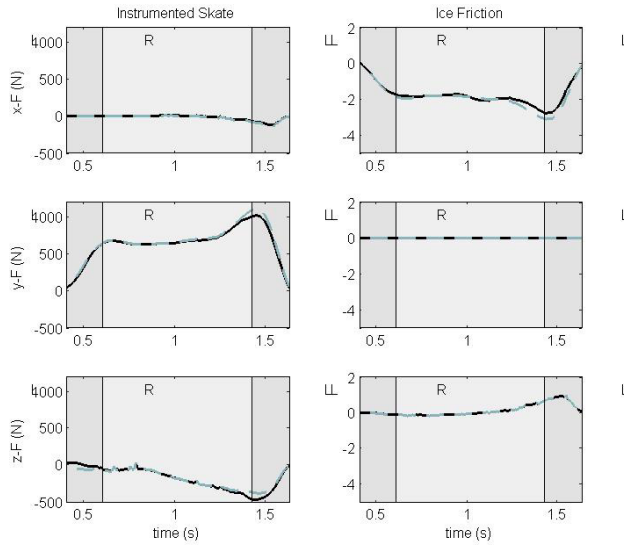


Figure 7.4 Optimizations of the PLS method for the measured forces and estimated ice frictional forces. Black line are the optimized data, the blue line are the measured data. Y is up, x is in the longitudinal direction of the straight and z is in the lateral direction of the straight part of the rink (right, facing forward), in agreement with the ISB convention

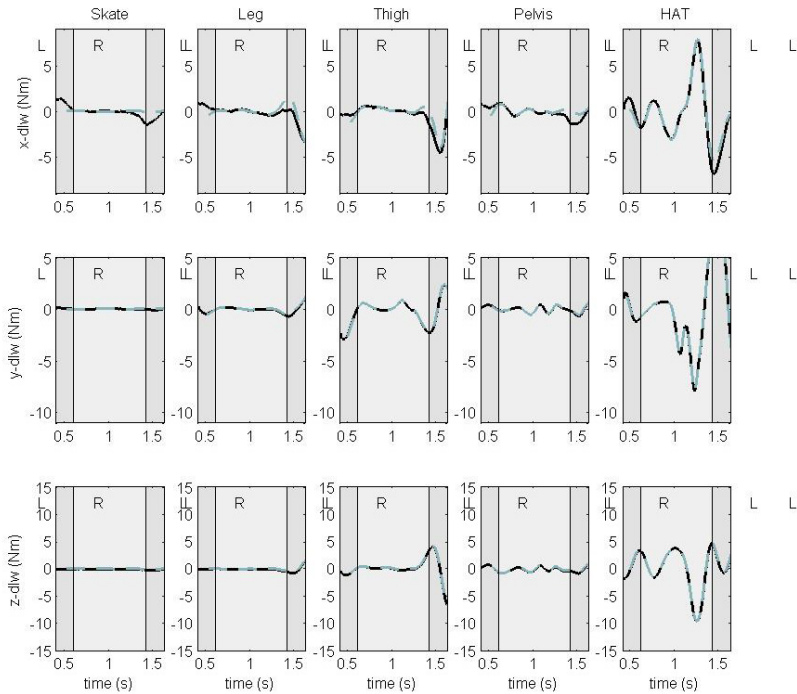


Figure 7.5 Optimizations of the PLS method to the change in angular momentum. Black line are the optimized data, the blue line are the measured data. Y is up, x is in the longitudinal direction of the straight and z is in the lateral direction of the straight part of the rink (right, facing forward), in agreement with the ISB convention

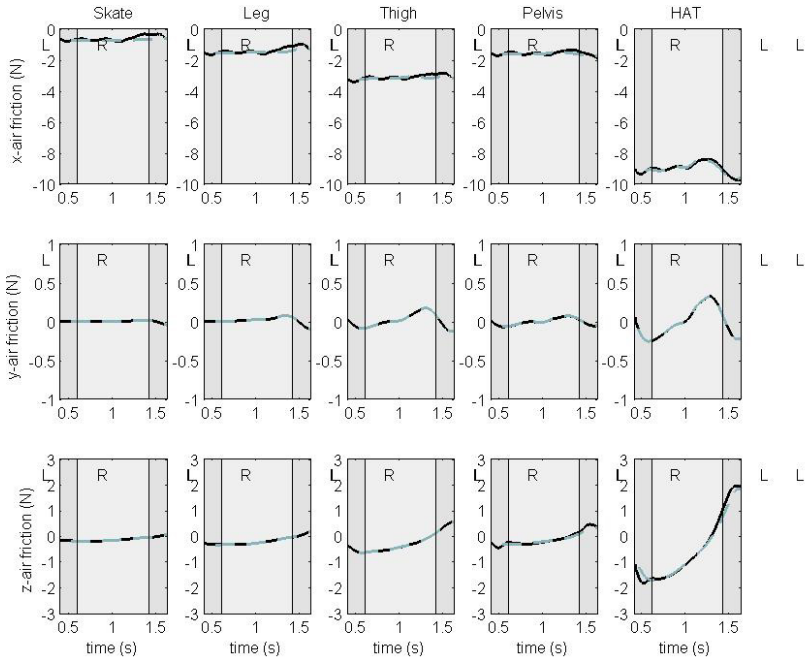


Figure 7.6 Optimizations of the PLS method to the air frictional forces of each segment. Black line are the optimized data, the blue line are the measured data. Y is up, x is in the longitudinal direction of the straight and z is in the lateral direction of the straight part of the rink (right, facing forward), in agreement with the ISB convention

Real-time Feedback Systems

PART IV

8

Getting the angles straight in speed skating: a validation study on an IMU filter design to measure the lean angle of the skate on the straights

This dissertation presented the design and calibration of a pair of instrumented klapskates that measure the push of forces during skating (CH3). The direction of this push-off force, and thus the orientation of the skate, is essential. An Inertial Measurement Unit (IMU), when filtered with the right algorithm, is an exquisite choice to continuously measure orientation. Unfortunately, disturbances on an indoor rink hamper the functioning of the commercially available orientation measurement units and their filters. In this chapter we validate the lean angle estimation in speed skating measured by an IMU and determined by an Adaptive Gain Complementary Filter on the straight parts. The system is designed such that it can be used for real-time applications.

van der Kruk, E., Schwab, A. L., van der Helm, F. C. T., & Veeger, H. E. J. (2016). *Getting the Angles Straight in Speed Skating: A Validation Study on an IMU Filter Design to Measure the Lean Angle of the Skate on the Straights*. *Procedia Engineering*, 147, 590-595.

Abstract

To assist speed skaters in improving their skating performance, we would like to provide them with real time feedback on the orientation of the skate within a single stroke. In this study we focus on the validation of the lean angle measurements of the skate, which distributes the push-off forces over the global vertical and transverse component. To measure this angle, an inertial measurement unit (IMU) would be a logical choice, but two aspects render measuring with commercially available IMUs and their filters on an ice rink rather difficult, first the ferromagnetic materials in the vicinity of the IMU and secondly the large linear accelerations. In this paper we therefore propose filters that bypass these problems. In total three complementary filters with adaptive gain were validated with a motion capture system. The filter based on the assumption that the lean angle can be reset to zero (upright) when there is no change in steer angle of the skate, showed the most accurate results (mean RMSE error of 5.30 and 3.60, for the left and right skate respectively). Integrated into the filter is an IMU based stroke detection, which as a stand-alone system could provide feedback on stroke frequency, stroke length, contact time or double stance phase time. It is concluded that an IMU used with this filter can provide individual elite speed skaters reliable feedback on their skate lean angle.

1. Introduction

Lean, steer and pitch, these are the three angles which together determine the orientation of a skate on the skate rink. While of course the forces generated by the skater on the ice determine the acceleration of the skater, the orientation of the skate determines in which direction this force, and thus acceleration, is headed. The lean angle of the skate distributes the force on the skate into a global horizontal and vertical direction, while the steer angle directs the forces in either the forward direction of the rink or the sideways direction (Figure 8.1). With pitch we refer to the pitch angle of the skate shoe. Pitch only occurs at the end of push-off, when the klapskate opens, and in the repositioning phase, while the skater repositions his skate in the air for the next stroke.

For the purpose of providing speed skaters with real-time feedback within a stroke to improve their skating performance, we would like to determine the skate orientation. The orientation can firstly provide insight into the direction, and therefore effectiveness, of the skate push-off, secondly the lean angle proved to be related to velocity in previous studies (Yuki et al. 1996). Up to now, no determination of the orientation of the skate in speed skating was established yet, except for (Yuda et al. 2004; Yuki et al. 1996), who performed measures of the lean angle at specific points in the stroke by a camera analysis. In this study we focus on validation of the lean angle of the orientation measurements with an IMU over the complete stroke.

An Inertial Measurement Unit (IMU), when filtered with the right algorithm, is an exquisite

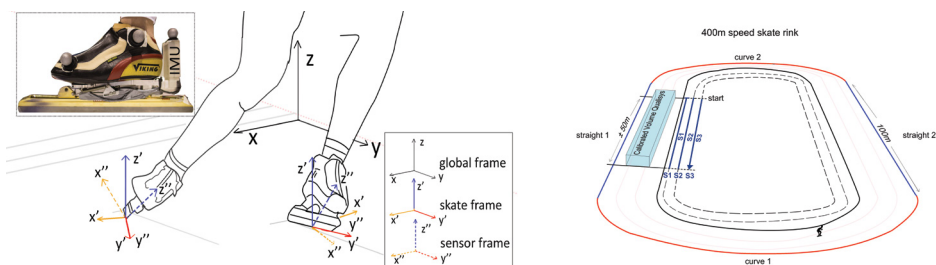


Figure 8.1 a) the three frames in speed skating, defined by the orientation of the skate; the global frame is a Newtonian frame aligned to the rink b) experimental set-up in the ice rink of Thialf (van der Kruk et al. 2015); 50m of the straight part were measured by the Qualisys motion capture system. The participants skated three consecutive rounds where one straight part of each (S1,S2,S3) was used for validation of the measurement system.

choice to continuously measure orientation with low interference. These systems are light weight, small sized and low cost. Unfortunately, disturbances on an indoor rink hamper the functioning of the commercially available orientation measurement units and their filters (van der Kruk 2013). Ferromagnetic materials in the vicinity of the IMU on the skate, e.g. the cooling pipes under the ice, disturb the local magnetic field and thereby render the first problem for the filtering algorithm. Second problem to address is motion dynamics. During speed skating, the skate moves uninterruptedly, either by gliding over the ice, or by repositioning the skate after retracting the skate from the ice (Allinger & Bogert 1997). This causes linear accelerations which disturb gravity-based algorithms. Contrary to studies in walking or running, where the foot has no velocity during push off, there is no static condition in speed skating to reset the drift of the IMU. In addition, when the skater passes through the curve, the centrifugal forces interfere with the measurements. Accurate measurements of the orientation of the skate with an IMU can therefore only be tackled by determining an algorithm which can by-pass these interferences.

The Extended Kalman Filter (EKF) is an accepted basis for the majority of the orientation filter algorithms and is the most applied one in commercially available orientation sensors. However, tuning the variables in the filter is a precise and difficult job, and the result is sensitive to changes in the environment. This can become a problem in speed skating when different rinks, each with their own cooling system, produce different noise levels for the sensors or when the difference in dynamics in speed skating between short and long distances call for a different gain in the EKF. The common alternative to the EKF is a Complementary Filter (CF) because of its simplicity and effectiveness. A complementary filter fuses accelerometer, magnetometer and gyroscope data for orientation estimation such that low pass filtering is applied on accelerometer and magnetometer data and high-pass filtering on the gyroscopic data (Mahony et al. 2008; Valenti et al. 2015; Madgwick et al. 2011). An adaptive gain, making the filter an Adaptive Gain Complementary Filter (ACF), improves robustness of the filter during dynamic motion.

In this paper we validate the lean angle estimation in speed skating measured by an IMU and determined by an Adaptive Gain Complementary Filter on the straight parts with an optical motion capture system (Qualisys 2015). Furthermore, two algorithms are tested, which improve the ACF filter for the application in speed skating, by adding a correction per stroke, based on established knowledge on the dynamics of speed skating. With this we want to provide useful feedback for speed skaters on the orientation of their skates. The algorithms are designed to be applied in real-time measurements.

2. Method

2.1. Adaptive Gain Filter (VAL1)

The filter described in Valenti et al. was employed in its original form as the adaptive gain filter and will further be referred to as VAL1 (Valenti et al. 2015). Input to the filter are the unfiltered data of the gyroscope, accelerometer and magnetometer. In this complementary filter first an estimation of the orientation in quaternion form is made by the gyroscope data. This estimation is then corrected by two steps: first the roll and pitch are corrected by an estimation of the accelerometer, second the yaw is corrected by the magnetometer data. In this paper the cut-off frequency for this correction was determined by the procedure described by Yu et al. (Yu et al. 1999). An adaptive gain compares the non-gravitational accelerations to the gravitational forces. If the non-gravitational forces rise and the error magnitude exceeds a certain threshold, the filter will rely less on the accelerometer output. This improves estimations in dynamic situations.

2.2. Self-Designed Filters

The filters are designed based on a reset point, where the estimation is reset to zero (upright). Although the lean angle is validated in this paper, the pitch angle is of influence on the lean angle estimation and is therefore also mentioned in this section. The following assumptions were made for the design of the additional two filters:

- I. When the skater places his skate on the ice, the skate is closed, so the pitch angle is zero.
- II. Since speed skating is a cyclic motion, we assume that the integral of the lean angular velocity, which determines the leaning of the skate, is approximately zero over one stroke.
- III. When the skate is perfectly upright (zero lean angle), it is impossible to have a change of heading. Therefore, the lean angle is zero when the change in steer is zero.

With these assumptions two filters were designed. The first filter is based on assumptions I and II (VAL2), the second filter is based on assumption I and III (VAL3). The filters start with an estimation of the orientation at time t via the VAL1 filter. The reset steps of the filter are explained in Figure 8.2.

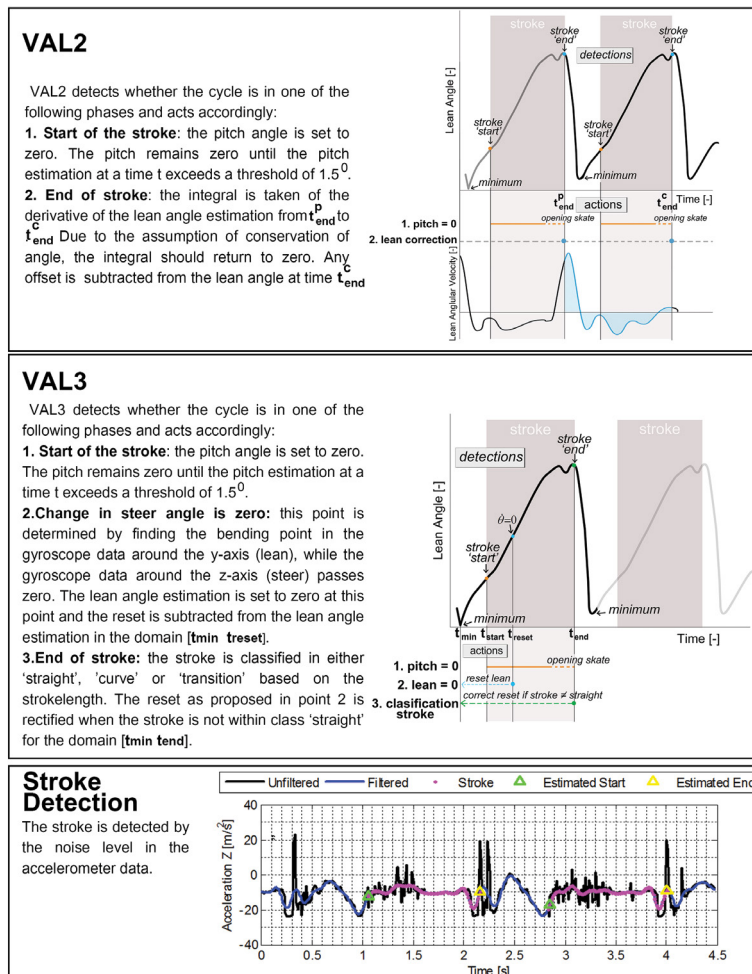


Figure 8.2 The infographics show the explanations of the filters VAL2 and VAL3 and the stroke detection algorithm. The graphs are divided into detections and actions. The detections set certain events (a.o. t_{end} , t_{reset} , t_{start}), the actions reset the current lean angle or reset the lean angle in a certain domain.

2.3. Stroke Detection algorithm

Stroke detection is necessary for the filters VAL2 and VAL3 to recognize the start and end of a stroke. When the skate is in contact with the ice, a high frequency noise appears in the accelerometer signal of the IMU, due to the structure of ice surface. By detecting this noise, an algorithm was made to perform stroke recognition via an IMU (Figure 8.2).

2.4. Experimental set-up

The validation of the filters was done with a data set recorded on the indoor ice rink in Thialf Heerenveen (januari 2015). Four passive markers on each skate were captured by 20 Qualisys motion capture cameras over 50m of the straight part to determine the reference orientation (Qualisys 2015). The number of strokes captured on each straight part varies depending on the participant. Data of three straight parts (S1,S2,S3) in three consecutive rounds of two elite speed skaters at a speed of 10.3m/s were used (Figure 8.1). The Qualisys orientation data were low passed filtered. Furthermore, the participants skated on instrumented skates with an integrated IMU on the bridge (see Figure 8.1) (100Hz) (Shimmer3 2015), which also measured the forces (van der Kruk et al. 2015). The instrumented skate and Qualisys system were synchronised via a digital start and end pulse. As the initial condition, the orientation measured by Qualisys at $t=0$ (start of S1) was taken.

2.5. RMSE

The accuracy of the three filters was determined by a sample wise root mean square error (RMSE) between the orientation measured by the Qualisys system and the value estimated by the filters with the IMU data for each complete stroke. A stroke was defined as the time were the skate was in contact with the ice (contact time). This was determined by the force data measured with the instrumented skate. The IMU results were validated for both the left and the right skate. Due to a different pattern of the left and right stroke on a full round (both are mainly on the medial side on the straights, but when entering the curve, the left skate changes to the lateral side, while the right skate remains on the medial side), we have treated their validation separately.

The contact-time determined with the instrumented skate was also used to verify the IMU stroke detection algorithm. The start and end point of the stroke were verified on one full round (curve and straight) for the two participants (50 strokes).

Table 8.1 RMSE error (in degrees) for two participants for the three straight parts on three consecutive rounds (S1,S2,S3) for each left (L1,L2) and right (R1,R2) stroke. The number of strokes varies with speed and may depend on the participant, due to the fixed measurement volume.

Participant 1	RMSE [°]	S1		S2		S3		mean	S1		S2		S3		mean
	stroke	L1	L2	L1	L2	L1	L2		R1	R2	R1	R2	R1	R2	
	VAL1	4.5	6.7	1.0	0.4	39.7	34.3	14.4	1.0	0.1	0.7		9.1	11.7	4.5
	VAL2	0.9	78.8	77.8	81.4	85.3	91.5	69.3	1.0	0.2	0.8		8.9	2.2	2.6
	VAL3	4.8	0.5	3.4	6.6	3.9	3.4	3.8	1.0	0.2	2.8		7.8	4.2	3.2

Participant 2	RMSE [°]	S1	S2	S3		mean	S1	S2	S3	mean
	stroke	L1	L1	L1	L2		R1	R1	R1	
	VAL1	11.8	34.6	10.2	7.8	16.1	4.0	24.2	18.3	15.5
	VAL2	11.8	14.5	9.4	2.1	9.5	3.9	3.0	14.9	7.2
	VAL3	0.8	13.0	12.9	0.7	6.9	4.0	0.2	7.4	3.9

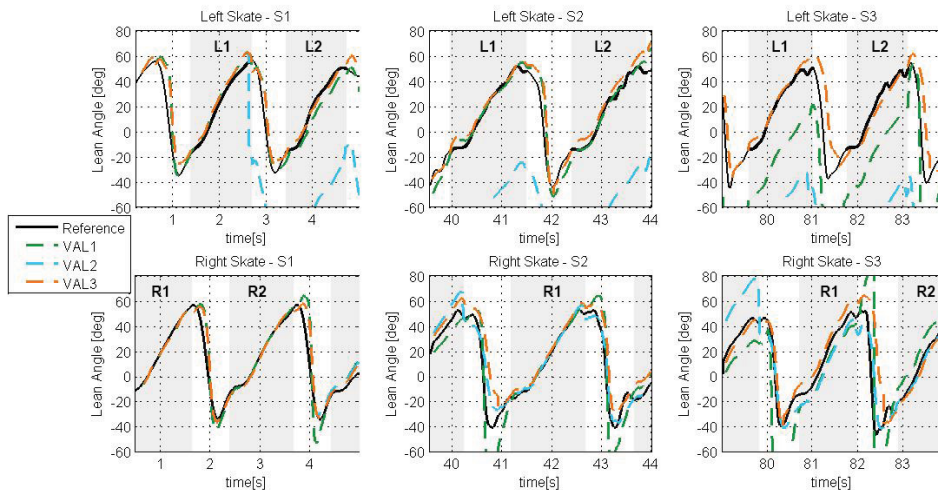


Figure 8.3 Measured lean angles with Qualisys (Reference) and the three ACFs (VAL1, VAL2, VAL3) for the three straight parts of the three consecutive rounds (S1, S2, S3) for participant 1. The grey areas indicate when the skate is in contact with the ice (measured via the instrumented skate).

3. Results

3.1. Stroke Detection

The start of the stroke was detected with an error of 0.002s (SD:0.08s) and 0.02s (SD:0.08s) for respectively the left and right stroke. The end of the stroke was detected with an error of respectively -0.02s (SD:0.02s) and -0.01s (SD:0.01s).

3.2. Filter validation

The estimation on lean angle of the three different filters and the measured lean angle for each recorded area (S1, S2, S3) for both the left and the right skate are shown in Figure 8.3. The RMSE errors are given in Table 8.1. The designed filter VAL3 shows improved estimations for the lean angle compared to the VAL1 filter. The VAL1 has a mean RMSE error of 15.30 and 100 for respectively the left and the right skate, the filter VAL3 has a mean RMSE error of 5.30 and 3.60.

The VAL2 filter also shows improved estimations in 3 out of 4 data sets compared to VAL1. The lack of robustness of this filter is evident in the left stroke of participant 1: one wrong correction affected the remaining data set.

4. Discussion

4.1. Validation

The VAL3 filter showed a remarkable improvement for the lean angle estimation in speed skating, compared to the standard VAL1 filter (Table 8.1). The question rises whether it would be accurate enough to provide (elite) speed skaters with real-time feedback on their orientation. While the exact relationship between the orientation and the performance is unknown, for now the variation within a subject can set the accuracy requirement for the lean angle. Figure 8.4 shows the lean angles of the two participants at several speeds measured by Qualisys. It illustrates that the lean angle varies in a range of 90 within a subject. The mean RMSE found in this study for the VAL3 filter falls within this variation and therefore appears to be accurate enough to provide a skater with useful feedback. For real-time feedback however, the accuracy on stroke level is important. On this level, the VAL3 estimations showed RMSE values of the measured angle of about 130 in two of the strokes. Both these strokes show increased noise in the gyroscope data, by which the wrong reset point was determined. These

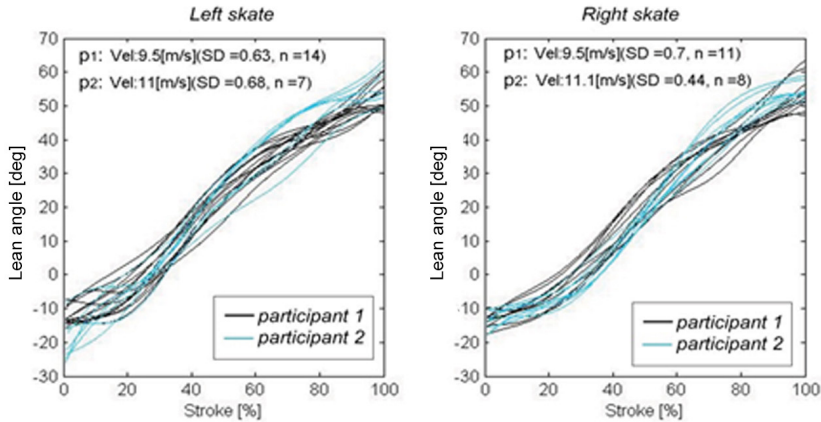


Figure 8.4 Lean angle measured by the Qualisys system in the study of (van der Kruk et al. 2015) for two participants. Of participant 1, 14 strokes for the left and 11 strokes for the right skate are presented at a mean speed of 9.5m/s ($SD=0.68$ m/s). For participant 2, 7 strokes for the left and 8 strokes for the right skate are presented at a speed of 11.1m/s ($SD=0.5$). The variations within a subject are around the 90.

erroneous reset points can however be recognized as outliers and rejected in future use, when the individual repetitive motions are taken into account.

Besides the direct feedback on lean angle, the orientation of the skate will be used in the determination of the direction of the push-off. Since the angle is then integrated into a rotation matrix, an error in lean angle will have impact on the global force estimation. Whether the found accuracy is then still valid remains a topic for future work.

4.2. Application

When providing skaters with feedback, it is important to decide on what would be an interesting variable for a skater to work with. Currently the exact relationship between lean angle and performance is unknown. However Yuki et al. showed that the lean angle of the skate on the straights increases with velocity (Yuki et al. 1996). This implies that skaters can be trained on increasing their angle. Furthermore, based on physics, we foresee that whenever the skate has a negative lean angle, the forces that are put on the skate by the skater, will be directed in the opposite direction of motion. It seems therefore plausible that this negative angle should be minimized. It is however unclear whether this would at all be possible and what its influence on the steer angle would be. With an IMU and the VAL3 filter we are able to investigate this on the ice rink.

The algorithm for stroke detection proved to be accurate in both the curves and the straight parts. With this the skater can be provided with feedback on, among other things, his stroke frequency, stroke length, contact time or double stance phase time. Furthermore, the algorithm provides classification of the strokes in either Straight part, Transition stroke or Curve. All of these variables can be of interest to a trainer or skater.

5. Conclusion

The lean angle of the skate in speed skating can be measured reliably with an IMU combined with an adequate filter. The complementary filter based on the assumption that the lean angle can be reset to zero when there is no change in steer angle of the skate showed the most accurate results (Table 8.1). Integrated into the filter is a stroke detection algorithm, which as a stand-alone system could provide feedback on stroke frequency, stroke length, contact time or double stance phase time. An IMU in combination with the VAL3 filter can provide individual elite speed skaters with reliable feedback on their skate lean angle.

References

Allinger, T.L. & Bogert, A.J., 1997. *Skating technique for the straights based on the optimization of a simulation study. Medicine and Science in Sports and Exercise*, 29, pp.279–286.

van der Kruk, E., 2013. *Modelling and Measuring 3D Movements of a Speed Skater*. TU Delft.

van der Kruk, E. et al., 2015. *Wireless instrumented klapskates for speed skating. current under review in Journal of Sports Engineering*.

Madgwick, S.O.H., Harrison, A.J.L. & Vaidyanathan, R., 2011. *Estimation of IMU and MARG orientation using a gradient descent algorithm. In IEEE International Conference on Rehabilitation Robotics*.

Mahony, R., Hamel, T. & J.-M. Pflimlin, 2008. *Nonlinear complementary filters on the special orthogonal group. Automatic control IEEE transactions on*, 53, pp.1203–1218.

Qualisys, 2015. <http://www.qualisys.com/>.

Shimmer3, 2015. *Shimmer*. Available at: www.shimmersensing.com.

Valenti, R., Dryanovski, I. & Xiao, J., 2015. *Keeping a Good Attitude: A Quaternion-Based Orientation Filter for IMUs and MARGs. Sensors*, 15(8), pp.19302–19330. Available at: <http://www.mdpi.com/1424-8220/15/8/19302/>.

Yu, B. et al., 1999. *Estimate of the optimum cut-off frequency for the butterworth low-pass digital filter. Journal of Applied Biomechanics*, 15, pp.318–329.

Yuda, J. et al., 2004. *Changes in blade reaction forces in speed skating the curve. International Journal of Sport and Health Science*, 2(1996), pp.195–204.

Yuki, M., Ae, M. & Fujii, N., 1996. *ドケットのド反 (Blade reaction forces in speed skating). Society of biomechanics*, 13, pp.41–51.

9

Push-off forces in elite short-track speed skating.

'If you thought that science would present certainties, well that is just your mistake'
-Richard Feynman-

In addition to feedback systems for the long-track speed skating discipline, we spread the gained knowledge to the short-track discipline. This resulted in an instrumented short-track skate which measures push-off forces. In this chapter, the design and calibration of the skates is described and an exploratory analysis of the push-off forces within the Dutch national elite short-track speed skaters is presented.

van der Kruk, E., M.M. Reijne, B. de Laat & H.E.J. Veeger, *Push-off Forces in Short-Track Speed Skating (2017)*, accepted with revisions at Sports Biomechanics

Abstract

Push-off forces can provide valuable insights into speed skating technique for coaches and skaters. This study performed an analysis of the push-off forces of elite-short-track speed skaters using a new designed instrumented short-track speed skate (accurate up to 2.2% in normal direction and 1.4% in lateral direction), with the aim to improve short-track skating performance. The instrumented skate can be used in routine training. Four different skating strokes were distinguished for short-track speed skaters at speed. The strokes differed in stroke time, force level in both normal and lateral directions and the centre of pressure on the blade (COP). Within the homogeneous group of male elite speed skaters (N=6), diversity of execution of the force patterns in the four phases of skating was evident, while skating at the same velocities. The male participants (N=6) with a better personal record (PR) kept the COP more to the rear of their blades while hanging into the curve ($r = 0.82, p < 0.05$), leaving the curve ($r = 0.86, p < 0.05$) and entering the straight ($r = 0.76, p < 0.10$). Furthermore, the male skaters with a better PR showed a trend of a lower lateral peak force while entering the curve ($r = 0.74, p < 0.10$). Females showed a trend towards applying higher body weight normalised lateral forces than the males, while skating at imposed lower velocities.

1. Introduction

Short-track speed skating is a form of competitive ice speed skating where multiple skaters compete on a short (111 m) oval ice track. Skaters ride the curves of this oval at very high velocities, challenging the high centrifugal forces. Applying the right skating technique is crucial to pass these curves and maintain position in the group during a match. However, little is known on the biomechanical background of the short-track skating technique. It is therefore unclear what the ideal technique is and therefore also what to correct for in athlete skaters.

Although biomechanical research on short-track speed skating is limited, there has been much research done on the technique of long-track speed skating. However, the technique of long-track speed skating significantly differs from that in short-track. In the long-track discipline skaters make six to eight symmetric strokes at the straight part, before entering the curve, whereas short-track speed skating is mainly skating curves. Since the curves in long-track speed skating are wider, and the skaters wear klapskates instead of fixed skates, also these techniques differ from the short-track discipline.

The motion of a short-tracker at speed can be divided into four phases: entering the curve (EC), hanging into the curve (C), leaving the curve (LC) and entering the straight (ES). Apart from which skating technique, it is also not clear which phase is most critical for performance. These issues could be addressed by measuring the push-off forces of a skater. For short-track, there are no data available yet on the force patterns or force levels applied during skating for these four phases.

In long-track speed skating, an instrumented klapskate has been developed, measuring the push-off forces in normal and lateral direction and determining the center of pressure (COP) on the blade (Houdijk, de Koning, de Groot, Bobbert, & van Ingen Schenau, 2000; van der Kruk, den Braver, Schwab, van der Helm, & Veeger, 2016; Yuki, Ae, & Fujii, 1996). Different from the hinge-opening klapskate in long-track, in short-track skaters have a fixed blade, where the shoe is placed off-centre from the blade. An instrumented skate should enable a skater to wear her own shoes and ride her own blade.

The purpose of this paper is to perform an analysis of the push-off forces of elite-short-track speed skaters, to eventually improve the short-track skating performance. First we report on an instrumented short-track speed skate; Secondly, a general description of the force patterns in short-track speed skating in terms of stroke-time, normal and lateral force level and center of pressure on the blade (COP) is given, based on force data of elite speed skaters. Thirdly, we explore within-group differences in a group of elite speed skaters related to their ranking based on personal records (PR). We hypothesize that, despite the homogeneity of a group of elite short-trackers, the instrumented skate can determine differences in push-off techniques within the group.

2. Method

2.1 Data Collection

Data were collected on an indoor ice rink in Thialf Heerenveen. Twelve (eight male and four female) Dutch elite short track skaters participated in the experiment after signing a written informed consent, which had been approved by the local Human Research Ethics Committee. All riders were within the top 70 of the world ranking (WR). However, two males were excluded from the test, since one fell and one did not perform according to exercise, and one female was excluded due to failing equipment. All riders were equipped with an instrumented skate at their right foot which measured the normal and lateral forces at the skate and the point of application of the force (COP) (Figure 9.1). Force measurements were only performed for one side, due to the available means. In consultation with the national coach, the right side was chosen, it being the most interesting side during the curve. The skaters were filmed by five cameras, one at each end of the straight, one at the inside of each curve and one panning camera at the finish line. The skaters skated five rounds at constant velocity; The participants were asked to skate lap times of 9.2 s to 9.3 s for the males, and 9.8 to 9.9 s for the females. Lap times were measured with a transponder worn by the skaters, using the MyLaps system (MYLAPS Timing Services, Nijmegen, the Netherlands).

The skaters were ranked based on their PR in an XL (an all-out lap when the skater is at speed) during practice, which was obtained via the national coach. The average PRs and measured lap times with the corresponding standard deviations are given in Table 9.1.

2.2 Instrumented short-track skate

The instrumented short-track skate (ISTS) consists of two self-designed cups (mountable on high-end blades of the brand EVO) (Figure 9.1). Each cup consists of a sandwich construction that clasps a piezoelectric 3-component force sensor (Kistler 9602, Kistler Group, Winterthur, Switzerland). The output of the sensor is logged on a SD card and sent over Bluetooth via a data logger (Shimmer3, 2015). The force sensors are powered by rechargeable Li-Ion batteries. A digital start-end pulse can be logged, to enable synchronisation with external measurement devices. The weight of the instrumented cups and electronics is 400 grams. The instrumented cups replace the normal cups of the skate, so in total the added weight is 340 grams (around 25% of the total skate). The height of the instrumented cups is 18 mm (normal height differs among skaters, on average 12 mm).

The calibration of the ISTS was performed using a tensile testing machine (Zwick Z100, Zwick Roell, Ulm, Germany, principal accuracy 1 N). The set-up is the same as the one used in van der Kruk, (2016), with the single difference that not four, but five positions (P1-P5) were tested on the blade (applied force up to 2500 N). Calibration in normal direction resulted in correlations

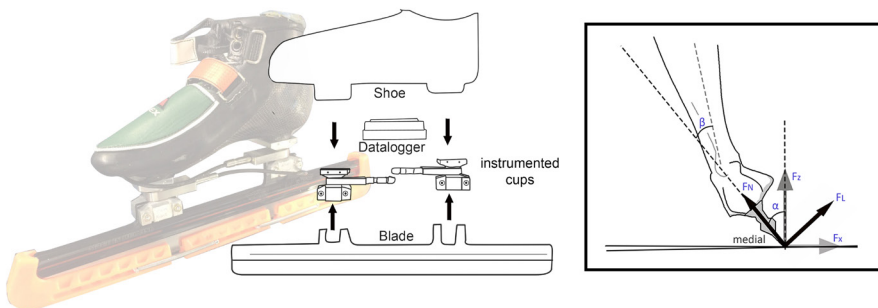


Figure 9.1 The instrumented short-track skate (ISTS) consists of two self-designed cups (mountable on EVO blades). The skate measures the forces in the normal (F_n) and lateral (F_l) direction of the blade. The lean angle of the skate (α) distributes these local forces into the horizontal push-off force (F_h) and the vertical force (F_v). Due to eversion of the foot (β), there is can be a skewed push-off on the skate.

of $R^2 = 0.989$, with a root mean square error (RMS) of 55 N (SEM = 1 N); the correlation for the lateral direction yielded $R^2 = 0.993$ with the corresponding RMS error of 23 N (SEM = 0.4 N). As the force in longitudinal direction (ice friction) likely to be lower than 10 N (Lozowski, Szilder, & Maw, 2013), which is lower than the cross-talk of the sensors, this force component is not used.

2.3 Data analysis

2.2.1 Push-off forces (force patterns)

The measured forces were divided into separate strokes over the four phases: entering the curve (EC), hanging into the curve (C), leaving the curve (LC) and entering the straight (ES). All measured force data were normalized to body weight. The mean and standard deviation of the peak (peak) and average (avg) normal (FN) and lateral forces (FL), the center of pressure on the blade (COP), and the stroke-time (ST) of nine participants (6 males, 3 females) were determined. Of each participant five strokes ($s=5$) were included for EC, C and LC and three strokes of ES ($s=3$), because fewer strokes were available since sometimes a short, corrective stroke was performed instead of ES. We will refer to this corrective stroke as a transition stroke (T). Since this stroke is only performed sporadically, we did not include the stroke in the statistical analysis.

A repeated measures ANOVA ($N=9$) was performed to compare phases (EC, C, LC, ES) for the within-participants variables: $F_{N\text{-peak}}$, $F_{N\text{-avg}}$, $F_{L\text{-peak}}$, $F_{L\text{-avg}}$, COP_{peak} , COP_{avg} , ST; sex was added as a between-participant factor. Only for the average normal force (FN-avg) an interaction effect between sex and stroke phases was found, however since the effects for average normal force within men and women were similar, it is justifiable to still take the groups together and look at the main effect. Pairwise comparison was done with a Bonferroni post-hoc analysis when a main effect was found. Only for stroke time (ST) sphericity was not met, for which a Greenhouse-Geisser correction was performed. A significance level of $p < 0.05$ was employed.

Table 9.1 A,B) Mean \pm SD of the PRs and Laptimes, and the average and peak measured normal and lateral forces (normalized to body weight), center of pressure at the blade (COP), and Stroke Time. For stroke EC,C and LC five strokes ($s=5$) per participant were included, for stroke ES three ($s=3$). B) males and females separately;

		[A]		[B]			
		N=9 (males and females)		N=3 (females)		N=6 (males)	
		avg	peak	avg	peak	avg	peak
PR	(s)	8.3 \pm 0.22		8.50 \pm 0.16		8.1 \pm 0.08	
Laptimes	s	9.49 \pm 0.37		9.95 \pm 0.19		9.26 \pm 0.10	
Normal Force	EC 5 (N/BW)	0.96 \pm 0.10	1.66 \pm 0.15	1.05 \pm 0.12	1.78 \pm 0.17	0.92 \pm 0.06	1.60 \pm 0.10
	C 5 (N/BW)	1.40 \pm 0.17	1.96 \pm 0.16	1.30 \pm 0.24	2.01 \pm 0.21	1.45 \pm 0.14	1.94 \pm 0.15
	LC 5 (N/BW)	1.02 \pm 0.09	1.55 \pm 0.16	0.99 \pm 0.12	1.56 \pm 0.14	1.04 \pm 0.08	1.55 \pm 0.18
	ES 3 (N/BW)	0.88 \pm 0.06	1.32 \pm 0.10	0.88 \pm 0.11	1.38 \pm 0.14	0.88 \pm 0.03	1.29 \pm 0.08
Lateral Force	EC 5 (N/BW)	0.24 \pm 0.08	0.77 \pm 0.22	0.32 \pm 0.03	1.00 \pm 0.14	0.19 \pm 0.07	0.66 \pm 0.16
	C 5 (N/BW)	0.41 \pm 0.08	0.74 \pm 0.23	0.48 \pm 0.06	1.02 \pm 0.10	0.37 \pm 0.06	0.59 \pm 0.09
	LC 5 (N/BW)	0.31 \pm 0.07	0.75 \pm 0.19	0.38 \pm 0.05	0.97 \pm 0.12	0.27 \pm 0.04	0.64 \pm 0.08
	ES 3 (N/BW)	0.28 \pm 0.08	0.66 \pm 0.24	0.35 \pm 0.05	0.91 \pm 0.21	0.24 \pm 0.07	0.53 \pm 0.12
COP	EC 5 (-)	0.45 \pm 0.03	0.83 \pm 0.14	0.46 \pm 0.01	0.91 \pm 0.10	0.44 \pm 0.03	0.79 \pm 0.15
	C 5 (-)	0.49 \pm 0.03	0.88 \pm 0.10	0.50 \pm 0.02	0.98 \pm 0.02	0.49 \pm 0.03	0.83 \pm 0.08
	LC 5 (-)	0.48 \pm 0.03	0.79 \pm 0.11	0.48 \pm 0.01	0.77 \pm 0.09	0.48 \pm 0.03	0.80 \pm 0.13
	ES 3 (-)	0.44 \pm 0.04	0.55 \pm 0.05	0.44 \pm 0.03	0.57 \pm 0.07	0.44 \pm 0.04	0.54 \pm 0.04
Stroke Time	EC 5 (s)	1.12 \pm 0.17		1.22 \pm 0.17		1.07 \pm 0.15	
	C 5 (s)	0.99 \pm 0.14		0.92 \pm 0.09		1.02 \pm 0.16	
	LC 5 (s)	0.61 \pm 0.08		0.68 \pm 0.09		0.57 \pm 0.04	
	ES 3 (s)	0.65 \pm 0.08		0.73 \pm 0.05		0.61 \pm 0.06	

2.2.2 Within-group differences and PR

To determine the correlation between PR and the average, and peak forces in normal, and lateral direction, a Pearson test was performed resulting in a pairwise linear correlation coefficient (r). Additionally, the correlation between PR and the average COP on the blade was tested. These analyses were performed on the males only ($N = 6$), due to the small sample size of the female group. From each participant, the peak and average push-off forces were determined for each measured stroke; the average was taken over the measured strokes to enter as number in the Pearson test. A significance level of $p < 0.05$ was employed, $p < 0.10$ was used for comparisons which are close to be significant.

3. Results

3.1 instrumented skate

The instrumented skate functioned well during the testing and the signals of the skate were stable throughout the experiment. Installing and de-installing the instrumented pots on the skater's shoe and blade was done on the ice in less than five minutes by the equipment manager of the team. In spite of the increased height and weight of the skate, the skaters felt comfortable riding the skate at high velocities.

3.2 push-off forces

A main effect was found between the different phases for the variables FN-peak, FN-avg, FL-avg, COPpeak, COPavg, and ST (Table 9.1). Based on the pairwise comparison (Table 9.2), the four different phases (EC, C, LC, ES) could be distinguished based on the normal and lateral force level of the push-off forces of the skaters. Figure 9.2 and Figure 9.3 show the skating motion together with the measured normal and lateral forces and COP (averaged over nine participants).

The strokes at the start of the curve (EC and C) are significantly longer than the other two strokes ($ST = 1.12$ s and $ST = 0.99$ s respectively). EC, the stroke in which the skater enters the curve, distinguished itself by the dip in normal force after the double stance phase (20-50% of the stroke) (Figure 9.3). Additionally, Stroke EC was characterized by the highest peak normal forces (1.66 N/BW) (together with stroke LC (1.55 N/BW)), and the lowest average lateral force, (0.24 N/BW) (together with stroke ES (0.28 N/BW)), with a mean peak lateral force of 0.77 N/BW.

Stroke C, the stroke where the skater hangs into the curve (see Figure 9.3) could be separated from the other three based on force profiles based on the high normal forces (average 1.40 N/BW, peak 1.96 N/BW) combined with the plateau-like lateral forces (average 0.41 N/BW, peak 0.74 N/BW).

The strokes where the skater exits the curve, stroke LC and ES, were significantly shorter than

Table 9.2 Repeated measures one-way Anova of the phases EC, C, LC and ES for the nine participants. Pairwise comparison is performed using a Bonferroni post-hoc analysis. x indicates a significant difference ($p < 0.05$).

N=9 avg	F-test	Mauchly's sphericity	Bonferroni					
			EC-C	EC-LC	EC-ES	C-LC	C-ES	LC-ES
Normal Force	$F(3,21) = 81.92, p = 0.000$	$\chi^2(5) = 7.66, p = 0.18$	x		x	x	x	x
Lateral Force	$F(3,21) = 34.47, p = 0.000$	$\chi^2(5) = 9.24, p = 0.10$	x	x		x	x	
COP	$F(3,21) = 16.62, p = 0.000$	$\chi^2(5) = 4.02, p = 0.55$	x	x			x	x
Stroke Time	$F(1.35,9.43) = 32.77, p = 0.000$	$\chi^2(5) = 16.01, p = 0.01^*$		x	x	x	x	
peak								
Normal Force	$F(3,21) = 68.10, p = 0.000$	$\chi^2(5) = 8.99, p = 0.11$	x		x	x	x	x
Lateral Force	$F(3,21) = 2.31, p = 0.105$	$\chi^2(5) = 6.93, p = 0.23$						
COP	$F(3,21) = 29.60, p = 0.000$	$\chi^2(5) = 8.20, p = 0.15$			x	x	x	x

*sphericity is not met, a Greenhouse-Geisser correction was performed.

Table 9.3 Pearson correlation coefficient of PR and the forces, COP, and StrokeTime, of the men (n=6).

		EC	C	LC	ES
Fn	avg	0.72	0.57	-0.01	-0.01
	peak	0.66	0.40	-0.14	0.18
Fl	avg	0.63	0.69	0.73	0.62
	peak	0.74**	0.55	0.48	0.48
COP	avg	0.60	0.81**	0.86*	0.76**
	peak	0.43	0.82*	0.52	0.45
ST	avg	-0.62	0.52	0.34	-0.40

* indicates a correlation where $p < 0.05$ ** indicates a correlation where $p < 0.10$

the other two (on average 0.61 s and 0.65 s respectively). The first stroke leaving the curve (stroke LC) was characterized by significantly higher average and peak normal forces (1.02 N/BW and 1.55 N/BW respectively) than the consecutive stroke, entering the straight (stroke ES) (0.88 N/BW and 1.32 N/BW respectively). The COP of ES differed significantly from the other strokes: it shifted to the rear of the blade at the end of the motion –resulting in a peak COP of 0.55 -, while in the other strokes, the skater moved to the front of the blade –resulting in a peak COP of 0.79 to 0.88.

The males were able to skate the specified lap time, while the females had a larger variation in maintaining their specified lap time. In Table 9.1B, the measured data for males and females are given separately. The lap times of the females were higher than lap times of the males, as instructed. Note however that, although there is a large difference in lap times between the males and females, there is no difference in normal forces. The lateral forces per body weight of the females, however, show a clear trend to be higher compared to the males. Ranking the lateral forces for all participants shows that the females have the highest FL-peak for EC, C, and LC, and the highest FL-avg for LC. For the other phases, the females were in the fourth highest FL-peak and FL-avg.

3.3 Correlation between measured force data and PR

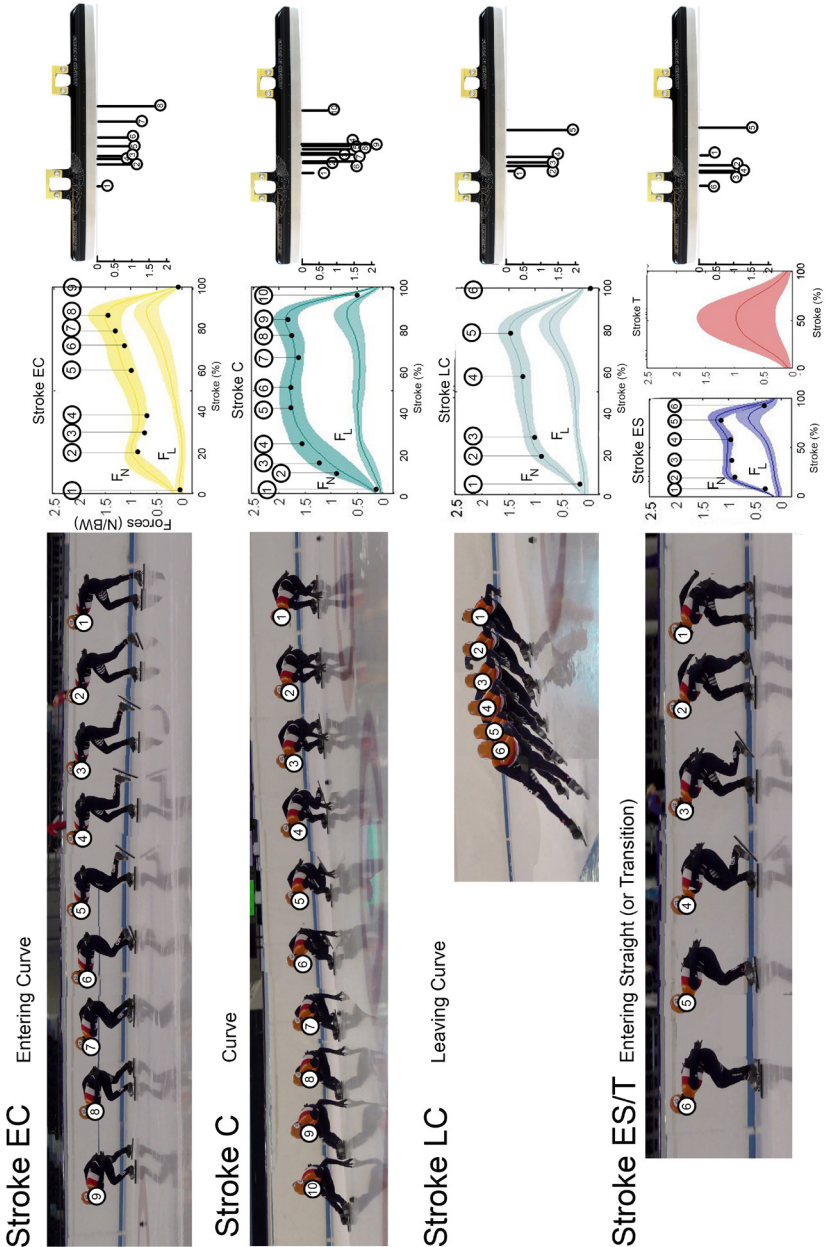
The Pearson correlation - performed on the group of males to determine the correlation between PR and lateral force, normal force, and COP at constant speed - showed relations between the COP and PR (Table 9.3, Figure 9.5). The average COP in LC and the peak COP in stroke C have a positive relation ($r = 0.86$, $p = 0.030$ and $r = 0.82$, $p = 0.048$, respectively) with PR, indicating that skaters with a better PR keep their COP more to the rear of their blade when riding and exiting the curve. Also, the average COP in the curve and while entering the straight appears to show a positive trend with PR ($r = 0.81$, $p = 0.052$ and $r = 0.76$, $p = 0.077$ respectively). Additionally, we found a positive trend ($r = 0.74$, $p = 0.096$) between PR and the peak lateral force in stroke EC, indicating that skaters with a better PR tend to apply lower lateral forces.

Although skating at similar speeds, the applied normal force levels (FN) differed between the skaters. Figure 9.4 shows the most distinct force patterns between male individual speed skaters. The graphs show diversity between the elite male speed skaters in the executions of the four strokes, but this diversity could, in this study, not be related to PR with the chosen measures.

4. Discussion and Implications

The practical usability of the developed instrumented short-track skate was demonstrated in this experiment. The four phases (EC, C, LC, ES) in the short-track round could be well distinguished based on the measured push-off forces. Within the elite speed skaters, we determined differences in skating technique and related these to the ranking of the skaters based on PR, which led to relations and trends with COP and the lateral forces. This makes the instrumented skate a useful tool for skaters and coaches during short-track practices. Despite the homogeneity of the group of elite short-trackers, the instrumented skate was able to determine differences in push-off techniques within the group.

Figure 9.2 Overview of the short-track speed skating motion, measured at constant velocity. Four strokes were distinguished, which are described in the results. The numbers indicated in the pictures correspond to the numbers in the graphs. Plotted are the mean measured normal and lateral forces of the six males and three females, the bandwidth indicates the standard deviation. The strokes are normalized to time. The numbers at the blades indicate the COP at the blade in that instant of the stroke.



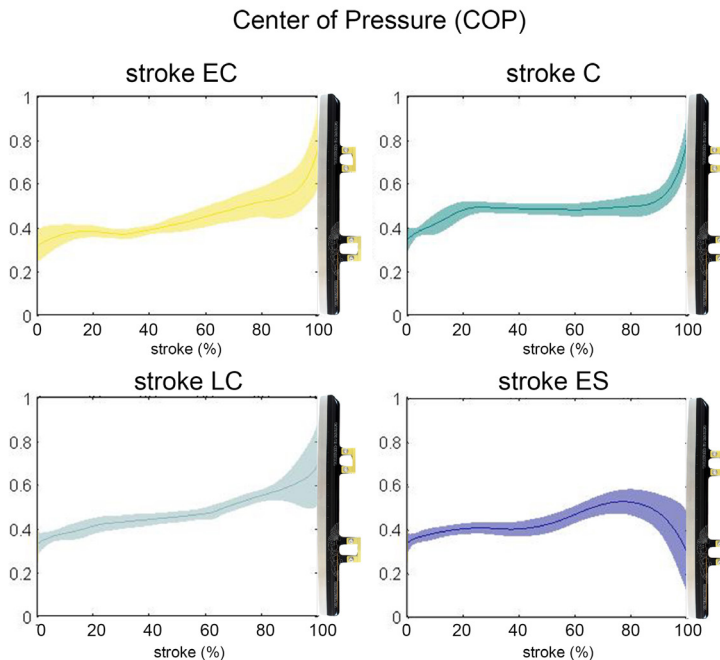


Figure 9.3 Plotted are the mean average positions of the COP throughout a stroke of the six males and three females; of each participant 5 strokes were included in the data. The bandwidth is the standard deviation. The strokes are normalized to time. The COP at the skate is indicated as a ratio, where 0 is at the rear of the blade and 1 is at the front of the blade. Remarkable is that in the stroke in which the skater enters the straight (ES), the COP shifts to the rear of the skate at the end of the stroke.

4.1 Force patterns

The four phases in short-track speed skating can be distinguished with the instrumented skate based on force level, stroke time and the center of pressure measured with the instrumented skate for the right side. The phase entering the curve, EC, distinguished itself by the dip in normal force after the double stance phase (20-50% of the stroke) (Figure 9.2). This is caused by the so-called shuffle, a motion where the skater changes from the medial (inside) to the lateral (outside) side of the blade and back. In this motion skaters move their upper body up and down, which shifts the center of mass of the skater, hence the dip in the normal force. Due to this shuffle, there is also a negative lateral force at the start of the stroke and the COP at the blade shifts from front to rear and back again. Stroke EC is also the only stroke where the skaters do not perform a cross-over with the left leg.

The force data of stroke C, where the skater leans into the curve, is most distinguishable from the other three by the high normal forces. The level of the normal force is here directly related to the centrifugal forces acting on the skater in the curve; these increase with an increased velocity. The decrease in normal force – just before the peak at the end of the stroke – is caused by the left (repositioning) leg in the air; this left leg is pulled to the front, thereby drawing it underneath the right leg, shifting the COM (Figure 9.3). This shifting in COM is what induces the decrease in the measured forces.

The COP of ES differs significantly from the other strokes: it shifts to the rear of the blade at the end of the motion, while in the other strokes, the skater moves to the front of the blade. This is caused by the fact that ES is a transitional stroke from the curve to the straight. The skater comes back upright, so most correction and steering is done here, which is linked to the COP on the blade.

In this study, only the forces on the right skate were measured. The comparison of average

normal forces between skaters should therefore be interpreted with care, since the force on the left skate –during double stance, when both skates are on the ice – influences this force level. For a complete picture, it would therefore be beneficial to measure the push-off forces of both skates synchronously, also because, based on the knowledge of long-track speed skating, different force patterns are expected between left and right, especially for the forces in the curve (van der Kruk, den Braver, et al., 2016).

4.2 COP and lateral forces on the blade

Results show that the male skaters with a better PR kept the COP more to the rear of their blades while leaning into (C) and leaving (LC) the curve, and entering the straight (ES). Additionally, we found that skaters with a better PR, showed lower lateral peak forces while entering the straight. Although these results are based on a small sample size of elite speed skaters ($n=6$), and may therefore not be as robust, it does seem to indicate that the handling of the skate is an important factor for short-track performance. We refer to handling as the actions to steer the skate. We expect that the skaters use the shifting of COP on the blade to steer, but also the lateral forces on the skate can be an intended action to induce a moment on the cups and thereby bending the blade, which will cause the skate to steer as well. The length and the stiffness of the blade then determine the necessary absolute lateral force level to bend it. Since the men and women skate on the same blade, and therefore likely need to apply the same absolute lateral forces, this might explain the fact that we found significant higher lateral forces when we corrected for body weight for the women.

Although not investigated yet, we hypothesize that this lateral force is, apart from the active steering control action of the skater, partly a result of an involuntary skewed push-off, due to a lack of active control to stabilize the knee and ankle. Felser et al. (2016) already found that the right ankle eversion's isometric and concentric maximum voluntary torque were significantly correlated to performance in short-track speed skating. A previous study in long-track speed skating already argued that a lateral force – in the frame of the skate - does not

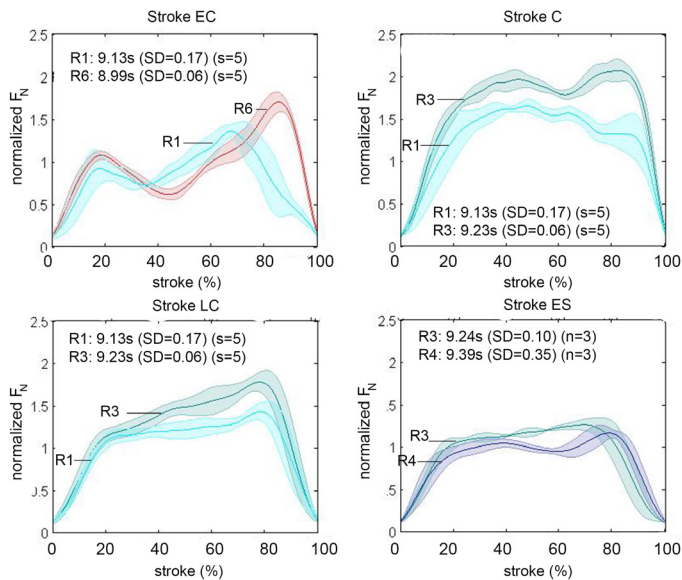


Figure 9.4 Most distinctive patterns between individual male skaters based on their normal force patterns. The ranking of the skaters is indicating with R# (ranking 1-6, based on PR). The differences in normal force levels (F_N -avg, F_N -peak) between the skaters were not related to PR ranking and therefore probably have their origin in the efficiency of the skating motion.

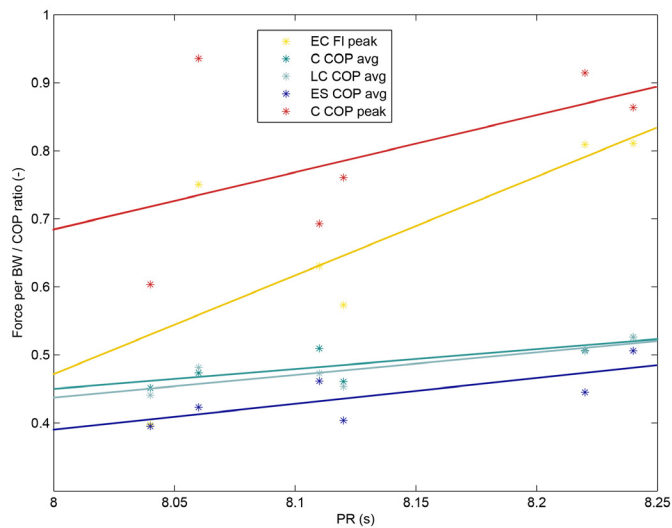


Figure 9.5 Scatterplot for the trends and correlations between PR and the normalized lateral forces, and COP position on the blade for the male participants (N=6).

directly contribute to the forward velocity (performance) of the skater (van der Kruk, van der Helm, Schwab, & Veeger, 2016). Therefore, from a mechanical point of view, the lateral force should be minimized if it does not serve the purpose of steering the skate. Hence, the relation between active control to stabilize the knee and ankle and lateral force on the ice is a topic well worth looking into. Especially, since the female short-track skaters showed a trend of applying higher lateral forces per body weight than their male colleagues, while they skated on a – imposed – lower velocity.

4.3 Force level and performance

Although all male participants skated at the same velocities, and the four general stroke patterns could be distinguished, we do see diversity between elite male speed skaters in the executions of the four strokes. The normal force levels (FN) differed between skaters at the same speed (Figure 9.4), but were not related to their ranking in PR. Since the skaters skated at the same velocities, differences in normal force levels seem to point at a difference in efficiency. Also, the fact that the female participants skated at lower velocities than the men, but did not apply lower normal forces (corrected to body weight), hangs towards an efficiency measure. To gain insight into this effect, data of individual skaters at different velocities and preferably some full-out exercises would be necessary. Also, measuring the velocity of separate strokes would be helpful. Expanding the number of participants would not only be hard –because the study is focussed on top-level athletes –, but also doubtful whether it would benefit the results. It would certainly increase the robustness, but also decrease the sensitivity of an already homogeneous dataset with small margins. In the future, the instrumented skate and push-off force profiles can be used to determine the efficiency of elite short-track skaters and help to give training advice whether the skater should focus on improving strength or technique.

5. Conclusion

A wireless force measuring instrumented short-track speed skate was constructed and calibrated on a tensile testing machine (accurate up to 2.2% in normal direction and 1.4% in lateral direction), which could be used in routine training. Within the homogeneous group of male elite speed skaters, diversity of execution of the force patterns in the four phases of

skating is evident, while skating at the same velocities. Higher ranked male skaters show a trend to have a COP more to the rear of the blade, and lower lateral forces for several phases. Females showed a trend towards applying higher body weight normalised lateral forces than the males, while skating at imposed lower velocities.

Acknowledgements

The authors gratefully acknowledge ir. Jorine Koopman of the Hague University and the students of the Hague University and Delft University of Technology that contributed to the design of the instrumented skate. We acknowledge Sjinkie Knecht for the manual fabrication of the custom cups. We thank dr. ir. J.C.F. de Winter for his advice on statistics. Furthermore, we want to acknowledge the national coach Jeroen Otter and assistant coach Kip Carpenter for their endless ideas and curiosity. And finally, the national Dutch speed skating selection for participating in this research. This study was supported by NWO-STW under Grant 12870.

References

- Felser, S., Behrens, M., Fischer, S., Heise, S., Bäuml, M., Salomon, R., & Bruhn, S. (2016). Relationship between strength qualities and short track speed skating performance in young athletes. *Scandinavian Journal of Medicine and Science in Sports*, 26(2), 165–171. <http://doi.org/10.1111/sms.12429>
- Houdijk, H., de Koning, J. J., de Groot, G., Bobbert, M. F., & van Ingen Schenau, G. J. (2000). Push-off mechanics in speed skating with conventional skates and klapskates. *Medicine and Science in Sports and Exercise*, 32(3), 635–641. <http://doi.org/10.1097/00005768-200003000-00013>
- Lozowski, E., Szilder, K., & Maw, S. (2013). A model of ice friction for a speed skate blade. *Sports Engineering*, 16(4), 239–253. <http://doi.org/10.1007/s12283-013-0141-z>
- Shimmer3. (2015). Shimmer. Retrieved from www.shimmersensing.com
- van der Kruk, E., den Braver, O., Schwab, A. L., van der Helm, F. C. T., & Veeger, H. E. J. (2016). Wireless instrumented klapskates for long-track speed skating. *Journal of Sports Engineering*, 19(4), 273–281. <http://doi.org/10.1007/s12283-016-0208-8>
- van der Kruk, E., van der Helm, F. C. T., Schwab, A. L., & Veeger, H. E. J. (2016). Giving the Force Direction: Analysis of Speed Skater Push-Off Forces with Respect to an Inertial Coordinate System. In *Proceedings of the 34th International Conference on Biomechanics in Sports* (pp. 112–115).
- Yuki, M., Ae, M., & Fujii, N. (1996). ドケットのド反 (Blade reaction forces in speed skating). *Society of Biomechanics*, 13, 41–51.

10

Conclusions and Discussion

Voetballen is simpel...maar het lastigste
wat er is, is simpel voetballen.
-Johan Crujff-

The aim of this dissertation was to determine the interconnectivity of technique variables and performance determining variables within a skating stroke by measuring and modelling the speed skating motion, which eventually can be used for real-time feedback in speed skating training. This is done by the development and verification of a simple 3D biomechanical skating model (SSM) that simulates the skating motion, and developing new instrumented klapskates to measure the push-off forces. To analyse the mechanical power, a well-known performance characteristic, an 8-segment mechanical power model (8SM) of a speed skater has been developed and verified. This dissertation led to the following conclusions:

I. & IV. Measurements and real-time applications:

- State-of the art **human motion capture measurement systems** are not capable of measuring position indoors with a <50mm accuracy in a volume of an indoor ice rink (area of 12,000 m²) (**CH2**). The largest volume we were able to capture with an extensive measurement set-up was 50x4x2m, with an accuracy of 4.5-4.7 mm (**CH6**).
- A pair of **wireless force measuring instrumented klapskates** was constructed and calibrated on a tensile testing machine, where they proved to be unaffected by temperature conditions and accurate up to 1.7% in normal direction and 4.4% in lateral direction. The design of the skate allows skaters to attach their own shoe and Maple blade to the bridge. On-ice measurements showed the possibility of recording with the skates simultaneously and synchronously both straights and curves, and the capability of the system to send data wirelessly and real-time to other devices, which makes it possible to eventually provide skaters and coaches with visual real-time feedback during practice (**CH3**).
- A wireless **force measuring instrumented skate for short-track speed skating**, which has been developed and calibrated in this project, showed that there are four distinctive strokes in short-track speed skating. The explorative study performed on the Dutch national team revealed that the COP on the blade and the lateral forces are related to the level of the skater (**CH9**).
- This thesis proposes a **lean-angle algorithm** for an Inertial Measurement Unit (IMU) to measure the lean angle of the skate on the straights. Two aspects render measuring the orientation with commercially available IMUs and their filters on an ice rink rather difficult, first the ferromagnetic materials in the vicinity of the IMU and secondly the large linear accelerations. A complementary filter based on the assumption that the lean angle can be reset to zero when there is no change in steer angle (angular velocity, measured with a gyroscope) of the skate was used to bypass these problems for the real-time lean angle measurements (**CH8**); verification showed a maximum mean Root Mean Square Error (RMSE) of 5.3° for this filter. We have not found an ambulant system to accurately measure the steering angle of the skate in a global frame.

II. Simple Skating model:

- This dissertation presented a **simple biomechanical skating model (SSM)** which mimics the observed forces and motion of a speed skater on the straights. The skater is considered as three point masses, which are situated at the upper body and at each skate. The input of the model is the changing distance between the upper body and the skate. The model was verified with 3D kinetic data of elite speed skaters measured at an ice rink (**CH4**). The model is most accurate for the position and velocity estimation (respectively 1.2% and 2.9% maximum residuals) and least accurate for the force estimations (underestimation of 4.5-10%). The model provides insight into the interconnectivity between the skating variables within a stroke.

III. Mechanical Power:

- **A systematic overview of the studies on mechanical power** in sports revealed that estimates of mechanical power are usually limited by the capabilities of measurement systems, resulting in the need for simplified power models. Validation of these simplifications has however only been done for running. Furthermore, in the open literature, inconsistency and imprecision were found in the determination of joint power, resulting from inverse dynamics methods, incorporation of translational joint powers, division in negative and positive work, and power flow over segments. Most inconsistency in terminology was found in the definition and application of external, and internal work, and power (**CH5**).
- **An eight body segment model (8SM)** together with a global optimization method with revolute joint in the knee and in the lumbosacral joint is the most realistic model to use for the inverse kinematics in long-track speed skating (**CH6**). Reporting on the Body Pose Reconstruction (BPR) technique and the inverse dynamic method is crucial to enable comparison between studies. This dissertation showed an underestimation of up to 74% in mean joint power when no optimization procedure was applied for BPR and an underestimation of up to 31% when a bottom-up inverse dynamics method was chosen instead of a least square error approach (**CH6**).
- The **new proposed inverse dynamics method PLS** allows minor modifications to the input variables under the assumption that the measurements can be slightly off. Different from other methods, the PLS method introduces the mechanical power balance as a constraint to the optimization function. PLS improves therefore both the input data and the power estimation. For speed skating, PLS showed significantly reduced residual powers in the complete mechanical power balance compared to the existing LSE method, by improving the kinetic power estimation (**CH7**).
- **Sensitivity analyses of the mechanical power balance (CH7)** showed that the normal force and steering angle accuracy, as well as the COM position of the HAT, are of significant influence on the joint power estimation; a 5° inaccuracy in steer or 5 cm inaccuracy of the COM position of the HAT resulted in a 9.7 % and 12.6 % error in joint power estimation respectively.

I. Measurements and real-time applications

I-1 skating power meter

Mechanical power is a metric often used by sport scientists, athletes, and coaches for research and training purposes in sports. In this thesis, the terminology on mechanical power in sport research was analysed (CH5), the influence of choice in inverse kinematics method on joint power in speed skating quantified (CH6), and a new inverse dynamics method introduced (CH7). However, the ultimate aim to develop a real-time feedback system on mechanical power was not established. This has two main causes.

First, the design of a real-time power system requires an ambulant measurement system that does not hamper skaters in their training, and a simplified mechanical power model, with minimal input (measurement) variables. The results from sensitivity analyses of the mechanical power balance (CH7), the literature survey on existing models (CH5), together with a preliminary investigation to compare simplified models to the mechanical power balance, showed that two variables are minimally needed for a reliable power estimation: the global push-off force and the global velocity vector of the skater's Center of Mass (COM) relative to the skate.

At the start of the project, the concept-design of the real-time power measurement system consisted of instrumented klapskates with integrated IMUs, and an IMU near the COM (since the COM lays outside of the body during the skating motion) to measure velocity and orientation. Preferably, this system would be supported by position measurements from a local position measurement system (LPM) (available at the ice rink) by applying a Kalman filter. Based on sensitivity analyses (CH7), we determined that to be within a 5% accuracy of joint power estimation, the accuracy of the orientation of the skate needs to be $<3^\circ$ for the steering angle, and $<4.4^\circ$ for the lean angle, <48 N for the normal forces and <53 N for the lateral force, and <20 mm for the position of the COM. Except for the push-off forces, these accuracies are not met by state-of-the-art ambulant measurement systems (CH2,CH8). Especially the steering angle is currently a concern for speed skating measurements since this cannot be measured by an ambulant system at an ice rink, as ferromagnetic materials of the construction of the building and the cooling pipes under the ice, highly disturb the magnetometer based measurements of the steering angle. Furthermore, after repeated verification of the position measurements of the LPM system, the accuracy met by this system was 288 mm (standard deviation) in the static trials, and 130 mm (standard deviation) in the dynamic trials (see Appendix 10.A) at the ice rink, and thus insufficient for our purpose. Therefore, a reliable real-time ambulant measurement system is currently not available due to the limitations in orientation and velocity measurements at an (artificial) ice rink.

Second, if an actual power meter is eventually established in speed skating, the usability will be different from its application in cycling. In cycling a real-time power meter added significant value in race planning, using for example the critical power concept (the concept is that there is a hyperbolic relationship between power output and the time that the power output can be sustained (Hill 1993)), and the fact that the cyclist with the highest generated power (or power/(BW+equipment) in case of uphill cycling) will in general be faster (assuming the same frictional and gravitational conditions, and correct steering). These results are however not expected in speed skating. The concept of critical power, when based on mechanical power estimations, will probably not hold for speed skating, since the metabolic power to keep the stooped, static position is an important factor of fatigue, but not incorporated in the mechanical power estimations. As Van Ingen Schenau et al. (1983) described in their study on physiological and anthropometrical aspects of speed skating, a skater needs to be able to skate at a deep knee angle during the gliding phase, to reduce air frictional forces. Maintaining this stooped position requires a large quadriceps force, which also explains why skaters with a relatively shorter upper leg have an advantage, as this stooped position will require less joint moments in the knee and hip for them. However, a power meter can serve a different

purpose in speed skating. The skater with the highest generated mechanical power will not be automatically fastest. The generated mechanical power causes a zig-zag motion of the upper body of a skater, while the actual performance is only measured in forward direction. Mechanical power in speed skating when combined with the forward velocity of the skater on the rink could therefore be a useful indication of the efficiency of technique. This can be a valuable variable for coaches and trainers.

Recommendations for the design of a real-time power meter are therefore:

- For **continuous velocity determination** of the COM of a speed skater, and the relative velocity of the COM of the skater to the skate, visual based tracking should be explored (a large number of open source codes are available (Scaramuzza & Fraundorfer 2011)). Since cameras are relatively cheap nowadays, a large number of cameras at the rink can be used for the velocity detection. Another option is to attach three cameras to the skater and skate itself (pointing forward): after mapping the environment with these cameras in a pre-test, the mapped environment could be used to determine the position, and also orientation of the skater and the skate real-time within the chosen frame during testing ([Monocular Scene Reconstruction](#)) (Einhorn et al. 2009). These techniques are currently used in the automotive and robotics industries, and developments are ongoing. Whether there is sufficient illumination at the rink and enough texture to extract the motion with enough accuracy needs to be investigated.
- Concerning the **steering angle of the skate**, the above mentioned monocular scene reconstruction with a small camera at the nose of the skating shoe might result in orientation measures in the future. Until then, the focus should be brought to measuring the velocity vector of the skate, since the steering angle in the global space can be conducted from the velocity vector of the skate: a skate can (mostly) only glide in the direction of the blade. For these global positional and velocity estimations, a camera based measured system seems most promising in the near future (see above).
- Further recommendation concerning mechanical power estimation:
- In this dissertation a new **inverse dynamics technique** (PLS) has been introduced. Limitations of the verification of this technique is that the speed skating data did not contain a full-body marker set (the trunk, head, and arms were assumed to be the HAT segment). In order to further evaluate the benefit of the PLS method, a full-body marker set of a baseball player is currently being used for verification (Gasparutto et al. 2016). Ultimately, the inverse dynamics technique should be verified in a system where all external forces can be measured, (e.g. in ergometer cycling with instrumented handle bars and pedals), since the residuals can then be better verified.

I-2 Steering Angle

The variable that showed to be very important in both performance indication and mechanical power estimation, is the steering angle of the skate. The steering angle of the skate depends on the geometry of the skate (curve and bend of the blade), and the active steering actions of the skater (COP, lean angle and lateral force). The curve of the blade sets the curvature the skate makes over the ice, dependent on the COP on the blade, and the lean angle of the skate. Solely looking at the curve of the blade and the lean angle of the skate, theoretically, the skate will glide in a forward line when the skate is upright, and in the line of the curve of the blade when the skate is flat on the ice (Oonk et al. 2006). The bending of the blade, which, from a top-view, is that both blades are slightly bended to the left, in the direction of the curve of the rink, enhance a better grip in the curves. The exact interplay between these factors, the ground contact forces, and the curve the skate makes on the ice, has not been discovered. Due to limitations in resources, we have not been able to put these separate parameters into further investigations regarding their relation to performance in long-track speed skating. However, in the explorative research performed with the instrumented skates in short-track speed skating (CH9), a trend between the level of the skater and lateral forces and COP was indeed found. The measurement systems to measure the lateral force and COP (CH2, CH9), and the lean angle of the skate (CH8) in long-track speed skating have now been designed and verified, and can therefore be used in future research on performance indicators.

Whether skaters are able to adjust their steering angle when provided with real-time feedback, has been investigated in this project (Bruins 2015). Her results show that subjects were able to apply the real-time feedback of their steering in their technique. Also, subjects were able to retain changes when visual feedback was removed on the same trainings day, and, as a long-term effect, one week after the last (fourth) trainings day. This shows that when the optimal steering technique has been determined, skaters will probably be able to adjust their steering angle with the use of real-time feedback, and, evenly important, can keep these changes after removal of the visual feedback.

Recommendations on technique variables:

- Currently the exact interplay between the geometry of the skate (curve, bend and stiffness), the active steering actions (lean angle, COP, and lateral moment), the ground contact forces (ice characteristics), and the eventual curve the skate makes on the ice is unknown. A mechanical model that can **simulate the behaviour of a skate** on the ice which incorporates the geometry of the skate, the contact force distribution of the ice, the orientation of the skate (lean and steer), the velocity of the skate, and the force distribution acting on the blade (normal force, lateral force, and their COP) would be of high value, since it can provide valuable insights for performance, strength and stability training, technique in the curves and straight parts, and the design of skates. Modifications of the blade, the shoe, or construction of the skate involved in steering could lead to a more effective push-off, such as a double push.
- Concerning the lateral force, we have argued in a conference paper (Van der Kruk et al. 2016) that the lateral force (in the skate frame), together with the steering and lean angle behaviour during skating, does not directly contribute to the forward velocity (performance) of the skater. Therefore, from a mechanical point of view the force can be minimized. Although not investigated yet, we hypothesize that this lateral force is, apart from the active steering control action of the skater, partly a result of an involuntary skewed push-off, due to a lack of **active control to stabilize and ankle**. Felser et al. (2016) already found that the right ankle eversion's isometric and concentric maximum voluntary torque were significantly correlated to performance in short-track speed skating. Hence, the relationship between active control to stabilize the ankle and lateral force on the ice is a topic well worth looking into.
- Integrated into the lean angle algorithm is an IMU based stroke detection, which as a

stand-alone system could provide feedback on stroke frequency, stroke length, contact time, or double stance phase time. Whether these latter measures can provide valuable improvement of the skating motion using real-time feedback, is currently investigated within this project (van der Eb 2017).

I-3 Instrumented Klapskates

This dissertation presented the design and verification of wireless instrumented klapskates (CH2). The design goals for these skates were to accurately and synchronously measure the push-off forces and center of pressure on the blade (COP) of a skater in normal and lateral direction during skating practice, without adjusting the height of the skate and the hinging principle. The skaters should be able to use their own blade and shoe during testing and the skate had to be interchangeable between skaters. Furthermore, the data needed to be transmitted wirelessly and real-time. Additionally, the instrumented skate should be equipped with an IMU for orientation determination (lean angle), a thermometer for temperature compensation (which in retrospect proved to be not required), and had to be able to be synchronised with other measurement systems, which in this design can be established via Bluetooth, or a digital input signal. During the use of the instrumented klapskates in research trials, we became aware of some of their limitations.

Main limitation was the necessity to change the shoe from the skater's own skate to the instrumented bridge. Skaters are reluctant to remove their shoe from their own bridge, since their shoe is positioned in a very specific individual orientation. And if skaters approved in the transfer of the shoe, it took the researchers and participants up to 60 minutes of measuring, adjusting, and habituation.

The second limitation was the weight of the skate. The instrumented skates added about 0.5 kg to the skates, which, although skaters were very well able to train with the skates, does lead to more fatigue than regular klapskates (a regular klapskate weights approximately 0.8-0.9 kg). This is mainly expected in the repositioning phase of the stroke. Research on the consequences of added mass to an instrumented skate is not available. Based on a study on treadmill running, where the metabolic effects of added foot mass (0 - 450 gr) have been quantified by strapping lead strips to the dorsal surface of the foot, an increase in average metabolic rate of 1% per 100 g of mass (per foot) can be expected (Franz et al. 2012; Frederick et al. 1982); we expect however, that the actual increase in metabolic rate will be lower for speed skating than for running, since the repositioning foot has lower accelerations in skating than in running. So, the maximum increase in metabolic rate of the instrumented bridge (0.51kg) is estimated at 5%.

For both these limitations of the design, a new generation of instrumented klapskates has been developed. The design goal of this new generation was to increase the interchangeability between skaters by allowing the shoe to stay on the bridge, while also reducing the added mass. The requirement that skaters need to be able to use their own blade was let go in this new design. In the next section the new design is presented and evaluated before proceeding to the recommendations on instrumented klapskates.

I-3.1 SARA: new design instrumented klapskates

The new design instrumented klapskates SARA (Skate Analyses for Real-time Applications) integrates the force sensors in the blade of the skate instead of the bridge (figure 1). SARA consists of a standard Nagano Viking skating blade with two integrated Kistler Force sensors (Kistler 9602, Kistler Group, Winterthur, Switzerland). The force sensors lay in steel containers, which are, after milling of the Viking blade, welded in the tube of the blade. SARA replaces the skaters' own blade, so installing only requires (de)mounting of the hinge axis. SARA has an added weight of 0.41 kg per skate, which is a 20% reduction compared to the instrumented bridge (0.51 kg). SARA was calibrated using the calibration set-up of the first version of wireless instrumented klapskates (CH2). The calibration in normal direction yielded a linear regression



Figure 10.1 New design instrumented Klapskates.

correlation of $R^2 = 0.99$ and $R^2 = 0.98$ for respectively the left and the right skate, with a root mean square error (RMS) of 2.3% (SEM = 1.6 N) and 2.8% (SEM = 1.8 N). The calibration in lateral direction, also performed with a first order regression, yielded a correlation of $R^2 = 0.98$ and $R^2 = 0.99$ for left and right with the corresponding RMS errors of 6.2% (SEM = 1.4 N) and 4.3% (SEM = 0.6 N) for respectively the left and the right skate. The remaining error of the fit proved to be random.

I-3.1.1 Evaluation of the design

SARA could accurately measure the normal and lateral push-off forces. Furthermore, SARA is 20% lighter than her predecessor and met the requirement of being easily installed under a skater's own shoe and bridge. However, the design did introduce several new limitations and challenges. First, by integrating the sensors in the skating tube, the stiffness of the blade was changed. During the design phase, FEM simulations were performed to test the strength of the blade, and to ensure that the stiffness of the blade would be comparable to the commercially available blades. The load case used in the analysis was based on an actual load case measured at the rink (2000 N normal force, 1200 N lateral force). The exact load application and ground constraint were estimated, since the actual conditions are unknown. (distributed load over the blade). With this FEM analysis, the maximum deformations of a commercially available Viking Nagano skate, a commercially available Maple Blizzard, and SARA were compared and interpreted as an indication of the differences in stiffness (Figure 3). The simulations showed maximum deformations of respectively 1.95 mm (Viking), 3.33 mm (Maple), and 2.85 mm (SARA), indicating that the stiffness of SARA falls within the range of commercially available blades. During pilot testing, however, several participants indicated to feel the difference in stiffness compared to their own blade. Furthermore, the bending and straightening of the blade, which was performed by equipment technicians of the speed skating teams, was more complicated due to the position of the containers in the tube, and due to the change in stiffness these gave to the blade.

Second limitation was a design choice in the joint between the stiff straight edge of the steel container to the less stiffer edges of the tube of the skating blade which induces a stress concentration on the welded connection. In the FEM-simulations, this part of the design was the most critical part, but did hold in the simulated load cases (see above). However, detailed welds were not included in the FEM analysis. The high carbon steel material complicated welding, which forced the use of laser welding. This experimental weld, executed by hand with no supply of filling material, resulted in, what afterwards proved to be, an undercut in the welds. Therefore, the strength of the welds appears to be lower than assumed in the FEM simulations. After a few pilot tests on ice, the welding on the foremost part of the container of one of the skates showed a hairline crack. Since such a crack immediately affects the bending behaviour and strength of the blade, the blade became unusable for further testing.

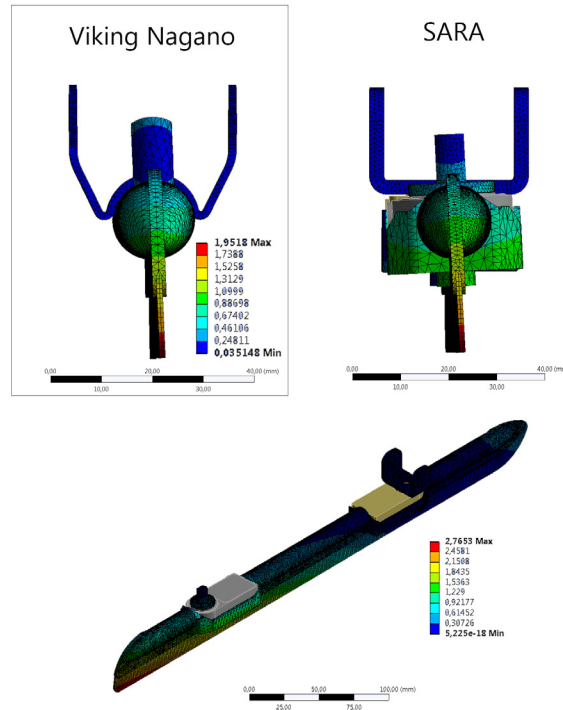


Figure 10.2 Deformations in the Viking Nagano and SARA

I-3.1.2 Requirements for SARA's redesign

The main issues the redesign of SARA has to cope with, are the stiffness of the blade and the strength of the blades. However, setting the correct requirements is a problem, because actual established quantifiable requirements on stiffness, bending, and straightening of skating blades do not exist. Elite skaters mainly chose their blades based on a mix of feeling, testing, and experience.

This was also evident during pilot testing. When participants were asked for their experience after the test, contradicting answers were received on the stiffness of the blade (stiffer/less stiff than a normal Nagano blade), the straightness of the blade (unable to skate on it/didn't notice any difference), and the bend of the blade. Also the instructions that the skaters were given beforehand, influenced the experience of the skaters, which is a well-known psychological phenomenon in sports research (a literature study on the placebo effect in sports showed a total of eleven studies in which authors were able to demonstrate increased athletic performance based on belief alone (Beedie & Foad, 2009)). Nonetheless, since the geometry of the skate is strongly related to the steering of the skate, and thus performance, a redesign of SARA should only be done if concrete requirements can be set for the blade behaviour, which are currently not available.

Recommendations for future directions with the instrumented klapskates are highly related to the results this thesis brought forward on the importance of the steering angle in speed skating the straights. Since this steering angle is related to the COP and the lateral forces on the blade, instrumented skates can play a significant role in the exploration of this performance determining factor. However, since the steering angle is related to the geometry of the blade, it seems counter effective to then adjust this geometry too much. Therefore, the following recommendations are brought about, based on these insights:

- The first version of the instrumented skate, **the instrumented bridge, is currently more applicable for research**, since the exact influence of the stiffness of SARA's blades on the steering angle is undiscovered, and the stiffness of a commercial blade cannot directly be reproduced in the instrumented blades. Short-term developments should therefore focus on the design of a tool to easily install the skater's shoe on the instrumented bridge without changing the original position. Also possible mass-reductions of the instrumented bridge should be explored. Options in fabricating the instrumented bridge from composites and details FEM modelling offer possibilities here.
- When looking further into the future, the ideal design of the instrumented skates would be to **replace the hinge and the cup of the skates by small sensors**. Hinge-like sensors (pin-load sensors) are applied in e.g. vehicles and off-shore applications. However, currently these sensors are too large ($\varnothing = 10$ mm) to implement in the hinge of klapskates ($\varnothing = 4$ mm, Maple blade).

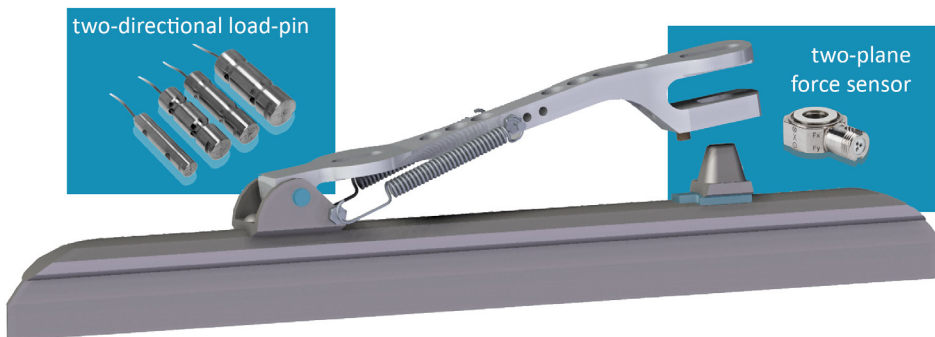


Figure 10.3 Possible design in the future: replacing the hinge by a two-directional load pin, and placing a load cell under the heelcup of the skate.

II. Simple skating model

II-1 Optimization of speed skating motion

We developed a biomechanical skating model with minimal complexity (simple skating model (SSM)). The benefit of a simple model is that the assumptions are comprehensible, and the number of parameters is limited, which eases the interpretation of the results. During verification (CH4), the model proved to be of the right amount of complexity to mimic the observed forces and motions. The model is therefore useful to further investigate the interconnectivity of the variables within a speed skating stroke. The benefit of a model over data analysis of actual skaters, is that one variable can be adjusted, while keeping the other variables constant, and extreme cases can be investigated which provide insight into the basic principles of the variable interaction. The model could also provide insights into possible different optimal motion strategies for different body built (mass, leg length) or strength (leg extension acceleration and velocity, human power), different motion strategies at different velocities or, in other words, for different distances (stroke-frequency), investigate whether optimal techniques are related to the drag at a rink (air frictional constant), or determine the dependency of the motion strategy on the behaviour of the klapskates (steering behaviour, ice frictional forces). To investigate these topics with a simple skater model, a realistic optimization strategy is a necessity.

As post-hoc analysis of CH4, first explorations of optimizing the simple skater model have been performed, of which the method is described in Appendix 10.B. Preliminary results from this optimization procedure have led to two observations; first, the simple skater model, with its limitations and assumptions, proved to be able to mimic the observed forces and motion of a speed skater using optimizing to determine the control input (BOX 1). Second, the key performance determining factor within the speed skating stroke is the interplay between the steering of the skate and the leg extensional velocity. Varying the boundaries of the control

input (the leg extension acceleration, \ddot{u}_s , \ddot{v}_s , and the steering angular acceleration, $\ddot{\theta}_s$) led to different motion strategies. Some of these optimizations found a solution with a *double push* like motion within a speed skating stroke when the steering acceleration boundaries were increased (BOX 2), this double push is discussed later on (II-1.2).

These preliminary results of the SSM look promising for further optimizations, however, we need to be aware of the current limitations of the simplified model.

BOX 1: PRELIMINARY RESULT FROM OPTIMIZATION PROCEDURE - VERIFICATION

The first optimization step was a verification step (for details see appendix 10.B). The results show that despite the simplicity of the model and optimization, the optimization finds a motion strategy that is similar to the observed motion (figure 10.4-6). The forward velocity determined via optimization, which is only fixed at the start and end of the stroke, shows a similar path compared to the measured data, which is first a decrease in velocity and then an increase ($e_{v_x} = 0.08$ m/s (1%)). Also for the lateral velocity the path is comparable, but the optimization uses a larger lateral movement throughout the stroke ($e_{v_y} = 0.38$ m (14%), $e_{\dot{y}} = 0.57$ m/s (27%)) (figure 10.6 d,e). This larger lateral motion is also evident in the steering angle (figure 10.6 h), which is therefore larger in the optimization data than the measured data ($e_{\theta} = 2.6^\circ$ (14%)). Based on the verification results of the simple skater model in CH4, we expect that this larger lateral motion has to do with the neglected swinging leg. The simulation uses the larger lateral motion to decrease the forward velocity in order to reach the fixed distance at exactly \tilde{t}_f , this decrease in forward velocity is in the real data probably due to the swinging leg motion. The leg extensional velocity of the optimization is slightly lower than the measured data, but again show a similar strategy (figure 10.6 f,g). Only the component u_s , which is restricted by a constraint function, does not reflect realistic values ($e_{u_s} = 0.04$ m (5%)) (figure 10.5), which was expected. The work per stroke of the optimized data is 275 J, in the measured data 209 J, the force profile however is very similar ($e_{F_x} = 58$ N (6%)). The difference in work is due to the larger covered distance of the optimization, implied by the larger lateral movement.

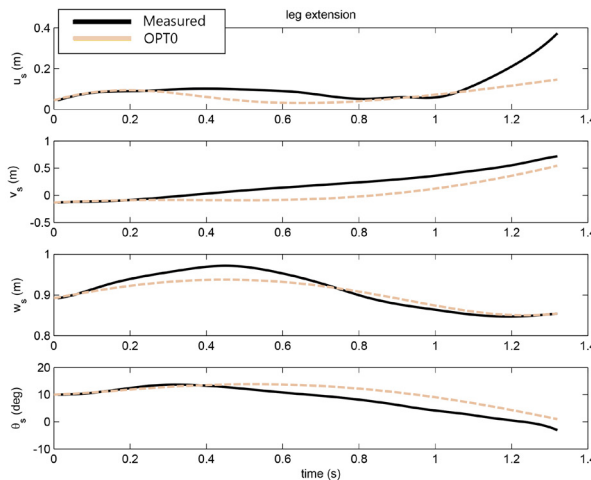


Figure 10.4 measured and optimized (simulated) leg extension of the speed skater. Except from u_s , which was restricted and therefore expected to show different results, the components of the leg extension show similar motion strategies to the measured data.

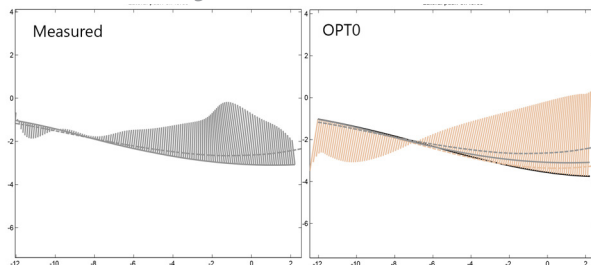


Figure 10.5 The push-off forces in the horizontal frame, presented along the line of the path the skate makes over the ice. Left are the measured kinematic and force data, Right the optimized data (pink), with in grey the measured paths of the skate and the upper body.

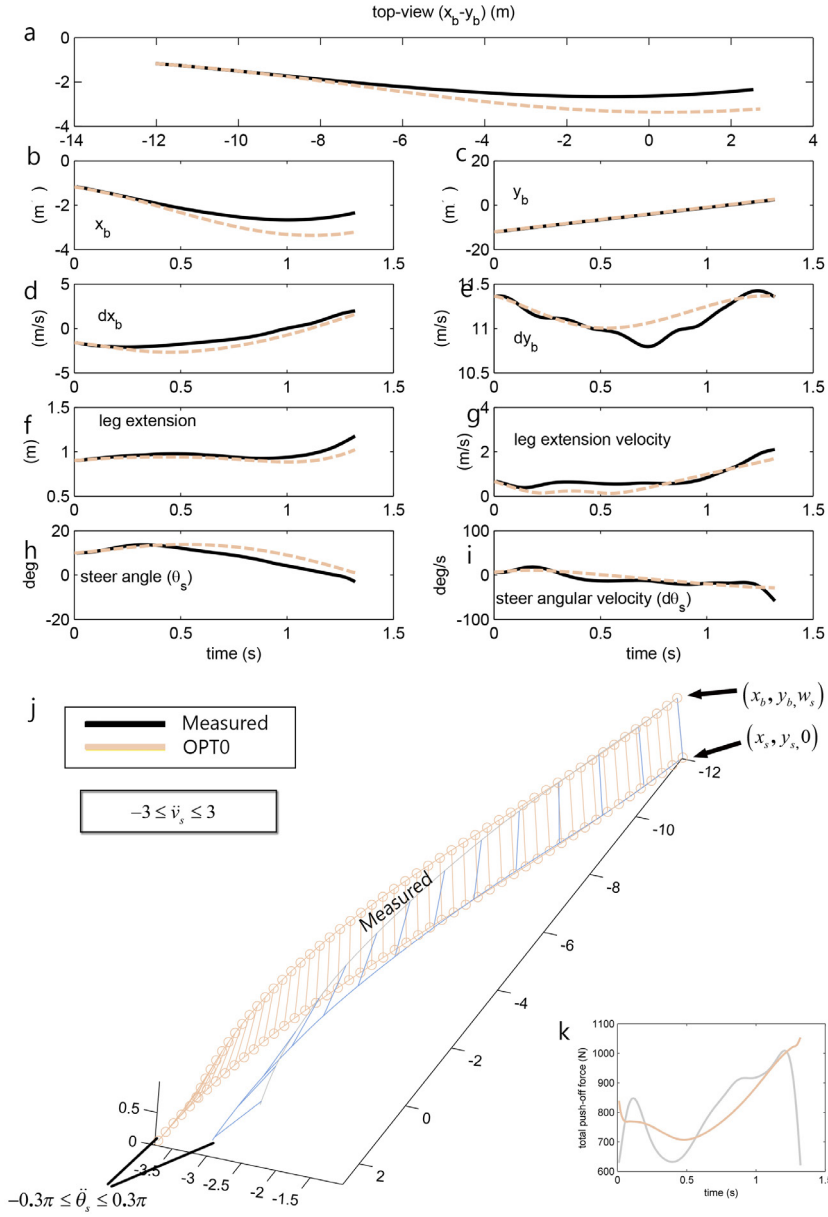


Figure 4 Overview of the output variables of the simple skater model for OPT0; a) topview of the motion of mass B; b) lateral position versus time mass B; c) longitudinal position versus time of mass B; d) lateral velocity of mass B; e) longitudinal (forward) velocity of mass B; f) leg extension, defined as the norm of u_s , v_s and w_s ; g) leg extension velocity; h) steering angle; i) steering angle velocity; j) 3D plot of the movement of mass B and mass S skate. The initial position at the rink is $[-1.17, -12.02 \text{ m}]$. k) total push-off force of the measured data,

BOX 2: PRELIMINARY RESULT FROM OPTIMIZATION PROCEDURE- DOUBLE PUSH

Next step after the verification was to find the optimized motion with adjusted control input boundaries. When the steering angular acceleration was increased, some optimizations found their solution in applying a double push. An example of such a motion strategy is given in figure 10.7 (OPT9). The control input boundary was here increased to $3\pi \text{ rad/s}^2$, for the initial velocity we used

the measured velocity $v^{\text{in}} = 12 \text{ m/s}$. Figure 10.7 shows the push-off forces in the (horizontal frame), presented along the line of the path the skate makes over the ice. In the double push like motion, the skate is steered back and forth, in which the skater pushes off several time. The benefit of a double push, is that because of the back-and forth steering, more of the push-off forces are directed into the forward direction, while the forward velocity is also sustained. Further research is necessary to determine when the optimization goes into a double push strategy. The preliminary results show that double push can be more efficient (increased average velocity with no increase, or even a decrease in

W_{SMW}), however this is not always the case.

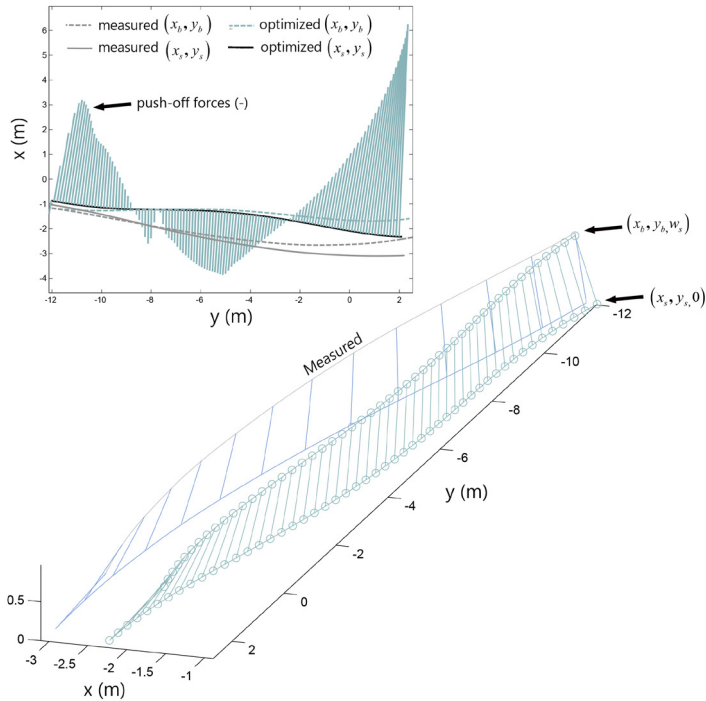


Figure 10.7 Example of an optimization (OPT9) is which the double push showed up as the best solution to cover the fixed distance in a minimal amount of time. The initial velocity of this trial is $v^{\text{in}} = 12 \text{ m/s}$, the input control boundaries were set to 3 m/s^2 for \ddot{u}_s, \ddot{v}_s , and $3\pi \text{ rad/s}^2$ for the steering angular acceleration $\ddot{\theta}_s$.

II-1.1 Limitations of the optimization

The simple skating model has been verified in this dissertation, but not validated. Validation is reached when the skating motion of a skater is improved with the outcome of the model via real-time feedback. There are several limitations that should be resolved before validation of the model. Preferable the optimal motion strategy is found, which will be a balance between efficiency (being aware of its limitations regarding the energy related to static posture (I-1)) and forward velocity. Therefore, the following parts need to be added to the simple skater model: the repositioning leg and balance control, human power restrictions, steering limitations, and air frictional force.

II-1.1.1 The repositioning leg and balance control

The balance control of the skater is currently not incorporated in the simple skating model, since we prescribe the upper body vertical motion (w_s). The simulated skater will therefore not fall over. In the current model, where the repositioning leg, and therefore the double stance phase is neglected, balance cannot be determined. Adding the repositioning leg is necessary if we want to determine if the optimized motion strategy is feasible, and will benefit the applicability of the model when translated into feedback for a skater. Implementation of the repositioning leg holds two things: modelling the swinging leg and determining the timing of the double stance phase. Currently, the simple model does not incorporate the swinging leg of the skater. As the results from van der Kruk et al. (2017) show (CH4), this leg does influence the forward velocity of the skater during a stroke. Modelling the trajectory of this leg in a separate simple two-mass model can provide insight into this motion, and could be used to optimize the motion trajectory of this leg in the air. If proved to be necessary, the results from this model (forces) could be integrated into the simple skater model as external forces acting at the COM. Also the double stance phase is not incorporated in the simple skater model. Since this double stance phase is basically overlaying parts of two strokes, the model does already exist. To transform the simple skater model into a bi-pedal skater, the timing of the double stance phase (placement of the skate and take-off) needs to be determined. The forces acting at the start and end of the stroke on the COM of the skater (determined with the simple skater model) can then be added as external forces to the active skate system. Introducing the double stance phase is most important for the start of the stroke, since the steering of the placed skate decides the direction the force of the other leg is directed to. When these two elements of the repositioning phase are added to the model, also the balance of the model can be incorporated.

II-1.1.2 Human Power constraints

When optimizing for a maximal performance, a constraint on maximum mechanical power and work should be added. The maximum voluntary joint torque is a function of joint angle (force-length relationship and change in moment arm) and angular velocity (force-velocity relation (Hill-model)), and could therefore be well integrated in the optimization of a biomechanical model. Since the simple skating model does not allow for direct joint power estimations, nor joint angular velocities, an estimation of these should be made. In the simple skater model, the athlete is modelled as just three point masses and a piston-like joint between them (upper body - skates), which is the direct distance between the COM of the body and each skate. The leg extension of the simple model is therefore an indirect measure of the knee joint angle (mostly extension) and hip angle (mostly extension and abduction). The benefit of this simple input is that the leg extension velocity and acceleration can relatively easily be determined for actual speed skaters (Allinger & Bogert 1997). This way, the model can be driven by individual constraints measured from the speed skater, by adding a path constraint to the existing optimization problem.

II-1.1.3 Steering of a klapskate.

In the SSM, the variable u_s decides the position of the COM of the skater relative to the skate in line of the blade. Therefore, u_s determines the position of the COP on the blade. Since the steering of the skate is related to COP, we might need to incorporate this relation into the simple skater model, in order to obtain more realistic results on the steering actions of the skate. In these first optimizations, this relation was not incorporated. Therefore, a path-constraint was necessary for u_s , to avoid unrealistic movements. In reality, u_s is related to balance and steering.

II-1.1.4 Air frictional forces

The estimation of the air frictional force was of influence on the fit of the model. In this dissertation, published data on static wind tunnel experiments were used to estimate the air frictional forces (van Ingen Schenau 1982). Furthermore, the air frictional force is currently dependent on the velocity in the horizontal plane, but independent of the posture of the skater. The model would benefit from an additional relation between the upper body position

(w_s) and the air frictional force. Since the pitch of the upper body (flexion-extension of the hip) is not modelled, a relation with respect to frontal area, needs to be estimated.

The segments of the skater constantly move during the skating motion, thereby changing both the frontal area of each segment and the drag coefficient. Although the frontal area per segment was estimated based on video recordings, exact knowledge on how the aerodynamics (drag coefficient) interact within a speed skating stroke has not been published. Both simulations of speed skating motion and mechanical power estimations in speed skating can benefit from improved aerodynamics data. If a more precise estimation per segment is possible in the future, it will be interesting to determine whether different techniques should be employed under divergent drag-conditions.

II-1.2 Accurate Kinetic data

The accuracy of the (input) measurements is of high importance for the model outcome. Differences in performance in top-level speed skaters are very small. As demonstrated by Noordhof et al. (2015), the smallest worthwhile improvement (0.3 times the standard deviation of an elite athlete's race-to-race performance) which reflects a 10% increase in the chance of winning the event by an athlete who is already winning medals regularly, is on average 0.23% for males and 0.25% for females senior elite speed skaters. This medal of course has two sides: small improvements can quickly improve the chance of winning, however, since the differences are so small, the requirements for accuracy of methods and measurement systems to improve performance are very high, and has, with the current state-of-the-art technology for biomechanical analysis, not yet been met.

II-1.3 Double push

The preliminary results of the optimizations underline the main interplay of the skating technique: the interchange between pushing sideways and moving forwards. The optimizations all aim at as much forward movement as possible, however, since the skate needs to have a steering angle in order to generate a push off that results in forward velocity, an optimal motion seems to steer the skate back-and-forth as much as possible during one stroke, resulting in a, for inline-skaters well-known, *double push* like motion¹. Since the inline skating technique and its restrictions are very similar to the ones in ice speed skating, a speed skater should physiologically and balance-wise be able to make this double-push. However, even the man who invented the double push in inline skating in 1993, Chad Hedrick, who also is

¹ video: double push on treadmill: <https://www.youtube.com/watch?v=KLrFqq6gGg8&t=27s>

a top-level long-track speed skater, does not apply the double-push technique on the ice. Apparently, there seems to be a restriction to perform this technique. Although scientific research on the ground contact reactions of speed skates and inline skates is not available, we hypothesize that this is due to the steering and handling restrictions of the design of a klapskate on the ice compared to a skeeler on the road². The steering of a skeeler can probably be done quicker (and more stable) than a speed skate and seems less sensitive in handling than a klapskate; for example, an inline skater can be more to the front of the wheels (which results in steering), where in speed skating this would automatically result in increased ice friction (de Boer et al. 1987).

Although the double-push is believed to be the most optimal technique to use in inline skating, no scientific research confirming its efficacy has been published. In cross-country skiing, where the double push is also applied, the steering of the ski is done by a jump in between the first and the second push to re-position the ski in an abducted orientation (Stöggli et al. 2008). This emphasizes that a double push is only beneficial when the ski can be turned quickly. This jump however, must result in lost energy by impact and high demands of muscle force. The double-push seems therefore less efficient in cross-country skiing compared to inline-skating. With further optimizations of a simple skating model (Bruzzo et al. 2016; E. van der Kruk et al. 2017) further insights can be made on the basic mechanism of the double push in both skiing and skating (Stoeggli et al. 2010). Experienced double-push cross-country skiers still seem to improve and develop the skating technique, a skating model might be able to accelerate these developments. The benefit of a model is that research is not dependent on the technical proficiency of the available participants.

Recommendations for the simple skater model:

- The simple biomechanical model neglects the **swinging leg in the repositioning phase** of the skating stroke. It seems relevant for the validation of the model to further analyse the motion of this swinging leg during repositioning, which can be done through optimization of a simple two-mass model. More important for the optimization is incorporating the timing of the placement of this swinging leg (the start of the double stance phase) in the simple skater model. This so to transform the model in a bipedal model which incorporates the balance of the skater throughout the stroke.
- When optimizing for a maximal performance, a **constraint on maximum mechanical power and work** should be added. The maximum voluntary joint torque is a function of joint angle (force-length relationship and change in moment arm) and angular velocity (force-velocity relation (Hill-model)). A simplification of the restrictions in mechanical joint power could be integrated in the optimization of a biomechanical model.
- The **aerodynamics of a speed skater** can currently not be measured directly. Two technological developments can be of importance for this topic; first development, are the improvements of CFD simulations for dynamic motions and the possibilities of 3D scanning of athletes. Combining the 3D scanning technology, with the 3D motion capture of athletes, 3D simulations of an athlete can be constructed, which thereupon can be used for dynamic CFD simulations. Second development is a new test set-up based on particle image velocimetry (PIV) called *the ring of fire*, which might be able to display the air flow around an athlete at an actual ice rink in the near future (Terra et al. 2017). In this method, a cloud of ultrafine bubbles is produced, which is shone by lasers or LED light to visualize the bubble flow (air flow) around the athlete during actual exercise.
- Since the steering is related to **COP**, and thus to the position of the COM of the skater relative to the skate in line of the blade, we might need to incorporate this relation into the simple skater model, in order to obtain more realistic results in the steering actions of the skate (in the model, this relation is defined by u_s). First, the relation between the COP and the steering of the skate should then be fully understood.

² video: double push inline vs speed skating (Bart Swings) : <https://youtu.be/3BSELHRSYYw>

- The results and insights of this dissertation obtained with the simple biomechanical model are of a **relative character**. The fact that there is an optimum in the steering angle of the athlete is established, however more advanced measurement technologies will be necessary to obtain accurate data than can provide absolute feedback for an athlete.
- Due to the limitations in measurement equipment, facilities and time, we had to restrict the current research to analysis of the straight part of the rink only. However, speed skaters seem to generate most acceleration and power in the **curves**, which makes analysis of this part of the rink very important for future studies. In the curve, the stroke frequency goes up, enabling the skater to generate more push-offs.

Future directions for speed skating research.

Recommendations for elaboration on the work of the thesis have been provided in the previous paragraphs. Based on the results of this dissertation and these recommendations, the following three focus points are defined for future directions in speed skating research:

- **Design and verification of a measurement system** that can measure the **position and velocity** of the center of mass and skate in a global space continuously over the whole rink with a position accuracy of (at least) 20mm. As stated in the recommendations, it is advised to look into the possibilities of either camera based tracking (cameras placed either at the ceiling and/or in the boarding of the rink), or monocular based tracking, where frontal pointing cameras are attached to the skaters trunk and skates. Apart from its application for mechanical power estimation, the relative position of the skate towards the trunk (COM) of the skater will provide significant insights into the skating technique within and between skaters, and is therefore directly applicable for skaters and coaches. In short-track speed skating, the position and velocity measurement will also be of benefit for the analysis in tactics. Furthermore, the measurements will eventually be of use for the feedback based on the optimizations of the skater model.
- Design and validation of a mechanical model that can **simulate the behaviour of a skate** on the ice which incorporates the geometry of the skate, the contact force distribution of the ice (ice characteristics), the orientation of the skate (lean and steer), the velocity of the skate, and the force distribution acting on the blade (normal force, lateral force, and their COP). This can provide valuable insights for performance, strength and stability training, technique in the curves and straight parts, and the design of skates. Modifications of the blade, the shoe, or construction of the skate involved in steering can lead to a more effective push-off, such as a double push.
- The results in optimization of the simple skater model are promising. Therefore, the **focus for the development of the model** should be on adding the double stance phase, incorporate stability into the model, and adding a constraint on the maximum power output of the skater. Optimizations of such a model can provide valuable insights on our general understanding of speed skating, which will be applicable in speed skating practice, but also in other skating motions as inline skating and cross-country skiing. If the dynamics of steering are understood and can be modelled (see above), these relations should be added to the skating model (mainly applicable for the COP positioning).

References

- Allinger, T.L. & Bogert, A.J., 1997. *Skating technique for the straights based on the optimization of a simulation study. Medicine and Science in Sports and Exercise*, 29, pp.279–286.
- Anderson, D.E., Madigan, M.L. & Nussbaum, M.A., 2007. *Maximum voluntary joint torque as a function of joint angle and angular velocity: model development and application to the lower limb. Journal of biomechanics*, 40(14), pp.3105–3113.
- Beedie, C.J. & Foad, A.J., 2009. *The placebo effect in sports performance. Sports Medicine*, 39(4), pp.313–329.
- de Boer, R.W. et al., 1987. *Physiological and biomechanical comparison of roller skating and speed skating on ice. European Journal of Applied Physiology and Occupational Physiology*, 56(5), pp.562–569.
- Bruins, N.T., 2015. *The effects of real-time visual feedback on skate orientation in skaters, Master Thesis VU University Amsterdam Faculty of Human Movement Sciences*.
- Bruzzo, J. et al., 2016. *A simple mechanical model for simulating cross-country skiing, skating technique. Sports Engineering*, 19(2), pp.91–104.
- van der Eb, J., 2017. *In search of good performance indicators for speed skating. In International Society of Biomechanics. Brisbane*.
- Einhorn, E., Schröter, C. & Gross, H.-M., 2009. *Monocular Scene Reconstruction for Reliable Obstacle Detection and Robot Navigation. In ECMR. pp. 7–12*.
- Felser, S. et al., 2016. *Relationship between strength qualities and short track speed skating performance in young athletes. Scandinavian Journal of Medicine and Science in Sports*, 26(2), pp.165–171.
- Franz, J.R., Wierzbinski, C.M. & Kram, R., 2012. *Metabolic cost of running barefoot versus shod: is lighter better? Medicine & Science in Sports & Exercise*, 44(8), pp.1519–1525.
- Frederick, E.C., Daniels, J.T. & Hayes, J., 1982. *The effect of shoe weight on the aerobic demands of running. Int. J. Sports Medicine*, 2(2), p.28.
- Gasparutto, X. et al., 2016. *BALL VELOCITY AND ELBOW LOADING IN FASTBALL PITCHING. In ISBS-Conference Proceedings Archive*.
- Hill, D.W., 1993. *The critical power concept. Sports medicine*, 16(4), pp.237–254.
- van Ingen Schenau, G.J., 1982. *The influence of air friction in speed skating. Journal of Biomechanics*, 15(6), pp.449–458.
- van Ingen Schenau, G.J., de Groot, G. & Hollander, A.P., 1983. *Some technical, physiological and anthropometrical aspects of speed skating. European Journal of Applied Physiology and Occupational Physiology*, 50(3), pp.343–354. Available at: <https://www.scopus.com/inward/record.uri?eid=2-s2.0-0020530772&partnerID=40&md5=90751a8580e56394d4ba897e50bba11>.
- van der Kruk, E. et al., 2016. *Giving the Force Direction: Analysis of Speed Skater Push-Off Forces with Respect to an Inertial Coordinate System. In In: Proceedings of the 34rd*

International Conference on Biomechanics in Sports. pp. 112–115.

van der Kruk, E. et al., 2017. Design and verification of a simple 3D dynamic model of speed skating which mimics observed forces and motions. *Journal of Biomechanics*.

Noordhof, D.A. et al., 2015. Race Factors Affecting Performance Times in Elite Long-Track Speed Skating. *International Journal of Sports Physiology and Performance*, (October). Available at: <http://journals.humankinetics.com/ijsp-in-press/ijsp-in-press/race-factors-affecting-performance-times-in-elite-long-track-speed-skating>.

Oonk, H. et al., 2006. The relationship between the rocker of the blade, the bending of the blade and the angle of the push off in speed skating | Relatie tussen ronding, bending en afzethoek bij schaatsen. *Geneeskunde en Sport*, 39(6).

Scaramuzza, D. & Fraundorfer, F., 2011. Visual odometry [tutorial]. *IEEE robotics & automation magazine*, 18(4), pp.80–92.

Stoegg, T. et al., 2010. Double-push skating versus V2 and V1 skating on uphill terrain in cross-country skiing. *Medicine and science in sports and exercise*, 42(1), pp.187–196.

Stögg, T., Müller, E. & Lindinger, S., 2008. Biomechanical comparison of the double-push technique and the conventional skate skiing technique in cross-country sprint skiing. *Journal of sports sciences*, 26(11), pp.1225–1233.

Terra, W., Sciacchitano, A. & Scarano, F., 2017. Aerodynamic drag of transiting objects by large-scale tomographic-PIV. *Experiments in Fluids*, 58(7), p.83.

Appendix 10.A Accuracy of Local Position Measurement System (LPM) and Indoor GPS (iGPS)

This Appendix is concerned with the comparison of the LPM and iGPS system in a field test concerning their accuracy and applicability in measuring the kinematics of a speed skater.

A.1 Method

A.1.1 Static and Dynamic measurements

The tests were performed on an unfrozen ice rink, of Thialf Heerenveen, the Netherlands in April 2013. The sensors of two measurement systems (two Nikon iGPS single detectors (I4is) (30Hz), two LPM transponders (100 Hz), were positioned on a frame (measurement cube, 320x320x320mm), thereby maintaining a constant relative position. The set-up consisted of eight iGPS transmitters and twelve LPM base stations. For the static measurements, the global position of the measurement frame was changed, into nine different positions in the horizontal xy-plane at two different height positions (0.5m and 0.9m). This test was repeated twice. The output variable of this test was the relative position error. The outcomes were compared with a set value of the measurement cube.

The purpose of the dynamic measurement was to find the accuracy of the systems with regard to position and velocity in a dynamic situation. A measurement cube was placed on the rear of a bicycle (Figure 10.A.1a), which was then ridden at three different velocities, thereby changing the global position dynamically while maintaining the relative positions of the sensors. Cycling speeds were 15 km/h, 20km/h and 25km/h and each test was performed three times, and ended a coasting recording (the cyclist stops pedalling). The velocity of the bicycle was kept constant by the cyclist with the aid of a cycling computer. Additionally a data logger was used (Arduino) to afterwards examine if the average velocity was as intended. Only the straights were measured.

The LPM data were filtered with a Kalman filter in the hardware. In the LPM software the outliers were removed and the data were filtered with a linear filter. The analysis of the iGPS data was done using the raw data. The raw data showed outliers which were removed using the z-scores of the distribution, as described in (Field 2005).

A.1.2 Comparison of LPM and iGPS in speed skating

The final test was a qualitative test to compare the LPM measurement system with the iGPS measurement system, performed at the ice rink Heerenveen in July 2013. Each participant (skater) was equipped with two iGPS single detectors (I4is) at the skates (30 Hz). At the upper body the skater was equipped with an iGPS double detector (I4is) (30 Hz). The benefit of the double detector was an increased accuracy and robustness. All iGPS sensors were connected to an amplifier and to the battery on the back of the skater. The iGPS sensors measured the position coordinates of the skates and the upper body. Additionally two LPM sensors (100 Hz) were attached to both skates (Figure 10.A.1b). The set-up consisted of twelve LPM base

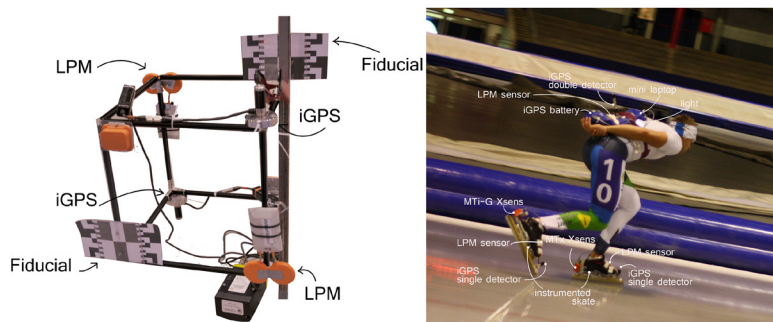


Figure 10.A.1 (a) measurement cube, the fiducials are not used the study here; (b) Fully equipped skater.

Table 10.A.1 The mean STD and maximum absolute error of the dynamic tests.

LPM	Set value (mm)	Mean (mm)	STD (mm)	Max abs error (mm)
15km/h	439(±17)	616.7	128.7	329.7
25 km/h	439(±17)	614.6	131.9	312.1
iGPS				
15 km/h	564(±17)	569.8	1.2	4.3
25 km/h	564(±17)	567.0	1.7	5.9

stations and thirteen iGPS transmitters. A Casio Exilim high speed camera was used to capture motion of the speed skaters in high speed (300 fps). The synchronization procedure was based on the internal clock of the high speed camera. Written consent was signed by the participants according to the guidelines of the Ethical Committee of the Technical University of Delft.

A.2 Results

A.2.1 Static position measurements

For LPM the results showed a large deviation in relative position error, ranging up to 790 mm error from the found mean, which was lower than the desired 50 mm accuracy. The maximum error and standard deviation relative to the found mean indicated that the variation in longitudinal direction (in line with the straight) (y) was lower than the perpendicular measurements (x), respectively 195 mm versus 288 mm standard deviation from the found mean. The mean measurements in x direction did however have a smaller deviation from the set value (180mm versus 235mm). The maximum deviation from the found mean for the iGPS system was found in y-direction and was about 20 mm, which is within the desired 50 mm accuracy. The maximum difference between the mean and the set value was 11 mm. There was no significant difference in performance for the three separate directions.

A.2.2 Dynamic measurements

For LPM the results showed that the standard deviation of the error was around 130 mm for all measured speeds (Table 10.A.1). The results also indicated a large deviation from the set value (>180mm). The results showed that the iGPS data were very accurate and had almost no variation in the data. The standard deviation of the error ranged between 1.2 mm and 1.7 mm for the increasing speeds. The largest deviation from the set value was found in one of the three tests at 20 km/h with a difference of about 40 mm from the found mean value. Due to signal loss during the measurements, the number of samples of the iGPS system fluctuated in time, with a lowest sample rate at 25 km/h of 24.4 Hz. The number of samples per time was negatively related to the velocity. The numbers are averaged over nine straight parts.

The performance of the systems in terms of velocity were scrutinized with the analysis of the coasting exercise (Figure 10.A.2). The speed could only decrease since the cyclist stops cycling.

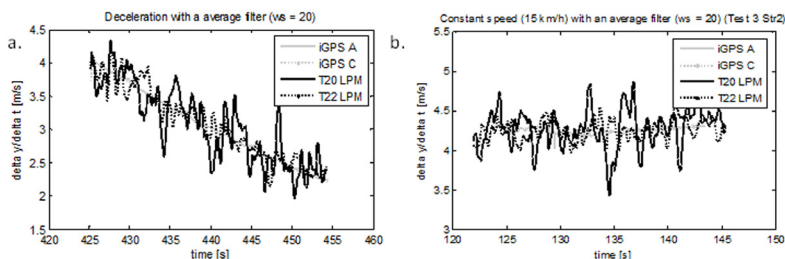


Figure 10.A.2 The LPM data is filtered with a linear filter and sampled at 100 Hz. The data from the iGPS system was sampled at 30 Hz and filtered using an averaging filter with a window size of 20. (a) Difference in y position over time during a coasting exercise. The figure should give a smooth deceleration; T20, T22 LPM sensors; A, C iGPS sensors. (b) Difference in y position over time during constant speed.

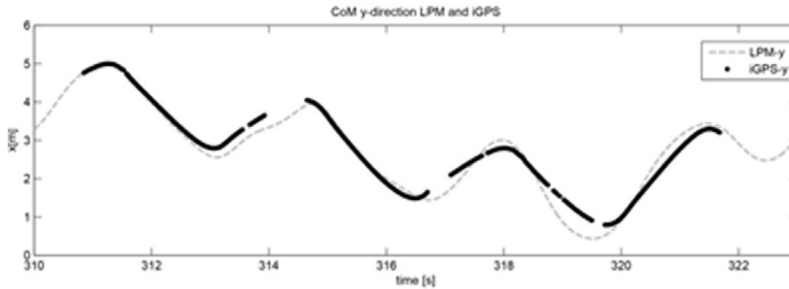


Figure 10.A.3 Position of the LPM and iGPS sensor at the upper body. The LPM data show more smooth curves, while the iGPS data show asymmetry.

The LPM results showed unrealistic accelerations in the data; The data obtained at the straight part with a constant velocity showed a correct global average velocity (4.2 m/s), however the LPM system showed far more fluctuations than the iGPS system (Figure 10.A.2).

A.2.3 Speed skating measurements

During the test it became evident that the iGPS infrared measurement system was influenced by the reflection of the ice. This resulted in time gaps in the data. The coverage of the iGPS measurement system was about 60% in time for the sensors at the skate and 80% for the sensor at the back of the skater (1.2m from the ice). This became evident after resurfacing of the ice, which increased the reflection and reduced the iGPS performance.

Figure 10.A.3 shows the position measurements of a sensor at the back of the skater along the straight part of the rink. The LPM data show more symmetric, smooth curves compared to the iGPS data.

A.3 Discussion

It is appropriate to do static as well as dynamic calibration of large-range measurement systems, as the motion might affect the accuracy of the systems. The LPM results for the static and dynamic tests are in line with the results described in (Fintelman 2011), also in Heerenveen, who reported that static error ranged up to 730 mm and the dynamic error ranged up to 130 mm standard deviation.

The iGPS system was never applied in sports applications before and therefore no reference data were available for comparison. In the dynamic tests the iGPS system showed maximum errors of 6 mm, which are lower than the errors found in the static test (20 mm). Increased speed leads to lower position accuracy and a decreased number of samples. The average number of samples at 25 km/h (24.4 samples per second), lead to a time accuracy of 0.04 s, which is within the requirement for the model verification (0.05s). The system proves to be applicable for accurate kinematic measurements in a dynamic environment. Drawback for the application in sports are the size of the sensor (the I4is used \varnothing 20mm x 63,5 mm + battery 150mmx100mmx50mm), the low sample frequency and the necessary line of sight.

In the speed skating tests it became evident that the infrared beam reflection on the ice influences the iGPS measurements in terms of time coverage. The closer the sensors are placed to the ice, the more gaps there are in the data. Possible solutions would be interpolation of the data or selection of data parts, or by performing sensor fusion, by combining iGPS with a system with a high sample rate, e.g. combining iGPS with inertial sensors.

The velocity measurement of both LPM and iGPS on average indicate a right estimation; the velocity over time in the LPM data however suffers from incorrect fluctuations. Based on the position measurements during the speed skating tests, the LPM data show a more smooth pattern. Unfortunately there was no insight in the hardware filtering of the LPM system, but it is hypothesized that the distortion can be partly attributed to the Kalman filter in the hardware.

A.4 Conclusion

The results show that the iGPS system has a maximum static error of 19.6 mm and a maximum dynamic error of 5.9 mm at a speed of 25 km/h. A maximum static error of LPM of 447.9 mm was found and a maximum dynamic error of 312.1 mm. The iGPS system reaches the required position accuracy of 50 mm for the speed skating data collection. The time accuracy of 0.05s can be reached with the iGPS system, however the data contain large time gaps, which are related to the reflection of the ice. It may be concluded that the iGPS measurement might find application in sport, although further developments should be made on the sensor size and robustness. The application in speed skating has its limitations due to distortions from ice reflection.

References

Field, A. (2005). *"Discovering statistics using spss."*

Fintelman, D. M. (2011). *Simplest skater model. Master Final Thesis, Technical University of Delft.*

Nikon. (2013). *"[http://www.nikonmetrology.com/en_EU/Products/Large-Volume-Applications/iGPS/iGPS/\(brochure\).](http://www.nikonmetrology.com/en_EU/Products/Large-Volume-Applications/iGPS/iGPS/(brochure).)"*

Appendix 10.B: Optimization of the simple skater model.

This Appendix describes the optimization procedure used to obtain the preliminary results presented in the discussion of this dissertation. First, a short introduction is given on the aim of the optimizations. Second the optimization method is presented.

B.1 Aim of the optimization study

Currently, there are three skater models that describe the coordination patterns of skaters (Allinger & Bogert, 1997; Otten, 2003; van der Kruk, Veeger, van der Helm, & Schwab, 2017). Allinger & Bogert (1997) were, up-to-now, the only ones to use their biomechanical model of a skater to optimize the skating technique in order to find the fastest steady-state speed. Their optimization was constrained by three relationships: the leg length, instantaneous power (determined from the push-off force and velocity of the leg extension in the horizontal plane), and the average power per stroke. Their biomechanical model is driven by the horizontal leg length which is a function in time. The steering angle was prescribed by this input, since the leg extension (horizontal leg length) was assumed to occur perpendicular to the skate blade. Their results show, among others, that a number of skating techniques can be used to achieve the same steady-state speed, that as skating speed increases the range of techniques decreases, and that full leg extension is not necessarily optimal to reach a top speed. However, the applicability of their results is limited, since the model is driven by a pre-scribed function for leg extension and the model, and the optimizations have not been verified with measured kinetic data of speed skaters. The simple skater model (SSM) of van der Kruk et al. (2017) is a simple three-dimensional biomechanical skater model driven by the three dimensional measured leg extension (defined as the changing distance between the upper body and the skate), and the measured skate steering, which is called the motion coordination. This model has been verified with measured kinematics and forces of elite speed skaters on an ice rink, and might therefore be suited to use in an optimization procedure.

This study is the start of this quest, and focusses on the main restriction in speed skating: the trade-off between gliding forward and pushing sideways. The aim of this study is to gain insight into the question: given an initial total velocity, what is the optimal trade-off between lateral and forward motion within one stroke to cover a fixed forward distance in a minimum time span? A fixed measured distance of one stroke was used, since in this first approach, we will only optimize for one stroke, and need to have a realistic stroke length that can actual be made an even number of times (allowing the skater to leave and enter the curve with the correct leg). In reality skaters might want to choose for a different stroke length (different stroke-frequency) under different conditions (Allinger & Bogert, 1997), this was left for future studies. Furthermore, the maximal power output of a skater and the efficiency are not incorporated in the optimization criteria in this first approach. We specifically chose to not incorporate these measures, since mechanical power estimated with a simplified model highly differs from joint power (which is, from the mechanical power estimates, closest related to muscle power) (van der Kruk, van der Helm, Veeger, & Schwab, 2017). Furthermore, even if joint power was incorporated, it remains unclear what the exact energy expenditure for a speed skater is. Therefore, this measure was not used in this first approach. Future possibilities and possible approaches are discussed in CH10 of this dissertation.

The aim of this study is to determine the optimal trade-off between lateral and forward motion within one stroke to cover a fixed distance in a minimum timespan. This aim is approached in two steps; first we determine if the optimization strategy, with the chosen boundaries and constraints, finds a realistic control input and model output, compared to observed forces and motions. Second, we determine the optimal trade-off between lateral and forward motion to minimize the time to cover a distance of one stroke, thereby using the control input boundaries (leg extension acceleration, steering angular acceleration) and the total initial velocity as independent variables. The optimized control strategies are compared based on the final time and the mechanical power output, together resulting in a measure of efficiency.

B.2 Method

B.2.1 Simple Skater Model

The model and its verification are fully described in CH4 (van der Kruk, Veeger, et al., 2017). , here we give a brief summary. The skater is considered as a combination of three point masses, which are situated at the upper body (mass B) and at each skate (mass S) (Figure 4.2). Since the double stance phase is rather short, it is assumed that there exists no double stance phase. Therefore, only one skate at the time is on the ice, alternating left and right. The point of alternation is defined as the moment in time where the forces exerted on both skates are equal. So at any point in time, only two masses are considered in the model, which we refer to as the *active masses* (mass B and one of the skates). The repositioning phase of the inactive skate in the air is therefore neglected. Each mass has three degrees of freedom. The set of parameters is restricted to the position coordinates of mass B (x_b, y_b, z_b), two translations in the transverse plane of mass S, with the position coordinates (x_s, y_s) (because the skate is assumed to be on the ice, making $z_s=0$ at all times) and one rotation in the same plane, the steer angle (θ_s). This steer angle is of importance for the constraint forces acting on the skate, since we assume that the skate can only glide in the direction of the blade, restricting lateral slip. All other rotations of the skates and the upper body rotations are neglected. The bodyweight of the skater is distributed over the two active masses by a constant mass distribution coefficient (α). Furthermore, the arm movements are assumed to be of marginal effect on the overall power and are therefore neglected.

The input of the model is the changing distance between the point mass position of the upper body and the skate (Euclidean distance in 3D space), which will be indicated as the leg extension in the remainder of this study, and the steering angle of the skate; The output of the model are the upper body motion of the skater in global space together with the forces exerted by the skates on the ice.

The global coordinates describing the position of upper body B and skate S are,

$$\mathbf{x} = [x_b \quad y_b \quad z_b \quad x_s \quad y_s \quad \phi_s] \quad (\text{B.1})$$

We express the coordination of the skater in terms of leg extension. Instead of describing the position and orientation of the body together with the constraints imposed by the joints on these coordinates \mathbf{x} we use a minimum set of coordinates \mathbf{q} ,

$$\mathbf{q} = [u_b \quad v_b \quad w_s \quad u_s \quad v_s \quad \theta_s] \quad (\text{B.2})$$

Where (w_s, u_s, v_s) describe the leg extension, and (θ_s) the steering angle which are actively controlled by the skater and therefore serve as the input coordinates to the model (Figure 4.2).

The remaining coordinates (u_b, v_b) are the generalized coordinates of the upper body, which will be a result of the system dynamics (Table 10.B.1).

The environmental forces acting on the skater are the gravitational force, the air frictional force and the ice frictional force. We described the air friction forces based on the study of van Ingen Schenau, 1982:

$$F_{b,f} = \frac{1}{2} AC_d \rho \mathbf{v}_{xyz}^2 = k_1 \mathbf{v}_{xyz}^2 \quad (\text{B.3})$$

where C_d represents the drag coefficient, A the frontal projected area of the skater, ρ the air density and \mathbf{v}_{xyz} the velocity of the air with respect to the skater. Based on the verification

Table 10.B.1 Clarification on the generalized coordinates.

q	Generalized coordinates
u_b	Absolute position of mass B in x-direction (global)
v_b	Absolute position of mass B in y-direction (global)
w_s	Vertical distance between the mass S and mass B
u_s	Horizontal distance between mass S and mass B in heading direction of the skate
v_s	Horizontal distance between mass S and mass B perpendicular to the heading direction of the skate
θ_s	Heading of the skate (counterclockwise)

results, we use $k_1 = 0.14$ in this study (van der Kruk, Veeger, et al., 2017). $F_{s,f}$ is the ice friction working on the skate, which is described using Coulomb's law of friction (De Koning, De Groot, & Van Ingen Schenau, 1992):

$$F_{s,f} = \mu F_N \quad (\text{B.4})$$

where μ is the friction coefficient and F_N is the normal force of the skate on the ice. Since the normal force is one of the outcomes of the model and μ is small, the normal force is approximated by $F_N \approx mg$ in which m the mass of the skater and g the earth gravity. Based on the verification results, we use $\mu = 0.006$ in this study (van der Kruk, Veeger, et al., 2017).

B.2.2 Model Optimization

The aim of this study is to determine the optimal trade-off between lateral and forward motion to cover a fixed forward distance in a minimum time span, given a fixed initial total velocity, by optimization of the simple skater model. This question is approached in two steps;

STEP1: first we determine if the optimization strategy, with the chosen boundaries and constraints, finds a realistic control input and model output, compared to observed forces and motions. As a constraint, the final time is set to the measured final time. For this validation we use the measured data of one stroke of one speed skater.

STEP2: Second, we determine the optimal trade-off between lateral and forward motion to minimize the time to cover a distance of one stroke, thereby using the control input boundaries (leg extension acceleration, steering angular acceleration) and the total initial velocity as independent variables.

The optimization problem and the constraints are the same for STEP1 and STEP2. The steps differ in their final minimization criterion, the initial conditions of the optimization, and the boundaries for the control input (Table 10.B.2), which are explained next.

B.2.2.1 General optimization set-up and constraints (STEP1 & STEP2)

To transcribe the simple skater model into an optimal control problem, we first rewrite the input and output of the simple skater model, to a state vector and control input. Since the second derivative of the leg extension (leg extension acceleration) is necessary to solve the simple skater model, we defined this as the control input for the optimization problem:

$$\mathbf{u} = \begin{bmatrix} \ddot{w}_s & \ddot{u}_s & \ddot{v}_s & \ddot{\theta}_s \end{bmatrix} \quad (\text{B.5})$$

the acceleration of the leg extension is taken as an input, therefore the leg extension and its velocity need to be added to the state vector, which is then defined as:

Table 10.B.2 The minimization criteria, the initial conditions and the state boundaries define STEP1 and STEP2. The constraints, which are part of the general optimization set-up, are the same for STEP1 and STEP2. In STEP1 the optimization control inputs and output are verified by comparing the results to observed data. In STEP2 the optimal motion strategy is search for different initial velocities (v^n) and different control boundaries.

	STEP1	STEP2
Minimization criterion	$E^{STEP1}(t_f) = \ t_f - \tilde{t}_f\ $	$E^{STEP2}(t_f) = t_f$
Initial conditions	$\mathbf{x}_{t_0}^{STEP1} = \tilde{\mathbf{x}}_{t_0}$	$x_b, y_b = \tilde{x}_b, \tilde{y}_b$ $\sqrt{\dot{x}_{b,t_0}^2 + \dot{y}_{b,t_0}^2} = v^n$ $0.65 \cdot LL \leq \sqrt{u_{s,t_0}^2 + v_{s,t_0}^2 + w_{s,t_0}^2} \leq 0.75 \cdot LL$ $0 \leq \sqrt{\ddot{u}_{s,t_0}^2 + \ddot{v}_{s,t_0}^2 + \ddot{w}_{s,t_0}^2} \leq 1$
Control Boundaries	$\mathbf{u}^{lb} = [-2 \quad -3 \quad -3 \quad -0.3\pi]$ $\mathbf{u}^{ub} = [2 \quad 3 \quad 3 \quad 0.3\pi]$	$\mathbf{u}^{lb} = [-2 \quad \ddot{u}_s^{lb} \quad \ddot{v}_s^{lb} \quad \ddot{\theta}_s^{lb}]$ $\mathbf{u}^{ub} = [2 \quad \ddot{u}_s^{ub} \quad \ddot{v}_s^{ub} \quad \ddot{\theta}_s^{ub}]$
Constraints	<p><i>Fixed distance</i> $y_{b,t_f} = \tilde{y}_{b,t_f}$</p> <p><i>Cyclic motion</i> $\dot{y}_{b,t_f} = \dot{y}_{b,t_0}$ $\dot{x}_{b,t_f} = -\dot{x}_{b,t_0}$ $\dot{w}_{b,t_f} = \dot{w}_{b,t_0}$ $w_{b,t_f} = w_{b,t_0}$</p> <p><i>Leg length</i> $\frac{1}{2}LL \leq \sqrt{u_{s,t}^2 + v_{s,t}^2 + w_{s,t}^2} \leq LL$</p> <p><i>$U_s$-constraint</i> $u_s \leq 0.1 \quad 0 \leq t \leq \frac{t_f}{2}$ $u_s \leq 0.4 \quad t > \frac{t_f}{2}$</p> <p><i>No pulling forces</i> $v_{s,t} \cdot \dot{v}_{s,t} \geq 0$</p>	<p>$y_{b,t_f} = \tilde{y}_{b,t_f}$</p> <p>$\dot{y}_{b,t_f} = \dot{y}_{b,t_0}$ $\dot{x}_{b,t_f} = -\dot{x}_{b,t_0}$ $\dot{w}_{b,t_f} = \dot{w}_{b,t_0}$ $w_{b,t_f} = w_{b,t_0}$</p> <p>$\frac{1}{2}LL \leq \sqrt{u_{s,t}^2 + v_{s,t}^2 + w_{s,t}^2} \leq LL$</p> <p>$u_s \leq 0.1 \quad 0 \leq t \leq \frac{t_f}{2}$ $u_s \leq 0.4 \quad t > \frac{t_f}{2}$</p> <p>$v_{s,t} \cdot \dot{v}_{s,t} \geq 0$</p>

$$\mathbf{x} = \begin{bmatrix} x_b & y_b & \dot{x}_b & \dot{y}_b & u_s & v_s & w_s & \theta_s & \dot{u}_s & \dot{v}_s & \dot{w}_s & \dot{\theta}_s \end{bmatrix} \quad (B.6)$$

The general constraints (used for both STEP1 and STEP2) contain final state constraints and path constraints (Table 10.B.2). The final state constraints define the state at time t_f . First, the covered forward distance is fixed at t_f :

$$y_{b,t_f} = \tilde{y}_{b,t_f} \quad (B.7)$$

Where the actual measured distance of a stroke \tilde{y}_{b,t_f} is used. Second, several constraints on the final state of mass B in three directions were set, since skating is a cyclic motion, and therefore the end of one stroke is the start of the next stroke. This is done for the forward velocity:

$$\dot{y}_{b,t_f} = \dot{y}_{b,t_0} \quad (B.8)$$

the lateral velocity,

$$\dot{x}_{b,t_f} = -\dot{x}_{b,t_0} \quad (B.9)$$

and the upwards velocity and position,

$$\begin{aligned}\dot{w}_{b,t_f} &= \dot{w}_{b,t_0} \\ w_{b,t_f} &= w_{b,t_0}\end{aligned}\tag{B.10}$$

Since the optimization of the motion of mass S is only half a cycle (the repositioning phase in the air is neglected), no final state constraints were set for S.

Next, three path constraints are set, which can restrict the state and input vector for each timestep t . First, the leg extension is restrained not to exceed the maximum leg length LL and not to be smaller than half the leg length:

$$\frac{1}{2}LL \leq \sqrt{u_{s,t}^2 + v_{s,t}^2 + w_{s,t}^2} \leq LL\tag{B.11}$$

The second path constraint is set for one of the components of the leg extension, u_s . In preliminary optimization approaches in which we only set boundary constraints for u_s (based on observed data in the skating trials ($-0.1 \leq u_s \leq 0.4$)), the optimal motion strategy found by the optimization was to first increase u_s to the maximum extension, before increasing the other components of the leg extension. However, such a motion is infeasible for an actual skater, due to balance control and steering of the skate, which will be further discussed in the discussion section. Since this motion strategy is not feasible for an actual speed skater, a path constraint was added for u_s , which defined that u_s can only increase after half of the stroke time (t_f).

$$\begin{aligned}u_s &\leq 0.1 & 0 \leq t \leq \frac{t_f}{2} \\ u_s &\leq 0.4 & t > \frac{t_f}{2}\end{aligned}\tag{B.12}$$

Third, since the input of the skater model is a piston-like joint without any attributes of real muscles, we need to add a constraint, that the leg extension cannot generate pulling forces in the horizontal plane. Based on the preliminary results, this constraint proved to be only necessary for the component $v_{s,t}$, therefore the following path constraint was added:

$$v_{s,t} \cdot \ddot{v}_{s,t} \geq 0\tag{B.13}$$

So for STEP1 and STEP2 the constraints are set for a fixed covered distance, enabling a cyclic motion, maximum leg length, u_s -constraint, and no pulling forces (see Table 10.B.2). Next, the STEP specific conditions are defined.

B.2.2.3 STEP1 & STEP 2: Initial Conditions, Minimization Criterion, and Control Boundaries

The minimization criterion, the initial conditions, and the control boundaries of the optimization define STEP1 and STEP2 (Table 10.B.2). The applied conditions are given here.

B.2.2.3.1 STEP1: verification of the optimization

STEP1 determines if the optimization strategy finds a realistic control input and model output, compared to observed forces and motions. The minimization criterion for STEP1 is to find a motion strategy with the same final time as the measured stroke

$$E^{STEP1}(t_f) = \|t_f - \tilde{t}_f\| \quad (B.14)$$

In which \tilde{t}_f is the measured time from the recorded data. The initial conditions of the state vector are set to the actual measured data $\tilde{\mathbf{x}}_{t_0}$ at the start of a stroke (t_0).

$$\mathbf{x}_{t_0}^{STEP1} = \tilde{\mathbf{x}}_{t_0} \quad (B.15)$$

There are no initial conditions set for the control input $\mathbf{u}_{t_0}^{STEP1}$. The control boundaries (the upper and lower bounds of the control inputs, \mathbf{u}^{lb} , \mathbf{u}^{ub}) are based on observed values in the measured data:

$$\begin{aligned} \mathbf{u}^{lb} &= [-2 \quad -3 \quad -3 \quad -0.3\pi] \\ \mathbf{u}^{ub} &= [2 \quad 3 \quad 3 \quad 0.3\pi] \end{aligned} \quad (B.16)$$

With the units

$$\mathbf{u}^{units} = \left[\frac{m}{s^2} \quad \frac{m}{s^2} \quad \frac{m}{s^2} \quad \frac{rad}{s^2} \right] \quad (B.17)$$

The control input, nor the state vector are further prescribed and therefore the motion strategy is free in the optimization. The results of this optimization is referred to as **OPT0**, and is the verification trial.

2.2.3.2 STEP2

STEP2 determines the optimal trade-off between lateral and forward motion to minimize the time to cover a distance of one stroke, thereby using the control input boundaries (leg extension acceleration, steering angular acceleration) and the total initial velocity as independent variables. The *minimization criterion* for STEP2 is

$$E^{STEP2}(t_f) = t_f \quad (B.18)$$

Except for the initial position ($x_b, y_b = \tilde{x}_b, \tilde{y}_b$) there are no *initial conditions* set for STEP2.

However, there are constraints set to the initial state vector $\mathbf{x}_{t_0}^{STEP2}$. First, the initial total velocity is set to the chosen initial velocity v^{in} , so

$$\sqrt{\dot{x}_{b,t_0}^2 + \dot{y}_{b,t_0}^2} = v^{in} \quad (B.19)$$

v^{in} is an independent variable which was tested for the measured velocity, and the velocities of 10,12,14, and 16 m/s (Table 10.B.3). Second, since the skater needs to start at a stooped

Table 10.B.3 Optimisations run with the simple skater model for STEP2.

Initial velocity (v^{in})	$-0.3\pi \leq \ddot{\theta}_s \leq 0.3\pi$, $-3 \leq \ddot{u}_s, \ddot{v}_s \leq 3$	$-0.3\pi \leq \ddot{\theta}_s \leq 0.3\pi$, $-10 \leq \ddot{u}_s, \ddot{v}_s \leq 10$	$-3\pi \leq \ddot{\theta}_s \leq 3\pi$, $-3 \leq \ddot{u}_s, \ddot{v}_s \leq 3$
$v^{\text{in}} = \tilde{v}^{\text{in}} = 11.48 \text{ m/s}$	(STEP1: OPT0) OPT1	OPT2	OPT3
$v^{\text{in}} = 10 \text{ m/s}$	OPT4	OPT5	OPT6
$v^{\text{in}} = 12 \text{ m/s}$	OPT7	OPT8	OPT9
$v^{\text{in}} = 14 \text{ m/s}$	OPT10	OPT11	OPT12
$v^{\text{in}} = 16 \text{ m/s}$	OPT13	OPT14	OPT15

position, the leg extension at t_0 is constrained to

$$0.65 \cdot LL \leq \sqrt{u_{s,t_0}^2 + v_{s,t_0}^2 + w_{s,t_0}^2} \leq 0.75 \cdot LL \quad (\text{B.20})$$

The boundaries are based on observed data. Finally, to restrain the optimization from starting at unrealistic leg extension velocities,

$$0 \leq \sqrt{\dot{u}_{s,t_0}^2 + \dot{v}_{s,t_0}^2 + \dot{w}_{s,t_0}^2} \leq 1 \quad (\text{B.21})$$

The boundaries are based on observed data. So although there are constraints put to the initial conditions, the separate variables of the motion strategy and the trade-off between gliding forwards and pushing of sideways are free. The control boundaries are independent

variables. From several preliminary optimizations and simulations it was clear that \dot{w}_s was of no influence to the forward motion (the upper body motion is prescribed in the simple skater model), therefore we did not change the boundaries of this control variable in the optimization.

Furthermore, we found that the boundaries of \ddot{u}_s, \ddot{v}_s should be changed together. The control input boundary is thus described by:

$$\begin{aligned} \mathbf{u}^{lb} &= \begin{bmatrix} -2 & \ddot{u}_s^{lb} & \ddot{v}_s^{lb} & \ddot{\theta}_s^{lb} \end{bmatrix} \\ \mathbf{u}^{ub} &= \begin{bmatrix} 2 & \ddot{u}_s^{ub} & \ddot{v}_s^{ub} & \ddot{\theta}_s^{ub} \end{bmatrix} \end{aligned} \quad (\text{B.22})$$

In which we used a lb and ub of 3 and 10 m/s^2 for the leg extensional accelerations (\ddot{u}_s, \ddot{v}_s), and 0.3π and 3π rad/s^2 for the steering angular acceleration ($\ddot{\theta}_s$) (see Table 10.B.3).

B.2.2.3 Solving the optimization

To solve the optimization problem, a multivariable approach is taken, by using the open-source optimal control software ICLOCS (Falugi, Kerrigan, & Van Wyk, 2010). The software first transcribes the control problem to a static optimisation problem by using direct collocation (trapezoidal method), which discretises the system dynamics using implicit Runge-Kutta formulae. After transcription, the solution is found via a selection of non-linear constraint optimization algorithms given by the open-source code IPOPT (Wächter, Laird, Margot, & Kawajir, 2009).

B.2.2.4 Outcome measures

For STEP1, the root mean square errors (e_{var}) have been determined between the measured input and output data and the optimized input and output data. Additionally we made an estimation of the mechanical work per stroke. Note however, that this was done via the simplified model, and therefore the resulting mechanical work cannot be compared to the estimated work of a joint power model (van der Kruk, van der Helm, et al., 2017). Results can only be interpreted relatively within this study. We determined the simplified mechanical power (SMP) as:

$$P_{SMP} = \mathbf{F}^q \cdot \begin{bmatrix} \dot{w}_s \\ \dot{u}_s \\ \dot{v}_s \\ \dot{\theta}_s \end{bmatrix} \quad (B.23)$$

In which \mathbf{F}^q are the forces in the generalized coordinate system. From this, we estimated the simplified mechanical work (SMW) per stroke as:

$$W_{SMW} = \int_{t_0}^{t_f} \|P_{SMP}\| dt \quad (B.24)$$

Here we take the absolute power, since part of the negative power also requires energy, but we cannot distinguish between the parts (van der Kruk, van der Helm, et al., 2017).

References:

Allinger, T. L., & Bogert, A. J. (1997). *Skating technique for the straights based on the optimization of a simulation study. Medicine and Science in Sports and Exercise*, 29, 279–286.

Bruzzo, J., Schwab, A. L., Valkeapää, A., Mikkola, A., Ohtonen, O., & Linnamo, V. (2016). *A simple mechanical model for simulating cross-country skiing, skating technique. Sports Engineering*, 19(2), 91–104.

de Boer, R. W., Vos, E., Hutter, W., de Groot, G., & van Ingen Schenau, G. J. (1987). *Physiological and biomechanical comparison of roller skating and speed skating on ice. European Journal of Applied Physiology and Occupational Physiology*, 56(5), 562–569. <http://doi.org/10.1007/BF00635371>

De Koning, J. J., De Groot, G., & Van Ingen Schenau, G. J. (1992). *Ice friction during speed skating. Journal of Biomechanics*, 25(6), 565–571. [http://doi.org/10.1016/0021-9290\(92\)90099-M](http://doi.org/10.1016/0021-9290(92)90099-M)

Falugi, P., Kerrigan, E., & Van Wyk, E. (2010). *Imperial college london optimal control software user guide (ICLOCS). Department of Electrical and Electronic Engineering, Imperial College London, London, England, UK.*

Otten, E. (2003). *Inverse and forward dynamics: models of multi-body systems. Philosophical Transactions of the Royal Society of London B: Biological Sciences*, 358, 1493–1500.

Stoeggli, T., Kappel, W., Mueller, E., & Lindinger, S. (2010). *Double-push skating versus V2 and V1 skating on uphill terrain in cross-country skiing. Medicine and Science in Sports and Exercise*, 42(1), 187–196.

Stöggl, T., Müller, E., & Lindinger, S. (2008). Biomechanical comparison of the double-push technique and the conventional skate skiing technique in cross-country sprint skiing. *Journal of Sports Sciences*, 26(11), 1225–1233.

van der Kruk, E. ., van der Helm, F. C. T. ., Veeger, H. E. J. ., & Schwab, A. L. . (2017). Power in Sports: a literature review on the application, assumptions, terminology and validity of mechanical power in sport research. Submitted at *Journal of Biomechanics*.

van der Kruk, E., Veeger, H. E. J., van der Helm, F. C. T., & Schwab, A. L. (2017). Design and verification of a simple 3D dynamic model of speed skating which mimics observed forces and motions. *Journal of Biomechanics*. <http://doi.org/10.1016/j.jbiomech.2017.09.004>

van Ingen Schenau, G. J. (1982). The influence of air friction in speed skating. *Journal of Biomechanics*, 15(6), 449–458. [http://doi.org/10.1016/0021-9290\(82\)90081-1](http://doi.org/10.1016/0021-9290(82)90081-1)

Waechter, A., Laird, C., Margot, F., & Kawajir, Y. (2009). Introduction to IPOPT: A tutorial for downloading, installing, and using IPOPT. Revision.

Acknowledgements Dankwoord

Het leven is alleen maar vrienden maken.

-Max Cramwinckel-



Frühlingsfest 2016, München



PhD Wintersport 2015, Val Thorens

Dan toch echt het aller-aller-laatste stukje van mijn proefschrift: het dankwoord. En er zijn heel wat mensen die ik wil bedanken, omdat de afgelopen vier jaar een stuk minder leuk waren geweest zonder hen.

Allereerst mijn drie promotoren;

Arend, mijn enthousiasme voor dynamica en modelleren heb ik vrijwel geheel aan jou te danken. Na mijn afstuderen bij jou, heb ik je in het eerste jaar van mijn PhD wegens ziekte helaas moeten missen, maar daarom heb ik des te meer genoten van de momenten erna waarop we samen konden puzzelen en rekenen aan een oplossing. Dankjewel voor je hulp, kennis, begeleiding en persoonlijke adviezen.

DirkJan, ook jij bent in mijn tweede jaar PhD meer en meer betrokken geraakt door de overstap van Amsterdam naar Delft. Waar we tijdens mijn afstuderen nog weleens botste, werd onze samenwerking des te sterker in de PhD. Ik heb veel van je geleerd op het gebied van bewegingswetenschappen, maar ook aan persoonlijke ontwikkeling. Dankjewel voor je aanmoedigingen en coachen hierin.

Frans, ik heb je denk ik nooit verteld dat ik mijn masterrichting heb gekozen na het zien van een presentatie van jou over implantaten bij Parkinson patiënten. Dat ik uiteindelijk bij jou zou promoveren had ik toen zeker niet voorzien. Je hebt zelf ooit gezegd: de beste samenwerkingen zijn met de mensen met wie je bier kan drinken, dus dat liep wel lekker. Dankjewel voor je onuitputtelijke enthousiasme en inspiratie.

Jullie hebben mij alle drie de vrijheid gegeven in het onderzoek en het project. En in het bijzonder ook om een week per maand in München te werken. Zoals DirkJan het verwoorde 'voor een promotor is een promovenda als je kind, als zij gelukkig is ben jij dat ook'. Dankjulliewel daarvoor!

Er zijn nog meer mensen uit het schaatsproject die ik graag wil bedanken; **Otto** voor het initiëren van het project en het introduceren van mij bij het project; **Jorine**, altijd gezellig om samen met jou studenten te begeleiden; **Wouter** dankjewel voor de prettige samenwerking aan de nieuwe meetschaats (laten we volgende keer geen schaats ontwerpen;)). **Nisse, Jos, Henny** en de andere mannen van DEMO en de werkplaats dank voor jullie vakmanschap over de jaren heen. Uit de schaatswereld wil ik **Bjorn** en **Jeroen** Otter bedanken voor jullie oneindige stroom aan ideeën en vertrouwen. Ook ik wil ik **Peter** Kolder bedanken voor het directe enthousiasme, meedenken en meewerken in de eerste jaren van het project; en tenslotte de **ijsmeesters van Thialf**, voor het faciliteren van het soms onmogelijke.

Dan mijn collega's, die ik gaande weg vrienden ben gaan noemen: **Jeroen, Paul, Bram, Annetje, Frédérique, David, Peter, Ingrid, Marco, Teun, Ewout, Awaz, Henri, Tonke, Marta, Nadia, Roos, Tricia, Xavier, Juan, Nick, Roel**. Dat er nog veel meer First-Fridays-

of-the-Months, sinterklazen, borrels, wintersporten, carnavals, phd-video's, lunches, derde kerstdagdinners, festivals, frühlingsfesten etc. met jullie mogen komen. Ik voel me enorm gezegend met zo'n toffe groep collega's. In het bijzonder wil ik van deze mensen nog **Fred** bedanken voor haar hulp bij de nachtmetingen (want laten we eerlijk zijn, het is twijfelachtig of ik hier anders nog had gestaan)); **Jeroen (en Eef)** voor jullie post-OFL-opvang en de introductie met de Science Battle; **David** voor je steun en hulp tijdens de laatste loodjes van mijn phd en de 'adoptie' in het hapticslab toen ik in mijn eerste jaar wat verloren was in het grote promotie systeem; **Peter** voor je gezelligheid in het kantoor; **Marco** voor het samen schrijven aan papers en omdat je het sports engineering stokje overneemt; **Ingrid** voor een paar onvergetelijke feestjes. En natuurlijk **Paul**, dankjewel voor alle biertjes op de meest uiteenlopende borrels, feestjes en gelegenheden, voor je gezelligheid tijdens lunches en de strijd bij Science Battles. Zonder jou zou een PhD een stuk minder gezellig en relativerend zijn; dankjewel dat je mijn paranimf bent.

Ook een dankjewel voor het hele ondersteunende team van BME: **Sabrina, Anoeke, Hanneke, Mirjam, Nancy, Karin** en alle andere: dank voor alles. **Erika** en **Terhas**, jullie zorgden er iedere ochtend voor dat mijn medium cappuccino met cacao klaarstond zonder te bestellen, jullie zijn heldinnen!

Tenslotte, Suzanne, René, Patrick en Richard en alle andere science battlers dank voor de bijzondere en leuke momenten in de Nederlandse theaters en podia met de **Science Battle**.

Maar ook buiten de TU Delft zijn er mensen die ik niet wil vergeten:

Pap, mam, dankjulliewel dat jullie me altijd de vrijheid hebben gegeven om te doen wat ik wilde, ook al was dat meestal veel te veel en iedere dag anders. Jullie hebben ons altijd met beide benen op de grond gehouden, en daarmee bijzondere mensen groot gebracht. **Dirk**, grote broer, dankzij jou kan ik mijn vrouw staan in deze mannenwereld. Ik heb bewondering voor hoe jij je eigen ideeën nastreeft en ze tot een succes maakt. En ik kan natuurlijk ook mijn grote nicht **Martine** niet vergeten, zonder jou zou ik nooit op de TU terecht zijn gekomen. En tenslotte **Oma**, dank voor alle wijsheden en liefde.

Ook dankjewel aan heel veel lieve vriendinnen; **Elsemieke** voor alle gezellige etentjes; **Josje** voor allerlei bizarre avonden; **Saskia** voor alle fijne en gênante gesprekken; **Katrien** omdat jij de enige bent die heel trots is dat je een nerd hebt als vriendin; **Yke** dat ik bij je in Londen langs kan komen; **Ninke** omdat je al zolang in mijn leven bent; **Merel** (peppie) omdat jij de aller-stoerste chick bent die ik ken; En **Dorine** omdat ik altijd bij jullie terecht kan.

Dan nog belangrijke mensen uit Den Haag; **Diedo**, jij bent al vanaf mijn eerste dag studeren erbij geweest in Huize K'sgaaf, Jansbrug, werktuigbouwkunde, en Den Haag. Bij jou en Dorine kom ik niet op visite, maar thuis. Ik ben trots en blij dat je op mijn promotie mijn paranimf wil zijn. En van de stoere mannen in Den Haag wil ik ook **Luc** niet vergeten. Luc, dankjewel dat ik je 's nachts voor alles mag wakker maken, van inbraken, tot blikseminslag (ahum), tot bier drinken. Zonder jou was mijn PhD tijd een stuk onveiliger en de kroeg een stuk veiliger geweest.

En dan natuurlijk nog de bijzonderste man van Den Haag: **Bas**. Lieve Bas, samen beleven we de meest gekke, lieve, onzekere, leuke, saaie, hilarische, droevige, nerderige, spannende, en gelukkige avonturen. Samen met jou ga ik alles aan. Op naar onze volgende avonturen in Zuid-Amerika.

Curriculum Vitae List of Publications

Ooit een normaal mens ontmoet?...En beviel 't?

- Stichting Pandora-

Curriculum Vitae

Nov 2013 – Dec 2017	Ph.D. in Biomechanical Engineering, Delft University of Technology Thesis: "Parameter Analysis for Speed Skating Performance." (co)promotoren: Prof. dr. F.C.T. van der Helm, Prof. dr. H.E.J. Veeger & dr. ir. A.L. Schwab
Sep 2011 – Sep 2013	M.Sc. in Mechanical Engineering, Delft University of Technology Specialization: Biomechanical Engineering (Sports Engineering) MSc Thesis: "Modelling and Measuring three-dimensional movements of a speed skater."
Sep 2007- Jul 2011	B.Sc. Industrial Design Engineering, Delft University of Technology BSc thesis: "Design of an occlusion-free earplug"
Sep 2001 – Jul 2007	Pre-University Education (High School/Gymnasium), Erasmiaans Gymnasium, Rotterdam, the Netherlands
14-02-1989	Born in Albranswaard, the Netherlands

Awards & Distinctions

2013	Cum Laude M.Sc. degree
2011	1 st place for UfD Bachelor Grant (€ 2000) for exceptional final bachelor's research paper, which met the requirements of technical innovation, practical applicability, collaboration between disciplines, social relevance and daring.
2007	Cum Laude pre-university degree

List of Publications

Journal Publications

1. **van der Kruk, E.**, den Braver, O., Schwab, A. L., van der Helm, F. C. T., & Veeger, H. E. J. (2016). Wireless instrumented klapskates for long-track speed skating. *Sports Engineering*, 19(4), 273-281 (impact factor: 1.1)

2. **van der Kruk, E.**, H.E.J. Veeger, F.C.T. van der Helm and A.L. Schwab, Design and verification of a simple 3D dynamic model of speed skating which mimics observed forces and motions. (2017), *Journal of Biomechanics* (impact factor: 2.66)

Journal publications accepted (with revisions)

3. **van der Kruk, E.**, A.L. Schwab, F.C.T. van der Helm & H.E.J. Veeger, Getting in shape: reconstructing three-dimensional long-track speed skating kinematics by comparing several body pose reconstruction techniques.

Journal submission: *Journal of Biomechanics* (impact factor: 2.66)

4. **van der Kruk, E.**, M.M. Reijne, B. de Laat & H.E.J. Veeger, Push-off Forces in Short-Track Speed Skating

Journal submission: *Sports Biomechanics*, revisions (impact factor: 0.826)

5. **van der Kruk, E.** & Reijne, M.M. Accuracy of Body Motion Capture System for Sport Applications

Journal submission: *European Journal of Sport Sciences*, revisions (impact factor: 2.69)

6. **van der Kruk, E.**, F.C.T. van der Helm, H.E.J. Veeger & A.L. Schwab, Power in Sports: a literature review on the application, assumptions, terminology and validity of mechanical power in sport research.

Journal submission: *Journal of Biomechanics*, revisions (impact factor: 2.66)

Journal publications under review

7. **van der Kruk, E.**, A.L. Schwab, H.E.J. Veeger & F.C.T. van der Helm, Balancing the power: determining the mechanical power balance in speed skating with a new proposed inverse dynamics method.

Journal submission: *Journal of Biomechanics*, May 2017 (impact factor: 2.66)

Peer-reviewed conference papers

8. **van der Kruk, E.**, Schwab, A. L., van der Helm, F. C. T., & Veeger, H. E. J. (2016). Getting the Angles Straight in Speed Skating: A Validation Study on an IMU Filter Design to Measure the Lean Angle of the Skate on the Straights. *Procedia Engineering*, 147, 590-595. (6-page article)

9. **van der Kruk, E.**, DirkJan (H).E.J. Veeger, Frans C.T. van der Helm and Arend L. Schwab, Measuring and modelling the mechanical power balance in speed skating, one-page abstract, ISB 2017, Brisbane, Australia

10. **van der Kruk, E.**, F.C.T. van der Helm, A.L. Schwab and H.E.J. Veeger, Giving the force direction: analysis of speed skater push-off forces with respect to an inertial coordinate system, ISBS conference 2016 (4-page paper)

11. **van der Kruk, E.**, Veeger, H. E. J., van der Helm, F. C. T., & Schwab, A. L. (2015). Two Body Dynamic Model for Speed Skating Driven by the Skaters Leg Extension. In *Workshop Modelling in Endurance Sports* (p. 14). (3-page abstract)

Dutch scientific publications

12. **van der Kruk, E.**, A.L. Schwab , Nog sneller schaatsen? Wie niet sterk is moet slim zijn!, Nederlands Tijdschrift voor Natuurkunde, Juni 2016

13. **van der Kruk, E.**, Niet over één nacht ijs: Real-time feedback voor betere schaatsprestaties, SportGericht nr.3, 2016

Outreach

Interviews in newspapers, magazines and books

- 2017 Trouw, Dutch National Newspaper
- 2017 De ingenieur, Dutch National Magazine, interview as 'inspiring engineer', chosen as 1 of 12 'best young engineers in the Netherlands'.
- 2017 Warmondse ijsclub, regional magazine
- 2016 SportKnowHowXL.nl, Dutch website
- 2016 Technisch Weekblad, Dutch National Magazine
- 2015 Volkskrant, Dutch National Newspaper, "Nieuw gezicht van de wetenschap"
- 2015 Metro, Dutch National Newspaper, interview on Science Battle
- 2015 Quest, (Dutch monthly technical magazine for adults)
- 2015 Leeuwarder Courant, Dutch Regional Newspaper
- 2013 TU Delft Highlights 2013, Chosen as highlights of TU Delft, 2013

TV and Radio coverage

- 2017 NPO2 (National TV), 'De Kennis van Nu', interview on Biomechanics in Speed skating, <https://youtu.be/5UALKDLgcGk>
- 2017 Universiteit van Nederland, Lecture on National TV 'How to determine the ideal motion for an individual speed skater', <http://www.universiteitvannederland.nl/college/hoe-bepaal-je-voor-elke-schaatser-wat-zijn-of-haar-ideale-techniek-is/>
- 2017 Start the Future , Online Broadcast, 10 min. documentary on the design and development of the instrumented skate, <https://youtu.be/oFFbUa8omt0>
- 2017 Korean EBS TV (National Korean TV), interview on biomechanics in speed skating
- 2015 NOS, Dutch National News, item on overnight speed skating measurements measurements, <http://nos.nl/artikel/2015565-schaatsster-van-beek-traint-in-3d-in-thialf.html>
- 2015 Omrop Fryslan, Dutch Regional News, item on overnight speed skating measurements measurements, http://omropfryslanvod.download.kpnstreaming.nl/video/2013/HQ/HJOED_2015-01-26.mp4
- 2015 Radio 1 (National Radio), Langs de lijn, item on overnight speed skating measurements measurements, <http://nos.nl/artikel/2015565-schaatsster-van-beek-traint-in-3d-in-thialf.html>
- 2013 NPO 1 (Dutch National TV), Omroep Max, interview as 'First Engineering of the Netherlands'
- 2009 SBS 6, (Dutch National TV), Interview on nomination for 'HEMA Design Contest'

Popular Science Presentations

- 2014 /7 Science Battle, Theatre Show to promote Science, 15 shows in different Dutch theatres, www.ScienceBattle.nl
- 2017 Weekend van de Wetenschap, interview as 'inspiring engineer'
- 2016 World Maintenance Congres, invited speaker 'Smart Sensoring'